NOTICE

The quality of this microform is heavily dependent upon the quality of the original thesis submitted for microfilming. Every effort has been made to ensure the highest quality of reproduction possible.

If pages are missing, contact the university which granted the degree.

Some pages may have indistinct print especially if the original pages were typed with a poor typewriter ribbon or if the university sent us an inferior photocopy.

Reproduction in full or in part of this microform is governed by the Canadian Copyright Act, R.S.C. 1970, c. C-30, and subsequent amendments.

AVIS

La qualité de cette microforme dépend grandement de la qualité de la thèse soumise au microfilmage. Nous avons tout fait pour assurer une qualité supérieure de reproduction.

S'il manque des pages, veuillez communiquer avec l'université qui a conféré le grade.

La qualité d'impression de certaines pages peut laisser à désirer, surtout si les pages originales ont été dactylographiées à l'aide d'un ruban usé ou si l'université nous a fait parvenir une photocopie de qualité inférieure.

La reproduction, même partielle, de cette microforme est soumise à la Loi canadienne sur le droit d'auteur, SRC 1970, c. C-30, et ses amendements subséquents.

ISBN 0-315-70496-9

UNIVERSITÉ D'OTTAWA
UNIVERSITY OF OTTAWA

to my mother

ABSTRACT

The main body of research reported in this thesis was concerned with studies of H, and OH or O, chemisorption on polycrystalline and single-crystal Pt surfaces, including studies of the anodic growth of thick oxide films and distinction between the several states in which they are formed.

The experimental conclusions on states of formation of thick-oxide films at polycrystalline Pt, reported in earlier literature, are not only quantitatively but qualitatively divergent from one research laboratory to another. It is shown that this was mainly due to the different pretreatments of the Pt electrodes that had been applied, which led to substantial irreproducibility. In the work reported in the first part of this thesis, a standard procedure has been worked out for preparing polycrystalline Pt electrodes. Such electrodes reveal and sustain the same physical and electrochemical properties over long periods of time; this is probably the result of the discovery and use of the "electrochemical annealing" phenomenon. Thus, polycrystalline Pt electrodes can be well characterized in a reproducible way after selected controlled thermal and/or electrochemical pretreatments and are found to become reconverted to the same, stable and final state (the "electrochemically annealed" state) after prolonged cycling between 0.05 and 1.40 V, RHE, regardless of their initial pretreatment.

Having thus established a standard procedure for preparation of polycrystalline Pt electrodes, controlled formation of thick-oxide films has been investigated. At Pt anodes subjected to regimes of anodization at high controlled potentials for various periods of time, it was found that at least five states of the oxide film can be distinguished, in reduction, using the cyclic-voltammetry technique. The extent of growth of the oxide film at Pt proceeds according to a direct logarithmic law in time of growth for polarization potentials between 1.80 and 2.30 V, RHE. Upon further increase of the polarization time,

the oxide growth rate increases some 400 times due to the onset of the high-field oxide growth mechanism of Mott and Cabrera. Contrary to some earlier results, no attainment of a finite limit of O "coverage" is reached, as continuous development of phase-oxide in fact takes place. However, the quasi-2-d oxide state does reach a limit of two monolayers of "PtO" and sustains it even if the Pt electrode is polarized up to higher potentials (4.0 V) and at elevated temperatures. Upon increase of the polarization potential and time, it has been shown that multilayer phase oxide is generated on top of the quasi-2-d oxide.

It is found that the quasi-2-d oxide can be reduced independently from the bulk-type oxide, leading to a situation where the thick-oxide film resides on bare Pt. It is also demonstrated that the quasi-2-d oxide resides between Pt and the thick-oxide film.

In earlier results, it was noticed, but not explained, that the oxide growth rate increased drastically (400×) once an oxide film having a reduction charge of ca. 1800 $\mu C\ cm^{-2}$ had been formed. Here it is demonstrated that the formation of two monolayers of "PtO" (880 $\mu C\ cm^{-2}$) and one monolayer of "PtO_2" (another 880 $\mu C\ cm^{-2}$) on top of it, is a slow process. However, once it has been completed, the oxide growth rate significantly increases. It is suggested that formation of the first monolayer of "PtO_2" is essential for the oxide growth rate to undergo drastic increase.

Preliminary ESCA measurements confirmed some earlier data indicating that Pt in the oxide films exists in two oxidation states: +II in the quasi-2-d oxide; and +IV in the thick oxide film. SEM EDX mapping analysis results suggest that the oxide film thickness varies amongst grains which, presumably, have different crystallographic orientations. This implies that the oxide growth rate depends on the crystallographic orientation of the underlying metal surface.

In order to clarify this matter, oxide films had to be grown at single-crystal Pt faces. For this purpose, it became necessary to investigate the characterization of single-crystal Pt electrodes, since the early results on both Pt(111) and Pt(100) surfaces were substantially at variance. The Pt(111) and Pt(100) electrodes were pretreated using

several thermal and/or electrochemical procedures. These experiments led to reproduction of the results of Hubbard and of Clavilier, respectively, depending on conditions. Apart from this, it was demonstrated that, for Pt(111), the H UPD cyclic-voltammetry (C-V) profiles depend on the thermal pretreatment history, e.g. quenching after heating to high temperatures, which leads, respectively, to distinguishable C-V profiles characteristic of each heating-quenching procedure. Moreover, the H UPD C-V profile, characteristic of "quenched" Pt(111), becomes the same as that for annealed Pt(111) by cycling up to 1.40 V, RHE. Interestingly, both the "quenched" and annealed Pt(111) have the same H UPD accommodation.

A similar result was found for Pt(100) which reveals different H UPD C-V profiles after various thermal and/or electrochemical pretreatments. The charge $Q_{H\ UPD}$ at annealed Pt(100) is found to be ca. 33% greater than that for the "ideal" (100)-(1×1) surface. This is explained in terms of surface reconstruction from the unstable (100)-(1×1) structure to the stable (100)-(2×1) "missing row" arrangement. Surprisingly, Pt(100) heated at 800°C and quenched, has an H UPD charge close to the calculated value for the (100)-(1×1) structure. It is suggested that the heating-quenching procedure results in metastable surface structures due to the induction of stresses in the surface region which, though close to the "ideal" (1×1) structure, contains small atomic displacements. These displacements might be of the order of 0.1-0.2 Å, i.e. close to the limit of LEED sensitivity. In such a case, the possible metastable surfaces with their displacements could be detected only by a more sensitive technique such as RHEED with use of grazing angles of incident and emergent beams. It is proposed that these metastable surfaces, with their small displacements, are responsible for the complex character of the H UPD C-V profiles both at Pt(111) and Pt(100) surfaces. It is also suggested that HSO_4^- adsorption at "quenched" (111) surfaces is greater due to small atomic displacements.

Cycling of "quenched" Pt(111) and Pt(100) into the oxide region results in surface restructuring (probably enhanced by the stress from quenching). Such pretreated Pt(111)

and Pt(100) surfaces exhibit the same electrochemical behaviours as those of annealed Pt(111) and Pt(100).

Having established and characterized the surface structural changes of the Pt(111) and Pt(100) surfaces (inferred from changes of C-V profiles), the oxide growth rates at Pt(111) and Pt(100) were investigated. One of the most interesting observations was that cycling to 1.80 V, RHE, and holding at this potential for up to 1000 s, did not result in any further significant surface restructuring.

The rate of oxide growth at Pt(100) was found to be greater than that at Pt(111) or Pt(poly). This is explained on account of different coordination numbers of Pt atoms within the (100) and (111) surfaces, which are 8 and 9 respectively. This corresponds to the place-exchange process being faster on the (100), less coordinated, surface than on the (111). The oxide growth rate at polycrystalline Pt is similar to that on Pt(111), indicating that the polycrystalline surface of Pt is comprised mainly of grains having the (111) orientation.

Studies of oxide growth at Pt(111), Pt(100) and Pt(poly) show that: (a) Q_{ox} vs log t_h plots are linear, i.e. a direct logarithmic growth law applies; (b) the slopes of the Q_{ox} vs log t_h plots are potential-dependent; and (c) Q_{ox} vs log t_h plots pass through the monolayer level of OH or O without any inflection or changes in the slopes indicating that the growth process is not directly coverage-dependent and that there is no change in the oxide growth mechanism through monolayer coverage. Contrary to some earlier observations, the Q_{ox} vs log t_h plots do not exhibit any "common intercept". This observation impairs the "nucleation-and-growth" mechanism previously proposed for early stages of oxide formation at Pt.

Publications and Conference Presentations

Some of the work described in this thesis has already been published or submitted for publication, and other papers are in preparation, as follows:

1. "Independence of Formation and Reduction of Monolayer Surface Oxide on Pt from Presence of Thicker Phase-Oxide Layers", B.E. Conway, G. Tremiliosi-Filho and G. Jerkiewicz, *J. Electroanal. Chem.* **297** (1991) 435.
2. "Time-Evolution of Structures of Annealed and Quenched Pt(111) Electrode Surface upon Potential Cycling", G. Jerkiewicz and B.E. Conway, *Journal de Chimie Physique*, in press.
3. "Characterization of the Sequence of States of Oxide Films Formed by Strong Anodic Polarization at Pt", G. Tremiliosi-Filho, G. Jerkiewicz and B.E. Conway, to be submitted.
4. "Investigation of the Oxide Growth at Pt(111) and Pt(100) Single-Crystal Electrodes by Anodic Polarization between 0.9 and 1.8 V", B.E. Conway and G. Jerkiewicz, in preparation.
5. "Characterization of Surface Structural Changes of Pt(111) and Pt(100) by Cyclic-Voltammetry Technique as a Result of Various Thermal and/or Electrochemical Pretreatments", B.E. Conway and G. Jerkiewicz, in preparation.

During the course of research, the work described in this thesis, and some other work, was presented at various conferences and symposia as follows:

1. B.E. Conway, T.C. Liu and G. Jerkiewicz, the Faraday Discussion on Catalysis by Well Characterized Material, University of Liverpool, April 1989.
2. G. Tremiliosi-Filho, G. Jerkiewicz and B.E. Conway, the Montreal Meeting of the Electrochemical Society, May 1990.
3. B.E. Conway, J. Wojtowicz and G. Jerkiewicz, the Ottawa Meeting of the Electrochemical Society, Canadian Section, November 1990.
4. G. Jerkiewicz and B.E. Conway, the Washington Meeting of the Electrochemical Society, May 1991.
5. B.E. Conway, J. Wojtowicz and G. Jerkiewicz, the Montreal Hydrogen Energy Symposium, May 1991.

Acknowledgments

I wish to express my sincere gratitude to Prof. Brian E. Conway, my research supervisor, for his generous help, guidance and support throughout the course of this work. The research project involved not only the use of electrochemical techniques which are well-established in this laboratory, but it also required the design of new pieces of equipment and Prof. Conway was very willing to undertake this difficult task and provide much professional advice. To me, Prof. Conway is not only an outstanding scientist but also a person of very human personality, an understanding friend, ready to support his younger colleagues in the ups and downs of a professional career. I would like to express my special thanks to Dr. Conway.

I also wish to express my gratitude to Dr. Halina Angerstein-Kozlowska. Her help and "hands-on experience", from which I benefited, were enormous and resulted in the completion of very many difficult experiments. Dr. Angerstein-Kozlowska was always willing to share her incredible experience with me and I have learned a lot from her. Like Dr. Conway, she was always helpful, understanding and a great friend for "better or for worse". I thank her very much.

During the course of this research, I worked a lot with Dr. Germano Tremiliosi-Filho, my Brazilian colleague and friend, with whom I conducted many fascinating experiments and had numerous fascinating discussions. I will never forget this great time of my life.

I wish to express my sincere thanks to my other colleagues, from this research group, Dr. Teresa Wrzesniewska, Mr. John McCaffery and Mr. Qian, for stimulating discussions and sharing their experience with me.

Conducting this research would have been impossible without electrochemical cells, the vacuum-line and many other pieces of equipment built by master glass-blower, Mr. Egon Kristof and by John Hopkins, whom I thank very much for their help, devotion

and professional advice.

I am very grateful to Ms. Wilma Nuyens for the accurate typing and beautiful presentation of this thesis. I very much appreciate her dedication and help.

I wish to thank Ms. Eva Szabo for drawing many figures and diagrams in a very short period of time.

I wish to thank very much Mr. Leonard Pement and Mr. Bob Hart of the Machine Shop in the Department of Physics for their help in designing and machining very unique pieces of equipment.

I wish to thank very much the Professors, the Support Staff members and all my colleagues and other graduate students of this department, for making my stay at this University and my first years in Canada so enjoyable. Thank you all very much.

I am much indebted to the Noranda Group and Mr. Alexander Stuart of Electrolyser Inc. for supporting me during graduate studies though the Noranda/Bradfield Graduate Fellowship Program. I also thank the Ontario Ministry of Colleges and Universities, and the University of Ottawa for financial support through the course of my studies.

Above all, I am greatly indebted and thankful to my Mom and my friend Shailja for love, patience, encouragement and support throughout this work.

Table of Contents

List of Tables

List of Figures

CHAPTER 1

Introduction

1.1 General Area of the Research

In physical and materials science, boundaries between different phases (solid-gas, solid-liquid and liquid-gas) are of special significance. It is well known that an interphase, i.e. matter of finite dimensions which resides just at the interface between two phases, exhibits different physical and often chemical properties form those of either of the adjacent bulk phases. The properties of such interphases are of practical importance in areas such as chemical and electrochemical heterogeneous catalysis, corrosion, metal-passivation, and chemical and electrochemical surface science. Out of all the many types of interphases, the solid-liquid-gas one is of special interest in electrochemistry; it usually also involves electron-transfer processes, making it even more complex.

The work described in this thesis is concerned with the interface between polycrystalline or single-crystal platinum electrodes and electrolyte solutions, and between Pt and its oxide film in contact with electrolyte solutions. In particular, it deals with reversible or irreversible changes which take place within or at the surface layers of the solid phase, i.e. the Pt electrodes. Noble metals (Pt, Au, Pd, Rh, etc.) are of special interest in electrochemistry on account of their adsorptive and catalytic properties, and their resistance to corrosion by electrolytes, so that their interfaces have usually excellent stability. In most electrochemical studies of non-noble metal oxidation, fairly thick oxide films, involving several tens or a few hundreds of atomic layers are examined [1-6]. In the case of noble metals, surface oxide film formation proceeds much more slowly and even

formation of the early, sub-monolayer stages of the first oxide monolayer can be examined [7-15], while in the case of non-noble metals it is much more difficult and requires special preparation of initially oxide-free metal electrodes, as for instance has been demonstrated for Ni electrodes [16,17].

Formation of relatively thick oxide films at polycrystalline Pt has been studied in the past [18-36] but the results are substantially at variance. This is for two major reasons: (a) in most cases, the thick oxide films were grown under galvanostatic conditions, i.e. without control of the important variable, electrode potential; and (b) the thick oxide films were grown on surfaces which were not initially well established or characterized, and often required such a drastic pretreatment as roughening with emery paper.

The present work involves both qualitative and quantitative improvements because: (a) thick oxide films were grown under potentiostatic conditions which allowed differentiation of various oxide states to be made as a function of polarization potential and time; and (b) thick oxide films were grown on well-defined surfaces which provided excellent reproducibility.

Direct formation of oxide films at Pt single-crystal electrodes, by potentiostatic or galvanostatic anodization, has not been studied in the past. The results presented in this thesis on this point are therefore original and significantly contribute to the overall knowledge of oxide growth at Pt. However, since oxide growth at Pt single-crystal electrodes required their polarization beyond 0.9 V, RHE, it was necessary to characterize any consequent structural changes (by evaluating changes in the C-V profiles) and evaluate their reversibility or irreversibility.

Previous research in this laboratory on noble metal oxidation processes has been described in three earlier theses by Sharp [10], Barnett [14] and Tellefsen [44], and in papers that have resulted from those works. Since they already contain extensive reviews of the pertinent literature, the present introduction will only be brief.

1.2 Metal Oxidation Mechanisms

1.2.1 Direct Dissolution as Metal Cations

This mechanism which can be described by the formal reaction equation

$$M \rightarrow M^{z+}_{soln} + z\,e \qquad (1.1)$$

is the simplest one and is of particular importance in corrosion and battery technology, especially that involving base metals. In this process, no oxide film is formed and the metal cations are present in the solution in a solvated form and each of them "carries" its solvation shell [3,4,44-46]. This type of mechanism is characteristic for active metals, such as Zn, in acidic media, or for some metals in strong alkaline media, where soluble metallate oxyanion species can be formed. This type of reaction is typical for metals undergoing corrosion processes or for anodic electrode reactions taking place in certain batteries [3,4,47] on discharge.

1.2.2 Dissolution-Precipitation

In this mechanism, the formation of metal cations (M^{z+}), as in Eq.(1.1), is followed by the formation of an insoluble metal oxide, hydroxy-oxide or hydroxide when the solubility product of such compounds is exceeded in the diffusion boundary layer. These species precipitate at the electrode surface usually forming a barrier, e.g. for a divalent ion:

$$M^{2+}_{soln} + 2\,H_2O \rightarrow M(OH)_2\downarrow + 2\,H^+ \qquad (1.2a)$$

or

$$M^{2+}_{soln} + 2\,OH^- \rightarrow M(OH)_2\downarrow \qquad (1.2b)$$

The formation of a porous, thick oxide film is possible because the oxide or hydroxide precipitation rate proceeds much faster than the metal cations can diffuse away. The oxide (hydroxide) growth is then usually controlled by the diffusion rate of M^{2+} cations through the film [48,49]. This type of oxide film formation often occurs in alkaline solutions on metals such as Ag or Zn, and is pH dependent when the anodically formed oxide or hydroxide has amphoteric properties.

1.2.3 Direct Oxide-Film Formation

Unlike the two previously mentioned mechanisms which are bulk processes, a direct surface process may be involved in the very initial stages of oxidation of some metals, as in the case of noble metals (Pt, Au, etc.), [9-15,48] or nickel under certain conditions [16,17]. In this case, no initial dissolution step is involved. The oxygen-containing species (O or OH) are reversibly electrosorbed (electrodeposited) at the metal surface:

$$M + H_2O \rightleftharpoons M\text{-}OH_{surf} + H^+ + e \qquad (1.3)$$

Although formation of a complete monolayer of oxygen-containing species, and subsequent formation of thicker oxide films, usually involves a more complex mechanism, the process starts with this sort of electrosorption step, which is therefore fundamental for metal oxidation reactions of this type. In fact, process (1.3) is probably more complex than that written, as the very initial steps of surface oxidation of noble metals take place on a surface on which an array of chemisorbed anions, amongst oriented water dipoles, already exists [11-13].

1.3 Oxide Film Growth Mechanisms

Several different kinetic laws have been proposed to describe oxide growth on a variety of metals under various experimental conditions. Depending on the metal and the conditions employed for formation or growth of oxide films of less than a monolayer or up to a few thousand atomic layers can result. Such films may have widely different physical properties, e.g. good or bad electronic conductivity, good or bad optical reflectivity, compact or porous structures, etc.

The growth of the oxide may be described in several different ways: (a) formation charge, Q, vs time, t; (b) fractional coverage, θ, (for sub-monolayer films) vs time, t; (c) thickness, x, vs time, t; and (d) mass, m, vs time, t. Since many reviews [5,6,51-60] have already covered the subject of oxide film growth mechanisms, it is only necessary here to describe briefly some of the general laws involved. These are: (a) the "direct" logarithmic law; (b) the "inverse" logarithmic law; and (c) the "parabolic" law.

1.3.1 The Direct Logarithmic Law

When an anodically formed oxide is highly conducting, as at noble metals [7,8,19,21,29,53,61-67] and some of the base transition metals [53], the oxide growth exhibits direct logarithmic kinetics in time, i.e. the extent of oxide formation increases in proportion to log[time]. In such cases, oxide growth often proceeds through the so-called place-exchange mechanism, where the initially deposited, i.e. chemisorbed oxygen species (O or OH) are "2-dimensionally" exchanged with surface metal atoms [48,68,69]. The direct logarithmic kinetics, originally treated by Tammann [70], arise formally whenever it can be postulated that the free energy of activation, $\Delta^{\ddagger}G$, for the oxide growth increases linearly with oxide thickness, x, i.e.

$$\Delta^{\ddagger}G = \Delta^{\ddagger}G^{\circ} + b\,x \qquad (1.4)$$

where b is a constant. Since the rate is proportional to the exponential of $\Delta^{\ddagger}G$, the resulting integrated rate law is:

$$x = k \ln t + k' \tag{1.5}$$

where k and k' are constants and t is time.

1.3.2 The Inverse Logarithmic Law

When an oxide film, formed either anodically or by atmospheric oxidation, is an insulator, then the oxide growth exhibits inverse logarithmic kinetics in time. This law applies to the valve metals (Al, Ti, Ta, Nb, etc.) at which thick, insulating oxide films are formed [5,53,57]. The inverse logarithmic kinetics, originally treated by Cabrera and Mott [51,71,72] and later modified by Ghez [73], assumes that the oxide film grows by injection of metal ions (generated at the metal/metal oxide interface) into interstitial positions in the growing oxide, followed by their transport through the oxide layer, assisted by the influence of the field across the film. Since the oxide film is more or less an insulator, a high-field arises across the film (this is the origin of the term Mott-Cabrera "high-field" mechanism) of many hundreds of V per cm.

The integrated form of this law is:

$$1/x = k' - k \ln t \tag{1.6}$$

where k and k' are constants and t is again time.

Experimentally, it is not easy to distinguish the applicability of this law to experimental results from that of the "direct" law, unless accurate measurements are available over 4 ~ 5 decades of time.

1.3.3 The Parabolic Law

The parabolic oxide growth law is found where field-assisted diffusion of ions through the film determines the rate of oxide growth [48,54]. The integrated form of this law is:

$$x = k\, t^{\frac{1}{2}} + k' \tag{1.7}$$

where k and k' are constants and t is time. In the case of this and other mechanisms, if the potential difference between the metal and the solution is constant, then the field diminishes due to the increasing oxide film thickness.

1.4 Experimental Methods for the Study of Metal Electrode Surfaces and Electrochemical Surface Process

1.4.1 Cyclic-Voltammetry

The cyclic-voltammetry technique, though relatively simple, has become increasingly useful in electrochemical studies, especially for electrode surface reactions. Information about electrode processes is gained from the i vs E profiles, colloquially called cyclic-voltammograms or C-V profiles [74-80], which arise in response to a linearly varying potential in time, applied to the electrode under investigation.

In cyclic-voltammetry, the potential, E, of the working electrode is changed linearly with time, t, at a constant sweep-rate, s ($V\ s^{-1}$), according to the equation

$$E = E_i + s\, t \tag{1.8}$$

or

$$dE/dt = s \tag{1.9}$$

where E_i is some initial potential that may or may not be held constant for some period of time. The method may employ either a single sweep (half-cycle) between the initial potential, E_i, and the final potential, E_f, or it may be programmed to give a repetitive response of the electrode by varying the potential between E_i and E_f, forward and backward, in a continuous manner (Fig. 1.1).

The information obtained from this technique (Fig. 1.1 shows a typical i vs E profile for a reversible surface process) includes the behaviour and characteristics of the electrochemical process involved, indication of any complicating side-reactions such as "pre-electrochemical" or "post-electrochemical" chemical reactions (such as place-exchange in oxide film formation), and general kinetic behaviour such as slowness of charge-transfer steps or the development of limiting currents due to "pre-electrochemical" chemical steps such as molecular dissociation, chemisorption, isomerization or ionization.

The standard electrical circuitry required for this technique has been shown in refs. 78-81.

The cyclic-voltammetry technique is very useful in electrochemical studies due to its high resolution and sensitivity. It is able to: (a) determine surface coverage down to 5% of a monolayer ($\theta = 0.05$); (b) resolve states which differ only 10 mV i.e. ca. 965 J (230 cal) of Gibbs energy; and (c) characterize time effects down to the 10 μs level.

The current response to the applied potential, E, i.e. the current recorded, may be represented as the first derivative of charge with respect to time:

$$i = \frac{dq}{dt} = \frac{dq}{dE} \cdot \frac{dE}{dt} \qquad (1.10)$$

Since $\frac{dq}{dt} = C$ (capacitance) and $\frac{dE}{dt} = s$ (sweep rate), the current response may be represented by the following formula:

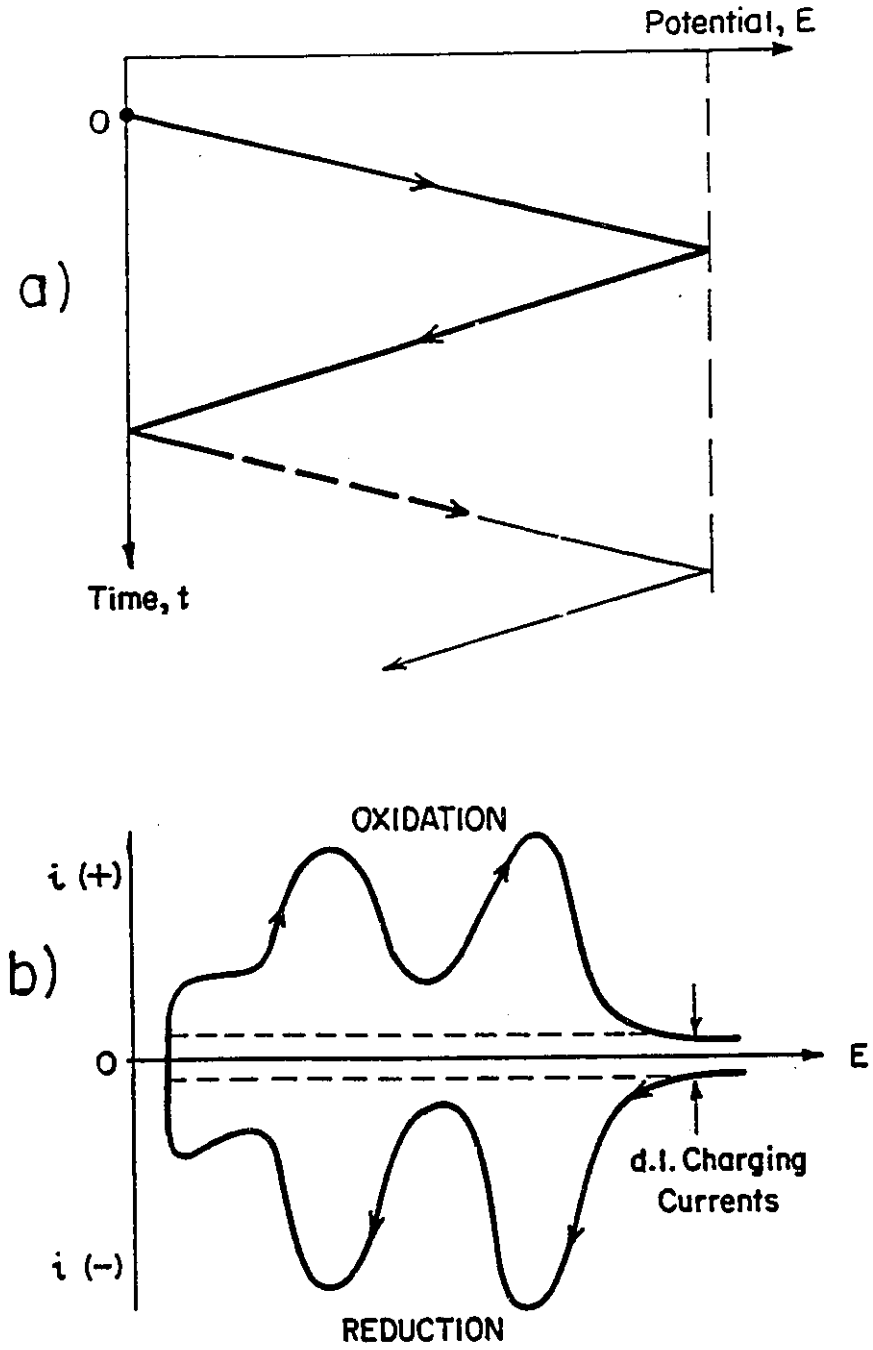

Fig. 1.1 (a) Schematic diagram of the cyclic potential sweep;
(b) Resulting cyclic-voltammogram for a reversible process.

$$i = C \cdot s \tag{1.11}$$

It is possible to calculate the total charge passed between two potential limits E_1 and E_2, by rearranging the equation (1.10) to

$$dq = i\,dt \tag{1.12}$$

Integration between the two potential limits allows us to determine the charge, q, according to the equations

$$q = \int_{E_1}^{E_2} dq = q(E_2) - q(E_1) \tag{1.13}$$

$$q = \int_{E_1}^{E_2} i\,dt = \int_{E_1}^{E_2} \frac{i}{s}\,dE = \int_{E_1}^{E_2} C\,dE \tag{1.14}$$

where C can be a function of potential, C = f(E).

For surface processes, small coverages may be determined using the formula

$$dq = q_1 d\theta \tag{1.15}$$

where q_1 is the charge required to form <u>one</u> monolayer of the adsorbed species.

<u>Process Reversibility or Irreversibility</u>

Amongst the kind of information available from the analysis of C-V profiles, that regarding <u>reversibility</u> or <u>irreversibility</u> of electrode processes seems to be the most fundamental. Fig. 1.2 shows four schematic diagrams of the principal types of i <u>vs</u> E

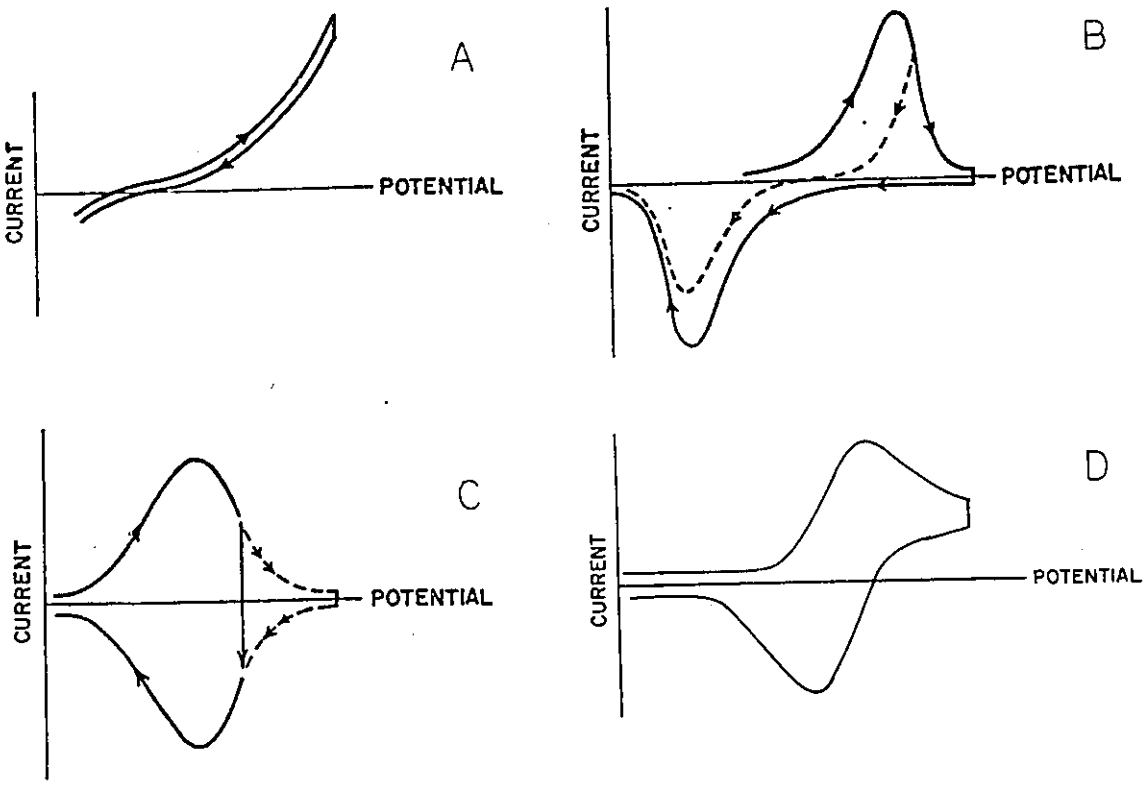

Fig. 1.2 Schematic diagrams of four principal types of i vs E profiles observable in cyclic-voltammetry: (a) irreversible Faradaic process not involving a surface species; (b) irreversible Faradaic process involving only electrodeposition and electrodesorption of a surface species; (c) reversible Faradaic process involving only a surface species; and (d) reversible Faradaic process under diffusion control.

profiles observable in cyclic-voltammetry. A typical and representative C-V profile is that for polycrystalline Pt between 0.05 and 1.40 V, RHE (Fig. 1.3). Here, the cathodic and anodic current profiles between 0.05 and 0.38 V, RHE, correspond to the reversible H underpotential adsorption and desorption of H which is found to be almost reversible in the absence of competitive effects due to anion chemisorption, while those between 0.85 and 1.40 V, RHE, represent the irreversible adsorption and desorption of OH and O species [9]. This profile is essential for understanding the general form of the i vs E profiles at Pt and other metals which undergo irreversible formation and reduction of a surface oxide layer.

Sweep-rate Dependence of Current : Diffusion Control

The electrode reaction rate (expressed as a current-density) is normally either under activation control (i.e. the reaction kinetics are determined by the rate of formation of activated complexes) or diffusion control.

For an electrochemical reaction

$$Ox + z\,e \rightleftharpoons Red \tag{1.16}$$

having a sufficiently large rate constant, and/or at sufficiently low reagent concentration, the process may be diffusion-controlled, with a concentration gradient developed normal to the electrode surface where the reagent is consumed. This process may be either reversible or irreversible. The activities (or concentrations) of oxidized, [Ox], and reduced, [Red], species at the electrode surface are related to potential by the Nernst equation:

$$E = E^{\circ} + (RT/zF) \ln [Ox]/[Red] \tag{1.17}$$

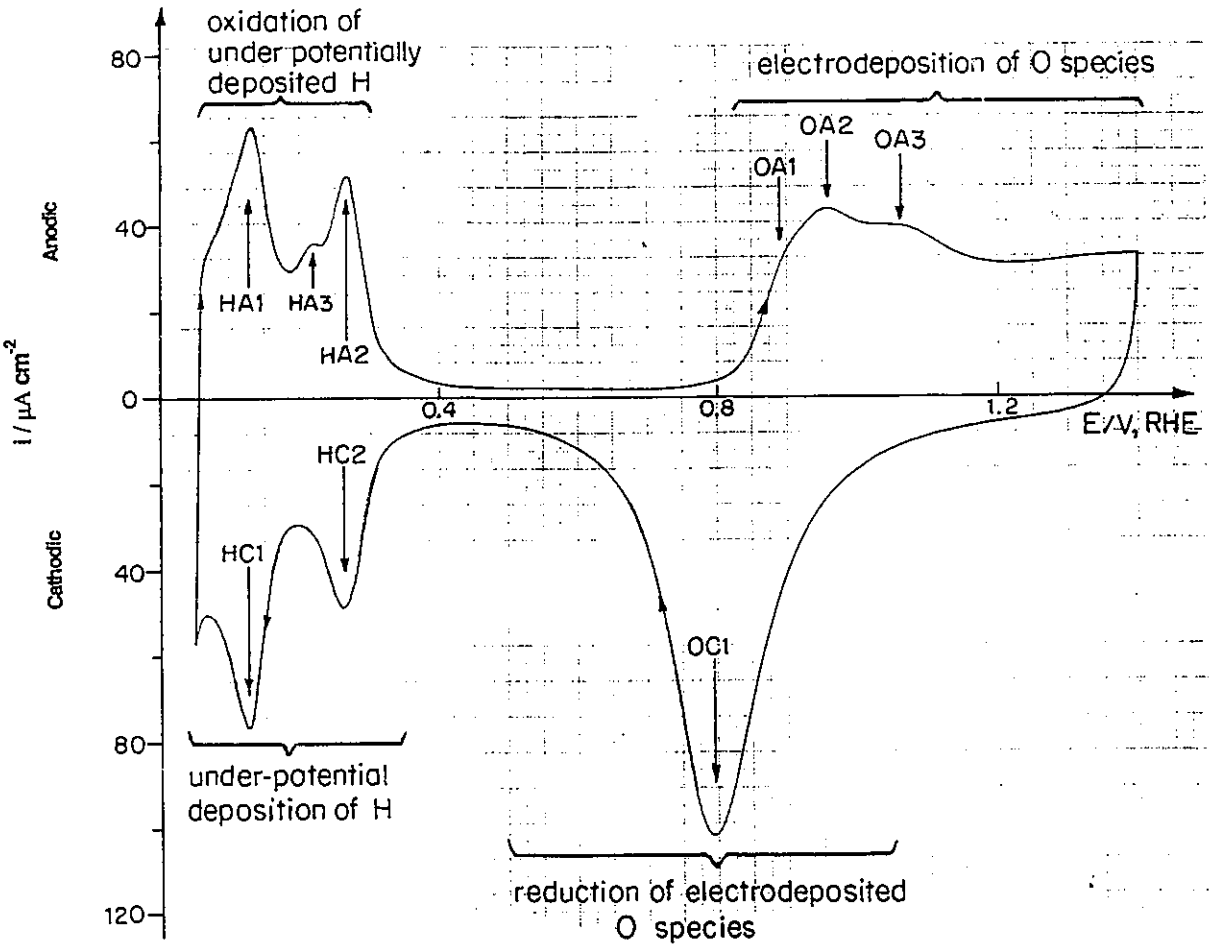

Fig. 1.3 Typical potentiodynamic i vs E profile for Pt at 0.050 V s^{-1} in 0.5 M aq. H_2SO_4 solution [9].

where E° is the standard reversible potential.

Various researchers [75,82-86] have solved the Fick equations for cyclic-voltammetry where the kinetics are under diffusion control. For such conditions, the peak current, i_p, varies linearly with the square-root of the sweep rate, $s^{\frac{1}{2}}$, both for reversible and irreversible processes, according to the equations:

$$i_p = (2.69 \times 10^5)\ z^{3/2} D^{\frac{1}{2}}\ c\ A\ s^{\frac{1}{2}} \quad \text{(reversible)} \tag{1.18}$$

$$i_p = (2.99 \times 10^5)(z\alpha)^{\frac{1}{2}}\ z\ c\ A\ (D\ s)^{\frac{1}{2}} \quad \text{(irreversible)} \tag{1.19}$$

where A is the electrode area (cm^2), D is the diffusion coefficient ($cm^2 s^{-1}$), c is the concentration (mol cm^{-3}), s is the sweep-rate ($V\ s^{-1}$), z is the number of electrons transferred, and α is the transfer coefficient in the irreversible case.

Under diffusion-controlled conditions, the following quantitative characteristics of the i vs E profiles are to be noted:

(a) The difference between anodic and cathodic peak potentials at 298 K is:

$$\Delta E_p = E_{p,c} - E_{p,a} = 2 \times (0.028/z) \tag{1.20}$$

(b) The difference between peak potential and the half-wave potential, $E_{\frac{1}{2}}$, is:

$$E_p - E_{\frac{1}{2}} = -1.1 \times (RT/zF) \tag{1.21}$$

Peak Potential and Peak Current for Surface Process Control

For the case of surface reactions, no mass transfer processes are involved in the kinetics so the current response behaviour to a potential sweep is simpler than for the diffusion-control case. A simple one-electron surface reaction, not influenced by

diffusion, may be represented by the reaction:

$$\underset{1-\theta_A \quad c_A}{M + A^{\pm}} \underset{k_{-1}}{\overset{k_1}{\rightleftharpoons}} \underset{\theta_A}{MA_{ads}} \mp \underset{E}{e} \qquad (1.22)$$

If the reaction is reversible and potential-dependent, then the current can be written as:

$$i = q_1[k_1 c_A(1-\theta_A)\exp(\beta\eta F/RT) - k_{-1} c_A \theta_A \exp(-(1-\beta)\eta F/RT)] \qquad (1.23)$$

where q_1 is the charge required to form a monolayer of species A, k_1 and k_{-1} are the standard rate constants at the reversible potential, η is the overpotential, c_A is the concentration of species A in the solution and β is the barrier symmetry factor. The Gibbs energy of activation is potential-dependent corresponding to the usual Butler-Volmer factor $\exp(\beta\eta F/RT)$, i.e. the Tafel exponent in the rate-equation for the current-density. For a reversible process, the exponential components of the above equation are comparable while for an irreversible process the first component is much greater than the second one ($k_1 >> k_{-1}$), or vice versa.

Srinivasan and Gileadi [87] have derived equations which relate current to potential as a function of sweep-rate for a simple surface process of the above kind.

For a reversible adsorption process, the peak current and potential are given by the equations:

$$i_p = (q_1 F/4RT)\, s \qquad (1.24)$$

$$E_p = (-RT/F) \ln K_1 \qquad (1.25)$$

For an irreversible process, i.e. $k_1 >> k_{-1}$,

$$i_p = 1/e\ (q_1\beta F/RT)\ s \tag{1.26}$$

$$E_p = (RT/\beta F)[\ln s + q_1\beta F/k_1 RT] \tag{1.27}$$

1.4.2 Kinetic Aspects of Electrode Processes: Tafel Plots

In general, the reaction velocity, v, of an electrochemical process having a rate-controlling discharge step can be expressed by the equation:

$$i = zFv = k_i nF\ c_R(1-\theta) \tag{1.28}$$

where the electrochemical rate constant, k_i, is given by

$$k_i = \tau(kT/h)\exp(-\Delta^{\ddagger}G°/RT) \tag{1.29}$$

and τ is the transmission coefficient (τ=1), k Boltzmann's constant, T the temperature, h Planck's constant, $\Delta^{\ddagger}G°$ the standard electrochemical Gibbs energy of activation for hypothetical zero metal/solution potential difference or the related value for the standard reversible potential of the process, zF the number of Coulombs involved, c_R is the reactant concentration at the outer Helmholtz plane and θ is the steady-state coverage of intermediates or products adsorbed at the electrode. The electrochemical Gibbs energy of activation is potential-dependent according to the formula:

$$\Delta^{\ddagger}\bar{G}°(E) = \Delta^{\ddagger}G°(E=0) \pm \beta FE \tag{1.30}$$

where β is again the barrier symmetry coefficient, $\Delta^{\ddagger}G°$ is the standard chemical Gibbs energy of activation at hypothetical E=0, and E represents the metal/solution potential difference expressed by

$$E = E_o + \eta \tag{1.31}$$

where E_o is the reversible potential and η is the overpotential [77,79,88]. For $E = E_o$, $\Delta^{\ddagger}\bar{G}\,(E_o)$ is the standard Gibbs energy of activation for the process, corresponding to its "standard rate constant".

For a simple discharge process, the above equations may be combined to give a general expression for the net-current-density, i, in the form of the so-called Butler-Volmer [79,88-92] equation which takes into account both the backward and forward components of the current-density (cf. eqn. 1.23):

$$i = i_f + i_b \tag{1.32}$$

$$i = zF[(1-\theta)k_f\, c_{ox}\exp(-\beta\eta F/RT) - k_b\, c_{red}\theta\, \exp((1-\beta)\eta F/RT)] \tag{1.33}$$

where c_{ox}, c_{red} are the respective concentrations of the oxidized and reduced species; k_f and k_b are the corresponding rate constants and θ is the surface coverage. At <u>high</u> values of (negative) overpotential, η, the first term of the above equation is much greater than the second one and the current-density, i, is:

$$i = i_o \exp(-\beta\eta F/RT) \tag{1.34}$$

or, explicitly in terms of η:

$$\eta = (RT/\beta F)\ln i_o - (RT/\beta F)\ln i \equiv (RT/\beta F)\ln[i_o/i]. \tag{1.35}$$

This is a form of the well-known Tafel equation [93]

$$\eta = a + b \log i \tag{1.36}$$

where a and b are seen, from eqn.(1.26), to be given by the equations

$$a = -2.303(RT/\beta F)\log i_o; \quad b = 2.303(RT/\beta F) \tag{1.37}$$

At low values of overpotential, η, the first and second terms are comparable and then linearization of the exponential terms gives:

$$i = i_o (\eta F/RT) \tag{1.38}$$

which allows a Faradaic charge-transfer resistance, R_F, to be defined as

$$R_F = RT/i_o F \tag{1.39}$$

by means of Ohm's law.

The Tafel slope, b, and the exchange current-density, i_o, are the two fundamental parameters characterizing steady-state electrochemical polarization behaviour of an electrode reaction.

Ideal kinetic behaviour for optimizing anodic and cathodic reaction rates in electrocatalysis requires a combination of high i_o and low b values. However, this is not always possible since i_o and b for a given multistep process are often mutually dependent quantities, e.g. both are closely related to the adsorption behaviour of the reaction intermediates adsorbed on the electrode surface. These kinetically-involved intermediates influence the exchange current-density of the process through their standard Gibbs energy of adsorption, and the Tafel slope through the potential-dependence of their coverage.

Treatment of Consecutive and Alternative Processes

Most electrochemical reactions, except perhaps one-electron ionic redox reactions, proceed by at least two steps. In such multistep processes, it is common to observe more than one Tafel slope, since a step which is rate-controlling at one potential, may not be the kinetically limiting step at another potential [79,88,94,95]. In consecutive reactions, it is always the step with the smallest rate constant that is rate-determining. For consecutive rate-determining reaction steps, a lower Tafel slope at low current-densities followed by a higher b value at larger current-densities will be observed. An opposite sequence of the Tafel slope values arises for alternative reactions. In this case, it is the path which proceeds with the greatest velocity that characterizes the kinetics in alternative rate-determining pathways (Fig. 1.4).

1.5 Characterization of Single Crystals: The von Laue X-ray Back Reflection Technique

The von Laue method is the oldest of the X-ray diffraction methods (1912). A collimated beam of continuous spectrum falls upon a fixed single crystal. For each set of planes (hkl), the spacing d(hkl) and the Bragg angle θ(hkl) are fixed. A reflected beam will be produced if the correct wavelength which satisfies the Bragg Law is contained in the continuous spectrum:

$$n\lambda = 2\, d(hkl) \sin\alpha; \qquad n = 1, 2, 3 \ldots \tag{1.40}$$

where α is the incident angle. The different reflected beams have different wavelengths and hence a Laue pattern is "coloured" [96-99].

The back-reflection Laue pattern is much used today for the orientation of single

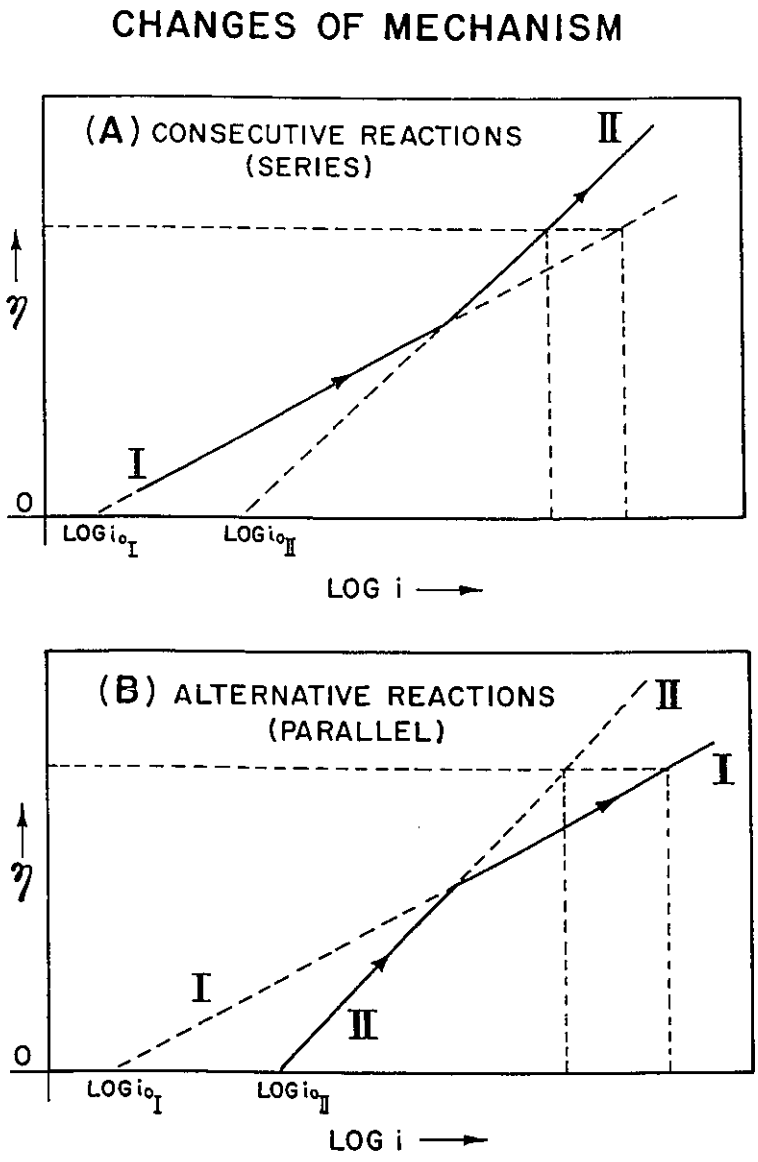

Fig. 1.4 Current-potential relaxation for consecutive and alternative electrode processes with exchange currents $i_{o,I}$ and $i_{o,II}$ and Tafel slopes b_1 and b_2. In (A), reaction I is slower than II, but its rate is more potential-dependent than that of II. II becomes rate-determining at high potentials even though $i_{o,II} > i_{o,I}$. In (B), if I and II are alternative, I passes more current than II even though $i_{o,I} < i_{o,II}$. (After refs. 79,94,95).

crystals, particularly for the orientation of single cubic crystals. Fig. 1.5 illustrates a schematic diagram of the back-reflection Laue camera. The interpretation of the back-reflection Laue pattern is greatly facilitated by the use of the Greninger chart [100]. Since the interpretation of back-reflection Laue patterns is a complex operation and consists of many steps, it will not be discussed further here, especially since the interpretation procedure is well explained in the literature devoted to X-ray diffraction [96-99]. However, it is worthwhile mentioning that to interpret a cubic pattern, one looks for the three most important spots on the pattern. These will be the low-index reflections (100), (110) or (111), and they will be characterized by the fact that they are quite black, that there is an appreciable open space around them, and that they arise at the intersections of several prominent zone lines.

1.6 Scanning Electron Microscopy and Electron Channelling Patterns

Scanning electron microscopy (SEM) provides the most informative procedure for the direct observation of the external form or surface morphology of solid-state objects. This technique, which combines large magnification and good resolution, can be used to analyse the quality of Pt polycrystalline and single-crystal electrodes. It is particularly useful in evaluating the quality of Pt single-crystal electrodes after mechanical polishing and annealing [101,102].

The Semco Nanolab 7 scanning electron microscope used for the experiments described in this thesis was also equipped with a backscattered electron detector. The backscattered electrons are considered to be electrons from the primary beam which have interacted with atoms in the specimen and have been turned back out of the specimen again. The backscattering takes place within the layers of the specimen down to ca 100 Å. The backscattered electrons form patterns characteristic of different principal

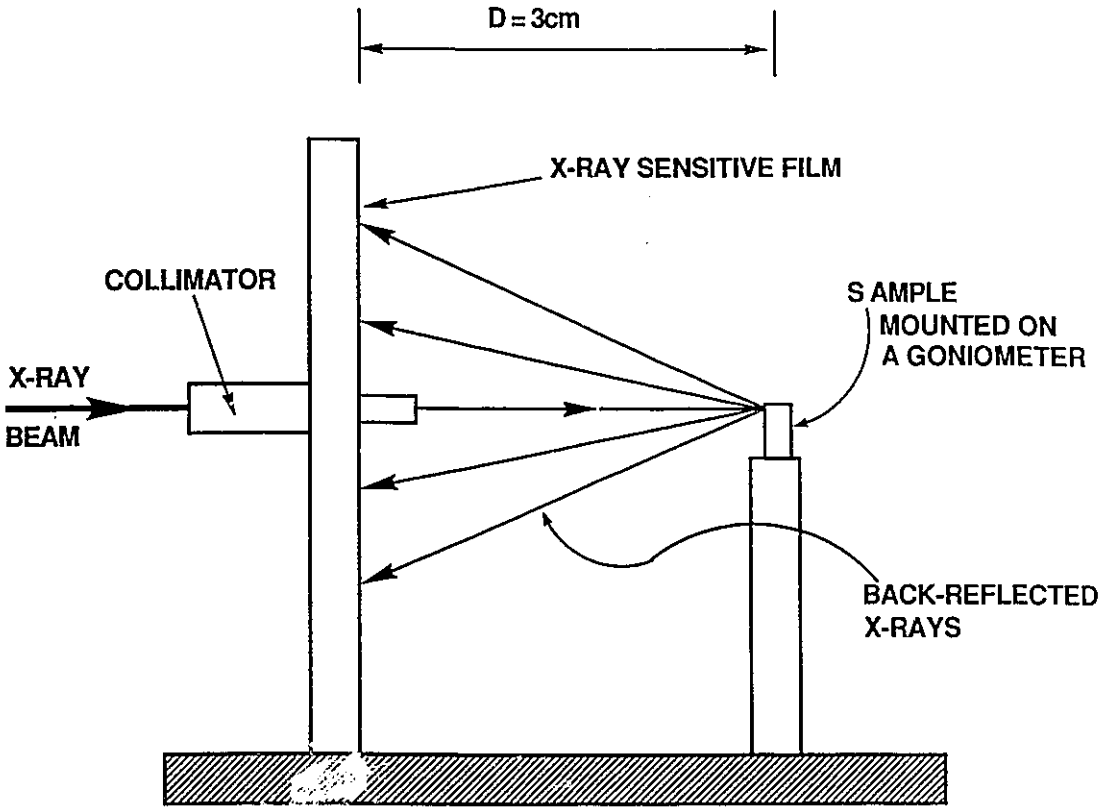

Fig. 1.5 Schematic diagram of an X-ray back-reflection camera.

crystallographic orientations of the metal sample (Fig. 1.6). Since this technique requires the specimen to be smooth and free from surface damage, such as a disturbed layer, it provides a good measure of the quality of single-crystal electrodes. Moreover, since the penetration of X-rays is a few hundreds of Å, the channelling patterns provide supplemental information about metal single crystals. However, this method is not sensitive enough to distinguish the first few surface layers from those lower in the bulk and therefore cannot provide any information about rearrangements in surface monolayers of the metal single-crystal sample. For that purpose, the techniques of LEED and preferably RHEED are required.

The recently developed technique of scanning tunnelling microscopy is capable of providing images which can clearly reveal such surface features as steps, terraces, etc. This technique is increasingly becoming applicable for surface science studies, as was shown by Somarjai and Van Hove [196].

1.7 Electron Spectroscopy for Chemical Analysis

Electron spectroscopy for chemical analysis (ESCA), developed by Seigbahn and co-workers [103], is a very powerful technique for the study of solid surfaces within the outermost 100 Å. This technique is based on the photoelectric effect in which an X-ray beam (each photon carries the hν quantum of energy) strikes atoms in the solid surface, ejecting electrons, called photoelectrons, each one carrying E_k amount of energy:

$$E_k = h\nu - E_b \tag{1.41}$$

where E_b is the binding energy in a given atomic level. Since each atom has a unique set of available energy levels, either in the state of a compound or a pure element, it may be

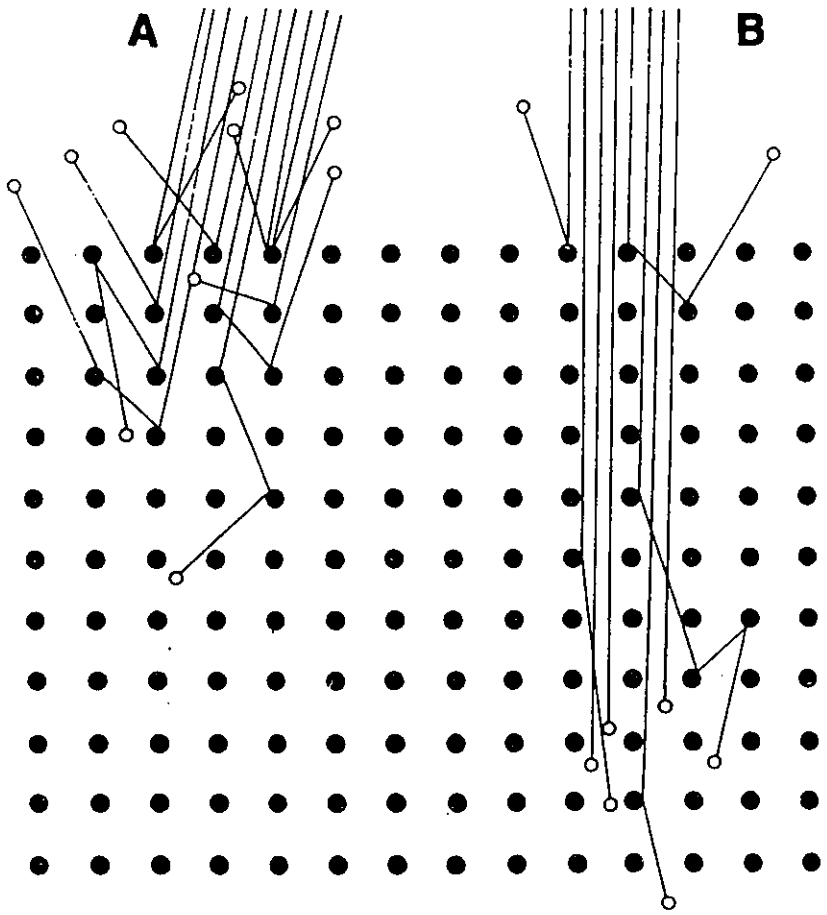

Fig. 1.6 Schematic representation of a crystal lattice. Two different beam-crystal orientations are indicated, demonstrating (A) a nonchannelling and (B) a channelling situation.

identified by the energy of the ejected electrons. Fig. 1.7 shows a schematic diagram of an arrangement used in an ESCA instrument. The technique requires rather sophisticated instrumentation to obtain adequate energy resolution; it uses characteristic X-ray radiation as the primary exciting beam and a high resolution electron spectrometer for analysis of the energies of emitted electrons. A notable feature of the type of spectrum obtained is the sharpness of the emission peaks. This is due primarily to the fact that the major energy loss process experienced by the escaping photoelectons is that of plasmon excitation which requires energy increments ≥ 10 eV. For maximum ionization efficiency the primary energy should be about three times the ionization energy; then the ejected photoelectrons under these conditions have energies of about $2E_b$, E_b being the binding energy [103-106].

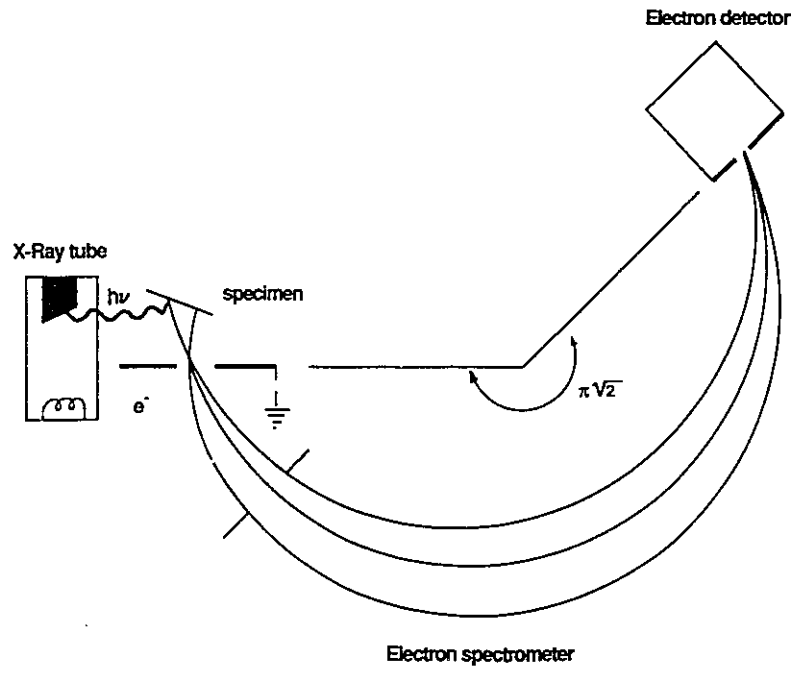

Fig. 1.7 Schematic view of an arrangement used in ESCA for the analysis of electrons ejected by X-rays.

1.8 Reflection High-Energy Electron Diffraction

Reflection high-energy electron diffraction (RHEED) differs form low-energy electron diffraction (LEED) in the range of energies used. While in LEED, "low" energies of about 10 to 500 eV are used, in RHEED "high" energies of about 5 to 50 keV are used. At higher energies, the mean free path increases from ca 20 to 100 Å and thus impairs the surface sensitivity on the atomic scale unless grazing angles of incidence and emergence are used.

Grazing angles of incidence put stronger requirements on the atomic scale planarity of the surface than the roughly perpendicular incidence directions used in LEED. Therefore RHEED samples the near-surface layers [105-109]. The penetration of high-energy electrons into the crystal in the direction of the normal is of the same order of magnitude as in a typical LEED experiment. This can be understood by noting that for an electron of energy 30 keV, incident at a glancing angle of about 3°, the component of its momentum normal to the surface is about the same as that for a 100 eV electron at normal incidence. However, because of the glancing angle used in RHEED, the diffracted beams are extremely sensitive to surface topography. This sensitivity is advantageous in studying such phenomena as the nucleation of oxides, epitaxial growth and faceting of surfaces, and, in fact, it is possible to obtain information on the morphology of surface nuclei at very small total coverages. With LEED, the long-range periodicity of positions of adsorbed atoms/molecules can be determined by examining a single diffraction pattern, while with RHEED it is generally necessary to examine at least two diffraction patterns obtained with the beam directed along different directions in the surface. Fig. 1.8 shows a diagram of the experimental arrangement in a RHEED apparatus and, as an example, RHEED patterns for Mo single-crystal faces [105].

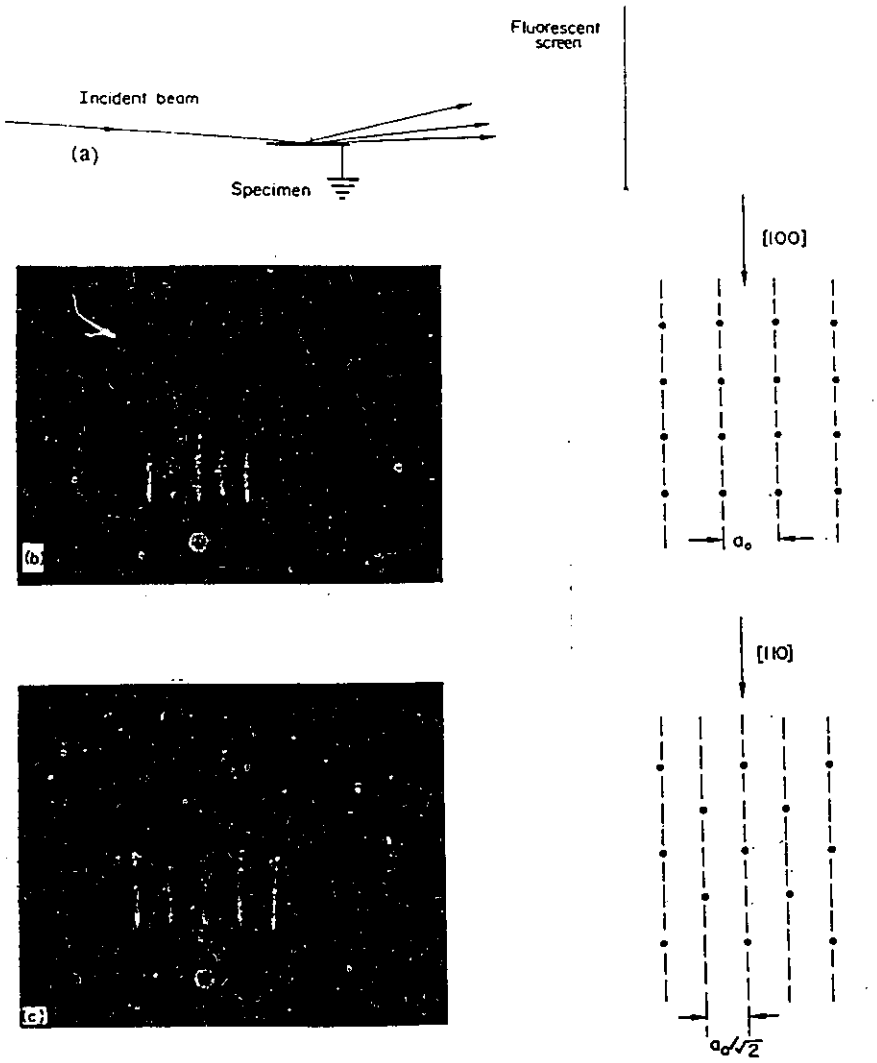

Fig. 1.8 (a) Diagram of the experimental arrangement in a reflection high energy electron diffraction (RHEED) apparatus. The primary energy is generally ~ 30 keV; (b) RHEED pattern of a (001) surface of molybdenum with the incident beam parallel to [100] (referred to as the [110] azimuth); (c) Corresponding pattern for the [11] azimuth. Note the reciprocal relationship between spacing of diffracted beams and inter-row spacing on the surface [105].

1.9 Electrochemical Surface Processes Involving Monolayer Deposition and Dissolution

Modern electrochemical surface science involves study of the deposition and dissolution of monolayers of species such as H, metal atoms, and OH and O species at noble metals. The species involved are often intermediates in some overall multistep electrode reactions such as H_2 and O_2 evolution, and metal crystal-phase formation etc. Since these species are deposited below (under) the reversible potential above which significant current-densities arise (due to bulk H_2 or O_2 evolution, or bulk metal deposition), they are called under-potential-deposited species (UPD).

Formally, the thermodynamic condition for UPD of a species A on a metal substrate M is the following, in terms of the Gibbs energies:

$$G_{AM} < G_{AA} \tag{1.42}$$

where AM represents electrochemisorption of A on M (bond free energy of AM) and AA the homonuclear species corresponding to the bulk phase of A. That is, bond formation of A to M is preferred to A with A which arises only above the reversible potential for bulk "A" formation.

Many electrochemical reactions occur in more than one step, thus giving rise to adsorbed intermediates which then undergo further chemical or electrochemical reactions leading to product formation. In most electrochemical processes where adsorbed intermediates are formed, the potential plays a characteristic role in addition to the reactant concentration and temperature in determining the surface coverage of an intermediate [10,79]. It should be mentioned that the intermediates in consecutive processes are not normally in the same state as the UPD species though they may be chemically identical but not necessarily in a charge distribution.

1.9.1 Electrochemical Langmuir Isotherm

The Langmuir isotherm is the simplest case and is based on the following assumptions:

(a) the Gibbs energy of adsorption of adsorbate species is potential dependent;

(b) the coverage (θ) of the species, in going from a bare substrate surface to one with full monolayer coverage, is potential dependent in a well-defined manner, determined by (a) above;

(c) the Gibbs energy of the adsorbed layer depends only on some configurational function of the occupied and vacant sites, and does not involve lateral interaction effects [110-113].

In the case of electrochemical adsorption of a species B arising by charge transfer from a reactant A in solution according to the process:

$$\underset{1-\theta_B}{M} + \underset{C_A}{A^{\pm}} \overset{K_1}{\rightleftharpoons} \underset{\theta_B}{MB} \mp E \qquad (1.43)$$

where A is a $\pm$ charged species, the Langmuir adsorption isotherm has the following form:

$$\frac{\theta_B}{1 - \theta_B} = K_1 c_A \exp\left(\frac{\Delta EF}{RT}\right) \qquad (1.44)$$

where ΔE is the difference of electrode potential at any θ_B from the standard potential [114] corresponding to $\theta_B = 0.5$; K_1 is the chemical equilibrium constant of the above surface reaction and is related to the standard Gibbs energy, ΔG°_1. Langmuir adsorption conditions are defined by independence of K_1 on coverage, θ_B. The statistical-mechanical basis for the Langmuir isotherm is well-known [115] and serves to define its limitations.

1.9.2 Temkin Isotherm

In the case of many real systems, the condition (c) of the Langmuir isotherm does not apply because K_1 depends on coverage due to: (a) lateral interactions and/or (b) variation of the standard free energy of adsorption with coverage due to heterogeneity of the surface.

The quantitative treatment of factor (b) was given by Temkin [79,116,117] who based his treatment of adsorption on experimental evidence that chemisorption energies often vary linearly with coverage. The relation between ΔH_{ads} and θ is approximately linear at intermediate values of θ (i.e. $0.2 < \theta < 0.8$). The standard Gibbs energy is assumed to decrease with θ according to the relation:

$$\Delta G^\circ_\theta = \Delta G^\circ_{\theta=0} + gRT\,\theta \tag{1.45}$$

where g is a parameter associated with intrinsic heterogeneity of the surface.

The Temkin adsorption isotherm can be derived formally for an electrochemical process such as that in eq. (1.43) under equilibrium conditions in the form:

$$\frac{\theta_B}{1 - \theta_B} = K_1\, c_A \exp\left(\frac{\Delta EF}{RT}\right) \exp(-g\theta_B) \tag{1.46}$$

At intermediate values of coverage and for sufficiently large g, i.e. when the term $\frac{\theta_B}{1 - \theta_B} \approx 1$, its variation with θ_B is small compared with that of the $\exp(-g\theta_B)$ term; then the above equation can be reduced to

$$\exp(g\theta_B) = K_1\, c_A \exp\left(\frac{\Delta EF}{RT}\right) \tag{1.47}$$

which upon rearrangement gives

$$\theta_B = \frac{\Delta EF}{gRT} + \frac{1}{g} \ln (K_1 c_A) \qquad (1.48)$$

which is a form of Temkin's isotherm although his derivation was based on a treatment of a heterogeneous surface having a distribution of K_1 values.

Hence, for constant values of K_1 and c_A, the coverage tends to increase linearly with increasing potential difference, ΔE, and increases logarithmically with increasing K_1 and c_A at constant potential difference, ΔE. Although Temkin's isotherm has been applied to the behaviour of many electrode processes, it should be noted that in recent years it has been found that chemisorption at electrodes often occurs in a sequence of discrete states with clearly distinguishable binding energies rather than with a continuous range of adsorption energies; each sub-state often behaves in a "Langmuir" way.

From an electrochemical point of view, an important feature of the Langmuir and Temkin isotherms is the relation between θ_B and ΔE. This means that a series of characteristic equilibrium values of θ_B between 0 and 1 exists for every value of potential as the atoms of the adsorbed layer are deposited or removed, provided that the kinetics of the deposition or desorption processes are such that electrochemical equilibrium is maintained.

1.10 Under-Potential Deposition (UPD) of Hydrogen at Polycrystalline and Single-Crystal Pt Electrodes

1.10.1 UPD of H at Polycrystalline Pt Electrodes

In recent years, the submonolayer states of chemisorbed H which can be displayed at noble transition metals have become a topic of interest in surface science, especially of single crystals. The state and reactivity of hydrogen on electrodes surfaces is also of great practical and fundamental interest in relation to electrocatalytic oxidation of H_2 and

related energy conversion technology, to the cathodic hydrogen evolution reaction (HER) and $H_2/D_2/H_2O$ catalytic exchange, and to catalytic electrochemical hydrogenation.

The application of the cyclic-voltammetry technique of Sevcik [75] to the study of surface processes at Pt by Will and Knorr [76] showed clearly, for the first time, the existence of more than one state of H adsorption. Inspection of the early charging curves (E vs t for i = const) of Frumkin and Slygin [118] also reveals two distinguishable states between 0.0 and 0.35 V, RHE. However, the significance of those states was neither recognized nor discussed at that time. In the A.C. impedance work, Dolin and Ershler [119], and Breiter [120] found similar behaviour. The interpretation was that different peaks arise from H electrosorption at different crystal faces of polycrystalline Pt. This viewpoint was tested by Will [121] who showed that well-resolved H states were still maintained on low index single-crystal faces. Similar results were obtained by Conway et al. [10,122,123].

Two principal states of chemisorbed H at Pt were also distinguished by their apparently different signs of relative reflectance change, $\Delta R/R$ [124,125]. However, potential-dependent changes of structure and charge-density at or within the double-layer also contribute to $\Delta R/R$, so that the interpretation of the experimental results depends on how the double-layer contributions to $\Delta R/R$ at Pt are calculated.

This problem is difficult since the energy of the surface excess of electrons may itself depend on the surface coverage by UPD H, the electronic state of adsorbed H, the presence or absence of coadsorbed anions and their orientation, the electronic state of water molecules in the double-layer and the direction of their orientation and, finally, by mutual interactions between UPD H, anions and water molecules, effects which may be potential-dependent.

Further discussion of the distinguishable H UPD states [9,126,127], as revealed by cyclic-voltammetry, and also analogous states indicated in experiments on Pt and W on low pressure H_2 gas/solid interactions [129-134] led to the final characterization of the

under-potentially deposited H as was shown by Angerstein-Kozlowska et al. [9] and by Conway et al. [128]. These papers serve as the "standard references" for research conducted at (polycrystalline) Pt electrodes; this work in very pure solutions clearly distinguished three anodic H UPD states and two cathodic ones in 0.5 M aq. H_2SO_4 solution for various temperatures between 273.7 K and 366.9 K (Fig. 1.3). In Fig. 7 of ref. 128 it can be seen that the H UPD C-V profile strongly depends on the concentration of H_2SO_4, i.e. of the HSO_4^- ion; the H UPD C-V profiles taken in 0.01 M aq. H_2SO_4 solution at various temperature differ dramatically from those observed in 0.5 M solution and are more complex, exhibiting fine structure consisting of several small peaks overlapping with one another.

1.10.2 UPD of H at Single-Crystal Surfaces of Pt Electrodes

While the discussion on the form of the H UPD C-V profile at polycrystalline Pt was basically over around 1973/74, and research laboratories world-wide could easily reproduce the profile of Conway et al. [135] for very clean solutions, and were also able to explain any differences or discrepancies in terms of adsorbed or solution impurities, the discussion on the fundamental significance of the H UPD C-V profiles at Pt single-crystal electrodes was in its very initial stage.

As was already mentioned, the first H UPD C-V profiles on low index single-crystal faces of Pt were obtained by Will [121] and, using the same crystals, were reproduced in this laboratory [10,122,123]. However, these results were unsatisfactory, since the single crystals used exhibited a certain amount of polycrystallinity.

Hubbard and coworker [136,137] studied the H UPD at Pt(100) and Pt(111) faces which were well-characterized in situ by LEED and Auger spectroscopy prior to contact with the 0.5 or 1 M aq. H_2SO_4 solution used. The C-V profiles are shown in Fig. 1.9.

The LEED patterns obtained for Pt(100) and Pt(111) after exposure to the aqueous solution of H_2SO_4 or $HClO_4$ indicated that both the above Pt single-crystal surfaces

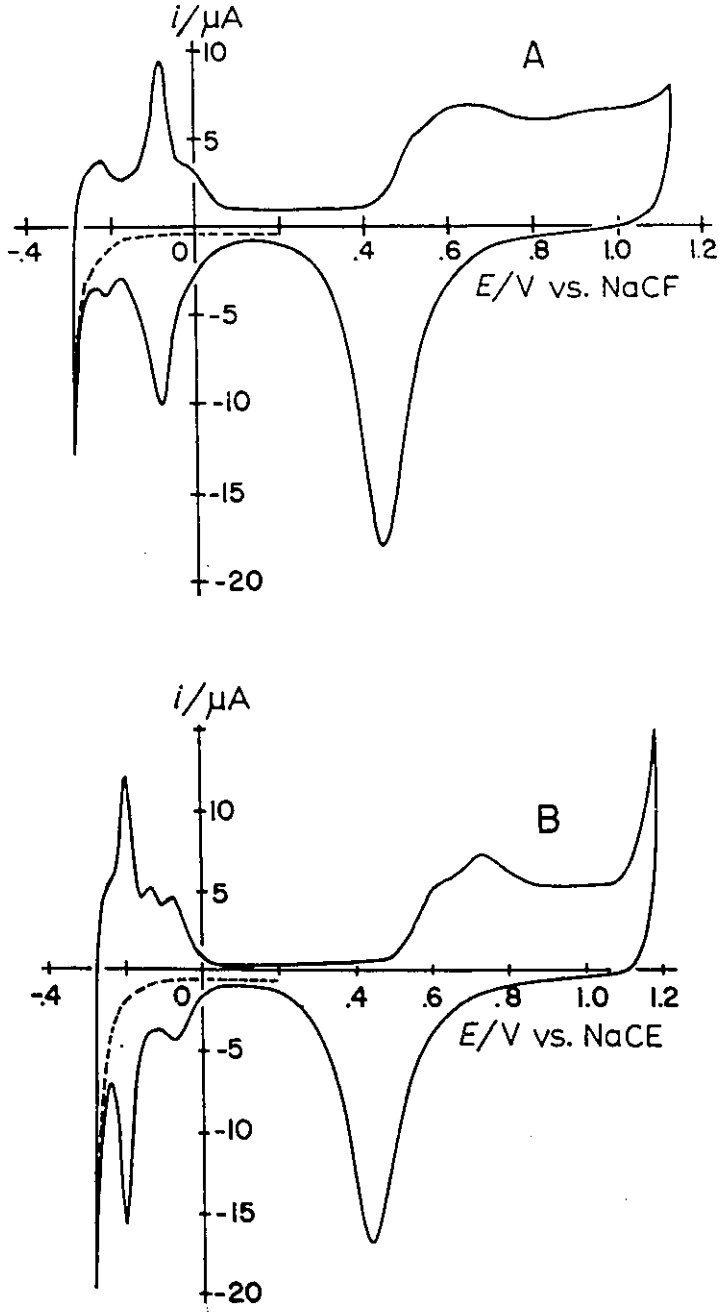

Fig. 1.9 (a) C-V profiles for Pt single-crystal electrodes in 1 M H_2SO_4 taken at t=23°C and at a sweep rate of 10 mV s^{-1}; (A) Pt(100), 0.622 cm^2; (B) Pt(111), 0.579 cm^2 [137].

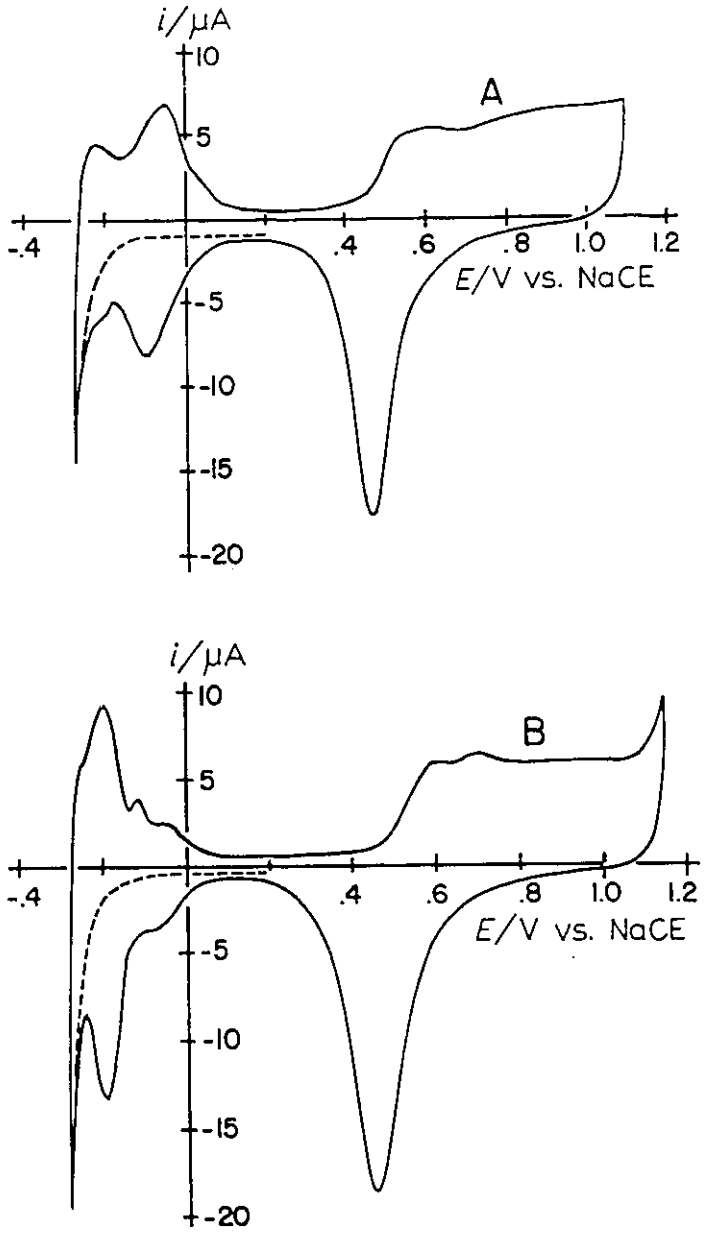

Fig. 1.9 (b) C-V profiles for Pt single-crystal electrodes in 1 M $HClO_4$ taken at t=23°C and at a sweep rate of 10 mV s^{-1}; (A) Pt(100), 0.622 cm^2; (B) Pt(111), 0.579 cm^2 [137].

acquired the simple (1×1) symmetry. However, it should be mentioned that ten or more C-V cycles were applied between 0.05 and 1.40 V, RHE, at a scan rate of from 2 to 10 $mV\ s^{-1}$ [137]. This procedure, well known as electrochemical cleaning, caused surface-structural rearrangements as was found by Wagner and Ross [138,139,172,173] and as will be discussed in the "Results and Discussion" Chapter.

The main controversy regarding electrochemistry at Pt single-crystal surfaces arose when Clavilier and coworkers [140-147] presented results of their experiments on low-index single-crystal faces. The H UPD C-V profiles of Clavilier for Pt single-crystal electrodes (Fig. 1.10) were completely different from the ones of Hubbard, and earlier of Will, both in H_2SO_4 and $HClO_4$. The experimental technique used by Clavilier [140,141,143-145] to prepare and pretreat Pt single-crystal electrodes involved heating single crystals in an hydrogen-oxygen flame followed by rapid quenching in distilled water. The purpose of this procedure was to isolate a supposedly very clean single-crystal face from the environment, by attaching a drop of water, so that no impurities present in the air could become adsorbed on the surface of interest. This procedure, though effective in preventing the single-crystal face from picking up impurities, might introduce stress not only within the surface layers of the crystal but also within its bulk, near the surface. Moreover, contact between a hot Pt single-crystal (800-1300°C) and air or water results evidently (cf. Figs. 2,3 of ref. 144 and Figs. 1-7 of ref. 142) in formation of Pt oxide on the Pt single-crystal, as was shown by Clavilier et al. [142-144] by recording the first negative-going sweep from ca. 0.90 to 0.05 V, RHE. An obvious question arises then, whether the Pt oxide thus present on the single-crystal face could lead to reconstruction of the surface and, if that was so, then to what extent (see "Results and Discussion" Chapter) did it occur?

The technique of Clavilier was also used to study H UPD at other than low-index crystal faces [145-147] as well as adsorption of CO, Bi, Pb, As and other atoms or molecules, and to study oxidation of CO, HCOOH and CH_3OH on low-index Pt

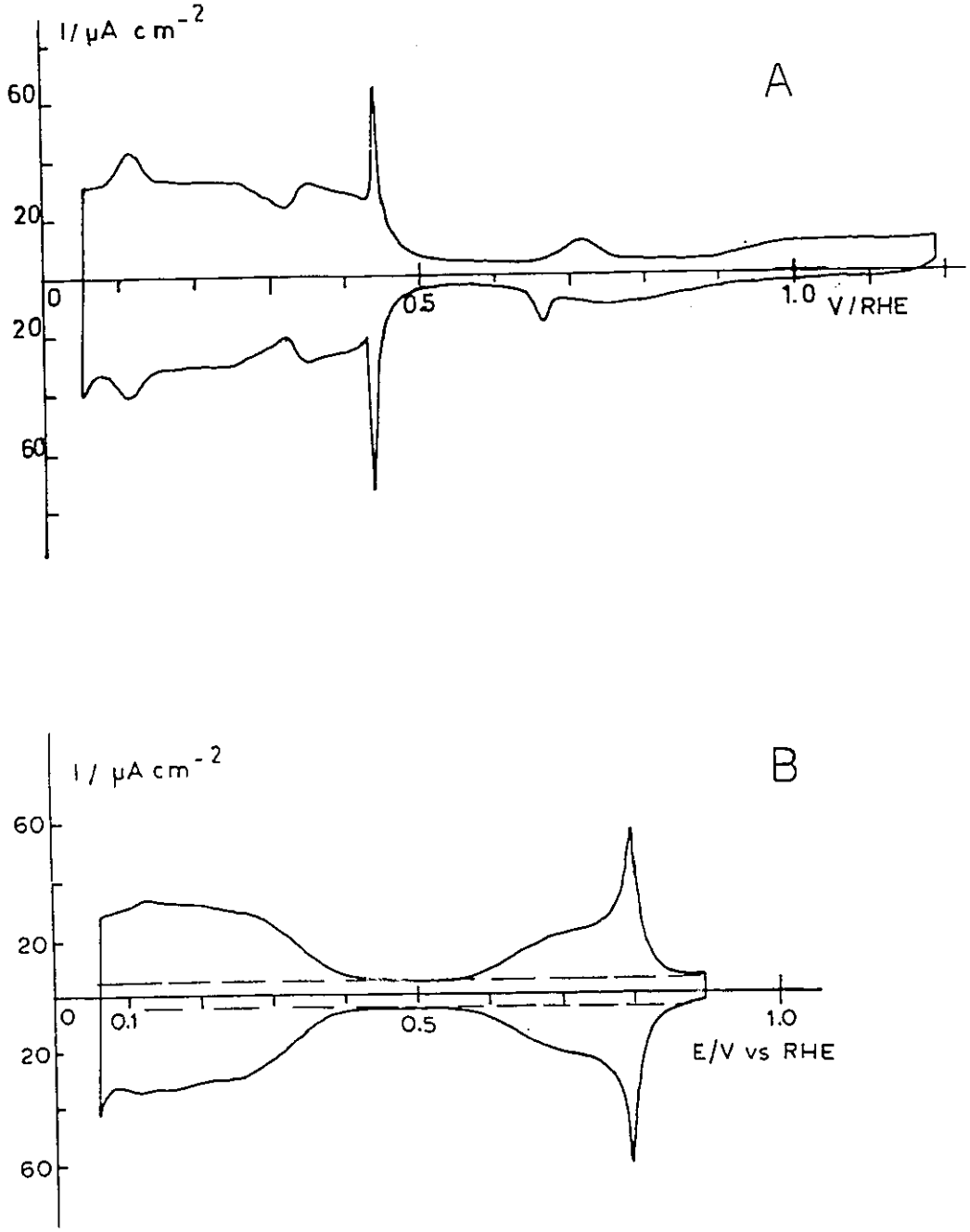

Fig. 1.10 (a) C-V profile for Pt(111) electrode in 0.5 M aq. H_2SO_4 (50 mV s^{-1}); (b) C-V profile for Pt(111) electrode in 0.5 M aq. $HClO_4$ (50 mV s^{-1}), [140,141].

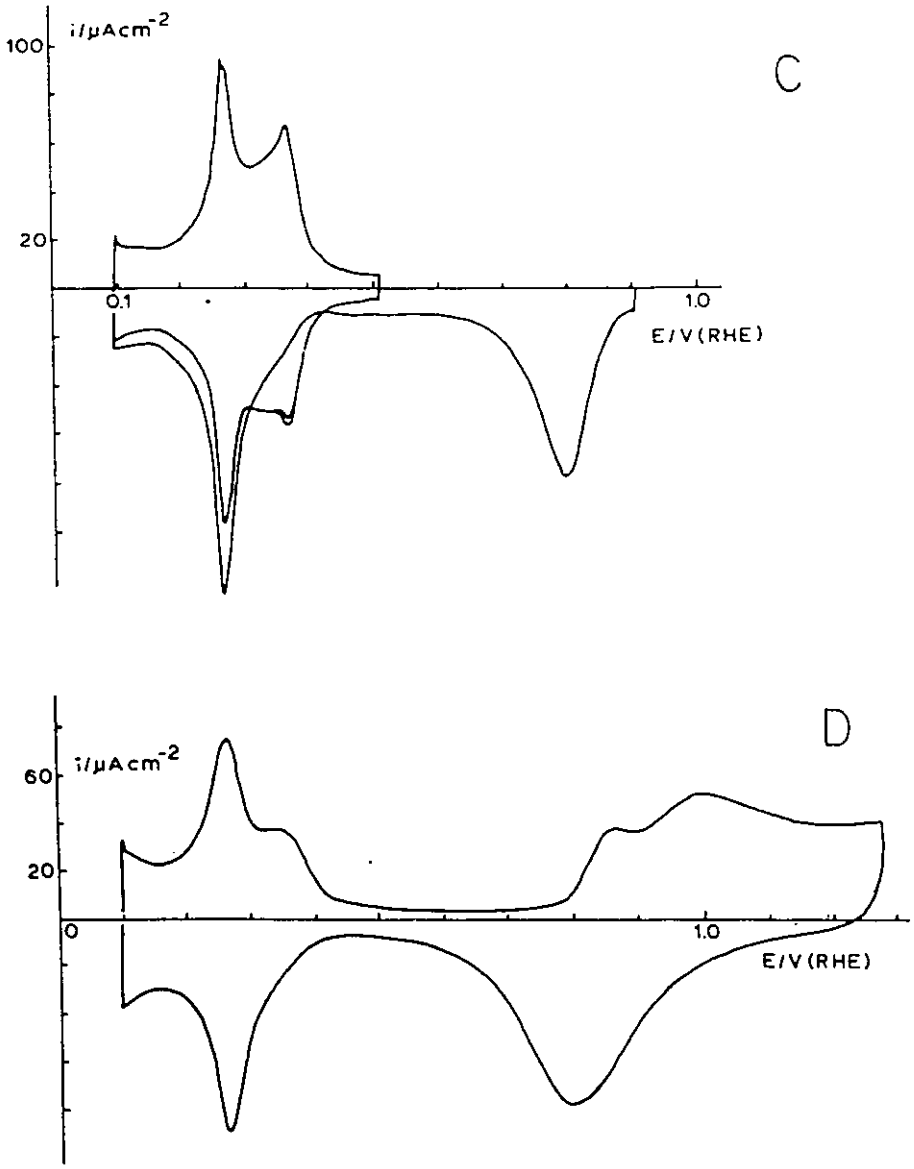

Fig. 1.10 (c) C-V profile for Pt(100) electrode in 0.5 M aq. H_2SO_4 (50 mV s^{-1}) after heating at ca. 1000°C followed by quenching (the C-V profile reveals the thermally-formed oxide which is reduced in the first negative-going sweep); (d) C-V profile for Pt(100) electrode in 0.5 M aq. H_2SO_4 (50 mV s^{-1}) after 6 cycles up to 1.40 V, RHE, [140,141].

single-crystal faces [148-161].

The heating and quenching technique has been used in various other research laboratories [162-168], including our own, and has usually resulted in reproduction of the results of Clavilier. However, it seems quite interesting and characteristic that the so-called "double-butterfly" i vs E profile of Clavilier is not the same in various of his own results and differs from one paper to another, i.e. the fine features, such as the "spike", are not the same and vary in height, sharpness, etc.

Significant contributions to the development of new procedures applicable to electrochemical measurements at single-crystal faces, were made by Hubbard [169-171] and Więckowski [172-176]. They developed the technique of coating Pt single-crystals by iodine, in order to prevent them from picking up impurities. Later on, it was shown [171-173] that iodine could be replaced by carbon monoxide (CO) which subsequently could be oxidatively desorbed from the single-crystal electrode by applying a single positive-going potential sweep. Więckowski et al. [174] further developed and simplified this procedure, working out a new method for in situ preparation of clean and well-ordered single-crystal Pt faces, which did not require either the heating-quenching procedure or an ultra-high vacuum. This technique, however effective, is fairly laborious and complicated. The C-V profiles for UPD of H acquired in aq. H_2SO_4 and $HClO_4$ solutions [174-176] are consistent with some of the results of Clavilier [140-142].

One of the most puzzling features of the C-V profiles for UPD of H at Pt(111) is that the experimentally-determined charge, $Q_{H\ UPD}$, in all cases is very close to the value calculated [137], for adsorption of one H per Pt atom, giving ca. 241 $\mu C\ cm^{-2}$, though the early C-V profile of Hubbard [137] is substantially different from the one of Clavilier, which he supposed was also a (111) surface.

Although the Pt(111) single-crystal face has been studied very extensively, many questions remain unanswered about its behaviour for electrosorption of H. For instance, it is not clear why the C-V profiles for UPD of H at Pt(111) or other low-index single-crystal

faces are so complex and an additive combination of contributions from these three does not give the C-V profile of polycrystalline Pt.

There are several interpretations of the form of the Pt(111) H UPD C-V profile. One of the most interesting is that which supposes the existence of two states of adsorbed hydrogen: a "conventional" (low binding energy) one and one having a high binding energy of the H [141]. However, this interpretation does not specify the source of energy which stabilizes the strongly bound H in the adsorbed state. It was also suggested that the "butterfly" could be accounted for by a metal surface oxidation process [138,177] instead of by H adsorption. Więckowski et al. [175] has critically reviewed the various concepts and proposed a new model which assumes the existence of subsurface hydrogen on Pt(111), an idea suggested earlier by Toya and Horiuti [179,180]. This model is based on experimental evidence such as the observed different optical properties of the weakly and the strongly adsorbed H on polycrystalline Pt electrodes [178]. It was suggested that the strongly bound hydrogen (low-energy hydrogen) had some metallic character due to mixing of the 1s hydrogen electron with the conduction band electrons of the metal. This property is consistent with the s-type of H adatom proposed by Toya [179,180]. Further electroreflectance studies showed that UPD H on Pt(111) appeared to correspond to a single adsorbed state [181]. Więckowski et al. [175] suggested that the second type of adsorbed hydrogen was not detected because it was located beneath the first metal surface layer, becoming the subsurface hydrogen. The implications of this model will be discussed in the Results and Discussion Chapter. Other models treat the multiple states of adsorbed H in terms of deposition of successive overlay array structures as θ_H is increased from 0 to 1.

1.11 Oxide Film Growth at Polycrystalline and Single-Crystal Pt Electrodes

1.11.1 Oxide Growth at Polycrystalline Pt Electrodes

At Pt and other noble metals, the initial stages of oxide film formation can be studied in detail, including the important transition from sub-monolayer, through monolayer oxide, to growth of multilayers corresponding eventually to quasi-bulk phase-oxide formation [7-9,18-23,61,182-184]. Knowledge of the states in which the oxide film on Pt can be formed is also of major importance for various continuous anodic Faradaic reactions since it determines the electrocatalytic surface on which O_2 [8,22,23,184] and Cl_2 [18] evolution, hydrocarbon formation (the Kolbe reaction [186]) and some ionic redox reactions take place [187]. The first three of these reactions occur on a surface that already bears an oxide film before significant current-densities for these processes arise. The state of the oxide film can also change with time and potential during the course of such reactions which can therefore be studied meaningfully only on oxide films that have been separately pre-formed to extents determinable by means of cyclic-voltammetry [194,195] and/or optical reflectivity measurements [198], so that further changes do not, or only minimally, take place during the kinetic examination of the reaction itself, e.g. O_2 or Cl_2 evolution. Hence, for studies of electrocatalysis in such reactions, the states and chemical properties of such oxide films require characterization.

At low submonolayer levels of OH or O coverage at Pt, Rh, Ru and Au, a reversibly depositable and reducible oxygen species can be distinguished voltammetrically [11,12,194] or optically [198,199] from oxide material that is reducible only irreversibly after formation at higher coverages (but initially still less than a monolayer) and/or after holding the potential constant at an appropriate value for controlled times. The process of conversion of the oxide films from the reversibly to the irreversibly reducible, but still quasi-2-dimensional state, has been attributed [9,10] to "place-exchange" between OH or O species (initially deposited in 2-dimensional arrays) and underlying metal atoms.

Results of various workers on the subject of oxide film formation and reduction at Pt have been substantially at variance. For example, early work of Vetter and Berndt [182] led to the conclusion that the charge for oxide reduction was ca. half that for its formation! It is now quite clear, however, that these charges match to within 1% in cyclic-voltammetry under well-controlled conditions especially of solution and electrode surface purity [9,135].

The kinetics of oxide film growth at Pt were studied by Gilroy and Conway [7] and later, in extended ways, by Gilroy [8] and by Biegler and Woods [25]. From the latter work, a second discrepancy arises in that, with more extensive surface oxidation for long times and/or at elevated potentials, oxide film formation had been said by Biegler and Woods [25,26] to attain a so-called monolayer limit of ca. 2.6 O atoms per Pt atom (but this clearly is not a monolayer!). Contrarily, Shibata [27,28] had shown (see below) that multilayer oxide film formation arises at Pt.

The formation of thick oxide films on Pt was demonstrated and studied by Shibata [27,28], James [32], and Balej and Spalek [33], and more recently by Vassiliev and Gromyko [30,31]. In studies of oxide film growth at high anodic potentials, Shibata [27] showed that a distinguishable phase oxide, virtually a bulk oxide film (designated the "β" state in his papers), could be formed on Pt and was reduced in a cathodic current peak separate from that for the usually observed, quasi-2-d oxide film and appearing at less positive potentials, in fact over the H UPD region. This state of the oxide had much higher resistivity [29] than that of the quasi-2-d film.

It was concluded by Shibata [27] that reduction of the quasi-2-d film in a negative-going potential sweep led to deposition of Pt atoms on the outside of the thicker, phase-oxide film. It was indicated in a paper by James [32], and by the referee of that paper (as referred to in a footnote to that paper), that Shibata's view of the course of reduction of the quasi-2-d film would result in the thick oxide being sandwiched between the bulk Pt metal and a film of newly generated Pt atoms on the outside of the remaining

thick oxide, resulting from the reduction of the "α" state of Shibata. Burke and Roche [34], and Burke in his review [35], developed a model of so-called thick "hydrous oxides" on Pt. In their work, the thick oxide films were grown by applying a cycling procedure (reversing the negative-going sweep at ca. 0.55 V, i.e. prior to the oxide film reduction). Burke and Roche also opposed Shibata's point of view that the "α" state of oxide resides on top of the "β" state, but did not provide any experimental evidence for this contrary view. Conway, in a paper co-authored by the present writer, [189] and Farebrother et al. [36], provided critical experimental evidence that the quasi-2-d oxide state lies beneath the thick-oxide film and can be reduced independently of the overlying thick-oxide (see the "Results and Discussion" Chapter). Settlement of this question was important for: (a) theories of growth of Pt oxide films [8]; and (b) identification of the state of the external surface of thick, anodically grown oxide films as electrocatalyst interfaces on which the Cl_2 (cf. ref. 185) and O_2 (cf. ref. 190) evolution reactions proceed.

Of the previous work, some of the most informative has been that of Shibata [27-29] and of Damjanović et al. [22,23] with regard to formation of thicker films, and of Kozlowska et al. [9] on the transition from submonolayer to post-monolayer film development, with reconstruction. Useful complementary information has been provided by XPS measurements [191-194] which indicate, variously, the existence of Pt in oxide films in oxidation states +II and +IV, depending on conditions of preparation.

Recent work by Vasilyev et al. [30,31] confirms qualitatively the observations of Shibata [27-29] but some details of their voltammograms are obscured by effects associated with reduction of impurities, probably anodically generated O_2, which makes difficult the quantitative evaluation of charges for reduction of different states of the oxide film.

The results that have been reported in the literature on Pt oxide film growth are thus divergent or, in some cases, unsatisfactory for the following reasons: (a) in many cases the oxide films were grown under galvanostatic conditions, so it was impossible to

relate different oxide states to the potential and duration of the polarization; (b) only in a few isolated cases [27,32,33] was the oxide grown potentiostatically but the potential range covered was quite narrow; and (c) the electrode preparation technique often involved such drastic pretreatment procedures as roughening the Pt electrodes with emery paper or depositing Pt black on Pt. Such prepared electrodes were highly unstable and results achieved were very irreproducible. Reduction and subsequent formation of a new oxide film never resulted in the same oxidizability of the Pt electrodes. Moreover, for a number of years it was thought [33-35] that thick-oxide films could be formed only on electrodes that had been pretreated with emery paper!

1.11.2 Oxide Growth at Single-Crystal Pt Electrodes

The oxide growth at polycrystalline Pt electrodes has been studied very extensively but hardly any data exist on the growth behaviour at single-crystal Pt electrodes.

An analysis of the C-V profiles for single-crystal Pt electrodes recorded by Clavilier [140-147], Hubbard [137] and other researchers [138,139,166,172,173,195] may be an indirect source of limited information on the oxide growth. For instance, the existing data on "quenched" Pt(111) indicate [140-143,147] that the formation of the quasi-2-d oxide does not occur below a potential of 1.10 V, RHE, while on an electrochemically cleaned Pt(111) surface it starts at the same potential as for polycrystalline Pt, i.e. at ca. 0.85 V, RHE. In the case of Pt(100), the formation of the quasi-2-d oxide begins at ca. 0.80 V, RHE, while for Pt(110) between 0.80 and 0.90 V, RHE, depending on the history of thermal pretreatment of the electrode [143,144,146,147].

Pre-electrochemical formation of oxide on single-crystal and polycrystalline Pt electrodes was observed [142-144] when electrodes were flame-annealed followed by quenching. The existence of an oxide film was detected by recording the first negative-going sweep from the rest potential of Pt electrodes, which was around ca. 0.9 V,

RHE. Interestingly, in the case of the "quenched" Pt(111) electrode, covered already with a thermally formed oxide, its reduction still resulted in a surface on which the UPD H gave the characteristic "double-butterfly" C-V profile [142,143].

Careful investigation of C-V profiles for single-crystal Pt electrodes up to 1.40 V, RHE, indicate [137,140,141,144,146,147,166,195] that the features of the profiles corresponding to oxide formation and reduction differ quite substantially from one single-crystal face to another.

The information mentioned above provides some qualitative data on quasi-2-d oxide formation and reduction on Pt single-crystal faces. However, virtually no data exist on potentiostatically controlled, direct formation of oxide beyond 1.40 V, RHE, and on any possible surface-restructuring processes which are likely to arise in oxide formation and reduction beyond that limit. The present author with Conway [166] showed that formation and reduction of the quasi-2-d oxide film on a "quenched" Pt(111) electrode surface, which initially revealed the "double-butterfly" C-V profile of Clavilier, results in an irreversible electrode-surface restructuring which, after ten cycles up to 1.40 V, RHE, leads to the H UPD C-V profile of Hubbard [137] Details of this work are given later in this thesis.

CHAPTER 2

Experimental

2.1 General Introduction and Choice of Methods

2.1.1 Thermal and Electrochemical Pretreatment of Polycrystalline Pt Electrodes with Respect to Their Oxidizability and Reproducibility of Experimental Results

The results that have been reported in the literature on Pt oxide film growth at polycrystalline Pt electrodes treated in various ways are divergent or, in some cases, unsatisfactory (see Section 1.11.1 of the Introduction). The need to be able to establish well characterized polycrystalline Pt electrodes and their reproducible oxidizability, has led, in the present work, to attempts to make definitive experiments on this problem.

In the work reported here, the polycrystalline Pt electrodes, prepared according to the procedure described in Section 2.8.1, were treated electrochemically by cycling between 0.05 and 1.40 V, RHE, at s = 50 mV s^{-1} and/or thermally by heating in an hydrogen-oxygen flame, followed by cooling in air or by quenching in pyrolytically-distilled water.

The state of the surfaces of polycrystalline Pt electrodes after various thermal and/or electrochemical pretreatments was examined with respect to their H and O adsorption characteristics by means of potentiodynamic i vs E profiles (cyclic-voltammograms), recorded by taking potential sweeps at s = 50 mV s^{-1} between 0.05 and 1.40 V, RHE, over an extended period of time. Qualitative changes in the i vs E profiles, which indicated reconstruction of the electrode surface, were examined by comparing the ratios of the principal anodic and cathodic peak currents, i_{HA1}/i_{HA2} and i_{HC1}/i_{HC2} [9,10] in the H UPD region (see Section 1.10 of the Introduction). Quantitative

changes were examined by determining values of the roughness factor, R, generated after various thermal and electrochemical pretreatments.

The oxidizability of polycrystalline Pt electrodes was determined by subjecting them to the same oxidation conditions (i.e. the same polarization potential, E_h, and polarization time, t_h) and examining the amount of oxide formed after various thermal and/or electrochemical pretreatments (see Section 1.11.1).

In a number of cases, reduction of a thick oxide film (10~50 equivalent O monolayers) resulted in an observably large increase of the real surface area which was determined by measuring the H UPD charges associated with the first i vs E profile, following the oxide reduction. Such a Pt surface with increased area was found to relax both qualitatively and quantitatively to a state having the initial surface characteristics after prolonged cycling between 0.05 and 1.40 V, RHE, at the sweep rate of $s = 50\ mV\ s^{-1}$. This behaviour was evidently attributable to an "electrochemical annealing" effect as described in Section 3.1.3 of the Results Chapter.

2.1.2 Formation and Study of Thick-Oxide Films in Relation to O_2 Evolution at Pre-formed Oxide Films

In the present work, thick-oxide films at Pt were generated by application of a linear, positive-going potential sweep at $s = 50\ mVs^{-1}$ to a controlled potential limit, E_h (the oxide "growth potential"), at which the potential was held constant (potentiostatic oxide-film growth) for various growth times, t_h. Values of the applied polarization potential were $E_h = 1.8, 1.9, ..., 2.3$ V, RHE, and polarization times, t_h, up to 48 h, were employed. During this procedure, purified N_2 was bubbled through the solution to displace anodically evolved O_2 which accompanied oxide film growth above 1.23 V, RHE. The potential vs time programme employed in these experiments is illustrated in Fig. 2.1. Controlled-potential growth was the preferred procedure in this work, as controlled-current [28,29] or cycling procedures [34,35] provide electrochemically less

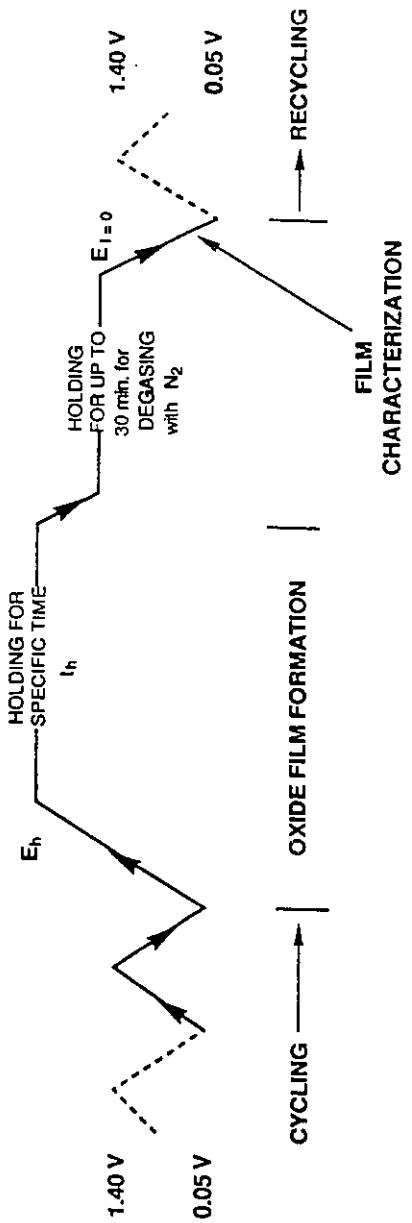

Fig. 2.1 Potentiodynamic and potentiostatic conditioning programmes for oxide film formation and reduction at Pt electrodes; E_h = polarization (holding) potential, t_h = polarization (holding) time, $E_{i=0}$ = zero current potential (N_2 bubbling).

well defined conditions for the formation of oxide films.

The state(s) of the anodically formed oxide film was (were) characterized by application of a negative-going potential sweep at $s = 50\ mV\ s^{-1}$ which generated cathodic current (i) vs potential (E) reduction profiles enabling the states of the anodically formed oxide to be distinguished electrochemically. It should be emphasized that only by means of the linear potential-sweep method can major, or more subtle, differences in the state of such oxide films be properly distinguished, since the procedure generates a differential response, $i = C\ (dE/dt)$, where C is the interfacial capacitance including the pseudocapacitance due to oxide reduction and the smaller double-layer capacitance.

In order to avoid cathodic currents in the negative-going potential sweeps due to reduction of O_2 formed in parallel with the Pt oxide formation, after potentiostatic oxide film formation at the E_h potential, the negative-going sweep was arrested at a potential $E_{i=0}$ (Fig. 2.1) between 1.60 and 1.75 V. In this potential range, virtually no anodic or cathodic currents (i=0) pass; then, by holding the potential at such values for up to 30 min, any anodically generated O_2 remaining in the solution can be completely expelled by the bubbled N_2. An $E_{i=0}$ around 1.70 V was usually chosen since, at this potential, neither continuing oxide film formation nor reduction of the oxide film takes place during this holding procedure. The reduction sweep was then continued to 0.05 V, RHE, in the usual way in order to record the cathodic current profiles for reduction of the oxide film.

This procedure for elimination of O_2 is essential for proper evaluation and resolution of the oxide-reduction i vs E profiles, otherwise accurate charge evaluation and resolution of oxide film states is impossible; this difficulty seems to have arisen in some works [30,31]. The above procedure satisfactorily led to virtually zero O_2-reduction currents being superimposed on the currents for the oxide film reduction.

It was found that the conditions of potential and time of anodization required to generate the distinguishable states of the oxide film at Pt must be carefully controlled; then a definitive distinction of the states of the oxide film at Pt could be made as described

later. This latter aspect is important for generating well-defined, pre-formed oxide surfaces on which electrocatalysis of anodic reactions such as O_2 or Cl_2 evolution could be examined. In the present work, the OER was studied by measuring the steady-state currents resulting from controlled but varied applied potentials. These log i vs η plots, commonly known as Tafel plots, provided the required information on the kinetics of the OER, occurring on pre-formed oxide surfaces, and their slopes could be diagnostic of the reaction mechanism(s) operative in the electrode process.

Finally, during the extended periods of oxide film formation, parallel anodic evolution of O_2, of course, took place [21,22]. The O_2 evolution behaviour in time was of interest in relation to the changing electrocatalytic properties of the oxide film as it grew and changed its state. This was measured as current density, i, vs time, t, on a Y-time recorder and attempts were made to relate the recorded O_2 evolution current-densities, i, to the oxide film development at the Pt. This could be reliably done since the currents for the latter processes were less than 0.1% of the O_2 evolution currents and states of oxide film development were separately characterizable by the cyclic-voltammetry experiments after removal of O_2.

2.1.3 Thermal and Electrochemical Pretreatment of Single-Crystal Pt Electrodes

Despite the fact that much interest has been devoted to the study of electrochemical processes at well-defined surfaces of Pt [136-143,171-177,195] as described in Section 1.10.2 of the Introduction, the results obtained by a number of researchers are not yet in agreement. In the present work, the single-crystal Pt electrodes were subjected to various thermal pretreatments as follows: (a) annealing or (b) heating, followed by quenching in pyrolytically-distilled water and (c) electrochemical pretreatment by cycling between the lower potential limit of 0.05 or 0.07 V, RHE, and an upper potential limit which varied from 0.70 to 1.40 V, RHE, depending on the electrochemical conditions desired. The states of the Pt single-crystal electrode surfaces

were studied by examining: (a) the i vs E profiles of the underpotentially-deposited H species (H UPD C-V profiles); (b) the charges corresponding to the H UPD C-V profiles arising from cycling to various upper potential limits; (c) the H UPD charge arising after various thermal and electrochemical pretreatments; and (d) the behaviour in the OH or O species region, also as a result of the different pretreatment conditions applied.

The phenomenon of under-potential deposition (UPD), e.g. of H, is a surface process in which virtually only non-continuous currents pass as the available surface of the electrode is either filled to the limit of full coverage (θ=1) or the deposited monolayer is stripped to zero coverage (θ=0). Methods used for the study of electrochemical surface processes must therefore be of a non-continuous, transient kind and include cyclic-voltammetry, galvanostatic charging/discharging, a.c. impedance spectroscopy; these procedures are usually employed in a complementary manner for better understanding of the electrochemical reaction involved. In the present work, the preferred technique for studying electrochemical processes at Pt single-crystal surfaces was cyclic-voltammetry, because it is the most powerful and sensitive method where small, time-dependent current-densities are to be observed, and where resolution of multiple-states of adsorption in a monolayer is required.

2.2 Experimental Methods

2.2.1 Cyclic Voltammetry

The cyclic-voltammetry technique is essential for electrochemical surface science studies, especially under-potential deposition, and uniquely provides detailed information about a particular surface process by provision of dynamic current-density (i) vs potential (E) profiles, colloquially called cyclic-voltammograms or C-V profiles. Usually, the potential of the working electrode is varied linearly with time at a constant sweep-rate, s,

between an upper and a lower potential limit. One transient from the lower limit to the upper limit and back is often called a "cycle", and can be repeated in a continuous manner ("cyclic-voltammetry" or C-V technique). During the potential cycling, the current is simultaneously recorded as a function of the potential, using either an X-Y recorder (for low sweep-rates) or a digital oscilloscope (for high sweep-rates). This is achieved by feeding into the potentiostat a pre-arranged, linearly-varying, time-dependent voltage program, controlled by an electronic function generator [10,14,77,78,80,197].

A standard electrical circuit was used in this work (as shown in Fig. 2.1 in ref. 80 and Fig. 6 in ref. 197) and consisted of the following components: (a) a High Power Potentiostat, Wenking HP72; (b) EG&G PARC Model 175 Universal Programmer; (c) two 7045B Hewlett-Packard X-Y Recorders connected "in parallel"; and (d) a Nicolet 3091 Digital Oscilloscope. Experimental current-density (i) vs voltage (E) profiles were recorded by means either of the X-Y recorders in the case of low sweep-rates ($s \leq 150$ mV s^{-1}) or the digital oscilloscope in the case of high sweep-rates ($s > 150$ mV s^{-1}). Continuous read-out of the working-electrode potential was available on a suitably connected Fluke 8050A Digital Multimeter while the current was measured on a Keithley 195A Digital Multimeter.

2.2.2 Steady-State Polarization (Tafel) Experiments

Measurements of the steady-state current (in this case, for anodic O_2 evolution), resulting from controlled but varied applied potential, provide useful information on the kinetics of any continuous electrode process of interest. Here, such measurements were complementary to those provided by cyclic-voltammetry. The general form of the log i vs E relation, commonly called a Tafel plot, provides information on: (a) the reaction mechanism operative in the electrode process; (b) any changes in the reaction mechanism that arise with change of potential or other conditions; and (c) the so-called exchange current-density, i_o, (determined from extrapolation of the linear part of the log i vs E

relation to zero overpotential) which characterizes the kinetics of the electrode process [77-79,198] at equilibrium.

All the "Tafel Plot" measurements made in the course of this work utilized an automated (computer-controlled) data acquisition system and employed software developed by Tessier [28] in previous years in this Laboratory. This procedure offers a number of advantages, for example: (a) a large number of i-E data pairs may be recorded which allow precise determination of the Tafel slope and exchange current density; (b) it allows precise and consistent adjustment of the holding potential; (c) it facilitates the processing and display of the experimental results; (d) it allows the latter to be compared quantitatively with predictions of possible physical and electrochemical models; and finally (e) it saves the operator's time when slow measurements are required (several seconds or more for each experimental point).

The procedure used in the present work involved pre-oxidation of the Pt electrode by applying a desired polarization potential, E_h, for a set polarization time, t_h, (consistent with those used in cyclic-voltammetry), directly followed by steady-state polarization that always began at the potential of 1.70 V, RHE, at which the pre-formed oxide could not yet be reduced and the oxidation current was virtually zero. This procedure allowed the OER to be studied on different states of preformed surface oxide at Pt, as revealed by separate cyclic-voltammetry measurements (see Section 3.2.2 of the "Results and Discussion" Chapter).

The controller (hardware) consisted of the following components: (a) an Hewlett-Packard (HP) 87 computer equipped with an HP 82909A 128K Memory Module, an HP 82936A ROM Drawer and an HP 82939 Serial Interface; (b) an HP 82901 M Flexible Disc Drive; (c) an HP 7470A Plotter; (d) an HP 2225H Jet Printer; (e) a Keithley 195A Digital Multimeter; (f) a Kepco SN488-122 Programmer; and (g) a Fluke 8050A Digital Multimeter. The schematic diagram of the experimental set-up described above and the electrical circuit has been already shown in ref. 198.

2.2.3 Compensation for Solution Resistance Effects

In many experiments in interfacial electrochemistry, the measurement of the relative potential drop between an electrode and the solution side of the electrical double-layer is of importance. However, when a net current, I, is passed across such an interface, a potential-sensing probe placed near the electrode surface measures a finite potential drop, $I \cdot R_s$, in the solution near the electrode, in addition to the desired interfacial potential difference:

$$E_{obs} = E + IR_s \qquad (2.1)$$

where E_{obs} is the observed potential, E is the real potential and R_s is the resistance of solution between the tip of the potential-sensing probe (the Luggin capillary) and the working electrode. The experimental error due to "IR-drop" becomes significantly large when appreciable currents are passed [77,78,198,199], depending on the conductance of the solution, as is well known.

In the present work, the Tafel plots were corrected for this effect of the solution resistance, R_s; the latter was determined by the current interruption method which involved opening the current-carrying circuit by means of a fast mercury-wetted reed relay and following the open-circuit potential decay transient at the test electrode using a Nicolet 3091 digital oscilloscope. A typical "potential-decay" curve (Fig. 2.2) consisted of two components: (i) a steep, almost instantaneous and linear part due to R_s and (ii) an exponential, dominating component due to the Faradaic impedance of the interface. By measuring the "length" of the linear component, E_{IR}, and the current, I, prior to its interruption, the value of R_s could be determined. For better accuracy, this procedure was repeated several times by applying different potentials, and a plot of E_{IR} vs I was constructed; as expected, such a plot was linear so the value of the slope gave the required R_s value for various experiments.

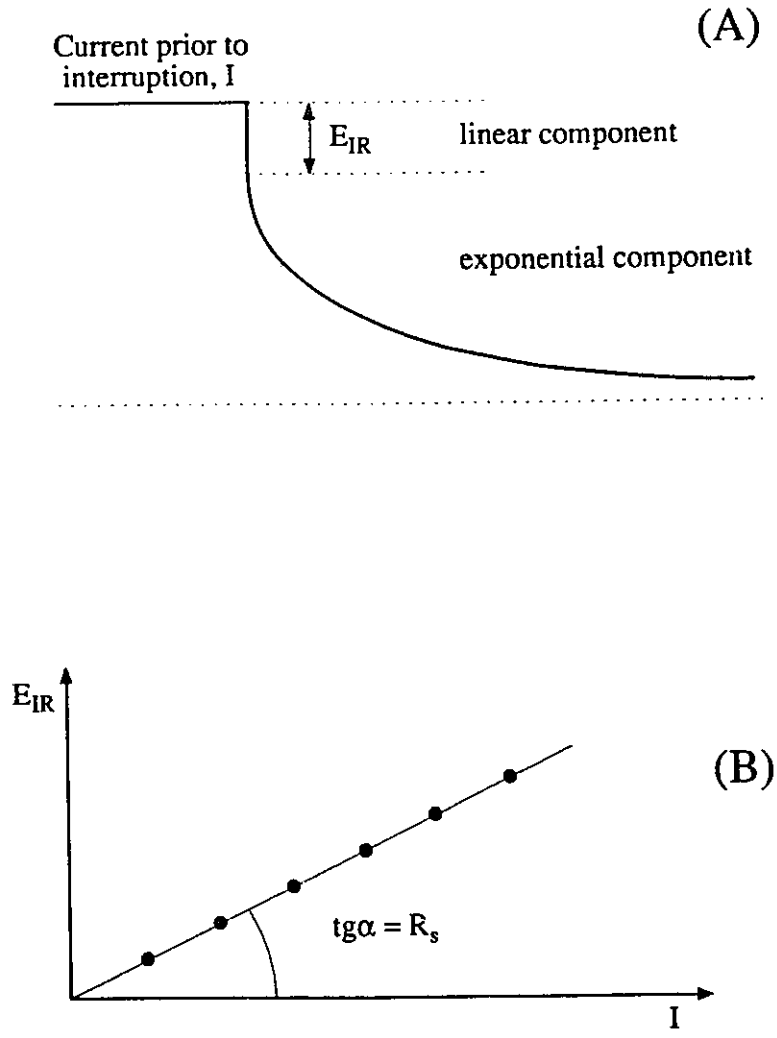

Fig. 2.2 (A) A typical potential-decay curve; (B) A typical E_{IR} vs I plot from which the value of solution resistance, R_s, can be determined.

2.2.4 Current vs Time Measurement

It was mentioned in Section 2.1.2 that the OER, taking place during the potentiostatic oxide film formation, was investigated by recording the oxygen evolution current-density, i, vs time, t. This was done by connecting in series with the current-carrying circuit a high-sensitivity HP 7101 BM Strip Chart Recorder.

2.3 Gases

Electrolytic H_2 and N_2 gases, used for the Pt/H_2 reference electrode and for deoxygenation (outgassing) of the solutions, respectively, were purified in conventional gas purification trains [200] before use, to remove any traces of O_2 since the latter is chemically reactive with some substances and electrochemically reducible.

Hydrogen gas was passed through a gas train consisting of $Mg(ClO_4)_2$ as a desiccant, molecular sieve (BDH type 4A), an oven containing palladized asbestos and Cu turnings at 623 K, and finally activated charcoal traps cooled by liquid N_2.

Nitrogen gas was passed through an identical gas purification train except that only Cu turnings were used in the oven for removal or O_2. The metallic surface of the Cu turnings was periodically regenerated by passing pre-cleaned H_2 through the oven.

2.4 Cleaning of Glassware

Electrochemical measurements are very sensitive to even trace-amounts of impurities, and it is necessary to clean all glassware prior to performing experiments. This was achieved by soaking the electrochemical cell and its glass components in fresh, concentrated chromic/sulphuric acid solution for ca. 12 h, then rinsing the glassware

several times with doubly-distilled water and finally soaking it in such water for ca. 12 h to leach out any adsorbed residual chromate ions. Prior to use, the cell was rinsed thoroughly with hot pyrolytically-distilled water (see below) and left to stand for ca. 1 h followed by rinsing. The assembled cell was then finally rinsed before filling it with the experimental solution. Between experiments, the cell was filled with fresh, concentrated H_2SO_4 [201].

An identical cleaning procedure was applied to the ancillary glassware used for preparing solutions or for storing doubly and pyrolytically distilled water.

2.5 Pyrolytically-Distilled Water

In the early seventies, it was found difficult, in this laboratory, to prepare pure water of high purity free from organic and other impurities, by means of a regular Barnstead still, as was demonstrated in a significant paper by Conway and co-workers [135]. Although the actual chemical nature of the impurities could not be established, a new method for removing these impurities was developed by "catalytic-pyrodistillation" [10,135]. The principle involved is pyrolysis of organic impurities by passage of the steam from boiling regular distilled water through a silica column at 1023 K in a stream of pre-cleaned oxygen. The hot column contains a closely-packed, 90% Pt - 10% Rh gauze for catalytic oxidation of any organic trace impurities in the water vapour, to gaseous oxidation products (e.g. CO_2, NO_2). The pyrodistillation apparatus is shown in Fig. 2.3 and the details of its construction have been described elsewhere [10,135]. Such purified water was found to be impurity-free as was determined by sensitive cyclic-voltammetry studies of electrochemical surface processes at Pt [10,135] and Au [10,14,44] in this laboratory.

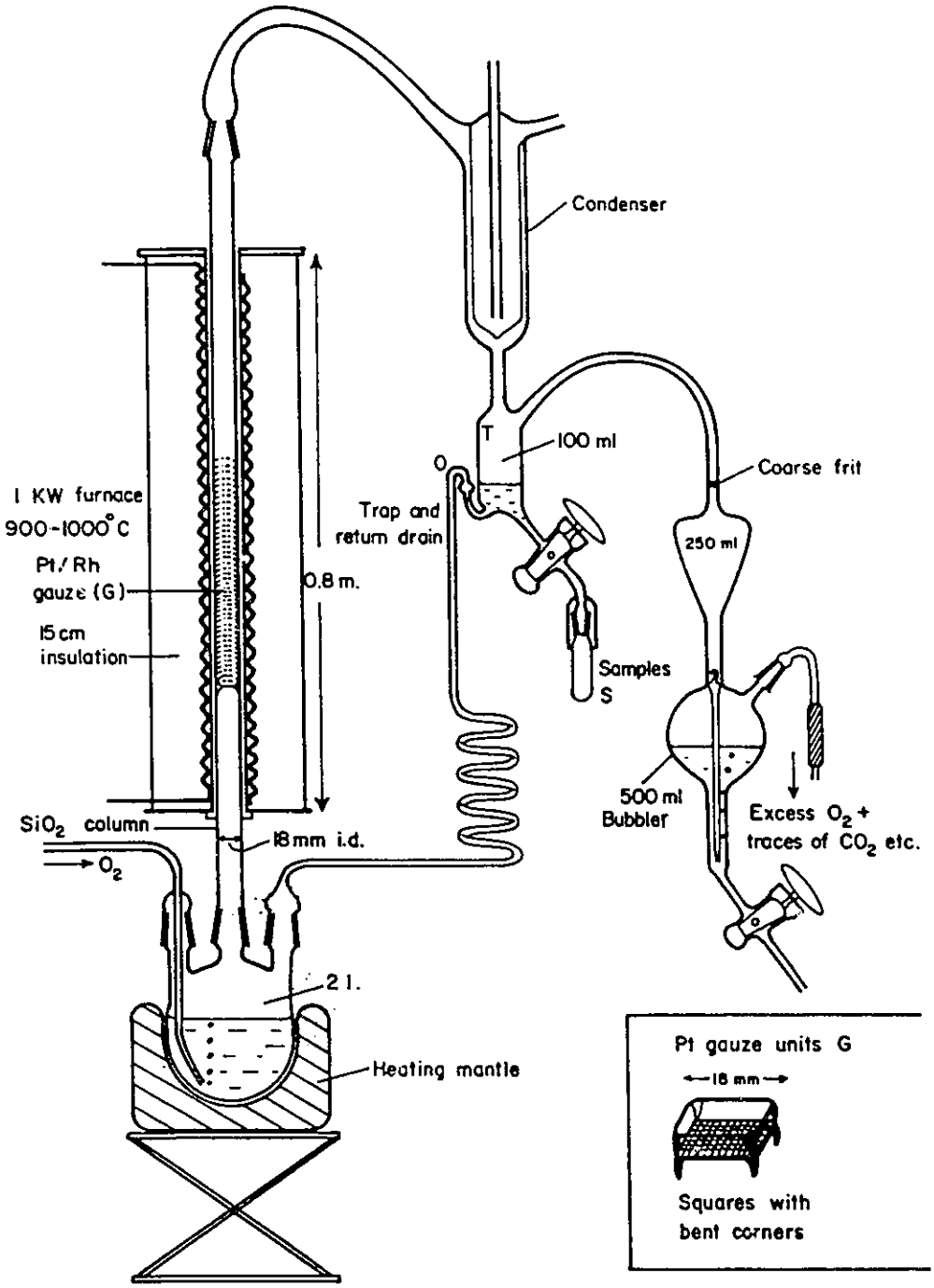

Fig. 2.3 Schematic diagram of pyrolytic distillation unit [135].

2.6 Solutions

The aq. H_2SO_4 solutions were made up from BDH "Aristar" grade conc. H_2SO_4 and pyrolytically-distilled water. The cyclic-votammetry profiles obtained at polycrystalline Pt electrodes were "clean" already after one or two cycles and were in excellent agreement with previous results obtained in this laboratory [10,135] which set a recognized "reference standard" for solution purity for other electrochemical research laboratories world-wide.

2.7 Electrochemical Cell

From previous experience gained in this laboratory with cells of various designs and sizes, it has been realized that a desirable cell should be of a suitably small size and simple design so that it is then much easier to clean and maintain in a clean state.

A conventional small three-compartment cell, as shown in Fig. 2.4, was therefore used. The reference-electrode compartment was separate but it was connected to the working-electrode compartment (main compartment) by a Luggin capillary. The main difference between this cell and most of the others used in this laboratory was provision of an exchangeable tip of the Luggin capillary as shown in Fig. 2.4. This allowed the same cell to be used for both single-crystal and polycrystalline wire electrodes, simply by changing the tip of the Luggin capillary. In each experiment, the tip of the Luggin capillary was adjusted to be close to the working electrode in order to minimize the "IR" drop (see Section 2.2.3) in the solution between the tip of the Luggin capillary and the working electrode. The counter-electrode compartment was isolated from the main compartment by a glass stopcock which could be opened slightly as necessary. The cell was provided with sleeved stopcocks so that during immersion in a thermostat (see

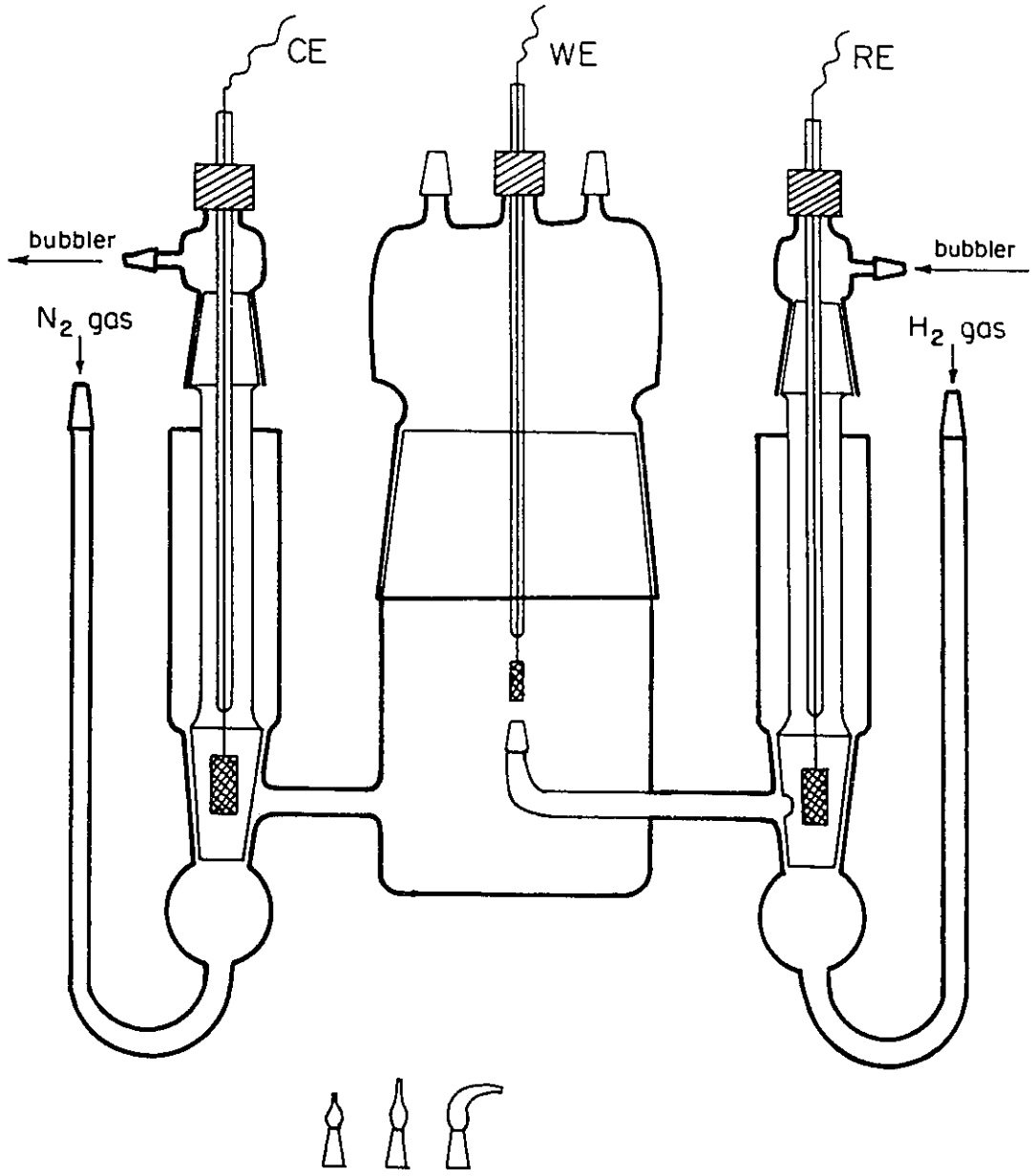

Fig. 2.4 A conventional three-compartment cell used in experiments for single-crystal and polycrystalline wire electrodes.

Section 2.9) no contamination of the test electrolyte with the thermostat fluid could occur.

All the glass components of the cell, prior to its construction and after, were thoroughly cleaned according to the procedure described in Section 2.4. When not in use, the cell was flooded with conc. H_2SO_4 and, prior to measurements, thoroughly rinsed and soaked in doubly- or pyrolytically-distilled water (see Section 2.4).

Solutions in the working-compartment were deoxygenated by bubbling a slow stream of purified N_2 (see Section 2.3). Both N_2 entering the working-electrode compartment and H_2 entering the reference-electrode compartment were pre-saturated with water vapour by passing them through bubblers. This procedure allowed both a constant volume of the solution to be maintained and a constant concentration of the electrolyte.

2.8 Electrodes

2.8.1 Polycrystalline Pt Working Electrodes

Polycrystalline Pt working electrodes were made from pre-annealed Pt wire of 99.99% purity and 0.508 mm in diameter, supplied by Johnson Matthey Inc., New Hampshire, USA. The electrode preparation procedures were: (a) initial "degreasing" of the Pt electrode by refluxing in acetone for 12 h; (b) flame-welding of the Pt electrode to a long piece of Ag wire to provide an electrical contact; (c) "degreasing" in acetone (as described above); (d) cleaning in conc. H_2SO_4 for ca. 12 h; (e) washing in pyrolytically-distilled water followed by soaking for ca. 12 h; (f) sealing into pre-cleaned soft-glass tubing (6 mm diameter) followed by repetitive cleaning as in the steps (c), (d) and (e). Then, the electrode was rinsed with the 0.5 M aq. H_2SO_4 solution and placed in the cell.

When not in use, the Pt electrodes were stored in conc. H_2SO_4 and, before using,

were thoroughly washed and soaked again in pyrolytically-distilled water.

In several experiments, the Pt working electrodes were made from pre-annealed Pt foil of 99.99% purity and 0.05 mm in thickness, supplied also by Johnson Matthey Inc. The Pt foil was pre-cleaned according to the procedure described above and then spot-welded to a Pt wire. Since the electrodes of the spot-welder were made of Cu, the electrode was immersed in aqua-regia for ca. 30 sec to remove any traces of Cu. Subsequently, the Pt foil electrode was cleaned as in the steps (c), (d) and (e).

2.8.2 Single-crystal Pt Working Electrodes

Electrical Connection

The pre-oriented Pt single crystals (Pt(111), Pt(110) and Pt(100)), supplied by Goodfellow, Cambridge, UK, had a cylindrical shape (3mm in diameter, 10 mm in length) and were of 99.999% purity. The electrical connection was made by flame-welding the Pt single crystals to a pre-cleaned Pt wire (99.99% purity, 0.508 mm in diameter) using a pre-formed Au bead of 99.99% purity (see Fig. 2.5). Such a connection was found to be very stable, reliable and non-contaminating, even when the Pt single crystals had to be re-annealed in a high-vacuum at ca. 900°C. EDX mapping, which could detect ca. 1% of Au or less within the surface monolayers, did not show any traces of Au as a result of re-annealing the Pt single crystals with their Au-Pt electrical connections.

Polishing Single Crystals

The Pt single crystals were mounted in a Teflon holder (Fig. 2.6) by means of epoxy resin and polished using, successively, silicon carbide paper of 800, 1000, 1200 and 2400 grades followed by an application of polishing cloths, polishing pastes (normal "N" and fine "F") and a polishing suspension containing 0.06 μ alumina. Such polished surfaces were mirror-like and did not show any scratches. All the above mentioned

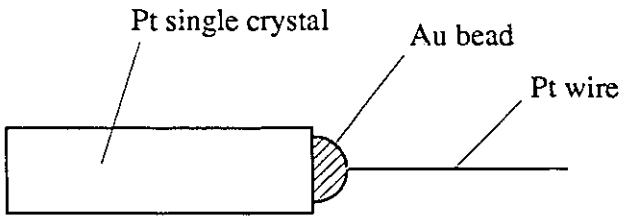

Fig. 2.5 The electrical connection of a Pt single crystal.

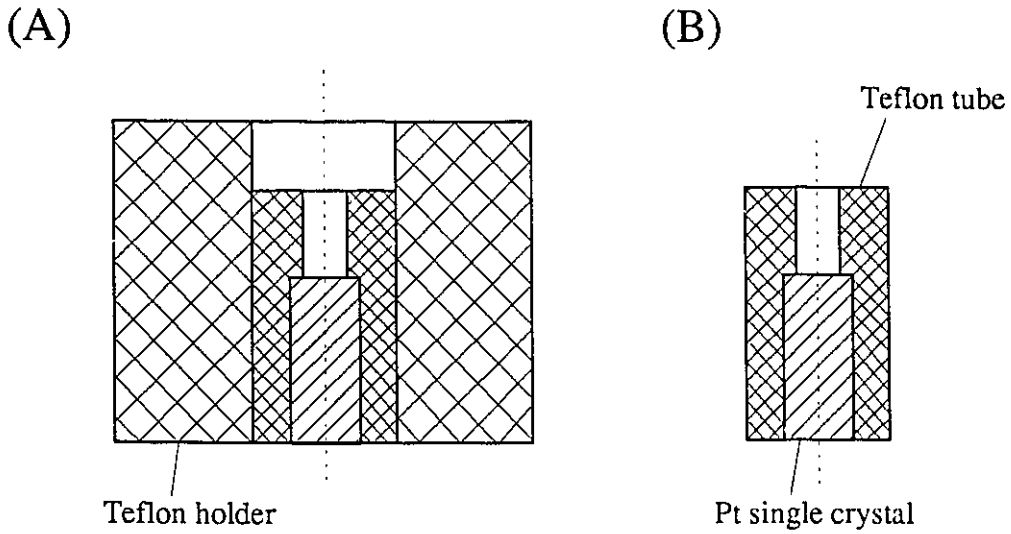

Fig. 2.6 (A) Pt single crystal mounted in a Teflon holder and a tube; (B) Pt single cystal in a Teflon tube.

polishing accessories were supplied by Struers Scientific Instruments, Copenhagen, Denmark.

Determination of Crystallographic Orientation

After polishing, the Pt single crystals were left in small Teflon tubes, but removed from the Teflon holders, and their crystallographic orientation was then checked using the back-reflection Laue method [99,202]. This required: (a) an X-ray generator; (b) a goniometer; (c) a Laue back-reflection camera; (d) a pin-hole collimator; and (e) a film holder. All of the above pieces of equipment were supplied by Enraf Nonius, Delft, Holland. The Diffractis 583 X-ray generator,the pin-hole collimator and the film holder were used as supplied, but the goniometer had to be re-designed to meet the desired requirements [99]. The re-designed goniometer consisted of the single-crystal holder placed in the head of the goniometer as shown in Fig. 2.7. The holder was made of stainless steel and was designed and constructed at the University of Ottawa according to the present author's design; high precision of the machining (±5 μm) allowed the experimental error associated with placing the Pt single crystals in the holder to be minimized, prior to taking back-reflection X-ray patterns.

The X-ray film was placed in a light-proof paper and, successively, in the film holder. The distance between the single-crystal face and the X-ray film was R=3.0 (±0.1) cm. The X-rays were generated using a Cu tube and applying a voltage of 30 kV at a current of 20 mA; the exposure time was 30 min.

Most of the pieces of equipment for single-crystal preparation and orientation were designed according to the requirements and specifications described by Hamelin in ref. 99. This procedure allowed the Pt single crystals to be oriented to within 1°. Also, the channelling patterns of the single crystals were checked using a SEM (see Fig. 2.8).

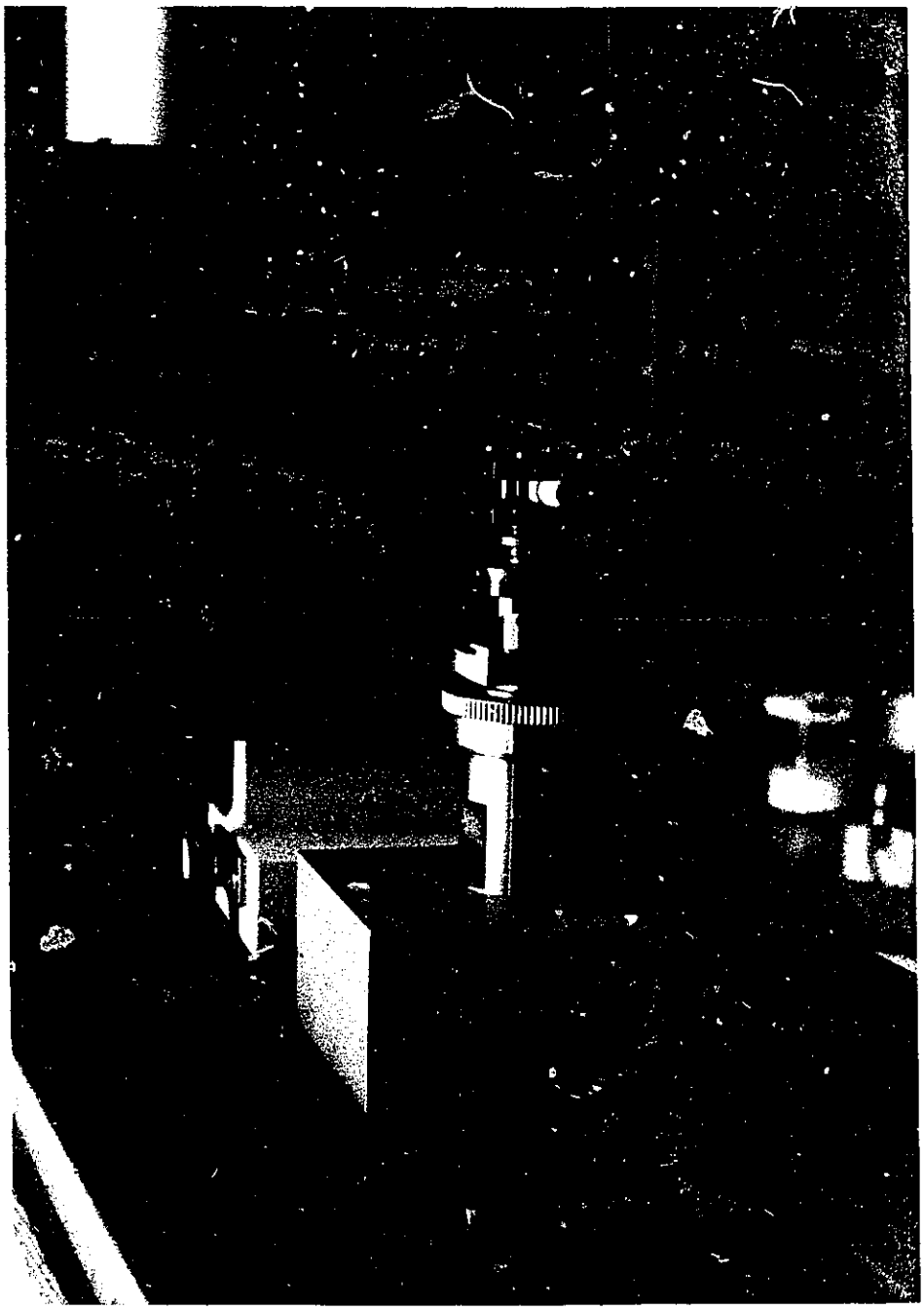

Fig. 2.7 Re-designed goniometer for taking back-reflection X-ray patterns.

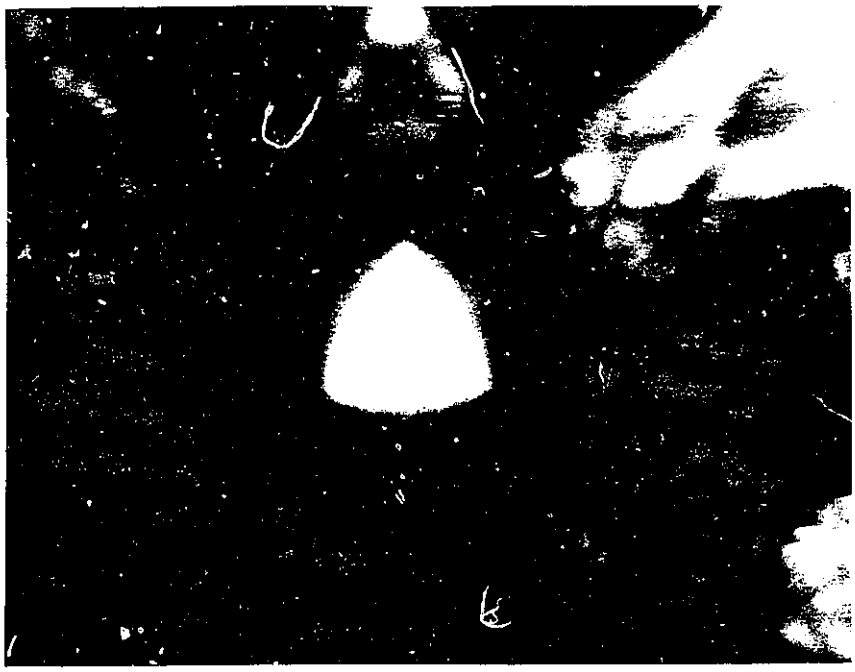

(A)

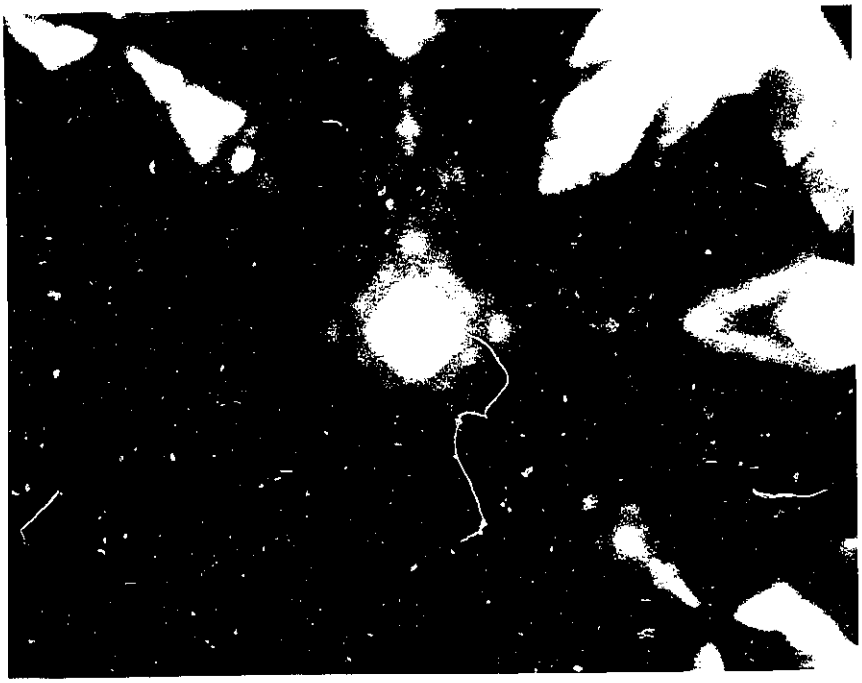

(B)

Fig. 2.8 Channelling patterns of Pt single crystals: (A) Pt(111); and (B) Pt(100).

Reorientation of Single Crystals

In one isolated case, the crystallographic orientation of a Pt single crystal was found to be unsatisfactory (3° off the required orientation) and the single crystal had to be re-oriented according to the following procedure:

1. A gentle (fine), vertical scratch was made on the surface of the crystal still mounted in the goniometer. This was done using a "knife" (Fig. 2.9) specially designed and machined at University of Ottawa; its precision was found to be ± 10 μm.

2. A hole was drilled in a large Teflon holder, which was to accommodate the Pt single crystal placed in a Teflon tube, at the angle required to re-orient the Pt single crystal. This was achieved by using a lathe-like machine (Fig. 2.10), again designed and machined at University of Ottawa. As with the previously mentioned pieces of equipment, the precision of the lathe-like machine was within 10 μm; the drill used and the thermal expansion of Teflon were the major sources of any inaccuracy, but it was still very satisfactory and precise enough to orient the single crystal to within 1°

The proper alignment of the single crystal in the Teflon holder was achieved by matching the fine scratch on the Pt single crystal with the vertical fine scratch on the Teflon holder. Since this step was the second possible source of a significant inaccuracy, the alignment was checked under a 5× magnifying glass.

3. Such a mounted Pt single crystal was polished according to the above procedure and its crystallographic orientation was checked using the back-reflection Laue method and taking a channelling pattern. The orientation was considered satisfactory when it was within 1°.

Final Surface Preparation

The final aim was to have the single-crystal face of interest chemically clean and physically well-defined. This meant removal of epoxy resin, leftovers of polishing pastes, suspension and silicon carbide, as specified by Hamelin [99] and Clavilier [140,147,203].

After having been oriented and polished, the Pt single crystals were removed from

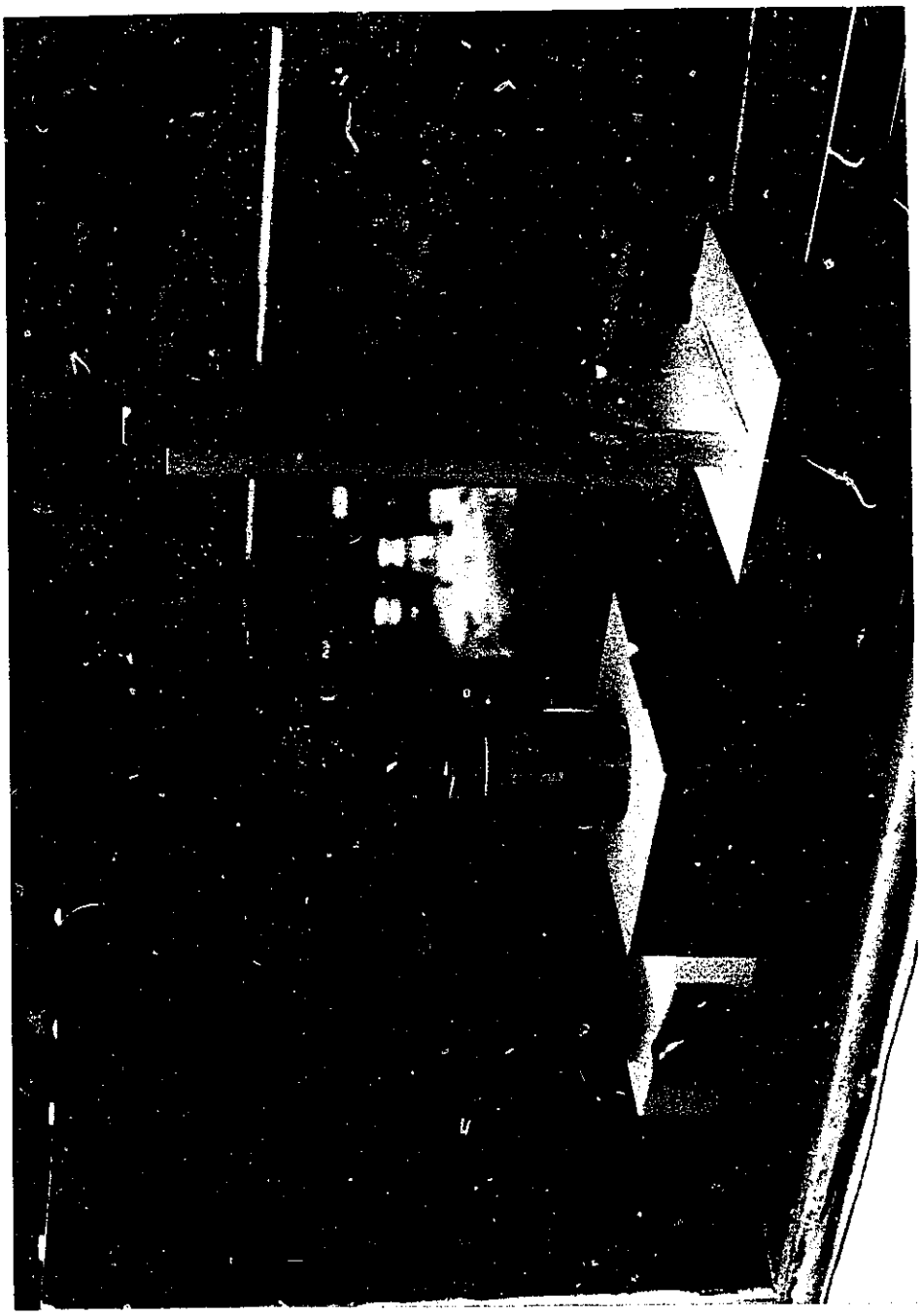

Fig. 2.9 "Knife" for making fine, vertical scratches on single crystals mounted in the head in the goniometer holder.

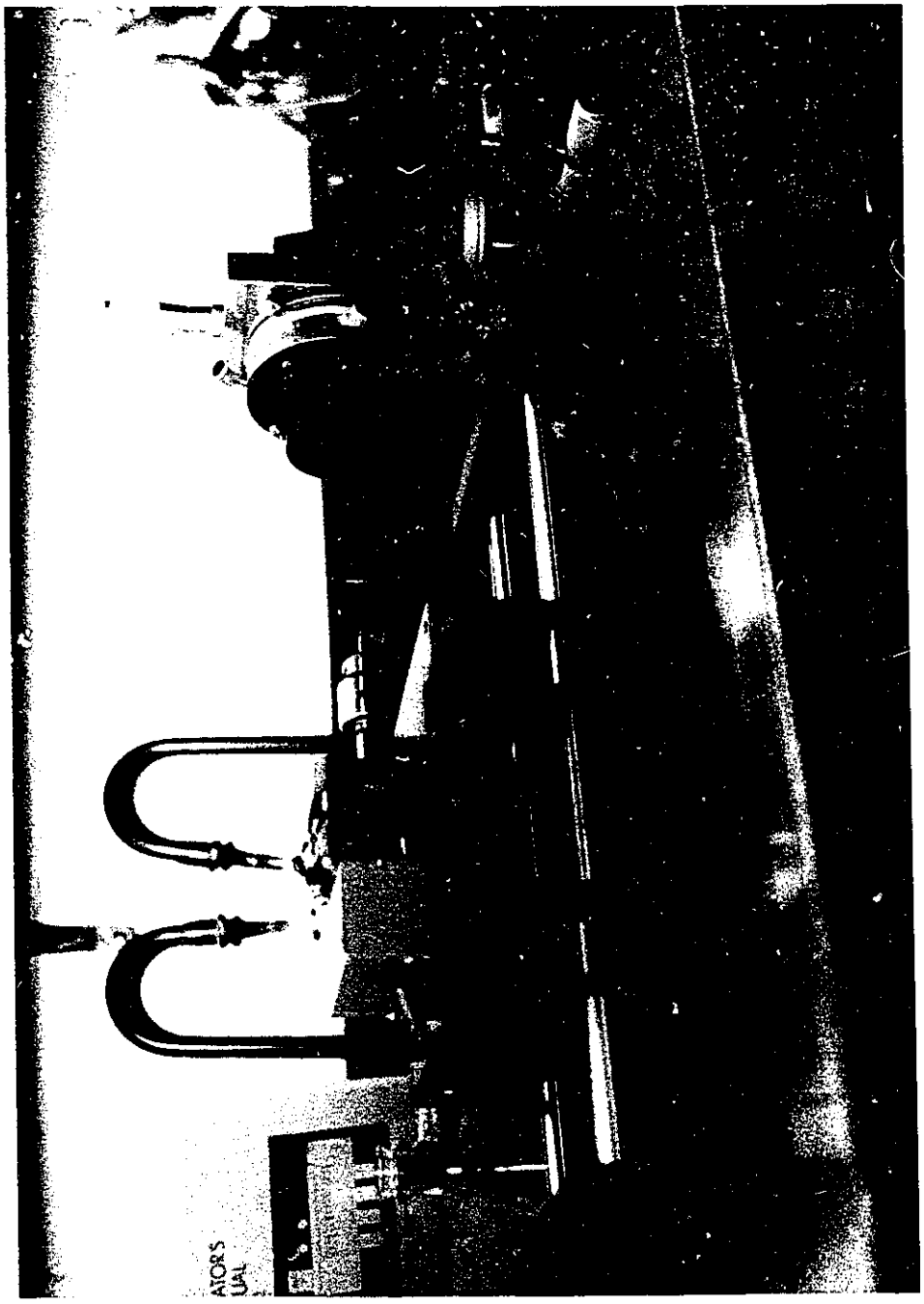

Fig. 2.10 Lathe-like machine for drilling holes at desired angles in Teflon holders.

the Teflon holder and tube, connected to a "regular" Pt electrode (Fig. 2.5) and cleaned in acetone under reflux for 24 h to strip off the epoxy resin. Subsequently, they were etched briefly in hot aqua-regia and rinsed with doubly-distilled water 10 times and soaked overnight. The single crystals were then soaked in conc. H_2SO_4 followed by rinsing 10 times with pyrolytically-distilled water and again soaked overnight. Following this procedure, the Pt single crystals were either annealed in a vacuum of 10^{-5} Torr at 900-920°C for 30 min, followed by slow cooling over at least 4 h or were heated in an hydrogen-oxygen flame to 500, 800 or 1000°C, followed by quenching (the "Clavilier procedure" [140]) in pyrolytically-distilled water in equilibrium with air, depending on the conditions applied. When not in use, the Pt single crystals were stored in conc. H_2SO_4 and thoroughly rinsed and soaked prior to use in further experiments.

Experimental Set-up for Annealing Single Crystals

Annealing of Pt single crystals was conducted using the experimental set-up shown in Fig. 2.11. The major components of the set-up were: (a) a Pyrex-glass vacuum line with high-vacuum stopcocks; (b) a quartz tube; (c) a two-stage mechanical high-vacuum pump (E2M5, Edwards, USA); (d) a vapour-diffusion pump (EO 40/55, Edwards); (e) a Penning gauge head (CP25K, Edwards); (f) a Penning gauge (Penning 8, Edwards); (g) a furnace (type 55035, Lindberg, USA); (h) an induction furnace (E1B2A, ENI Power Systems Inc., USA); (i) a power amplifier (1140LA, ENI Power Systems Inc.); (j) a function generator (130, Wavetek, USA); (k) a "getter" made of quartz and filled with charcoal [38]; and (l) a "getter" heater. All the glass or quartz components of the high-vacuum experimental set-up were cleaned prior to the construction according to the procedure described in Section 2.4. After construction, the glass components were baked at ca. 200°C in a vacuum of 10^{-4} Torr to desorb adsorbed gases and moisture. The quartz tube in the furnace was baked at ca. 1000°C for 1 h also to desorb adsorbed gases and moisture, and to burn any traces of impurities. Pt single crystals, which had to be

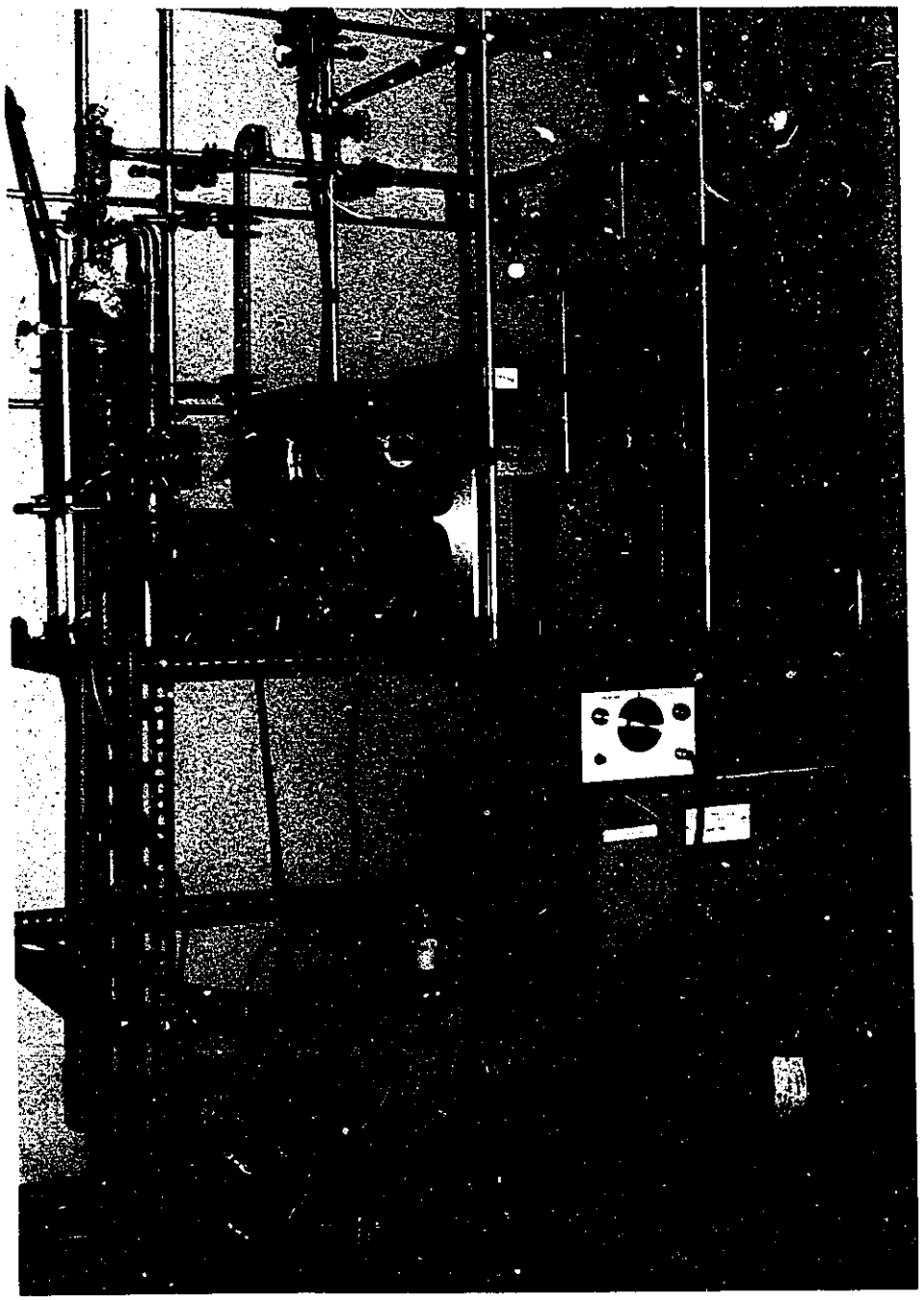

Fig. 2.11 Experimental set-up for annealing Pt single crystals in vacuum.

annealed, were placed in a pre-cleaned boat-shaped sample holder made of quartz. No silica was detected on the surface of Pt single crystals as a result of annealing in the quartz tube, as was revealed by EDX analysis.

2.8.3 Hydrogen Reference Electrode

Potentials of the working electrodes were referred to that of a platinized Pt hydrogen reference electrode (RHE) immersed in the same solution as that under study. The reference electrode was made of Pt gauze of 99.99% purity and 100 mesh, supplied by Johnson Matthey Inc. The Pt gauze was pre-cleaned as described in Section 2.7.1 and spot-welded to a Pt wire electrode. Trace amounts of Cu from the electrodes of the spot-welder were removed by immersing the electrode in fresh aqua-regia for ca. 30 sec. The further cleaning procedure applied was the same as that described in Section 2.7.1. Platinization of the Pt gauze was conducted according to the procedure given by Ives and Janz [205] using a 2% H_2PtCl_6 solution in 2 N HCl. The potential of the reference electrode was found to be very stable; when not in use, the electrode was stored under pyrolytically-distilled water in a closed vial to prevent deactivation by dehydration or by adsorption of impurities from the atmosphere.

2.8.4 Counter Electrode

A platinized Pt gauze, having a large surface area and prepared in the same manner as the reference electrode, was used as the counter electrode and was set in a separate compartment of the electrochemical cell. The large surface area minimized the Faradaic resistance of the hydrogen or oxygen evolution reactions occurring at the counter electrode during polarization experiments. Location of the counter electrode in a separate compartment in which N_2 was bubbled prevented significant migration of the gases (H_2 or O_2) evolved at its surface to the main compartment of the cell.

2.9 Temperature Control

2.9.1 Solution in the Electrochemical Cell

For experiments conducted above room temperature (298 K < T < 348 K), the electrochemical cell was placed in a large water-bath where the temperature could be controlled to ± 0.5 K by means of an Haake E3 circulating water heater. The level of the electrolyte in the electrochemical cell was kept below that of the thermostated fluid; the reference electrode was, in this case, at the same temperature as the working electrode, so that no thermal liquid-junction was involved.

In experiments where thick-oxide films were grown at elevated temperatures but reduced at room temperature, the electrochemical cell was removed from the water-bath and a stream of air was blown at it using a hair-dryer. The temperature inside the cell was monitored by means of a pre-cleaned mercury thermometer which was immersed in the test solution in the main compartment of the cell. This procedure was combined with the outgassing procedure and, though very simple, was found to be more than satisfactory.

2.9.2 Pt Electrodes During Thermal Pretreatment

The temperature of Pt electrodes, while being annealed, was controlled by means of a thermocouple built into the furnace. It allowed the temperature to be monitored with an accuracy of 10°C.

During the heating and quenching procedure, the temperature was monitored by means of an optical pyrometer. Such temperature readings were reliable to ±20°C. However, the exact temperature directly prior to quenching could not be precisely determined, since transfer via air to a beaker with pyrolytically-distilled water unavoidably resulted in some cooling the Pt electrode even though the transfer took only 1-3 sec. It should be mentioned that the accuracy of the optical pyrometer is 1-3°C, depending on the temperature range, but the manual handling of the Pt electrodes in the

hydrogen-oxygen flame decreases the exact temperature readings, hence the inaccuracy of 20°C. This procedure could be improved by using an IR-sensitive camera which could record the Pt electrode's temperature directly following its removal from the H_2/O_2 flame to its immersion in pyrolytically-distilled water. (Such a camera is not available in our laboratory.)

2.10 Determination of Real Surface Area of the Pt Electrodes

2.10.1 Polycrystalline Pt Electrodes

The real surface area of polycrystalline Pt electrodes was easily determined, in the usual way, from the measurable accommodation for the under-potentially deposited H species (H UPD) by taking 210 $\mu C\ cm^{-2}$ as the charge density for monolayer H deposition [25,76].

2.10.2 Single-Crystal Pt Electrodes

The Pt single-crystal surfaces had been highly polished to a mirror-like finish so that their roughness factors, R, could be assumed to be virtually equal to unity (R=1), i.e. the real surface area could be assumed to be equivalent to the geometric area. The respective diameters of the circular surfaces of the three single crystals were determined using a Vernier Microscope No. 13 (The Precision Tool and Instrument Co. Ltd., England) with an accuracy of 0.001 cm. The diameter of each Pt single crystal was measured five times and the average was determined. Such evaluated surface areas were:

Pt(111) 0.08951(±0.0050) cm^2;

Pt(110) 0.07059(±0.0050) cm^2;

Pt(100) 0.06281(±0.0050) cm^2.

CHAPTER 3

Results and Discussion

3.1 Characterization of Polycrystalline Pt Electrodes

Electrode preparation which involves thermal and/or electrochemical pretreatment is essential in studies of oxide film growth at (polycrystalline) Pt. As was discussed in Section 1.11.1 of the Introduction, in early work on oxide growth at Pt, it was thought that formation of the oxide film tended to a limit of ca. 2.6 O atoms per Pt atom [25], said to be a "monolayer" but obviously not. This conclusion was based on investigation of oxide growth on Pt electrodes prepared from Pt gauze, which had been aged by cycling (up to 350 cycles) between 0.05 and 1.54 V, RHE. Similar results were found for Pt/Pt black electrodes [25]. In later work, thick, quasi 3-d oxide films were grown on Pt electrodes which had been pretreated with emery paper [33-35] and it was thought that only on such mechanically disturbed (pretreated) Pt electrodes could thick-oxide films be grown. Lack of reproducibility of experimental results found by different researchers is the most striking feature of the results reported in the earlier literature (see refs. 25-35 and Section 1.11.1 of the Introduction).

In the work reported here, the final stages of preparation of polycrystalline Pt electrodes were: (a) flame-annealing, followed by slow or fast cooling; and (b) cycling between 0.05 and 1.40 V, RHE, at a sweep rate of $s = 50\ mV\ s^{-1}$. Fast cooling was achieved by placing a Pt electrode in a stream of ultra-high-pure N_2 or by immediate immersion of a hot (ca. 500°C to ca. 1000°C; see Section 3.3.1) Pt electrode in pyrolytically-distilled water. The latter procedure is referred to as quenching.

3.1.1 Flame-annealed Polycrystalline Pt Electrodes

Polycrystalline Pt electrodes were characterized quantitatively by recording the i vs E C-V profiles between 0.05 and 1.40 V, RHE, and by measuring the real surface area by determining the UPD H accommodation, taking 210 $\mu C\ cm^{-2}$ as the charge density for monolayer H deposition [25,76]. This allowed changes in the roughness factor, R, of the electrode to be determined in the course of various electrochemical treatments of the electrode. Qualitative characterization was made by measuring the ratios of the principal peak currents, i_{HA1}/i_{HA2} and i_{HC1}/i_{HC2}, in the UPD H region (see ref. 9 for significance of these peak designations and Fig. 1.3, p.13) which gives a characteristic indication of any reconstruction of the surface.

Fig. 3.1(a) shows the 5th C-V profile after annealing the Pt electrode in an H_2/O_2 flame at ca. 900°C followed by slow cooling. The ratio i_{HA1}/i_{HA2} was 2.06 while i_{HC1}/i_{HC2} was 2.52; the value of the real/apparent area ratio, R, was 1.23. Fig. 3.1(b) shows C-V profiles after 1, 3 and 20 h of cycling up to 1.40 V, RHE. Arrows indicate directions of changes in the i vs E C-V profiles. The dominant features are: (a) a decrease of the HA1 peak and increase of the HA2 ; (b) a decrease of the HC1 peak and increase of HC2; and (c) an increase of the real surface area (R=1.38 after 20 h of cycling). Fig. 3.1(c) shows C-V profiles after 30, 47, 92, 125 and 174 h of cycling. Similarly, the ratios i_{HA1}/i_{HA2} and i_{HC1}/i_{HC2} decrease and the real surface area increases; the value of R after 174 h of cycling is 1.59. Fig. 3.1(d) shows the C-V profile after prolonged (174 h) cycling (see Table 3.1).

Oxidation of such a pretreated Pt electrode, on which up to 50 monolayers of equivalent "O" could be formed, followed by the oxide reduction always results in a surface region which is highly disordered or porous (see Table 3.1 and Fig. 3.2) and having a high R value. Upon subsequent anodic polarization, the surface undergoes oxidation much faster and gives an oxide film having different properties from those of the film formed initially on the "well-cycled" Pt electrode. However, in the present work, it

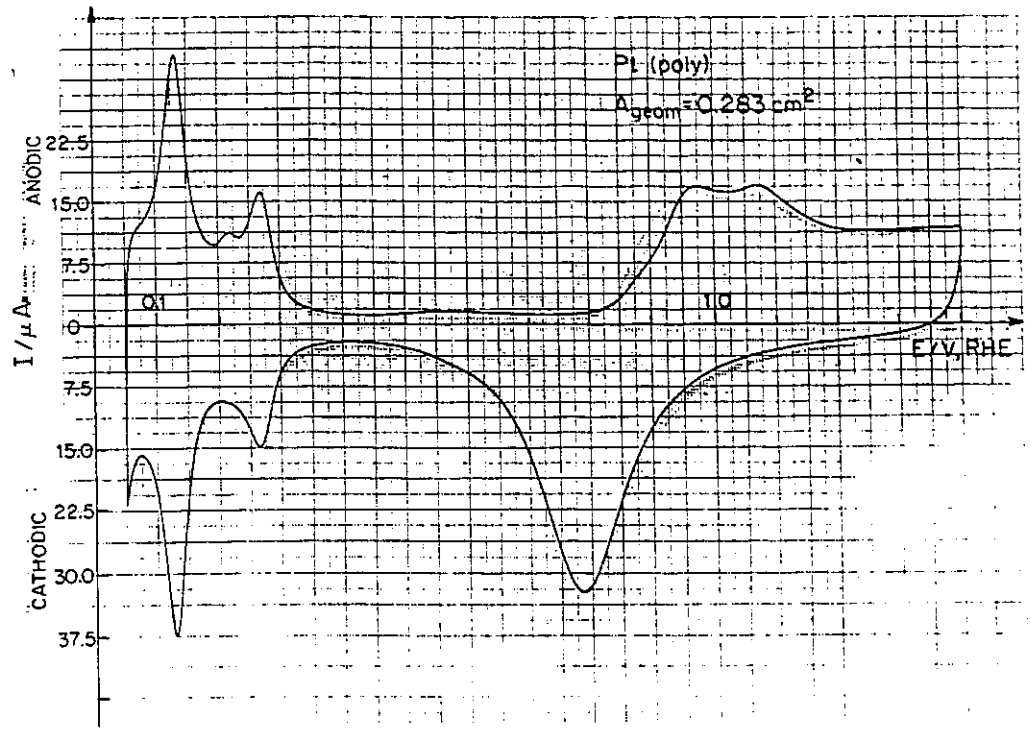

Fig. 3.1 (a) The 5th C-V profile after annealing the Pt electrode in an H_2/O_2 flame at ca. 900 °C followed by slow cooling (0.5 M aq. H_2SO_4, 298 K).

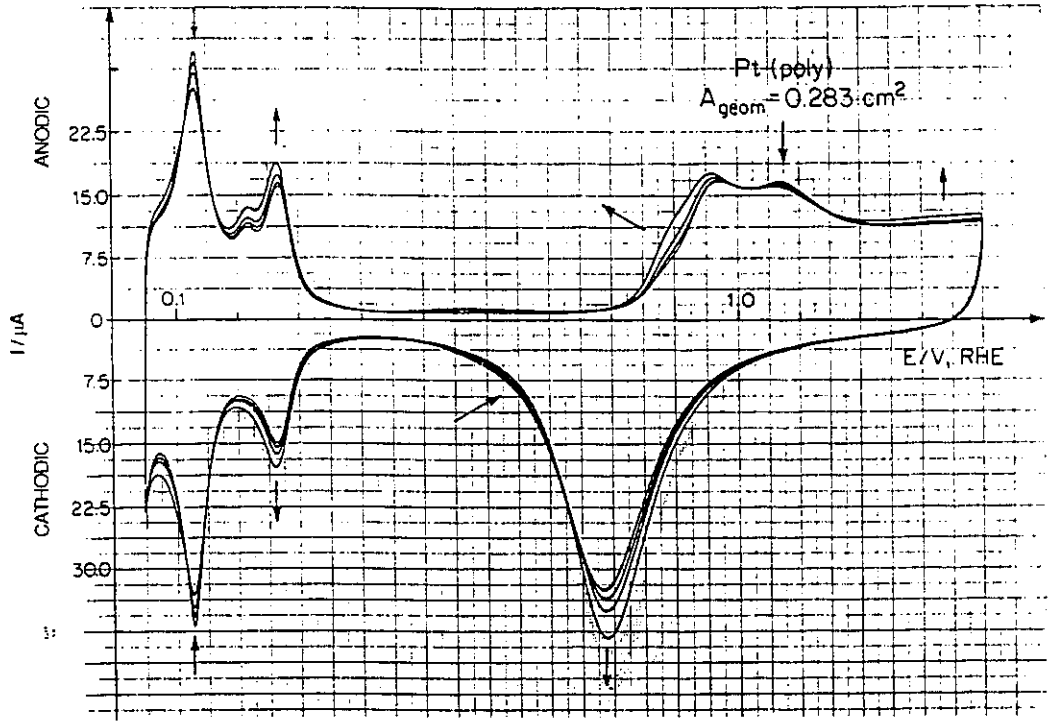

Fig. 3.1 (b) C-V profiles for the Pt electrode after 1, 3 and 20 h of cycling up to 1.40 V, RHE (0.5 M aq. H_2SO_4, 298 K).

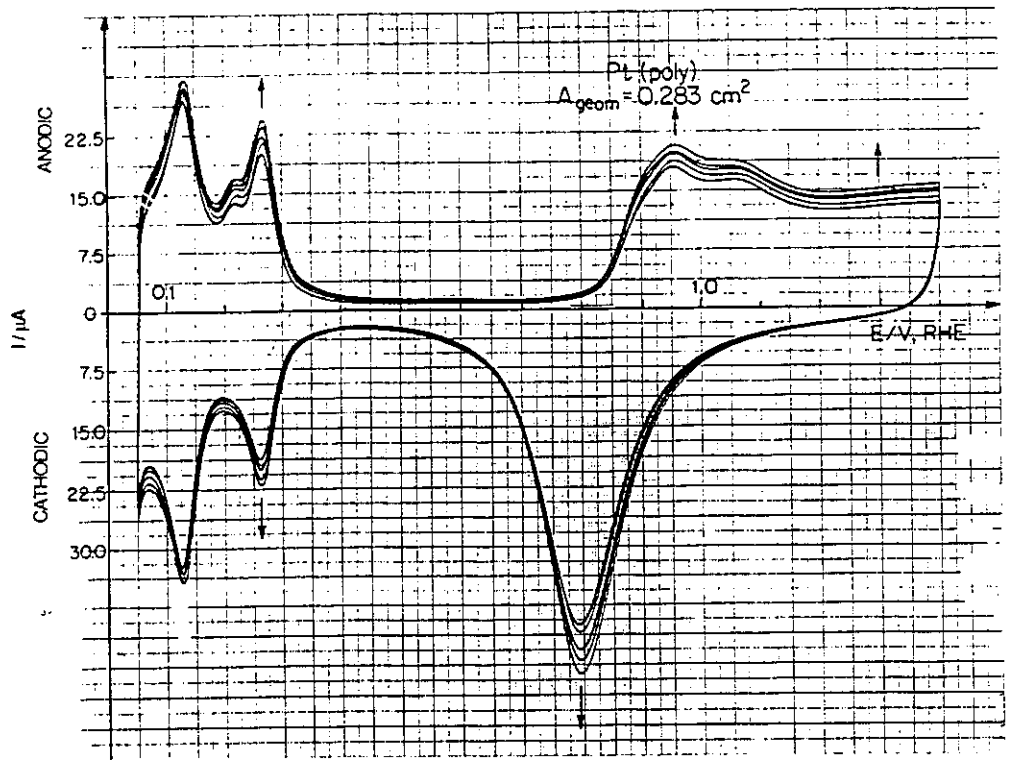

Fig. 3.1 (c) C-V profiles after 30, 47, 92, 125 and 174 h of cycling up to 1.40 V, RHE (0.5 M aq. H_2SO_4, 298 K).

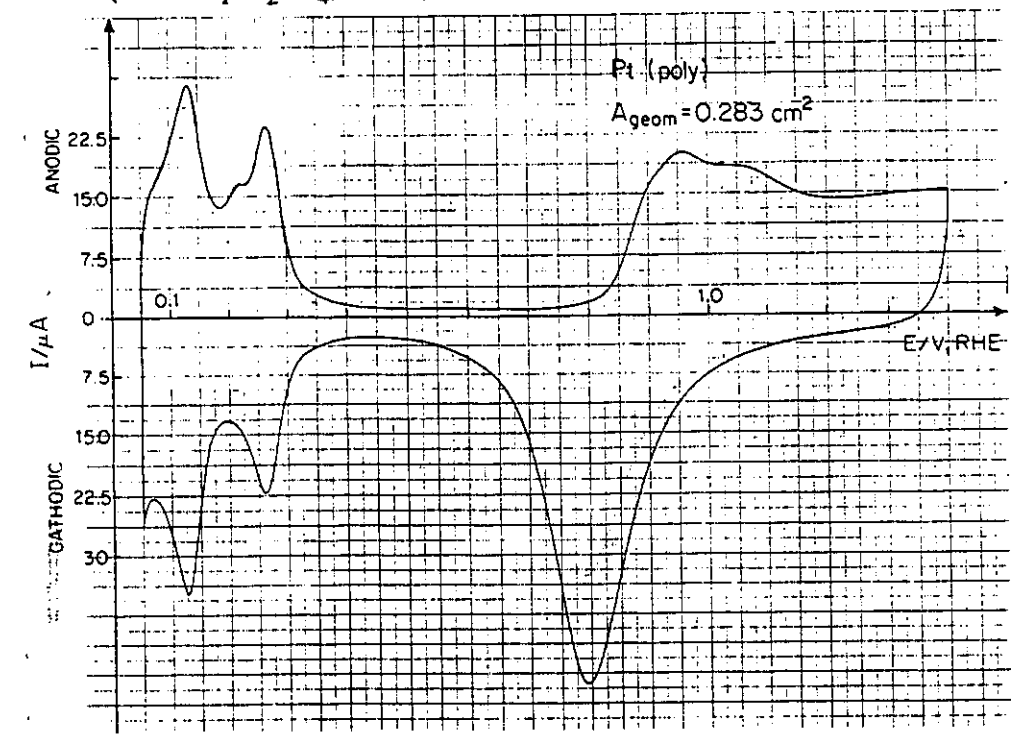

Fig. 3.1 (d) C-V profile after cycling for 174 h up to 1.40 V, RHE (0.5 M aq. H_2SO_4, 298 K).

Table 3.1 Real/Apparent Area Ratios (R), Currents and Changes of UPD H Profiles due to Changes of Crystallographic Orientation upon Cycling and Thick Oxide-film Formation

Electrode Description	i_{HA1} / i_{HA2}	i_{HC1} / i_{HC2}	R	Features
Fresh Pt electrode surface, prior to film growth and cycling	2.06	2.52	1.23	Regular anodic/cathodic i vs E profile
Electrode cycled for 174 h between 0.05 and 1.4 V, RHE ("electrochemically annealed")	1.21	1.56	1.59	Small changes in anodic and cathodic i vs E profiles
Pt electrode after multiple oxidation/reduction, followed by prolonged cycling	1.06	1.32	1.87	Small changes in distribution of currents in the UPD H profiles
Pt electrode after extended oxide growth and reduction, but before surface regeneration (2.1 V for 12 h; yellow oxide)	1.11	1.92	2.64	Distribution of currents in H UPD profiles changes significantly
Pt electrode after extended oxide growth and reduction but before surface regeneration (2.0 V for 48 h; brown oxide)	1.16	1.76	5.18	Distribution of currents in H UPD profiles changes significantly

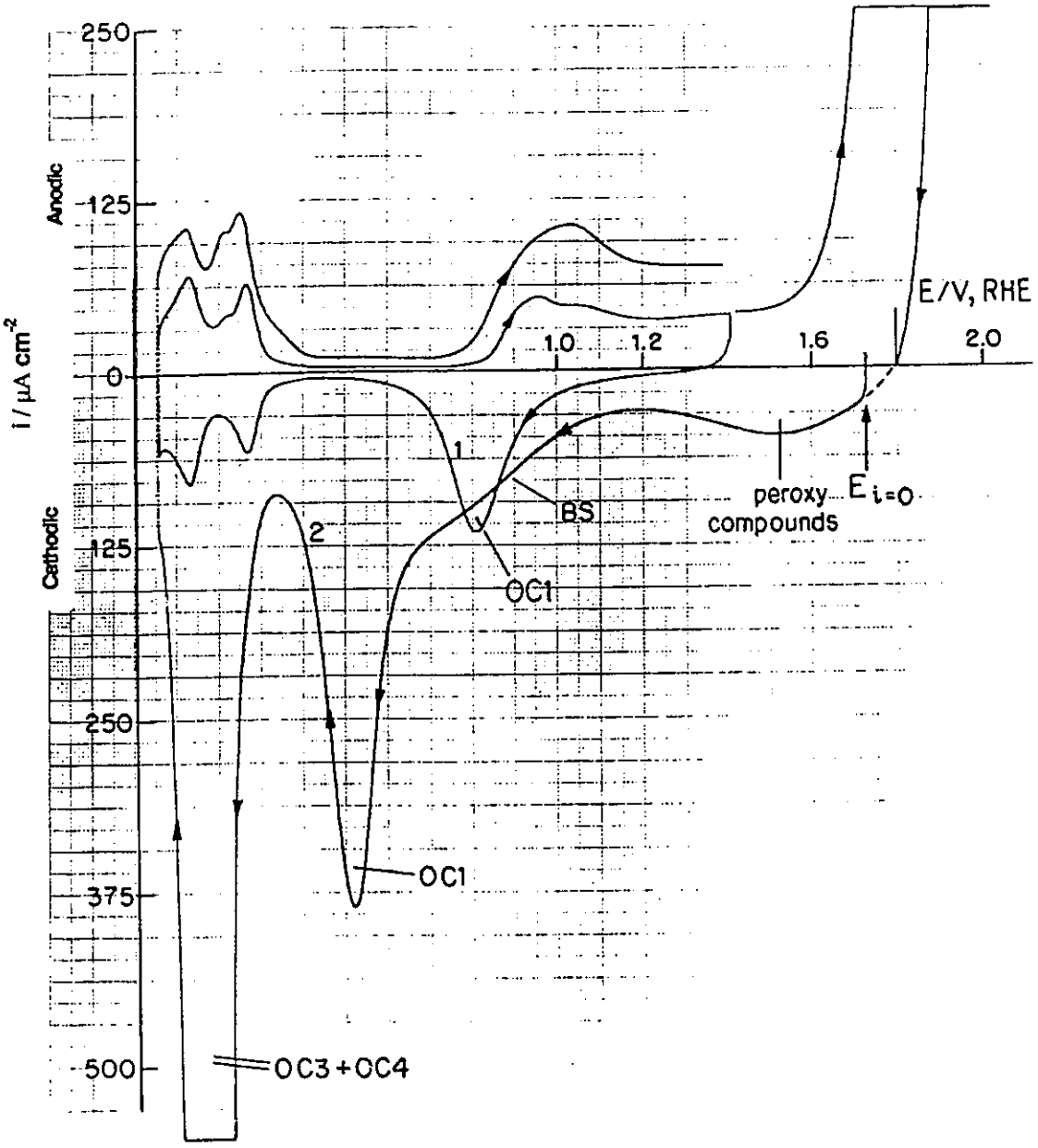

Fig. 3.2 C-V profiles for a Pt electrode in 0.5 M aq. H_2SO_4 at 298 K. (1) Original profile between 0.05 and 1.40 V, RHE. (2) Profile after oxide formation at 2.0 V, RHE, for 24 h, and reduction having a highly disordered and rough surface.

was found that after reduction of a thick oxide film resulting in an observably large increase in R, the state of the Pt surface could be returned both qualitatively and quantitatively to the initial one [9,206] by prolonged cycling between 0.05 and 1.40 V, RHE. Then a following oxidation on that surface reproduces almost exactly the behaviour of the initial surface of the polycrystalline Pt. This behaviour is the result of an "electrochemical annealing" effect (see Section 3.1.3) and cannot be due to dissolution and redeposition of Pt since: (a) it arises with undiminished efficiency when cycling is conducted in a N_2-stirred, large volume of solution; and (b) even more importantly, exchange of the "old" solution, right after the oxide reduction, for a "fresh" solution of the same concentration does not affect the C-V profiles at all.

3.1.2 "Quenched" Polycrystalline Pt Electrodes

In this procedure, the Pt electrode was heated in an H_2/O_2 flame to redness (ca. 900°C) and quenched in pyrolytically-distilled water when its temperature reached ca. 500-600°C. The quenching procedure was applied for four reasons: (a) to investigate surface-structural changes of the electrode, by means of the C-V technique upon prolonged cycling between 0.05 and 1.40 V, RHE, and to compare the C-V behaviour with the C-V profiles of the "flame-annealed" Pt electrodes; (b) to examine reproducibility of experimental results on "quenched" Pt electrodes; (c) to examine oxidizability of such electrodes and compare it with that of the "flame-annealed" Pt electrode; and (d) to examine how such a drastic pretreatment as heating to ca. 900°C, followed by quenching, may affect the C-V profiles of polycrystalline Pt and to relate such experimental data to results obtained (see later, Sections 3.3 and 3.4) at low-index surfaces of single-crystal Pt electrodes.

Since drastic (heating and quenching) thermal pretreatment of Pt electrodes might be "geometry-sensitive", i.e. results might depend on the shape of the Pt electrode, experiments were done using both Pt-wire and Pt-sheet electrodes. Interestingly, results

obtained were the same in both cases and did not depend on the physical shape of the electrode under investigation (but see Section 3.3 on single-crystal electrodes).

Fig. 3.1(d) shows a C-V profile of a polycrystalline Pt electrode prior to the thermal pretreatment. The electrode was cycled for 174 h and R was 1.57. Fig. 3.3(a) shows the profiles of the first 3 cycles between 0.05 and 0.80 V, RHE, after quenching the electrode. It reveals several interesting features: (a) absence of the HA3 peak; (b) sharpness and large height of the HA2 and HC2 peaks; (c) both the anodic and cathodic parts of the "butterfly" region are very symmetrical and are literally mirror images; and (d) the C-V profile reveals a hump between 0.3 and 0.4 V, RHE, previously noticed by Clavilier and Armand [143]; it will be discussed later in Section 3.1.4. R for such a pretreated electrode was 1.21. Fig. 3.3(b) shows the cyclic-voltammograms after increasing the upper-potential limit from 0.80 to 1.40 V, RHE. The following changes in the C-V profiles can be recognized: (a) the sharpness of the HA2 and HC2 peaks disappears right after the first sweep up to 1.40 V, RHE; (b) the HA3 peak appears and increases with further cycling up to 1.40 V, RHE, while currents in the HA2 and HC2 peaks decrease; (c) the HA1 and HC1 peaks undergo more complex changes which involve an initial increase, followed by a decrease; (d) the oxide region undergoes changes as indicated by the arrows on Fig. 3.3(b); (e) the hump between 0.3 and 0.4 V, RHE, disappears upon cycling; and (f) R increases upon cycling and tends to a "final" value of ca. 1.59 ± 0.03. The quantitative and qualitative changes in the C-V profiles, as a result of heating and quenching followed by cycling, are summarized in Table 3.2.

3.1.3 "Electrochemical Annealing"

It was mentioned earlier (see Table 3.1) that after reduction of a thick-oxide film, the resulting polycrystalline Pt surface can have its real surface area as large as 3.25 times its initial value. From the first positive-going C-V profile after oxide reduction (Fig. 3.2), it can be seen that the UPD H accommodation is also qualitatively different. Interestingly,

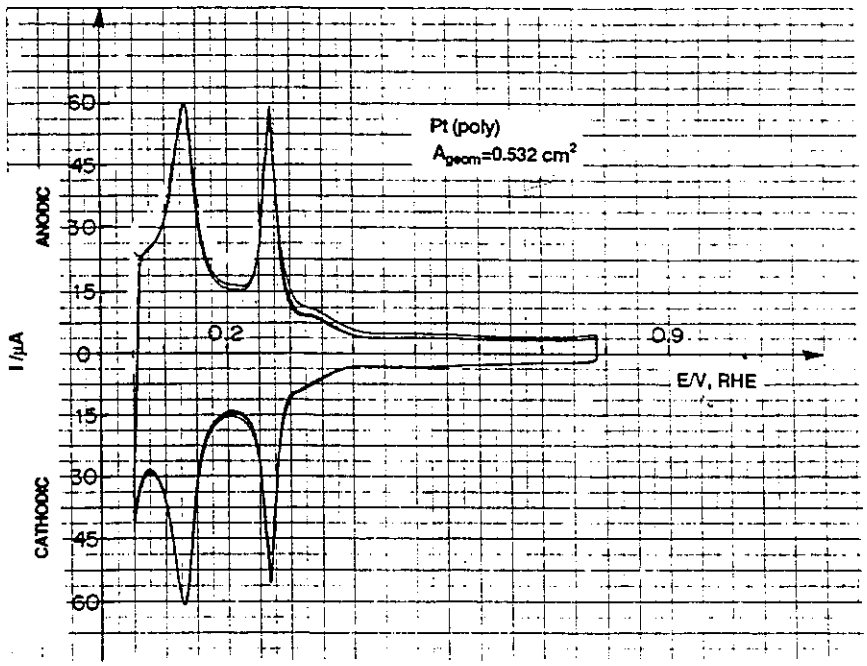

Fig. 3.3 (a) The first three H UPD C-V profiles for a Pt electrode in 0.5 M aq. H_2SO_4 at 298 K after heating in an H_2/O_2 flame followed by quenching.

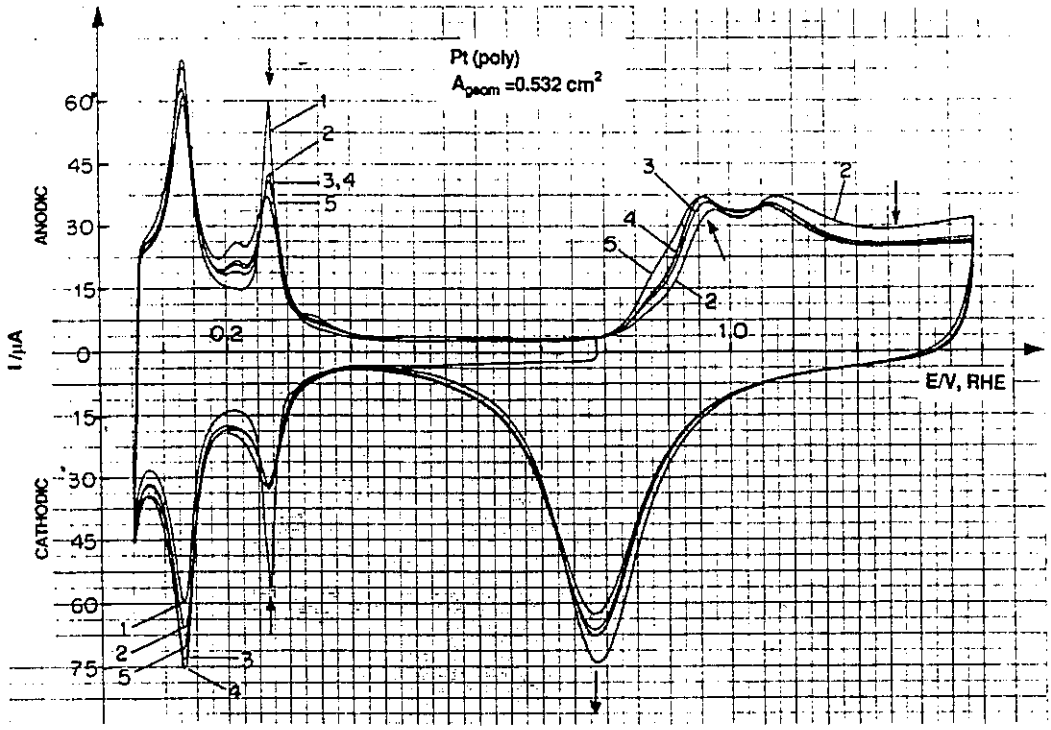

Fig. 3.3 (b) C-V profiles of a Pt electrode in 0.5 M aq. H_2SO_4 at 298 K after increasing the upper-potential limit from 0.80 to 1.40 V, RHE; Curve (1) up to 0.80 V; (2) 1st profile up to 1.40 V; (3) 3rd; (4) 10th; and (5) 200th.

Table 3.2 Real/Apparent Area Ratios (R), Currents and Changes of UPD H Profiles due to Changes of Surface Crystallographic Geometry upon Cycling

Electrode Description	i_{HA1} / i_{HA2}	i_{HC1} / i_{HC2}	R	Features
Electrode cycled for 48 h between 0.05 and 1.40 V, RHE, ("electrochemically annealed")	1.14	1.54	1.57	Regular anodic/cathodic i vs E profile (see ref. 9)
Electrode after heating and quenching, and prior to cycling into the oxide region	1.03	1.08	1.21	No HA3 peak; the HA2 and HC3 peaks are very sharp; hump between 0.3 and 0.4 V, RHE
Electrode after cycling into the oxide region	between 1.61 and 1.65	between 1.90 and 2.15	increases from 1.21 to 1.44	The HA3 peak appears; the sharpness of HA2 and HC2 disappears after the first cycle into the oxide region; the hump gradually diminishes; qualitative changes in both H UPD and the oxide region
Electrode cycles between 0.05 and 1.40 V, RHE, for 24 h after heating and quenching	1.28	1.67	1.53	The HA3 peak further increases in size; the C-V profile is similar to the one for a "well-cycled" Pt electrode

such a surface having substantially increased area can be qualitatively and quantitatively returned to its initial state by repetitive anodic/cathodic cycling at $s = 50\ mV\ s^{-1}$ between 0.05 and 1.40 V, RHE, for 12-24 h, depending on the extent of previous formation of the oxide film [206]. In general, the thicker the oxide film, the longer is the cycling time required to return the surface to its initial state. The "electrochemical annealing" must arise from reconstruction of a "high-energy", high area, surface that is left after reduction of the thick-oxide film, to a low-energy surface.

The high-energy surface is evidently microcrystalline [207], not amorphous, since the characteristic multiple states of H chemisorption are still clearly resolvable [9,207], though not in the same distribution as that for the original surface.

The surface resulting from quenching a polycrystalline Pt electrode has a real surface area smaller than that arising after prolonged cycling between 0.05 and 1.40 V, RHE (see Table 3.2). However, prolonged cycling results in qualitative and quantitative regeneration of the initial surface.

An obvious and important question arises whether the thermal and electrochemical pretreatment involves recrystallization of grains to form new ones and/or restructuring of grain surfaces.

It is well known that, for instance, thermal pretreatment of a carbon steel may change the size of grains, their chemical composition, and in this way affect its mechanical and physico-chemical properties [208-210], by transition between different phases. However, no different phases of Pt can arise in 99.99% purity material. Investigation by means of SEM did not reveal any significant changes in the mean size of grains as a result of thermal pretreatment. This phenomenon must, then, be explained in terms of restructuring of grain surfaces. In the surface layers, the reconstruction takes place through the formation and reduction of the quasi-2-d oxide which proceeds through the place-exchange mechanism [9,48,68]. The surface reconstruction releases stress from the outermost surface layer of the Pt electrode and slowly progresses in depth, also

releasing stress from the grain boundaries by restructuring in the Pt bulk, just below the surface layer. This proposed mechanism can explain why the C-V profiles for the thermally annealed Pt electrodes are qualitatively and quantitatively similar to those for the "electrochemically annealed" Pt electrodes, despite their previous quenching which, supposedly, introduced much stress and cold-work.

3.1.4 Calculations of the Roughness Factor of Polycrystalline Pt Electrodes: Introduction of the Micro-roughness Factor, R_m

Polycrystalline Pt electrodes, which are usually made from a wire or a foil exhibit non-uniformities in the form of scratches, depressions, etc. This non-uniformity is responsible for the electrode roughness, usually expressed as R. R is defined as the ratio between the real surface area and the geometric (apparent) surface area (which takes into account only the overall geometric dimensions, such as length, diameter, etc.). As shown in Sections 3.1.1 and 3.1.2, the H UPD profiles change drastically after thermal pretreatment or thick oxide formation-reduction, giving rise to new surfaces of different H UPD accommodation (different surface area). Since the grain size, scratches, depressions and the like do not undergo any significant changes (see Section 3.1.3), then the variations in UPD H accommodation must be explained in terms of micro-changes occurring on the electrode surface, as already suggested.

It is proposed that the micro-changes occurring on the electrode surface (i.e. formation of shorter terraces, more frequent steps, etc.) be characterized by a "micro-roughness factor", R_m, and the overall roughness of the electrode by the total roughness factor, R_t, where we define

$$R_t = R_1 \cdot R_m \tag{3.1}$$

and $R_1 \equiv R$, the commonly employed roughness factor. The following problem serves as a

good way of showing how the values of R_t, R_1 and R_m can be calculated and also how they can be related to the electrode's history, e.g., after thermal and/or electrochemical pretreatment.

PROBLEM:

(a) The UPD H accommodation of a polycrystalline Pt electrode after cycling for 48 h is found to be 169 μC and its geometric surface area 0.509 cm^2. Find the real surface area and the macro-roughness factors.

(b) The UPD H accommodation of the same electrode after heating and quenching is found to be 133.5 μC. Express the difference in terms of R_m. Find R_t.

(c) The UPD H accommodation right after reduction of a thick oxide, grown on the same electrode, is 358.0 μC. Express the difference in terms of R_m. Find R_t.

SOLUTION:

(a) The real surface area, A_r:

$$A_r = \frac{Q_{measured}}{Q_1} = \frac{169}{210} = 0.805 \text{ cm}^2 \qquad (3.2)$$

The micro-roughness factor, R_m, of a "well-cycled" ("electrochemically annealed") electrode is assumed to equal unity, i.e. $R_m = 1$. Then

$$R_1 = \frac{0.805 \text{ cm}^2}{0.509 \text{ cm}^2} = 1.58 \qquad (3.3)$$

and

$$R_t = R_1 \cdot R_m = 1.58 \qquad (3.4)$$

(b) The value of R_m is calculated using the following formula:

$$R_m = \frac{Q_{HUPD}(exptl)}{Q_{HUPD}(ea)} \tag{3.5}$$

where $Q_{HUPD}(ea)$ is the H UPD accommodation (determined experimentally) on the "electrochemically annealed" Pt electrode, and $Q_{HUPD}(exptl)$ is the H UPD accommodation measured at different stages of thermal and/or electrochemical pretreatment of the Pt electrode. Then

$$R_m = \frac{133.5}{169} = 0.790 \tag{3.6}$$

and

$$R_t = R_1 \cdot R_m = 1.58 \times 0.790 = 1.25 \tag{3.7}$$

(c)
$$R_m = \frac{358.0}{169} = 2.12 \tag{3.8}$$

and

$$R_t = 1.58 \times 2.12 = 3.35 \tag{3.9}$$

Based upon the above example, the following conclusions may be made:

1. The total roughness factor of a polycrystalline Pt electrode consists of two components: (a) the macro-roughness, described by $R_1 \equiv R$; and (b) the micro-roughness, described by R_m.
2. The value of the micro-roughness factor, R_m for a "well-cycled" ("electrochemically annealed") electrode is assumed to equal unity; the H UPD accommodation on such an "electrochemically annealed" Pt electrode, $Q_{HUPD}(ea)$, then serves as a reference.
3. The value of R_m may be calculated using

$$\frac{Q_{HUPD}(exptl)}{Q_{HUPD}(ea)} \tag{3.10}$$

where $Q_{HUPD}(exptl)$ is the experimentally determined H UPD accommodation at

a certain stage of thermal and/or electrochemical pretreatment.

4. The total-roughness is described by R_t where

$$R_t = R_1 \cdot R_m \tag{3.11}$$

5. For a given electrode, which has been well cycled, R_1 is constant and usually between 1.51 and 1.59 (±0.03); introduction of scratches, pores, etc., of course increases the value of R_1.
6. The value of R_m is 1 for an "electrochemically annealed" Pt electrode.
7. For a freshly heated and quenched Pt electrode, $R_m < 1$ and, upon cycling, $R_m \rightarrow 1$.
8. For an electrode at which a thick-oxide film has been grown and reduced, $R_m > 1$ and $R_m \rightarrow 1$ upon repetitive cycling.

Fig. 3.4 shows the H UPD C-V profile of Clavilier and Armand [143] obtained at a spherical Pt single crystal. This electrode, though a single crystal, exhibits a range of

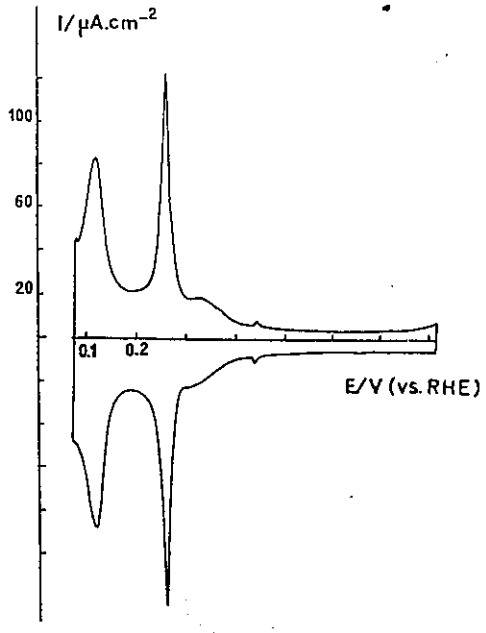

Fig. 3.4 C-V profile of a thermally treated spherical Pt single-crystal electrode recorded at 50 mV s^{-1} in 0.5 M aq. H_2SO_4 solution.

faces due to its spherical shape and has been proposed [143] as a model for a polyoriented Pt electrode surface. However, the electrode was treated thermally at "high temperature" [143] and quenched, hence it must be under a state of much stress at or near its surface. This surface-region stress can be released upon cycling into the oxide region, as shown in Section 3.1.2, by surface restructuring. Such an electrode could serve as a qualitative model of the polyoriented electrode if it were cycled between 0.05 and 1.40 V, RHE, for an extended period of time.

3.2 Growth of Thick-oxide Films at Polycrystalline Pt Electrodes

3.2.1 Introductory Remarks

Studies of the oxide film formation and reduction at Pt for various controlled polarization (holding) potentials, E_h, and for various polarization (holding) times, t_h, generated about two hundred cyclic-voltammograms. Here, only a selection from these curves is shown to illustrate the principal observations.

Oxide film growth on Pt was studied potentiostatically over the potential range 1.8 to 2.3 V, RHE, for a wide range of growth times, up to 48 hours. This choice of conditions was found to be necessary in order to demonstrate the complexity of the sequence of stages [27,184,206] of surface oxidation of Pt that can be observed in the reduction profiles, and also to resolve these stages. In most of Shibata's work, the oxide films were grown at controlled currents so his conditions did not allow differentiation of oxide states as a function of growth potential (here E_h). Also, he did not record oxide growth rates or any limits (cf. ref. 25) attained during the growth.

Burke and Roche [34] found that thick-film states of oxide, which they assumed to be in oxidation state +IV (cf. ref. 191), could be generated easily by a potential-cycling regime as for the cases of thick film generation at Ru [194] and Ir [211]. They considered

that such films were porous hydrous oxides containing water. However, the cycling procedure does not give the required conditions for characterization of formation of different states which the potentiostatic method [9] provides.

The results reported here will not include information on resolution of sub-monolayer states of surface oxide films at Pt since that aspect was already fully covered in earlier papers on Pt [9,10,197,212] and also on Au [12-14,207] from this laboratory.

It will be convenient to present the results comparatively, first in terms of the behaviour observed at a sequence of growth potentials from E_h = 1.80 V to 2.30 V, RHE. It will also be necessary to annotate the cathodic peaks (or shoulders) in the order that the reduction peak potentials arise in the negative-going sweep, viz. OC1, OC2, OC3, etc. as has been done in earlier papers which originated from this group [9,13], but note that the annotations here are not the same as those in other papers on Au [12,207] or earlier work at Pt [9,135] where thick-oxide films were not generated.

3.2.2 Oxide Film Growth as a Function of Potential and Time, and Resolution of Distinguishable States of the Anodically-Formed Films

The general reduction behaviour observed, following surface oxidation for extended periods of time at controlled potentials from 1.8 to 2.3 V, RHE, is as follows (see following Figures 3.5-3.12): the peak OC1, commonly observed [9,213], is the first resolvable feature. With more extended oxidation, its charge becomes increased (see Section 3.2.3) and its peak potential moves to less-positive potentials [9]. Depending critically on the holding (polarization) potential, E_h, and on the holding (polarization) time, t_h, other, electrochemically more stable states, designated OC2, OC3 and OC4 [189,206], are resolved, the latter two being equivalent, it seems, to the state "β" of Shibata [27,28]. Additionally, a new and eventually major broad-shoulder (BS) feature develops, as reported by Shibata [27,28] and denoted "α_1". An interesting feature of the

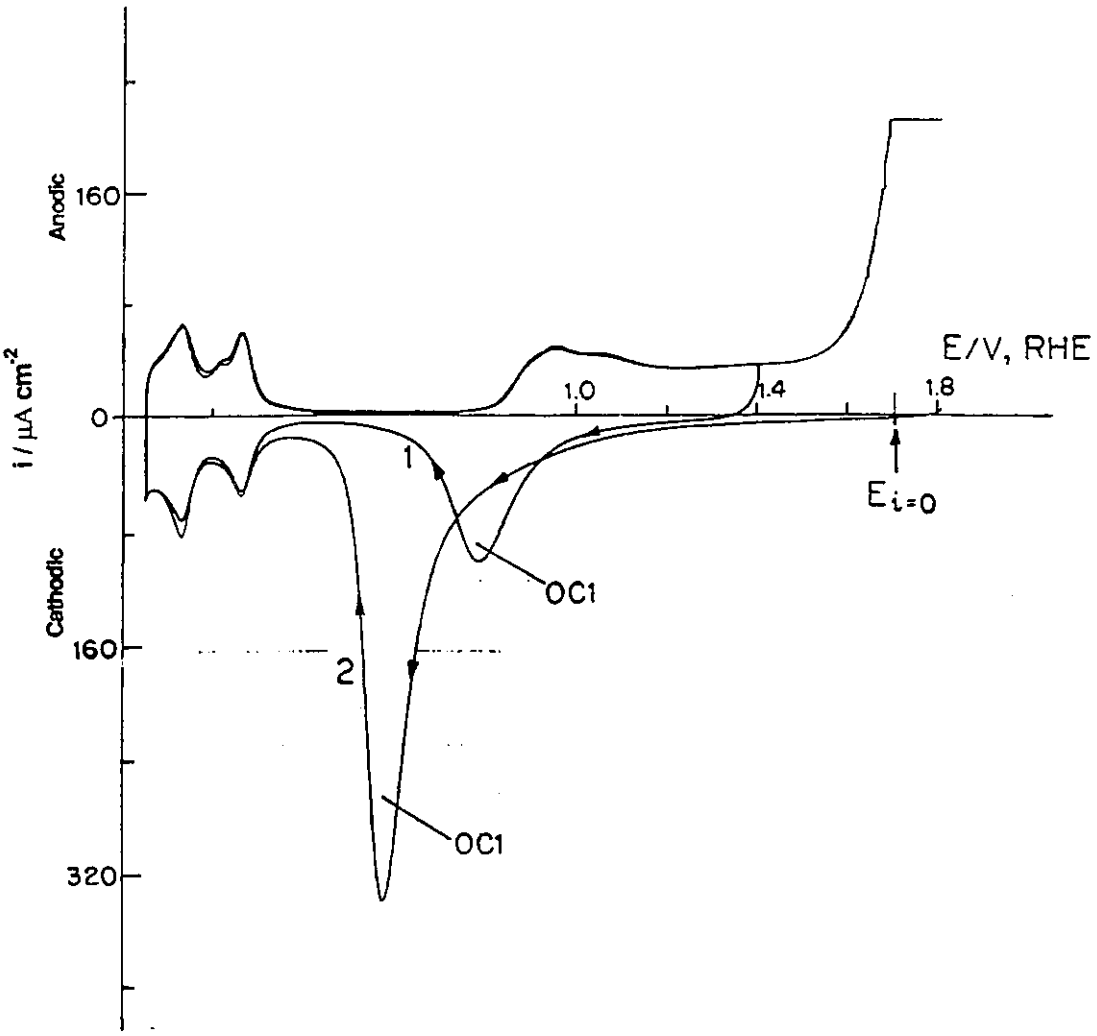

Fig. 3.5 Cyclic-voltammograms for a Pt electrode in high purity 0.5 M aq. H_2SO_4 (298 K); sweep rate = 50 mVs^{-1}. (1) Original profile between 0.05 and 1.40 V, RHE. (2) Profile after polarization at 1.80 V for 6 h 57 min; the negative-going sweep is arrested at $E_{i=0}$ (ca. 1.7 V, RHE) for 30 min with N_2 bubbling, followed by continuation of the negative-going sweep to 0.05 V; the profile reveals peak OC1.

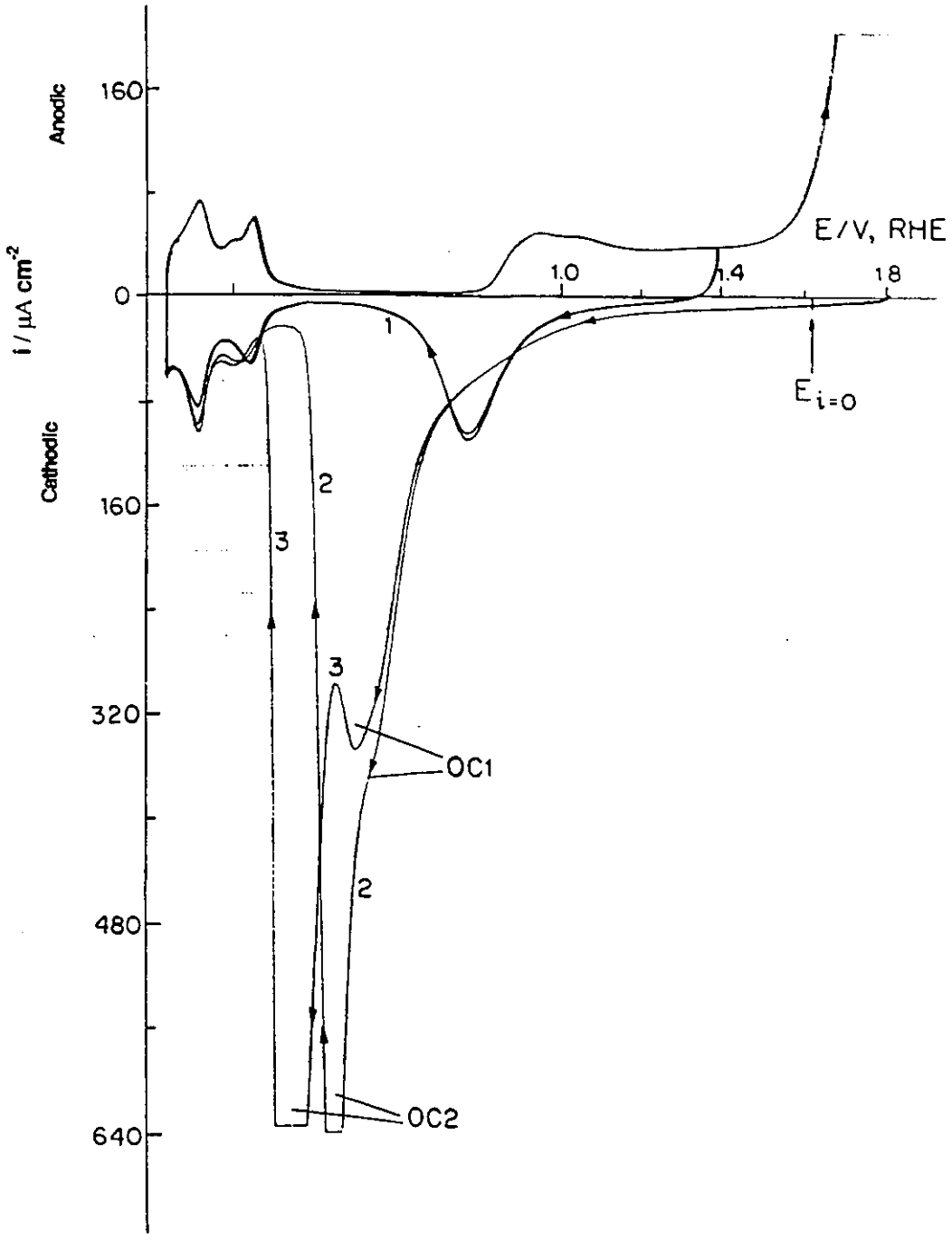

Fig. 3.6 Cyclic-voltammograms for a Pt electrode; sweep rate = 50 mVs^{-1} (298 K). (1) Original profile between 0.05 and 1.40 V. (2) Profile after polarization at 1.80 V for 24 h 57 min; the negative-going sweep is arrested at $E_{i=0}$ (ca. 1.70 V, RHE) for 30 min with N_2 bubbling, followed by continuation of the negative-going sweep to 0.05 V; the profile reveals two peaks OC1 and OC2. (3) As for profile (2) but for polarization for 49 h 47 min; the OC2 peak increases in charge and shifts towards less positive potentials.

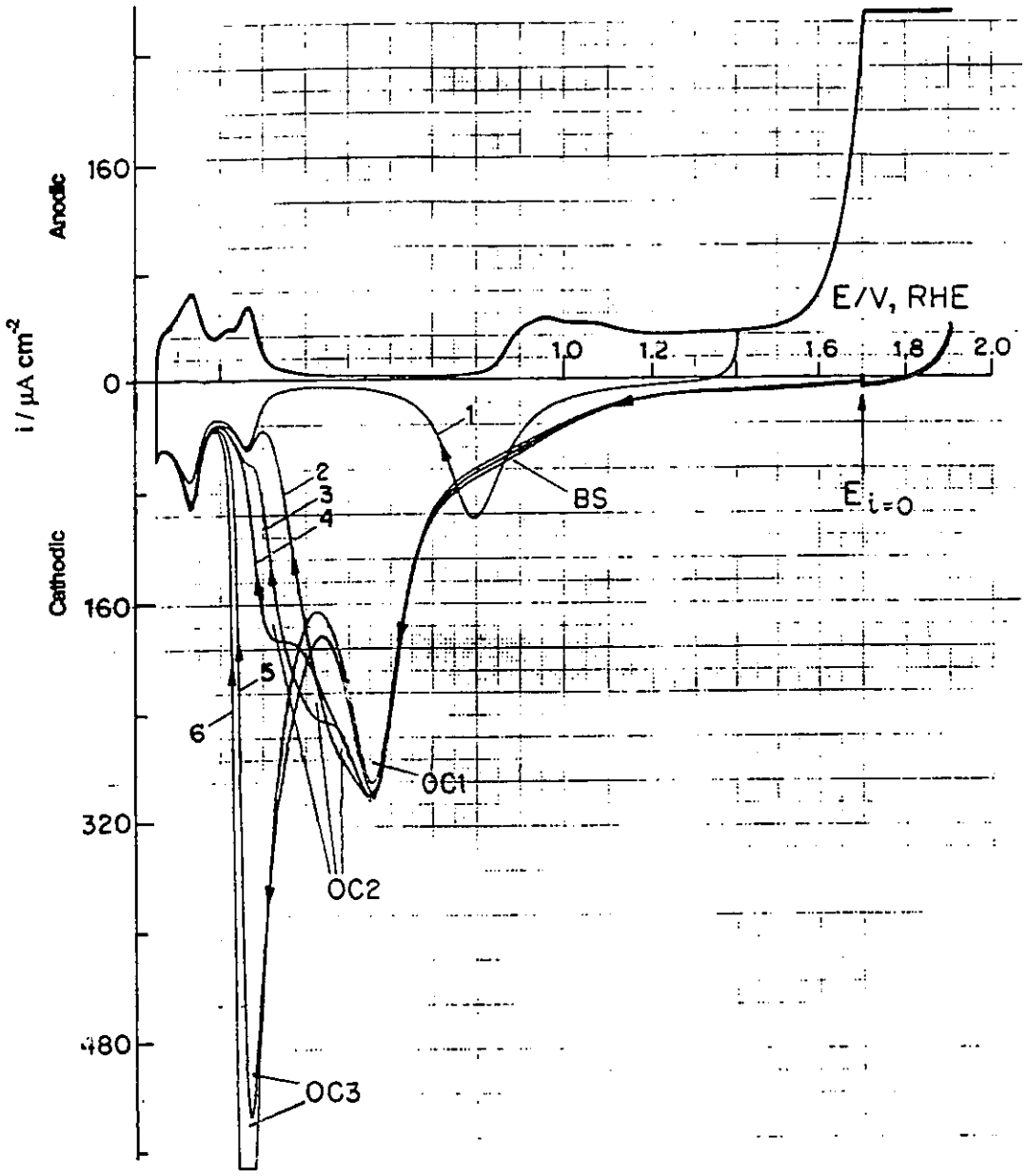

Fig. 3.7 Cyclic-voltammograms for a Pt electrode; sweep rate = 50 mVs^{-1} (298 K). (1) Original profile between 0.05 and 1.40 V. (2 to 6): Profiles after polarization at 1.9 V for different time periods. (2) 6h; (3) 8 h; (4) 9 h; (5) 10 h; (6) 12 h; the negative-going sweep is arrested at $E_{i=0}$ (ca. 1.70 V) for 30 min with N_2 bubbling, followed by continuation of the negative-going sweep to 0.05 V; the profiles reveal OC1, OC2 and OC3 states.

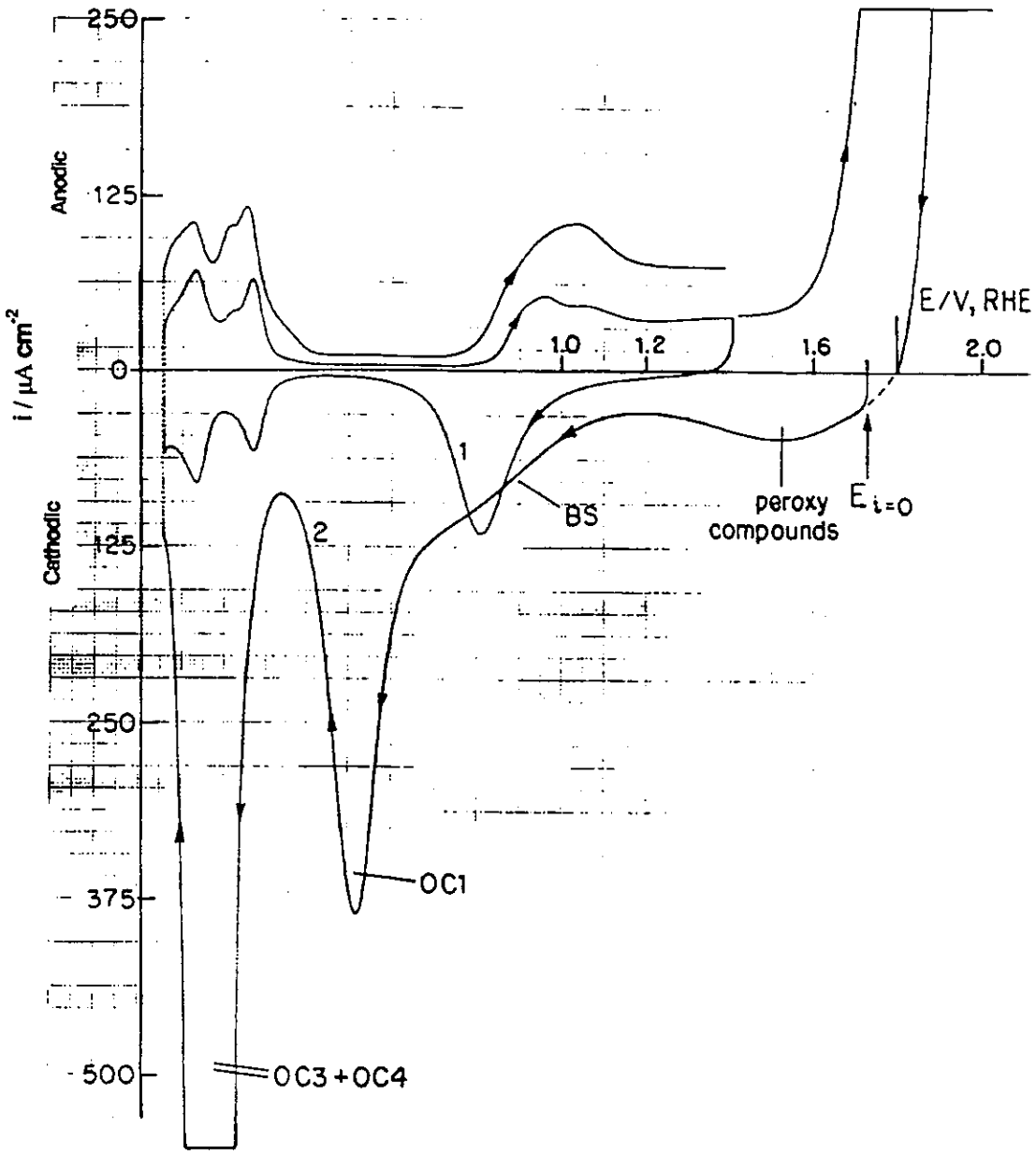

Fig. 3.8 Cyclic-voltammograms for a Pt electrode; sweep rate = 50 mVs^{-1} (298 K). (1) Original profile between 0.05 and 1.40 V. (2) Profile after polarization at 2.0 V for 24 h; the negative-going sweep is arrested at $E_{i=0}$ (ca. 1.70 V, RHE) for 30 min with N_2 bubbling, followed by continuation of the negative-going sweep to 0.05 V; the profile reveals peaks for OC1 and OC3 + OC4 states, the broad shoulder, BS, and a peak/shoulder with a maximum around 1.52 V (peroxy compounds formed?).

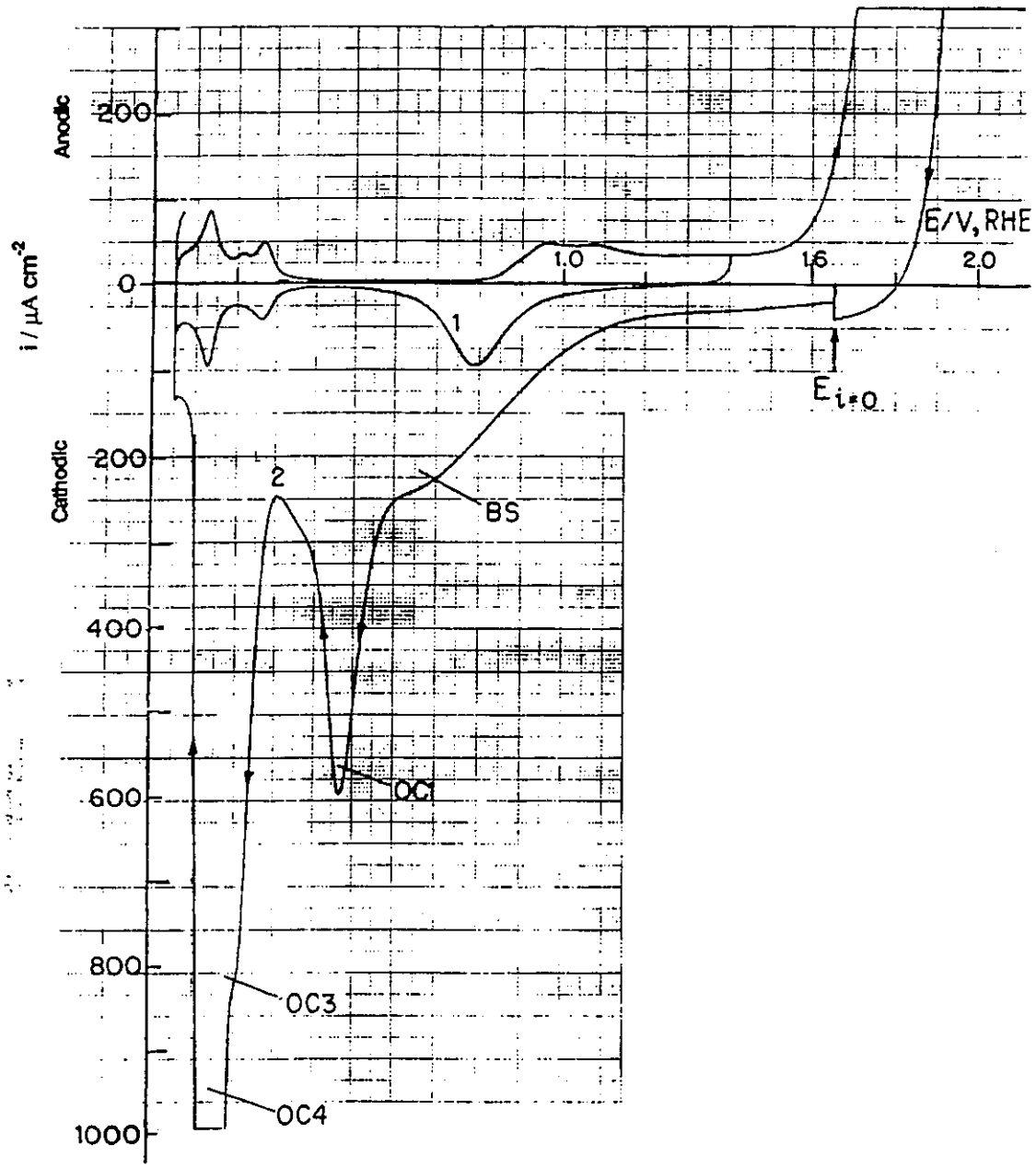

Fig. 3.9 Cyclic-voltammograms for a Pt electrode; sweep rate = 50 mVs^{-1} (298 K). (1) Original profile between 0.05 and 1.40 V. (2) Profile after polarization at 2.1 V for 18 h 50 min; the negative-going sweep is arrested at $E_{i=0}$ (ca. 1.65 V) for 30 min with N_2 bubbling, followed by continuation of the negative-going sweep to 0.05 V; the profile reveals peaks OC1, OC3 + OC4 and the broad shoulder BS.

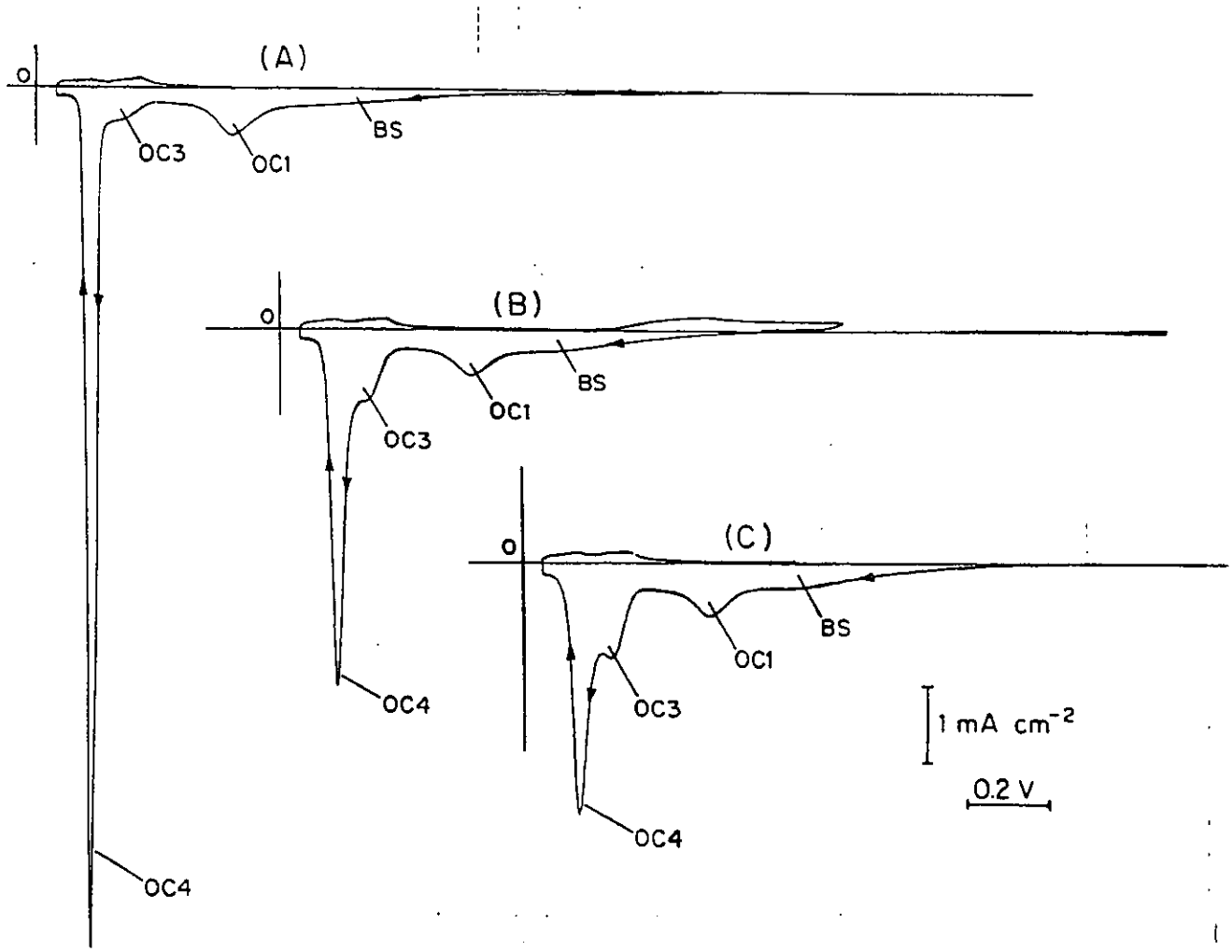

Fig. 3.10 Cyclic-voltammograms for a Pt electrode polarized at 2.2 V for different time periods. (A) 2 h 35 min, (B) 4 h and (C) 6 h 30 min; the polarization history was as noted in the caption of Fig. 9. Upon increase of the polarization time, the total charge for reduction of oxide states does not change significantly but the OC3 state increases at the expense of OC4, which decreases.

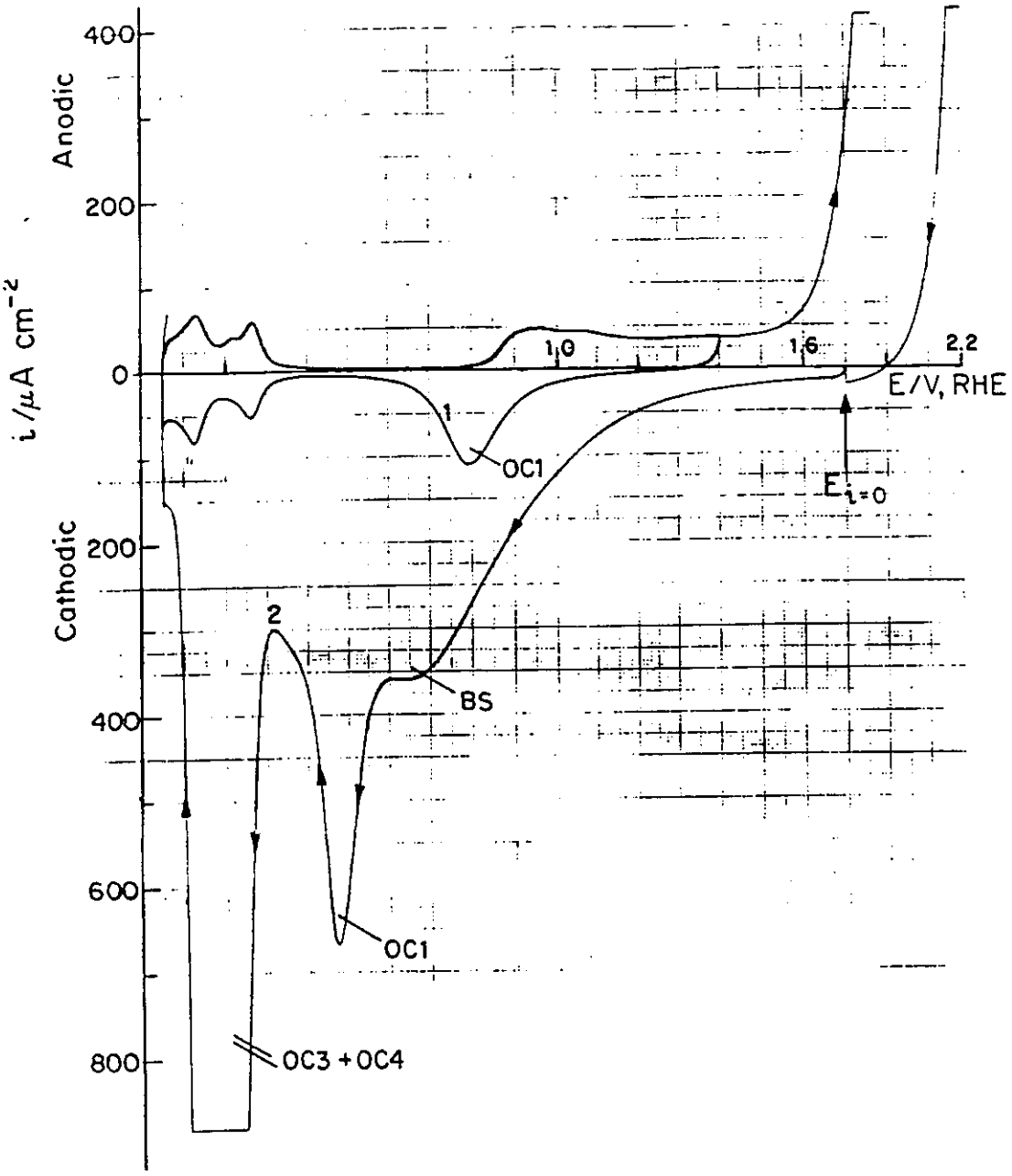

Fig. 3.11 Cyclic-voltammograms for a Pt electrode; sweep rate = 50 mVs^{-1} (298 K). (1) Original profile between 0.05 and 1.40 V. (2) Profile after polarization at 2.2 V for 6 h; the negative-going sweep is arrested at $E_{i=0}$ (ca. 1.70 V) for 30 min with N_2 bubbling, followed by continuation of the negative-going sweep to 0.05 V; the profile reveals peaks OC1, OC3 + OC4 and the broad shoulder BS.

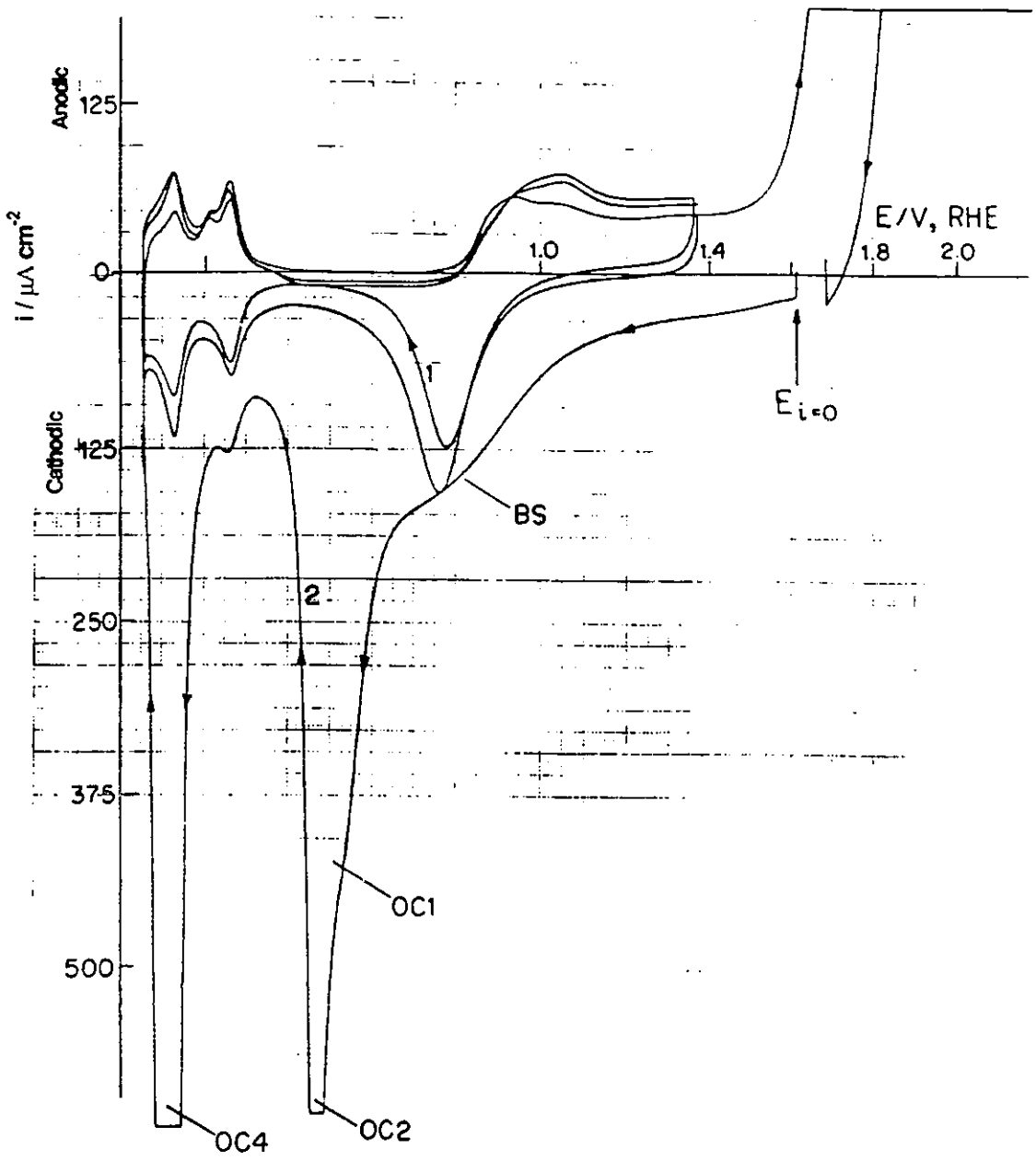

Fig. 3.12 Cyclic-voltammograms for a Pt electrode; sweep rate = 50 mVs^{-1} (298 K). (1) Original profile between 0.05 and 1.40 V. (2) Profile after polarization at 2.3 V for 1 h; the negative-going sweep is arrested at $E_{i=0}$ (ca. 1.71 V) for 30 min with N_2 bubbling, followed by continuation of the negative-going sweep to 0.05 V; the profile reveals peaks OC1, OC2, OC4 and the broad shoulder BS.

BS state is that it is reduced over a much wider potential range than the OC1, OC2, OC3 or OC4 states [206].

Oxide film development was followed at six E_h values: 1.8, 1.9, 2.0, 2.1, 2.2 and 2.3 V, RHE. It will be most convenient to describe the developed features of the reduction current profiles sequentially with respect to increasing E_h, stressing their differences where appropriate. In order to avoid a lengthy description, these features are recorded in tabular form (Table 3.3). Additionally, the logarithmic oxide film growth rates (cf. refs. 7,12), $dQ/d \log t_h$, are recorded for each of the E_h values and discussed in a later Section. However, before proceeding further, it is necessary to comment on apparent limits to oxide film development referred to in some previous papers [25,33].

3.2.3 Limit to Extent of Formation of the OC1 State

It has been stated by Biegler and Woods [25] that the extent of Pt surface oxidation reaches a so-called monolayer limit of 2.6 O atoms per Pt atom (but clearly this does not correspond actually to a monolayer of O species) with extended time of polarization. Qualitatively, this is clearly incorrect, as Shibata's and earlier work conducted in this laboratory indicates that an extended logarithmic growth in time to much larger extents of surface oxidation takes place.

However, the first resolvable feature on oxide film reduction is the commonly observed [3,213] OC1 peak. Upon extended oxidation, its charge becomes increased and its peak potential moves to less positive values, as observed in earlier work [7,9]. The apparent increases of reduction charge for OC1 in the present work are shown in Table 3.4, which indicates that for oxide film growth at or beyond 2.0 V the apparent charges for OC1 can increase well beyond the nominal, so-called "monolayer" limit [25] of 2.6 oxygen atoms per Pt atom. However, for such conditions of oxide film growth, other states of the oxide are also generated and, upon reduction, give rise to substantial changes of real area as determined by accommodation for H (see Section 3.1.2). Then, when the

Table 3.3 Characteristic Behavio

Films Following their

Table 3.3 Characteristic Behaviour of Reductively Resolved States of Pt Surface Oxide Films Following their Anodic Formation at Various Potentials (E_h) for Various Times

E_h/V RHE	Features of i vs E profiles and states resolved	Figure number for i vs E profile	Reduction peak potenti /V,RHE
1.80	OC1 only	3.5	E_p (OC1) = 0.58
	OC2 appears as a shoulder on OC1 and continues its growth	3.6 (curve 2)	E_p (OC1) = 0.55 Peak potential becomes positive with increasir OC2 develops on less positive side of OC1
	OC2 becomes a main cathodic peak but is completed positive to H UPD region	3.6 (curve 3)	E_p (OC2) = 0.37
1.90	OC1 only ; then		E_p (OC1) = 0.55 Peak potential becomes positive with increasin
	OC2 shoulder on OC1 ; then	3.7 (curves 2,3,4)	
	OC3 appears as a sharp peak	3.7 (curves 5,6)	E_p (OC3) = 0.27 (curve E_p (OC3) = 0.26 (curve
	Broad shoulder (BS)	3.7 (curves 5,6)	BS over potential range 1.10 to 0.70
2.00	Features similar to those for 1.90 V but changes develop in shorter times		
	OC1 only; then	3.8	E_p (OC1) = 0.51 Peak potential becomes positive with increasin
	BS begins its growth and remains a major feature	3.8	BS over potential range 1.10 to 0.70
	OC3 begins its growth; OC1 remains a major feature	3.8	E_p (OC3) = 0.22
	New broad small peak between 1.7 - 1.4 V (peroxy compounds or a new oxide state); OC3 continues its growth	3.8	1.70 to 1.40

Table 3.3 Characteristic Behavior of R

Films Following their Anodic

Table 3.3 Characteristic Behaviour of Reductively Resolved States of Pt Surface Oxide Films Following their Anodic Formation at Various Potentials (E_h) for Various Times

E_h/V RHE	Features of i vs E profiles and states resolved	Figure number for i vs E profile	Reduction peak potentials /V,RHE
1.80	OC1 only	3.5	E_p (OC1) = 0.58
	OC2 appears as a shoulder on OC1 and continues its growth	3.6 (curve 2)	E_p (OC1) = 0.55 Peak potential becomes less positive with increasing Q; OC2 develops on less positive side of OC1
	OC2 becomes a main cathodic peak but is completed positive to H UPD region	3.6 (curve 3)	E_p (OC2) = 0.37
1.90	OC1 only ; then		E_p (OC1) = 0.55 Peak potential becomes less positive with increasing Q.
	OC2 shoulder on OC1 ; then	3.7 (curves 2,3,4)	
	OC3 appears as a sharp peak	3.7 (curves 5,6)	E_p (OC3) = 0.27 (curve 5) E_p (OC3) = 0.26 (curve 6)
	Broad shoulder (BS)	3.7 (curves 5,6)	BS over potential range 1.10 to 0.70
2.00	Features similar to those for 1.90 V but changes develop in shorter times		
	OC1 only; then	3.8	E_p (OC1) = 0.51 Peak potential becomes less positive with increasing Q.
	BS begins its growth and remains a major feature	3.8	BS over potential range 1.10 to 0.70
	OC3 begins its growth; OC1 remains a major feature	3.8	E_p (OC3) = 0.22
	New broad small peak between 1.7 - 1.4 V (peroxy compounds or a new oxide state); OC3 continues its growth	3.8	1.70 to 1.40

ɔr of Reductively Resolved States of Pt Surface Oxide

Anodic Formation at Various Potentials (E_h) for Various Times

als	Time t_h for oxide film formation	$dQ/d \log t_h$ / $\mu C\ cm^{-2}$. (decade t_h)$^{-1}$	O monolayer (decade t_h)$^{-1}$	Other features and features not shown in any of the presented figures but revealed in other experiments
less g Q;	= 7.0 h 24.5 h	47	0.106	Up to t_h = 15 h only the normal cathodic peak, OC1, arises. The growth is linearly logarithmic in t_h up to ca. 2000 s. Beyond this point, the oxide growth rate becomes more rapid (Fig.3.14).OC1 tends to reach a limit. There is no limiting value for Q.
	49.8 h	c.a. 4000; no limiting value for Q_{OC2} (Fig.3.14)	ca. 9.1	
less g Q.	$<10.8 \times 10^3$ s	64	ca. 0.147	Up to t_h = 6 h only OC1 arises. Its growth is linearly logarithmic in t_h up to ca. 900 s. Again, beyond this point, the oxide growth rate becomes more rapid (Fig.3.14)OC1 reaches a limit, but there is no limit in the growth of OC3. The growth rate of BS is low (compared with values at higher potential).
	6 h to 12 h	64 OC1 tends to reach a limiting value (Fig3.7)		
5) 6)	12 h	ca. 4300; no limiting value for Q	ca. 11.1	
	$> 10^4$ s			
less g Q.	0 to 4 h	84 (for t_h < 500s);beyond this point the increase becomes more rapid	0.191	Fig.3.8 refers to polarization for t_h = 24 h and reveals all mentioned features. The broad small speak between 1.70 and 1.40 V is not due to physically adsorbed or occluded O_2 since it could not be dimished either by extended N_2 bubbling or ultrasonification of the electrode; it is either a new state of oxide or an adsorbed peroxy species. OC1 reaches a limit again but there is no limiting value for Q. The subsequently recorded H UPD profile reveals substantial increase of the surface area (2x) and some redistribution of the H oxidation peaks indicating changes of crystal surface orientation (Fig.3.8). Polarization for up to 48 h does not reveal the growth of OC4.
	2 h			
	>4 h	ca. 36000; no limiting value for Q	ca. 82	
	12 h			

	OC1 only and remains a major component	3.9	E_p (OC1) = 0.47 Peak potential becomes less positive with increasing Q.	0 to 1.5 h	(f ra th
	OC3 develops and remains a major feature up to t_h = 6h	3.9	E_p (OC3) = 0.22	1.5 h to 6 h	
2.10	BS begins its growth and remains a major feature	3.9	BS over potential range 1.10 to 0.65	1.5 h	
	OC4 appears on the less positive side of OC3 and continues its growth; it seems to grow at the expense of OC3 which disappears (at ca. 6 h).	3.9	E_p (OC4) = 0.15	5 h	
	Broad small peak again between (peroxy compounds)		1.70 to 1.40	6 h	Q (Q in
	OC3 reappears and continues its growth	3.9	E_p (OC3) = 0.22	16.5 h	be ti lo
	More complex behavior and similar to that at 2.1 V.				
	OC1 only	3.11	E_p (OC1) = 0.47	0 to 50 min	(f
	OC3 appears and continues its growth	3.11	E_p (OC3) = 0.22	50 to 100 min	th is
2.20	OC4 appears and OC3 disappears		E_p (OC4) = 0.14	2 h	
	BS begins its growth and remains a major feature	3.10,3.11	over potential range 1.10 to 0.60	2 h	
	OC3 regrows together with OC4	3.10,3.11	E_p (OC3) = 0.22 E_p (OC4) = 0.14	2.6 h	
	OC3 + OC4 reach a limit in Q; OC3 continues its growth but at the expense of OC4 (Fig.3.14).BS region becomes again further developed (ca. 18% of total Q)	3.10		6.5 h	In at at ca
	Similar behavior to that for 2.20 V.				
	OC1 retains a limiting charge but is difficult to resolve due to overlap by OC2 (see below)	3.12	E_p (OC1) = 0.55 E_p (OC2) = 0.46	0 to 900 s	(t is
2.30	BS continues to be an increasingly dominant feature	3.12	BS over potential range 1.10 to 0.65	0.5 h	
	OC4 becomes main species reducible at the least positive potential in H UPD region.	3.12	E_p (OC4) = 0.12	0.5 h	Q c i
	OC2 develops as an extended shoulder on OC1 which is thereby obscured	3.12		1 h	

less g Q.	0 to 1.5 h 1.5 h to 6 h 1.5 h 5 h 6 h 16.5 h	107 (for t_h < 200 s); rapid increase beyond this point Q reaches a maximum (Q ≃ 11,900 μC cm^{-2}) and inflects at ca. t_h=11 h; beyond ca. 28 h it continues growth but at a lower rate (Fig.3.14).	ca. 0,242	The OC1 growth is linearly logarithmic up to ca. 200 s. Beyond this point the oxide growth becomes more rapid (Fig.3.14). Again, OC1 tends to a limit. However, there is no limit for Q even though it reveals an inflection. The broad small peak between 1.70 and 1.40 V is not shown in Fig.3.9 since N_2 bubbling was conducted in the region of its reduction and the species was reduced.
	0 to 50 min 50 to 100 min 2 h 2 h 2.6 h 6.5 h	130 (for t_h< 70 s); beyond this point the increase is rapid Inflection in Q vs log t_h at Q ≃ 10,900 μC cm^{-2}, after fast growth, at ca. 2.5 h.	ca. 0.295	OC1 growth is linearly logarithmic up to ca. 70 s. Beyond this point there is a region of rapid oxide growth (Fig.3.14). BS region becomes much more developed with increased polarization time and there seem to be no limit to its growth.
ıe	0 to 900 s 0.5 h 0.5 h 1 h	150 (for t_h< 300 s); beyond this point the increase is rapid. Q reaches a limit of ca. 10,900 μC cm^{-2} and inflects at ca. 24 h.	ca. 0.340	OC3 starts to grow (t_h = 17 min) and OC4 right after. Further growth of OC4 continues at the expense of OC3 which practically disappears. When OC2 state has formed, OC3 begins to regrow at the expense of OC4 (t_h = 2 h). The maximum Q is for t_h = 4 h. since further increase of t_h does not change total charge, Q, (Fig.3.14) but only changes the charge distribution amongst OC1, OC2, OC3, OC4 and BS. After reduction of the thick oxide grown for t_h=1 h, the surface area increases ca. 1.7 x; also H UPD current components are redistributed.

Table 3.4 Approximate Evaluation of Charges Associated with Partially Resolved Peaks in Negative-going Potential Sweeps by Deconvolution

Table 3.4. Approximate Evaluation of Charges Ass
Peaks in Negative-going Potential Swe

Electrode description (reference to figure)	Charge under BS $\mu C\ cm^{-2}$	Charge under OC1 $\mu C\ cm^{-2}$	Charge under OC2 $\mu C\ cm^{-2}$	Charge under OC3 $\mu C\ cm^{-2}$
Polar. at 1.8 V for 6 h. 57 min. (Fig.3.5)	—	654	—	—
Polar. at 1.8 V for 24 h. 57 min. (Fig.3.6, curve 2)	—	837	621	—
Polar. at 1.8 V for 49 h. 47 min. (Fig.3.6, curve 3)	—	879	1210	—
Polar. at 1.9 V for 10 h. (Fig.3.7,curve 5)	—	894	726	—
Polar. at 1.9 V for 12 h. (Fig.3.7,curve 6)	—	896	864	—
Polar. at 2.0 V for 24 h. (Fig.3.8)	620*	1410** (ca. 880)	—	9 (OC3
Polar. at 2.1 V for 18 h. 50 min. (Fig.3.9)	1400*	2320** (ca. 880)	—	1220
Polar. at 2.2 V for 6 h. (Fig.3.11)	1850	2940** (ca. 880)	—	(OC3
Polar. at 2.3 V for 1 h. (Fig. 3.12)	970*	2270 (OC1 + OC2)		—

* BS overlaps the region where peroxy-compounds are reduced so the calculated BS charges

** As mentioned in Section 3.2.3 of Results and Discussion, the OC1 tends to a limit of c. OC1 charge for different E_h and t_h, shown in this table, are not contrary to the discus roughness of the Pt electrode causes the increase of OC1 charges up to 2940 $\mu C.cm^{-2}$. Th correcting for increases of the roughness factor of the electrode.

*** The initial roughness factor of the Pt electrode means the roughness it achieved after

of Charges Associated with Partially Resolved

Potential Sweeps by Deconvolution

Charge under $OC3_2$ $\mu C\ cm^{-2}$	Charge Under $OC4_2$ $\mu C\ cm^{-2}$	Features and Peak Potentials
—	—	OC1 ⟶ 0.58 V,
—	—	OC1 ⟶ 0.55 V, OC2 ⟶ 0.47 V,
—	—	OC1 ⟶ 0.52 V, OC2 ⟶ 0.37 V,
—	—	OC1 ⟶ 0.55 V, OC3 ⟶ 0.27 V,
—	—	OC1 ⟶ 0.55 V, OC3 ⟶ 0.26 V,
9570 (OC3 + OC4)		peroxy species ca. 390 $\mu C\ cm^{-2}$, deconvolution of OC3 and OC4 impossible due to their superimposition; the roughness factor of the electrode surface increased ca. 2.0 x with respect to its initial value. *** OC1 ⟶ 0.51 V, OC3 ⟶ 0.22 V, OC4 ⟶ 0.17 V.
1220	6500	peroxy species ca. 16 $\mu C\ cm^{-2}$; deconvolution of OC3 and OC4 carries an error of up to 10%; the roughness factor of the electrode increased ca. 2.6 x with respect to its initial value. OC1 ⟶ 0.47 V, OC3 ⟶ 0.22 V, OC4 ⟶ 0.15 V
5400 (OC3 + OC4)		deconvolution of OC3 and OC4 impossible; the roughness factor of the electrode increased ca. 3.3 x with respect to its initial value. OC1 ⟶ 0.47 V, OC3 ⟶ 0.22 V, OC4 ⟶ 0.14 V
—	4330	peroxy species ca. 250 $\mu C\ cm^{-2}$; the roughness factor of the electrode increases ca. 1.7 x with respect to its initial value. OC1 ⟶ 0.55 V, OC2 ⟶ 0.46 V, OC4 ⟶ 0.12 V.

d BS charges have a significant error (uncertainty) of up to 10%.

a limit of ç.a. 880 $\mu C.cm^{-2}$ (2.0 0 per Pt). The values of the
to the discussion in the text since drastic increase of the
0 $\mu C.cm^{-2}$. The values in brackets represent the OC1 charge after

hieved after prolonged cycling between 0.05 V and 1.40 V.

apparent OC1 reduction charges are corrected for these increases of real area, the OC1 charges are found to remain essentially constant (Table 3.4, Fig. 3.13), independent of growth potential in the range 1.8 V to 2.3 V. These observations clarify the controversial aspect of Biegler and Wood's results; thus it is only the OC1 component that reaches (understandably) a limit of ca. 880 μC per real cm^2, even up to 2.2 or 2.3 V growth potential, while concurrent growth processes leading to a quasi-3d or a 3d oxide film provide a continuous increase of the overall extent of oxide film formation revealed by the total reduction charge.

3.2.4 Sequence of Formation of States of the Oxide Film in Relation to Stabilities

The sequence in which states of the oxide film, formed anodically, are revealed in the negative-going sweep through reduction follows, in general, the commonly observed trend [9,201] which, however, requires comment. At sub-monolayer levels of oxide coverage (5 to 15%, depending on pH), the formation and reduction of the ad-species is almost reversible [9]. However, contrary to what might be expected thermodynamically, oxide species formed at potentials more positive than those for the reversible region (ref. 9) are, in fact, reduced only at progressively less positive potentials, e.g. as for the OC1 peak in Figs. 3.5 and 3.6. This behaviour has been attributed [9] to a totally irreversible process of place exchange, i.e. once a reconstructed state of the original 2-d ad-layer has occurred, it is reducible only at potentials much less positive than those for its formation, irrespective of how slowly the reduction is caused to take place. Such behaviour is even more strongly manifested with respect to the states OC2, OC3 + OC4 (Figs. 3.5 to 3.12). Only the new state, revealed in reduction over the potential range 1.7 to 1.3 V (Fig. 3.8), is an exception to the above statement; it could be a peroxy-species. Thus, the sequence of reduction current peaks in the negative-going sweep does not follow expectations corresponding to the thermodynamics of reduction of an oxide through two (or more) successive oxidation states where normally the lower one is always reduced at a potential

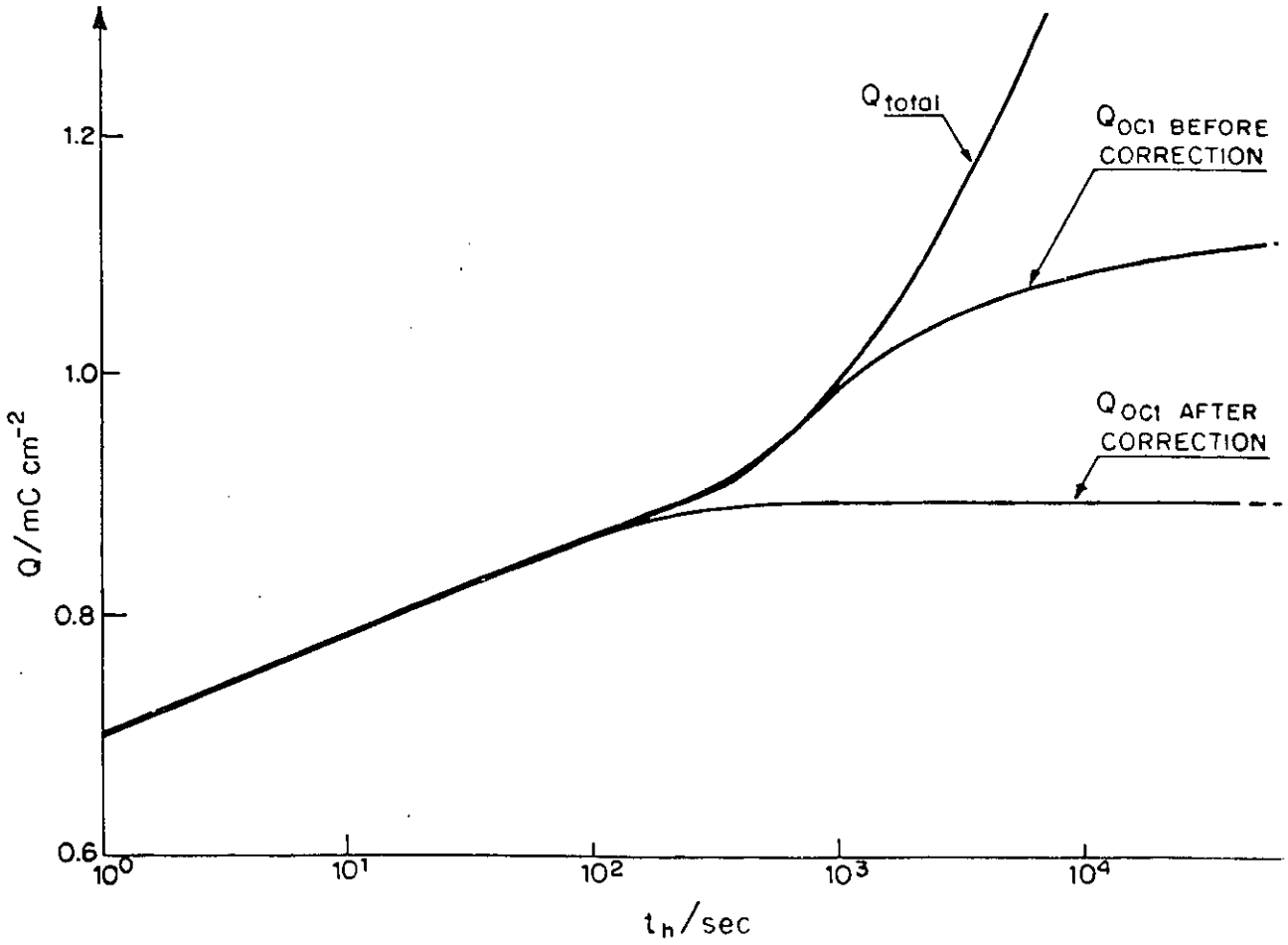

Fig. 3.13 The time dependence of the OC1 charge during oxide film growth at Pt (2.0 V), corrected for the real area change that occurs during extended film formation. Polarization at 298 K in 0.5 M aq. H_2SO_4.

less positive (or more negative) than that for reduction of the higher oxidation state to the lower. The distinguishable peaks OC2, OC3 and OC4 cannot, therefore, represent oxide species in which Pt, as ions, is in different oxidation states, since the species produced under strongest oxidation conditions is reduced over the least positive potential range. The observed behaviour must therefore be interpreted in terms of stability of the oxide phases that are sequentially developed. There are, however, some kinetic effects. Birss (private communication and ref. 36) has made the interesting observation that, given sufficient time at a potential positive to the potential of the reduction peak of Shibata's "β' oxide, this species can be completely reduced. This observation was confirmed and it was found that the species OC3 and OC4 can be reduced already at +0.4 V, RHE (i.e. well positive to the peak potential, Fig. 3.8), though not by holding the potential at 0.8 or 1.3 V, RHE.

At E_h = 2.1, 2.2 and 2.3 V a new type of behaviour is observed: following initial development of the OC1 peak, the OC3 peak develops first as a shoulder and continues its growth. However, the OC3 peak diminishes as the OC4 peak begins its growth, and eventually practically disappears (OC4 becoming the new dominant sharp peak). The OC4 reduction charge tends to a limiting value, and after having attained it, the OC3 peak reappears and continues its growth at the expense of OC4 (the total charge, Q, remains almost constant upon increase of t_h). The t_h's at which these features appear depend on the polarization potential, E_h, and are indicated in Table 3.3 (also see Fig. 3.10).

The very sharp peak, OC4, approaches the reduction behaviour expected for a single 3-d phase, i.e. reduction at only a singular, thermodynamically defined potential; the behaviour for OC3 + OC4 is for a multilayer state (formed eventually up to a thickness of ca. 50 equivalent O monolayers) of the oxide in which there will be lateral attraction interactions in three dimensions so that the film behaves almost like a bulk 3-d phase. An intermediate situation arises with the OC1 peak which has a half-width of ca. 120 mV but its peak potential moves progressively to less positive potentials with increasing Q,

reflecting increased stability with increasing mean thickness of the film. However, the Q values are not sufficient to correspond to a 3-d phase state, neither is the behaviour characteristic of increasing coverage in a purely 2-d array. The behaviour corresponds to progressive conversion of a 2-d array to a quasi-3-d film with increasing Q due to the place-exchange process [9,21,188].

3.2.5 "Logarithmic" Growth and the Dependence of its Rate on Potential

In the initial states of development of the oxide film on Pt, except at coverages below ca. 0.25 (as θ_{OH}), the growth of the oxide film is linearly logarithmic in t_h, as was found in earlier work in this research group [7].

Examination of the growth kinetics in the linear log t_h regions at the various potentials recorded above (Fig. 3.14) gives rise to a linear plot of dQ/d log t_h against E_h shown in Fig. 3.15, having a slope 204 (±5) $\mu C\ cm^{-2}$ (decade $t_h)^{-1}V^{-1}$. This behaviour is qualitatively similar to that reported by Gilroy [9] but cannot be compared quantitatively since his Q values were not scaled to values per cm^2.

The OC1 state continues to grow logarithmically with t_h until its charge for reduction is ca. 880 $\mu C\ cm^{-2}$ (Table 3.4). This presumably corresponds to the apparent limit for oxidation of Pt surfaces claimed by Biegler and Woods [25], as discussed in Section 3.2.3. This, however, does not represent a limit for overall growth since, concurrent with growth of OC1 and attainment of its own limit, the states OC2, OC3 + OC4 continue to be developed. In fact, for these states, the continued growth rate is much larger than that for OC1 (Table 3.4).

Generally, it is seen that the onset of the more rapid oxide film growth regime occurs at shorter t_h the higher is the potential, E_h. This is probably because a change of oxide growth mechanism takes place at a particular film thickness which is achieved, of course, at shorter times when the E_h potential, driving the growth, is larger [206].

Although some of the states of the oxide that are progressively formed with

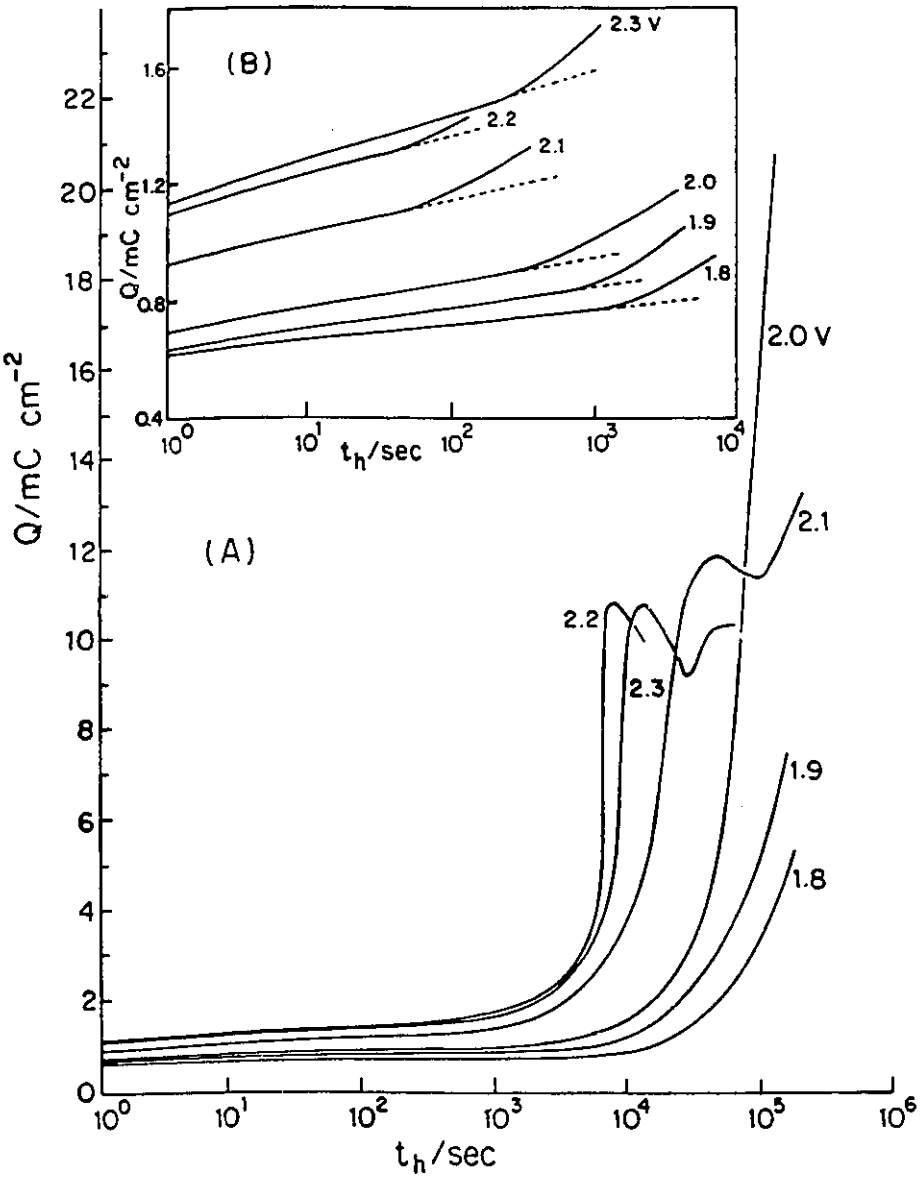

Fig. 3.14 Oxide film growth plots in log t_h at Pt electrodes in 0.5 M aq. H_2SO_4 at 298 K for various polarization potentials (cathodic total charge vs log t_h plots). (A) The overall plots. (B) The linear parts of the plots.

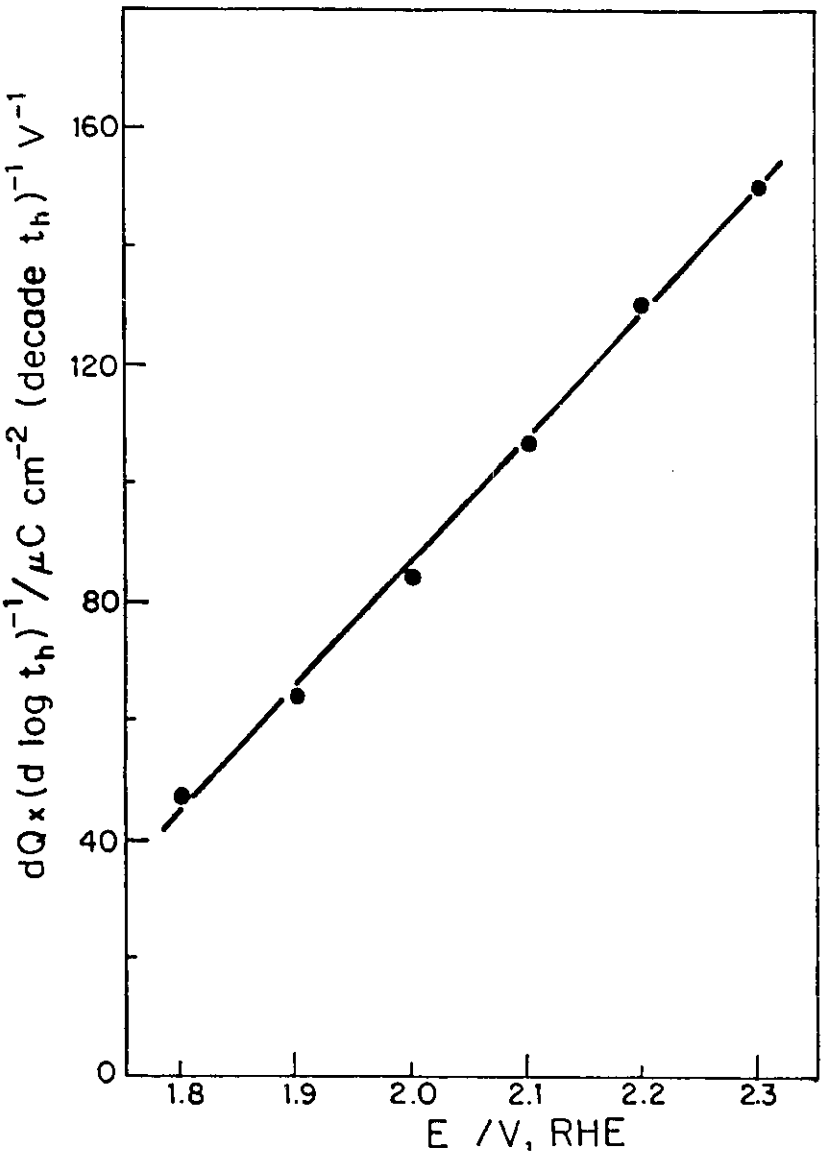

Fig. 3.15 Slopes of the linear regions of the plots of charge Q vs log t_h from Fig.3.14(B) as a function of the polarization (holding) potential, E_h.

increasing t_h and/or E_h have overlapping ranges of potential for their reduction, it is informative to attempt some deconvolution of the i vs E profiles in order to evaluate respective reduction charges for states that are distinguishable. Such charge data are recorded in Table 3.4 but it must be noted that they are reliable only to ca. 10 - 15%, except for conditions where OC1 is clearly resolved; then the Q is ± ca. 2% or better.

3.2.6 Significance of Distinguishability of the Thick-film States

The distinction between the OC1 and the other three peaks OC2 to OC4 seems qualitatively easy to make; this is because OC1 has the characteristics of a chemisorbed film type of oxide while the other states, which evidently grow quasi-independently of it and only at high anodic potentials for extended periods of time, have more the behaviour of bulk-type films (cf. refs. 20,21,32,33).

It is not at all easy to see the reason why the thicker, bulk-type film grows in three distinguishable states, separated maximally in average Gibbs energy by ca. 0.3 eV, with at least two being simultaneously present (in addition to the OC1 state) under some conditions (e.g. see Figs. 3.8, 3.3, 3.11 and 3.12).

It is possible that these states correspond to development of the thick film on distinguishable areas of the underlying polycrystalline Pt surface (see Section 3.5) having different crystal-face orientations, although there is apparently (see Fig. 3.10) "interconversion" between the distinguishable states, depending on time and potential of anodization. On the other hand, at single-crystal Au surfaces having (111), (110) and (100) orientations, the main oxide film growth peak at that metal (denoted OC3 in earlier papers [44,207]) is found [11,12] to develop similarly for the three surfaces, i.e., at Au, there is no specific epitaxial relation of the main oxide film to the underlying geometries of the surfaces from which it developed. (The submonolayer peaks at Au are, however, quite specifically characteristic of the surface orientation and hence geometry - refs. 11,12).

The behaviour observed at Pt may arise for several reasons. One is polycrystallinity, suggested by grain SEM EDX mapping (Section 3.2.11), and it may also be suggested that, as the film grows, there is a changing surface to volume ratio that determines the Gibbs energy of the film's formation and thus of its reduction potential. Accompanying the relative increase of volume to surface area there could be phase changes associated with minimization of Gibbs energy. As an example, the changes of state from OC2 to OC4 correspond to increases of extent of oxide formation, equivalent to reduction charges of ca. 1500, 3200 and 6300 $\mu C\ cm^{-2}$, i.e. apparent thickness of 3.4, 7.6 and 15 equivalent O monolayers, respectively. (Also refer to Table 3.4).

ESCA analysis data (see Section 3.2.11 and refs. 191-193) on the state of Pt in the oxide films at various stages of film development show that there is no indication that Pt is in a different average oxidation state in OC2, OC3 or OC4. A common oxidation state of Pt (+IV) is the main observation.

Later in this thesis, it will be shown that there is some significant dependence of the electrocatalytic activity of the different states of the thick film on their respective identities as revealed in the cathodic current profiles generated in the linear-sweep voltammetry experiments (see Sections 3.2.12 and 3.2.14).

3.2.7 iR-Drop Effect in the Oxide Films on Reduction

The progressive displacement of the reduction peak potentials for oxide films in the OC2, OC3 and OC4 states to less positive potentials could be due to internal film "iR" drop effects. Thus, as greater quantities of oxide film (larger Q values) are generated at higher E_h values at long times, the reduction peak currents become progressively larger; hence their displacement to less positive potentials could be due to an iR-drop effect in the film. This would be consistent with the increased resistivity [29] of the "β" film of Shibata (here OC2, OC3 + OC4 states). The progressive shift of OC1 is not,however, due to such an effect since the resistivity of the "α" film (≡ OC1 here) state is much lower and

its thickness much less. Such iR-drop effects, however, could not lead to appearance of the distinguishable states of the oxide in reduction.

3.2.8 Independent Deposition of the 2-d Oxide Film Beneath the 3-d Film, Following Partial Reduction of the Latter

In relation to the discussion in earlier paragraphs concerning the sequence of formation of distinguishable states of the oxide film, one of the most interesting results of this present Section of the work was as follows.

An oxide film that would have exhibited both the OC1 and the OC2 or OC3 + OC4 states in a negative-going sweep (as in Fig. 3.7 or 3.11) was formed by film growth at appropriate E_h and t_h values. If, for such a prepared film, the next negative-going sweep was reversed at +0.4 V (see Fig. 3.16) before commencement of reduction of the OC3 + OC4 states, then it was observed that this immediately subsequent positive-going sweep would trace out more or less the normal i vs E profile for 2-d monolayer oxide film development that would be observed on an initially oxide-free Pt surface, indeed, even with the usual fine structure being displayed [9]. This generation of the i vs E profile characteristic of the 2-d monolayer formation was, however, at a pre-oxidized Pt surface which, being incompletely reduced beyond the distinguishable OC1 stage, still retained on its surface (in this example) an intact oxide film of some 10.2 equivalent O layers corresponding to the OC3 + OC4 states that are eventually revealed, e.g. in the profiles of Fig. 3.16 when completion of the oxide reduction to +0.05 V, RHE, has been carried out.

This result must indicate that once the 3-d type of thick phase-oxide has been formed, and the OC1 state "in it" reduced, a renewed 2-d film of OH and/or O on Pt can be anodically generated on the Pt metal surface. Since the i vs E profile for this monolayer re-formation process shows all the characteristics (cf. ref. 9) of a first-sweep profile on an initially oxide-free Pt metal surface, it seems that the 2-d film must lie beneath rather than above the thick oxide film. This conclusion was suggested by Burke and Roche [34] but

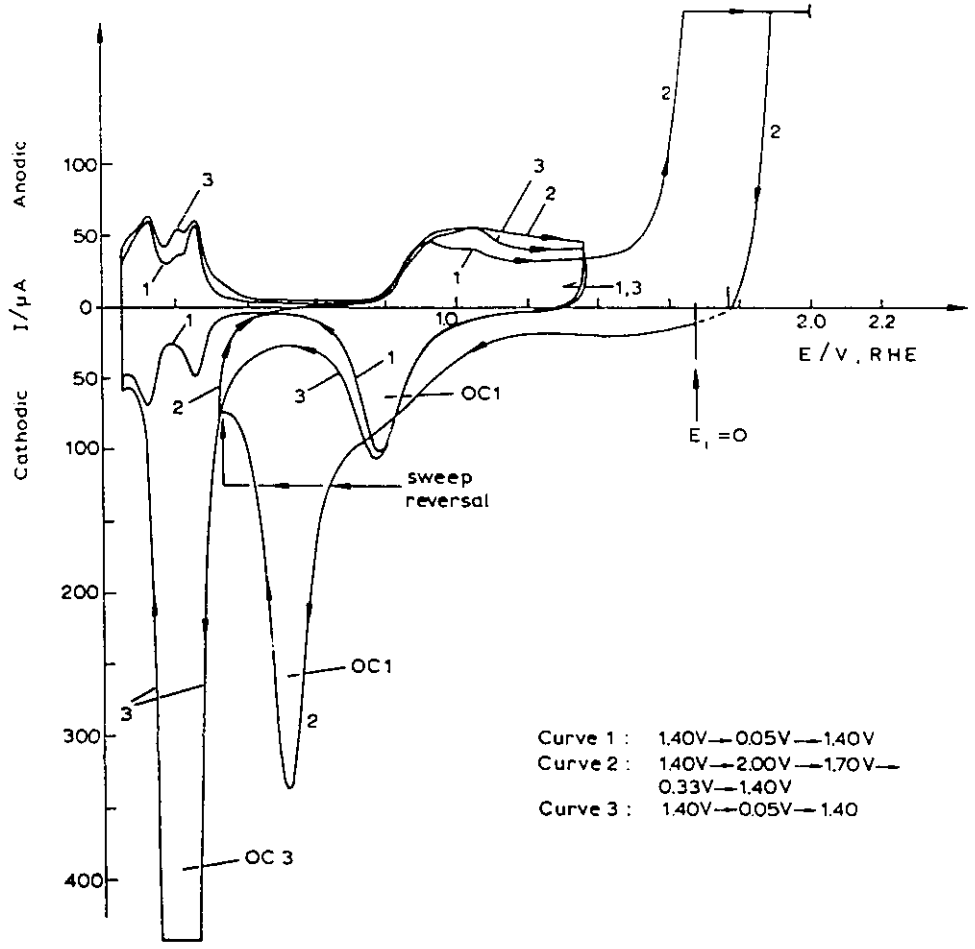

Fig. 3.16 Cyclic-voltammograms for Pt oxide formation and reduction at 50 mV s^{-1} (T = 298 K). (1) Regular cyclic-voltammogram taken from 0.05 V to 1.40 V, RHE, showing state OC1 in reduction. (2) Extension of potential sweep to 2.0 V, RHE, then held at 2.0 V for 12 h, followed by a negative-going sweep arrested at $E_{i=0}$ (ca. 1.7 V, RHE) for 30 min with N_2 bubbling, followed by continuation of the negative-going sweep to 0.33 V but with reversal at that potential giving positive-going sweep (continuation of curve (2) but in positive direction) revealing almost normal quasi-2-d oxide film formation over potential range 0.8 to 1.4 V, RHE. (3) Continuation of voltammetry by immediate re-application of negative-going sweep from 1.4 V, RHE, giving renewed OC1 peak but with continuation revealing existence of large OC3 + OC4 peaks over the region 0.4 to 0.1 V, RHE, for reduction of still remaining stable, quasi-3-d oxide states. Continuation of curve (3) in the positive direction (after sweep-reversal at 0.05 V, RHE) revealing re-formation of 2-d oxide, similar to that in curves (1) and (2) over the same potential range (0.8 to 1.4 V, RHE).

without any experimental evidence being given to support it. The latter thick film must therefore presumably be porous to H_2O and protons (cf. ref. 34) so that a 2-d film can separately be formed at the inner interface of the thick film with the metal, almost as though the remaining thick film were not present. Shibata had concluded [27] that reduction of his "α"-component (≡ OC1 here) left Pt atoms on the outside of the β-phase thick oxide film. In view of the result described above, such a conclusion seems unlikely to be correct since it is difficult to see how a monolayer equivalent of free Pt atoms on an underlying oxide film could, upon reoxidation reproduce the details of the i vs E profile for monolayer surface oxide formation on a bulk Pt metal surface for which it is known, e.g., that characteristic forms of the anodic i vs E profile are determined by lattice-plane geometries of the Pt metal surface. Thus, the picture envisaged here is, in some ways, just the opposite of Shibata's. Also Shibata proposed [27] that his β-oxide required UPD H for its reduction. While the OC3 + OC4 states are, in some cases, reduced over the H UPD region, this depends on the extent of formation (the Q values) of these states. Under less strongly oxidizing conditions, it can be seen from Fig. 3.6 or 3.12 that a multilayer (OC2) peak (well resolved from OC1) is already almost completely reduced over a potential range positive to that for commencement of H deposition, so the latter process is evidently not required to provide a mechanism for multilayer oxide film reduction [189].

The above results imply that a 2-d reconstructed state remains below the thicker oxide film that can be formed together with it, at sufficiently high potentials, and can evidently be reduced (as the OC1 state) independently of the thicker 3-d phase oxide that is reduced in the peak OC2, or OC3 + OC4 (Fig. 3.16).

Fig. 3.17 shows an analogous experiment to the one described above and demonstrated in Fig. 3.16, but in this case the negative going sweep was reversed twice, i.e. first at 0.63 V and then at 0.32 V, RHE. After the first sweep reversal (after reduction of the BS state), the immediate subsequent positive-going sweep does not trace out exactly the normal i vs E profile for 2-d monolayer oxide film [9]. This is, presumably, because

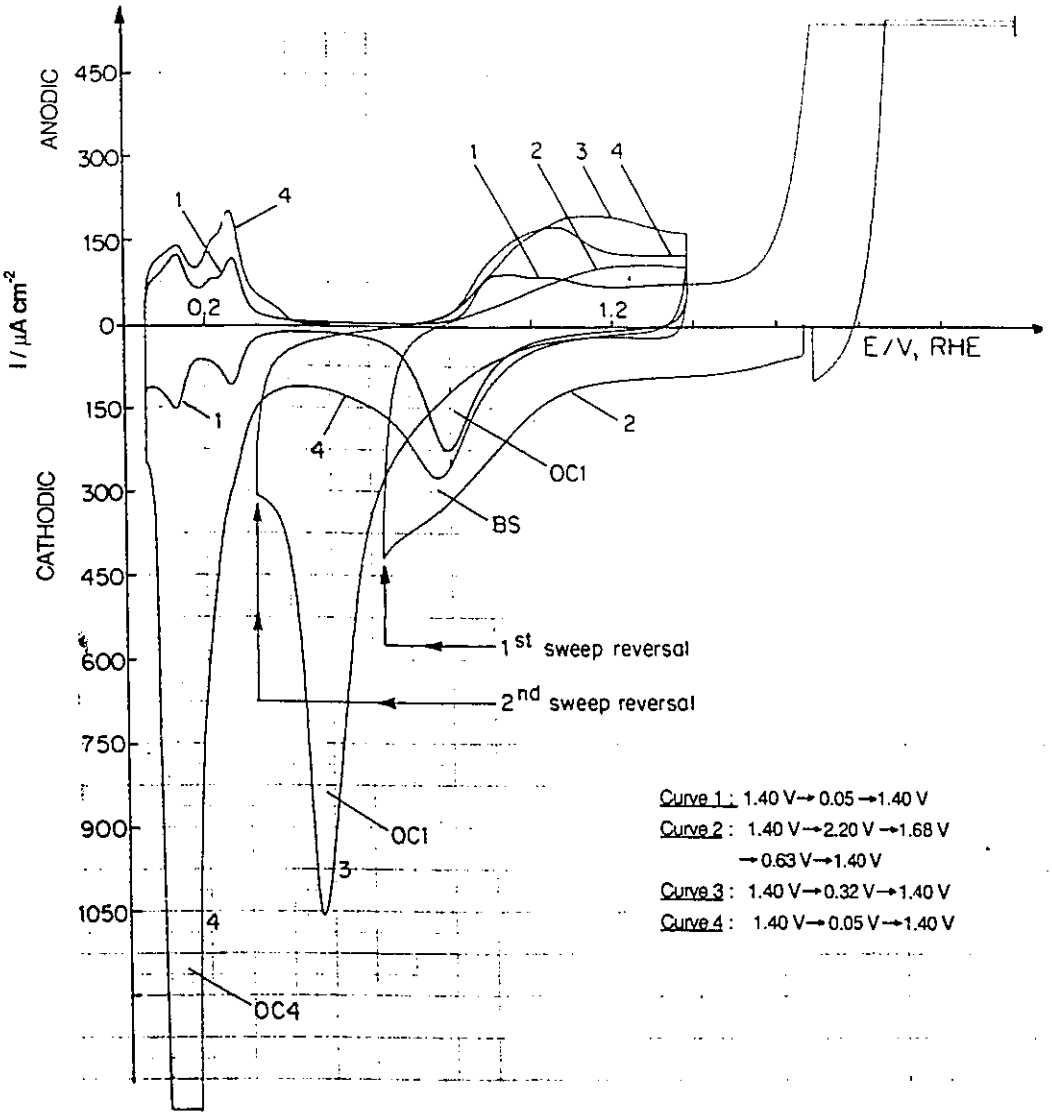

Fig. 3.17 Cyclic-v...mograms for Pt oxide formation and reduction at 50 mV s^{-1} (T = 298 K). (1) Regular C-V profile taken from 0.05 V to 1.40 V, RHE, showing state OC1 in reduction. (2) Extension of potential sweep to 2.2 V, RHE, then held at 2.2 V for 5 h 30 min, followed by a negative-going sweep arrested at $E_{i=0}$ (ca. 1.7 V, RHE) for 30 min with N_2 bubbling, followed by continuation of the negative-going sweep to 0.63 V but with reversal at that potential giving positive-going sweep (continuation of curve (2) but in positive direction) which does not trace exactly the normal quasi-2-d oxide film formation over potential range 0.8 to 1.4 V, RHE. Curves (3) and (4) are analogous to curves (2) and (3) in Fig. 3.16 (see the caption for details).

the BS state represents "Pt_2O_3" (i.e. PtO + PtO_2) which exists at the boundary between the "PtO" and "PtO_2" phases. Since the reduction potential of the BS state is the most positive of all the Pt oxide states, it may be concluded that the "Pt_2O_3" state is the least stable one and is the first to undergo reduction. The second reversal at 0.32 V, RHE, represents the situation shown in Fig. 3.16 and described already in this Section.

The above experimental results imply that the BS state, i.e. "Pt_2O_3", can be reduced to an oxide of a lower oxidation state of Pt ("PtO") which subsequently is reduced to Pt upon application of a sweep down to ca. 0.32 V, RHE, i.e. the potential range within which the OC1 state ("PtO") is reduced.

3.2.9 Kinetics of the Oxide Film Growth Processes

Recent papers [12], which originated in this laboratory, dealt in some detail with the kinetics of oxide film growth in the regime of time and potential where the direct logarithmic law of film extension in time applies. Such kinetics were also examined by Gilroy [8] in terms of a nucleation and growth mechanism as has been referred to earlier in this thesis.

The main point to be stressed here is that the direct logarithmic growth law extends to the highest potential (E_h = 2.3 V) used in the present work and its slope, dQ/d log t_h, continues to increase with E_h, though at a small rate when E_h is low.

However, at sufficiently long times (t_h) of extension of the film, the oxide film growth rate changes rather suddenly to much larger values (some 400 ×; Fig. 3.14), a condition that coincides with the appearance of the most stable OC3 + OC4 states of the film, as resolved on reduction. It appears that a new mechanism of oxide film growth takes over when the above condition is reached. The time for onset of this mechanism is shorter the higher is the E_h value, which suggests simply that some certain degree of oxide film thickness or some new state of the film is required for the new mechanism to take over.

It is suggested that this is the result of the change of electrical conductivity of the film [27] so that a high field can become established over the initial oxide film formed to an extent of ca. 1800 $\mu C\ cm^{-2}$. Such a difference of conductivity of oxide films at Pt was directly measured by Shibata [29] who found that the thicker oxide-film state, designated "β" in his paper [27], had much higher resistance than the "α" state of the oxide. The onset of increased resistivity was shown to be at Q = ca. 2000 $\mu C\ cm^{-2}$, somewhat larger but of the same order of magnitude as the film reduction charge associated with the onset of rapid film growth beyond the direct logarithmic region. As the poorly conducting film (OC3 + OC4 states designated here) becomes formed, the high-field, "inverse" growth law of Mott and Cabrera [51] (modified by Ghez [73]) presumable becomes applicable, so the kinetics of further growth are expected to be quite different from those in the direct logarithmic region for smaller Q values, as indeed is observed.

For the state of oxide reduced in the OC1 region, the mechanism of growth is continued deposition of OH or O species from the solution with place-exchange between Pt and OH or O species. This progressively changes the potential profile across the interphase due to changes of surface potential, an effect analogous to that of specifically adsorbed anions on the potential profile across the double-layer at Hg. It has been shown [48] that this effect can lead to a "direct" logarithmic growth law in time.

When the thicker film is established, having high resistivity [29], the mechanism can then change to Pt cation injection into the previously formed film, with field-assisted ion migration in the film, according to the "high-field" Mott-Cabrera mechanism [51,73]. This mechanism was suggested for Pt oxidation by Ord and Ho [20], and considered by Shibata [27] and by Damjanović et al. [22] but in ref. 20 was not supported by the evidence of enhanced resistivity since only thinner films, that had not attained the "β"-state of Shibata, were involved.

It has been mentioned that the oxide film growth rate increases some 400× once the initial oxide film has been formed to an extent of ca. 1800 $\mu C\ cm^{-2}$ (see Fig. 3.14).

The following explanation is suggested.

In the initial stage of the oxide formation, only the OC1 state is formed to the extent of 2 monolayers of "PtO" (880 $\mu C\ cm^{-2}$). Subsequently, the formation of one further nominal monolayer of "PtO_2" (i.e. the state in which the Pt:O ratio is 1:2) occurs corresponding to 880 $\mu C\ cm^{-2}$ appearing in other states. Once one monolayer of "PtO_2" has been formed, the oxide growth rate drastically increases. The formation of the first monolayer of "PtO_2" on top of two monolayers of "PtO" is a slow process, and the Q vs log t_h curves (Fig. 3.14) may serve as indirect evidence. The total charge equivalent to 2 monolayers of "PtO" and 1 monolayer of "PtO_2" corresponds to 1760 $\mu C\ cm^{-2}$ which is very close to the value of ca. 1800 $\mu C\ cm^{-2}$ referred to above (see Section 3.2.5) and to the 2000 $\mu C\ cm^{-2}$ charge of Shibata [29].

It is puzzling that thick-oxide growth requires minutes or even hours but such thick films can be reduced within a few or several seconds in a single sweep at 50 mVs^{-1}. This implies that the activation energy of the bulk-type oxide growth is much higher than that for its reduction. In Section 3.2.10 it is shown that the thick-oxide states can be formed on a single sweep but only if much higher polarization potentials are applied at an elevated temperature.

3.2.10 Oxide Formation in a Single Sweep to Potentials between 2.4 and 4.0 V at Room and Elevated Temperatures

As has been mentioned in Section 3.2.2, states OC2 to OC4 (the bulk-type oxide) require large values of t_h to be formed, and cannot be grown in a single sweep to upper polarization potentials of 2.3 V or less. An obvious question arises: (a) whether any of the thick-oxide states could be grown in a single sweep if potentials were taken to values substantially higher than 2.3 V, RHE; or (b) whether increase of temperature would increase the growth rate sufficiently to form any of the above states in a single sweep. In a further series of experiments, the polycrystalline Pt electrode was polarized at potentials

2.4, 2.6, ..., 4.0 V, RHE, for t_h=0 time (a single sweep) at temperatures of 298, 323, 333 and 348 K, for each E_h (see Fig. 3.18). In the case of experiments where the oxide was grown at elevated temperatures, the reduction was done at 298 K, with N_2 outgassing at $E_{i=0}$, as before.

Application of single-sweeps to 4.0 V, RHE, at 298 and 323 K results in the formation of only the OC1 and BS states. However, polarization at 333 and 348 K is found to lead to the formation of the OC1, BS and OC3 states. The highest oxide-reduction charge, Q, is achieved for the polarization (holding) potential of E_h = 4.0 V, RHE, at T = 348 K; Q is then ca. 4960 $\mu C\ cm^{-2}$ and corresponds to ca. 11.3 monolayers.

It is important to record that the OC1 charge limit of ca. 880 μC per real cm^2, as discussed in Section 3.2.3, is still maintained, even up to 4.0 V and at elevated temperatures. Also, the sequence of states, observed in reduction, is again OC1, BS and subsequently OC3; the other states, OC2 or OC4, are evidently not observable in these single-sweep experiments.

3.2.11 ESCA Examination and SEM EDX Mapping Analysis

The preliminary results of an ESCA examination of the state of Pt in the oxide film (cf. refs. 191-194), after various states of the oxide films had been formed, showed that Pt is in the +IV oxidation state in OC2, OC3 and OC4, while the OC1 state corresponds to the +II oxidation state. This clearly indicates that the OC2 to OC4 peaks do not differ on account of differences of oxidation state of Pt (oxides of different Pt to O ratio) so that these oxide states must differ, rather, on account of their different Gibbs energies and to some extent also on account of the kinetics of their reduction.

SEM EDX mapping analysis results for Pt and O show that in the case of the oxide formed on a polycrystalline Pt plate, the film evidently has different thickness at different grains (Fig. 3.19). Sputtering with 5.0 keV Ar^+ ions gradually removes the oxide, but differentially: it is clear that different grains were covered with oxide to different

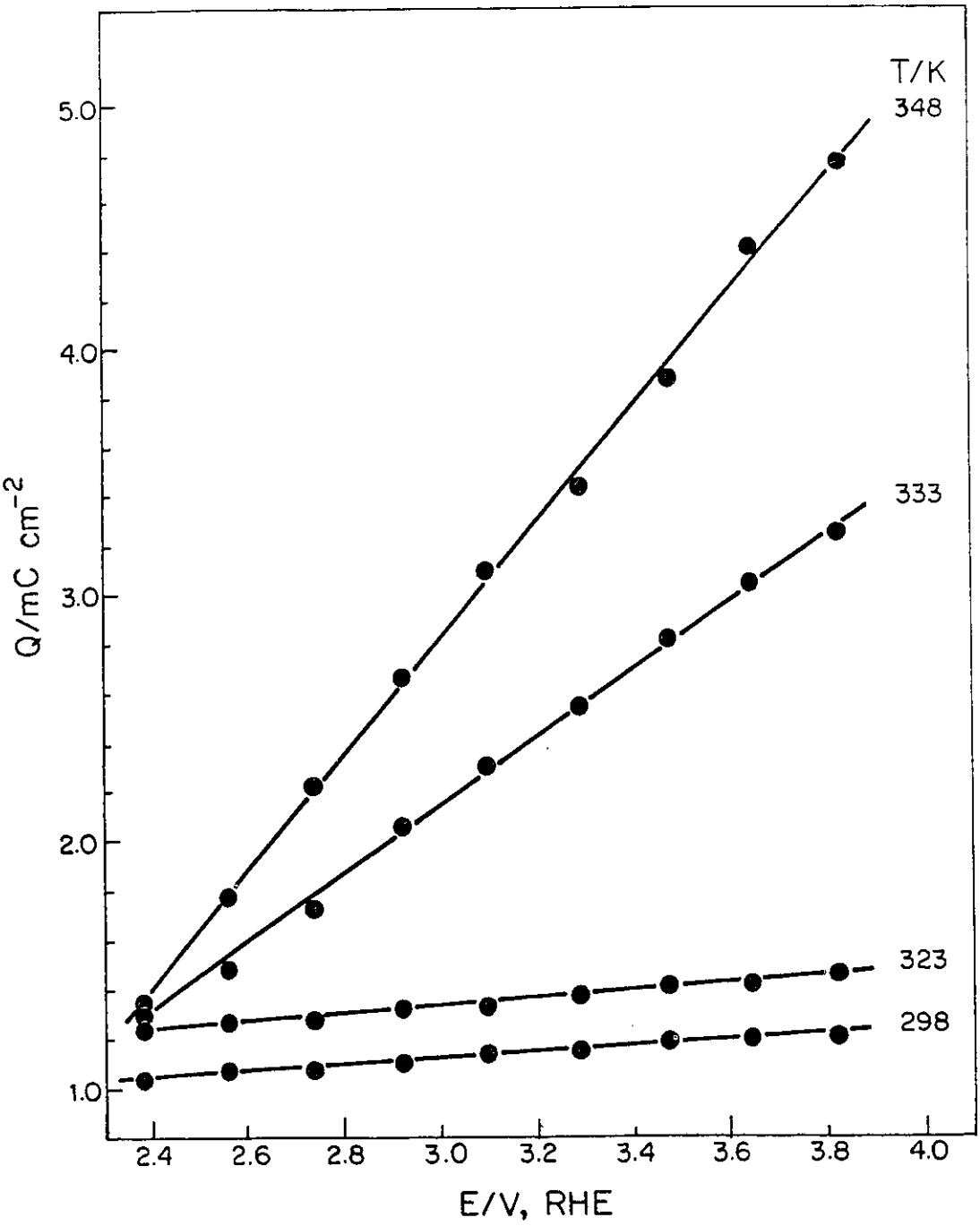

Fig. 3.18 Oxide growth at Pt electrodes upon application of a single sweep up to 2.4, 2.6, ..., 4.0 V, RHE, in 0.5 M aq. H_2SO_4 at 298, 323, 333 and 348 K (Figure shows potentials after the "IR" correction).

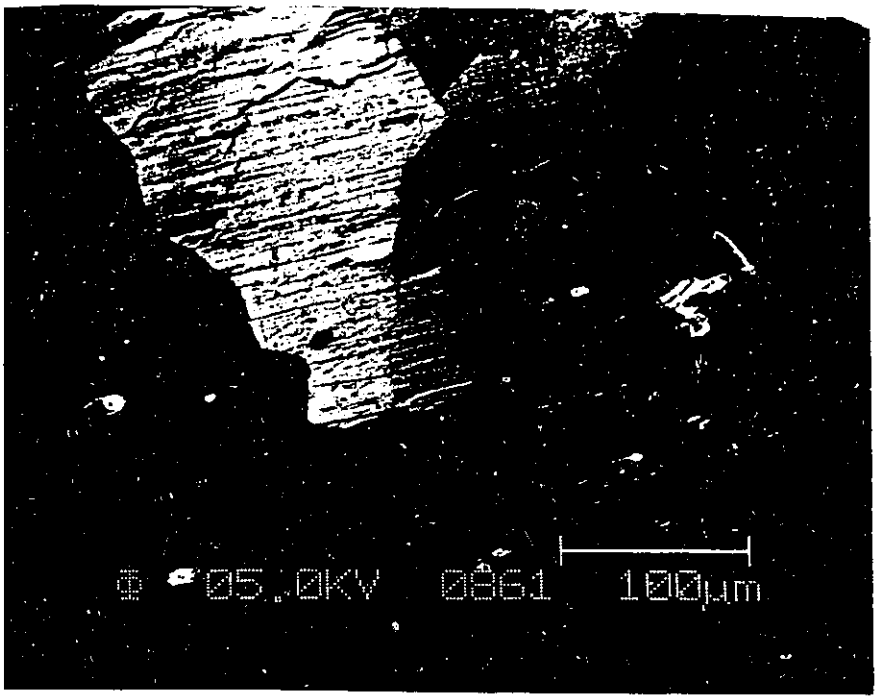

A

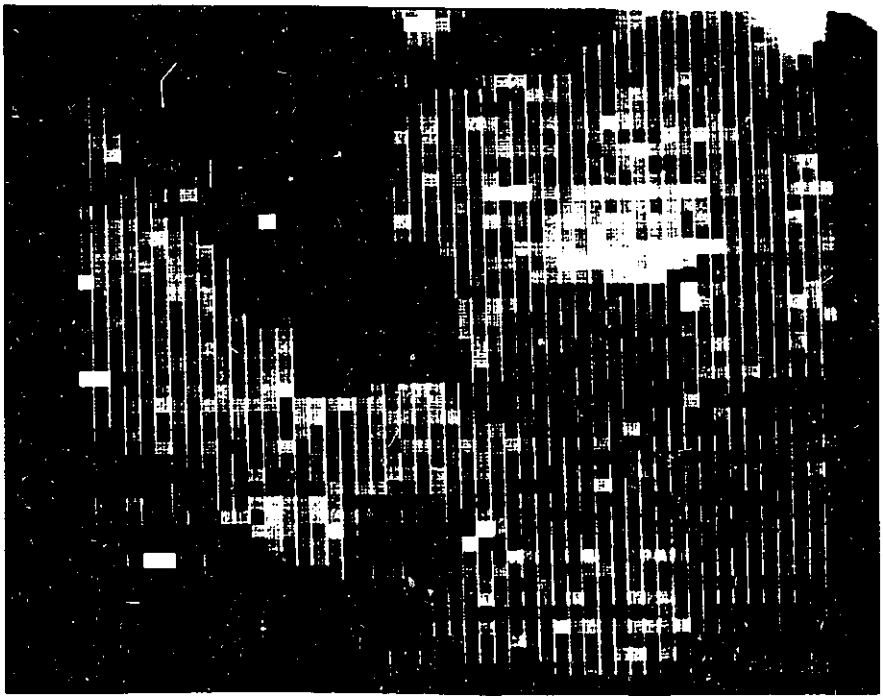

B

Fig. 3.19 SEM EDX mapping analysis micrographs: (a) shows different grains within a Pt polycrystalline sheet covered with Pt oxide; (b), (c) and (d) represent EDX mapping analysis micrographs after sputtering with 5.0 keV Ar^+ ions for 0, 20 and 40 s, respectively. Dark spots represent Pt and bright ones Pt oxide. (Different thickness [different numbers of monolayers] at different grains is indicated).

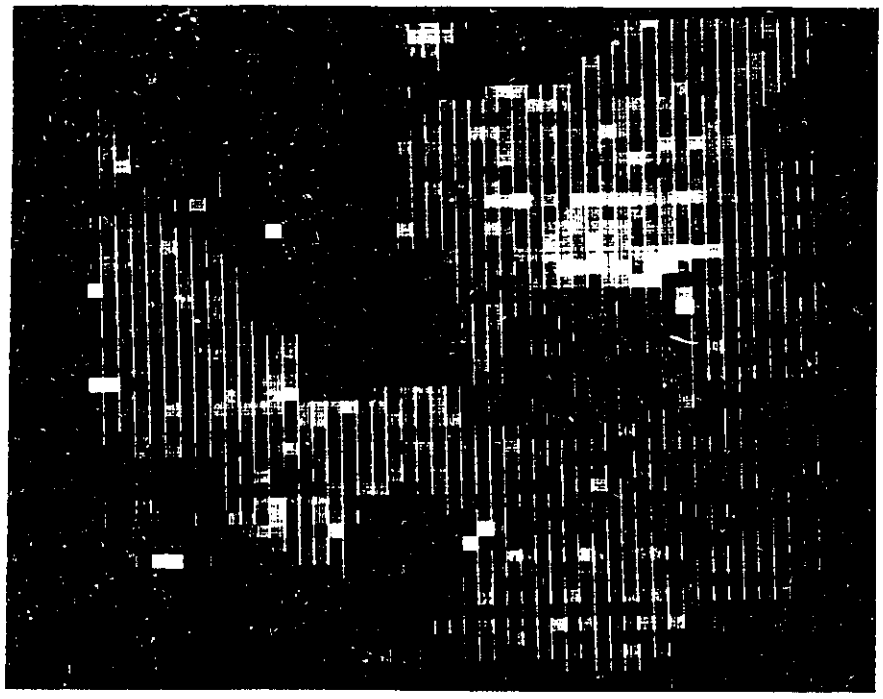

C

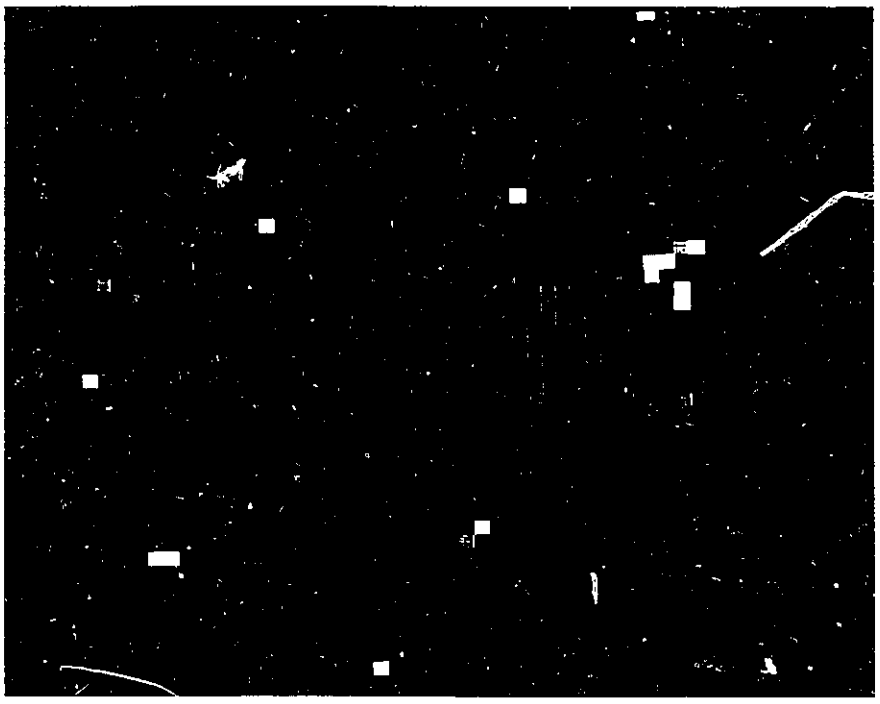

D

Fig. 3.19 (continued)

thicknesses, possibly correlated with the different energetic states. These results imply that the oxide growth rate is different at different principal crystallographic faces but, from the ESCA binding energy information, chemically the same oxide (i.e. the same Pt to O ratio) is formed across the surface [206].

3.2.12 Time Dependence of O_2 Evolution Rates in Relation to State of Formation of the Pt Oxide Film

During the extended periods of oxide film formation, parallel anodic evolution of O_2, of course, takes place [21,22]. The O_2 evolution behaviour in time is of interest in relation to the changing electrocatalytic properties of the oxide film as it grows and changes its state as indicated in the Figs. 3.5 - 3.12.

The rates of O_2 evolution were measured, as current-densities, i, on a Y-time recorder and attempts were made to relate the recorded O_2 evolution current-densities, i, to the course of oxide film development at the Pt. This can be reliably done since the currents for the latter processes are < 0.1% of the O_2 evolution currents. We summarize the behaviour as follows and illustrate it in Fig. 3.20 for three potentials. The behaviours described below are to be considered in the light of the progressions of oxide states revealed in the sweep-curves of Fig. 3.5 - 3.12 and referred to in Table 3.3.

Behaviour at 1.8 V: The initial i is 1.2 mA cm^{-2} but drops exponentially with time towards zero within 0.2 h, up to 60 h; the cyclic-voltammograms show only peak OC1. After 20 h, the peak OC2 appears but little effect on the i vs t_h relation is observed.

Behaviour at 1.9 V: The behaviour is similar to that at 1.8 V. The peaks OC2 and OC3, as well as OC1, are observed but no significant influence on the i vs t_h record is observable.

Behaviour at 2.0 V: At this potential, i is initially 7.5 mA cm^{-2} but decreases with t_h to a shallow minimum around 0.5 mA cm^{-2}. After this point, i has a slowly variable behaviour (between 0.65 and 1.40 mA cm^{-2}) in time. Only the peaks OC1 and OC4 are

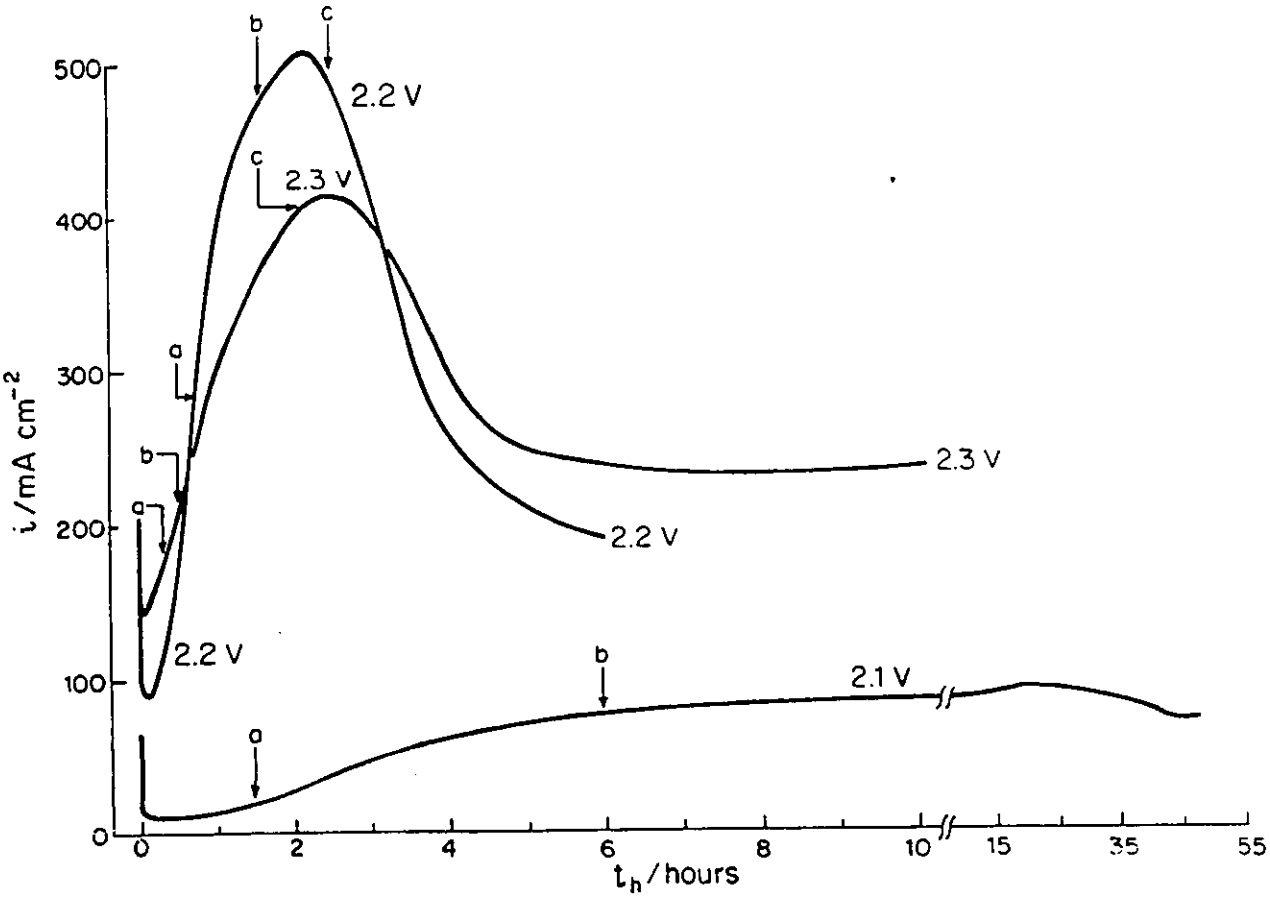

Fig. 3.20 The rates of O_2 evolution, measured as current-densities, during an extended period of oxide film formation at various holding potentials, (i vs t_h). Annotations to curves: (a) the peak OC3 develops; (b) the peak OC4 develops; (c) the peak OC3 regrows at the expense of OC4 and the total reduction charge remains practically constant.

distinguished at this potential but the appearance of OC3 is not correlated with the i vs t_h record.

Behaviour at 2.1 V: The behaviour is similar to that at 2.0 V but now both peaks OC3 and OC4 are observed but are not clearly correlated with the course of i in time (Fig. 3.19).

Behaviour at 2.2 V: The initial value of i is 190 mA cm^{-2} (Fig. 3.19) but then increases to ca. 500 mA cm^{-2} after 2 h 10 min and decreases again. The variation of i here depends on how many times the electrode has been oxidized and reduced. As the peak OC4 decreases (see description of this latter behaviour earlier) and OC3 regrows, the i vs t_h plot reaches a maximum as seen in Fig. 3.19. This may arise because, as the OC3 state increases at the expense of OC4, the resistivity of the oxide film increases (cf. ref. 29).

Behaviour at 2.3 V: At this potential, the situation is similar to that at 2.2 V. Correlated with the observable maximum in i vs t_h, the charges in the peaks OC2 and OC4 are decreasing while that in OC3 is increasing. Again, these are the conditions for which the film resistivity may be increasing.

On the linear scale of current-densities in Fig. 3.19 the electrocatalytic effect of the changing state of the oxide formed at 2.2 and 2.3 V after $t_h > 2.5$ h looks substantial (ca. 4 to 5 times increase over the initial current density). However, it must be recalled that a decrease of activation energy of only ca. 5.5 kJ mol^{-1} at 298 K would be sufficient to cause this increase. Hence only subtle changes in the state of the oxide film are required to make apparently substantial changes in the electrocatalytic activity.

3.2.13 Stability of the Oxide Films

A separate reduction experiment was made in which an oxide film had been grown at 2.1 V for 12 h and then held on open-circuit for 24 h (with N_2 being bubbled) when the $E_{i=0}$ potential of 1.70 V had been reached on a following negative-going sweep. This experiment showed that no change in the state of this oxide occurred during this time in

comparison with that at an electrode at which the same quantity of oxide had been generated but reduced after only 30 min N_2 bubbling at ca. 1.70 V. The thick oxide films thus grown anodically are thus quite stable on open-circuit (in the absence of H_2; cf. ref. 28) as might also be deduced from the fact that they are only reducible at much lower potentials than those required for their formation, e.g. near or in the UPD H region.

The ESCA measurements also provide indirect evidence regarding the stability of the thick-oxide films. Since these measurements were conducted under ultra-high vacuum conditions (ca. 10^{-9} Torr) and Pt oxides, in which Pt had the +II and +IV oxidation state, were detected, it may be concluded that the thick-oxide films are stable under an ultra-high vacuum conditions. However, if the oxide(s) exist as porous and hydrous films (as suggested by Burke et al. [34,35]), then they might undergo dehydration under high-vacuum conditions.

3.2.14 Anodic Steady-state Tafel Polarization Relations for the Oxygen Evolution Reaction at Pre-oxidized Pt

Introductory Remarks

The anodic oxygen evolution reaction (OER) proceeds at all metals, base and noble, on oxide films that are developed anodically at potentials below those required for significant rates of O_2 to occur, or in many cases (e.g. Ni, Co, Pt), below the reversible potential for the OER. The oxide films on which O_2 is generated vary from relatively thick ones at base metals, such as Ni, Co or Pb, to very thin surface oxides in the case of Au or Pt [9,184,190,214-216].

The overall polarization behaviour of the OER at Pt was investigated in very clean solutions by Bockris and Huq [217] who were able to establish experimentally, for the first time, an approach to a true reversible potential for the O_2/H_2O equilibrium and determine the exchange current density, i_o, for the process. Schultze and Haga [218]

related the polarization behaviour at 353 K (pH=0.3) to the oxide film thickness and treated the mechanism at high overpotentials in terms of resonance tunnelling [219] of electrons via the higher oxidation state of Pt in the oxide film.

Various mechanisms of anodic O_2 evolution have been considered in some previous papers [217,220-222] but with little relation experimentally to the state of the oxide film on which the reaction proceeds at the given anode metal. Schultze and Haga [218] recognized the importance of evaluating the OER kinetics at Pt on definite states (thicknesses) of the oxide. Damjanović et al. [223], and Birss and Damjanović [23] recognized that at low oxygen overpotentials, parallel currents arise for oxide film growth and Faradaic O_2 evolution. After sufficiently long times, the film growth rate is almost zero and the OER then continues on a more or less unchanging state of the oxide film determined by the time and anodic potential (see Section 3.2.2). In the case of Pt, a considerable amount of information on the kinetics of the OER taking place on pre-oxidized Pt is available from: (a) the research conducted in this laboratory [184,190,224,225] on the OER at pre-oxidized Pt electrodes; (b) the resolution of the reversible from the irreversible stages in the formation and reduction of the 2-d oxide [9,10]; (c) the kinetics of the Pt oxide growth or extension [7,8]; (d) the chemical state of Pt in surface oxide films at Pt through XPS measurements [191-194,226]; and (e) the involvement or otherwise of the O atoms in the film itself in the electrochemical formation of O_2 molecules, through $^{16}O/^{18}O$ isotope labelling experiments [227].

The OER differs in several important ways from the HER at metals, as follows: (a) the reaction (OER) proceeds always on a bulk-oxide surface or on the surface of an oxidized metal bearing a thick (as at Ni) or thin (as at Pt or Au) oxide film; (b) the oxidation state of such oxide materials can, and often does, depend on the electrode potential; (c) the intermediates in the OER can be both OH and/or O species and higher oxidation states of metal ions in the exterior surface of the oxide film; the latter species can act as mediator states in the anodic O_2 evolution mechanism [190]; and (d) the

oxide-film growth proceeds simultaneously with the OER [23,184,190,224,225,228,229].

In the experiments reported here, steady-state polarization measurements (Tafel plots) were conducted at pre-formed oxide films which were well defined as manifested through prior C-V measurements (see Section 3.2.2 and Table 3.3). The measurements were done in such a way that the Tafel plots were taken either prior to the appearance of OC2, OC3 and/or OC4 states or after their development. This sequence of experiments allowed the development of a new oxide state(s) to be correlated with any possible changes in the kinetics of the OER as revealed by Tafel slope values.

For simplicity and clarity, the results are grouped in two sections: Section I - for which the polarization potential, E_h, was held constant while the polarization time was varied; and Section II - for which the polarization time, t_h, was held constant while the polarization potential was varied. All the presented data are "iR-corrected"; the resistance of the solution between the tip of the potential-sensing probe (the Luggin capillary) and the working electrode was determined using the method described in Section 2.2.3 and R_s was found to be 0.502 Ω (this is an average of four values).

The Tafel plots were recorded for oxide films formed at four different polarization potentials, 2.0, 2.1, 2.2 and 2.3 V, RHE, and were taken between 1.70 V and one of the upper potential limits.

An obvious question arose, which of the following commonly accepted "Tafel-plot" programmes should be applied:

(a) ascending staircase or rectangular;

(b) descending staircase or rectangular?

In a separate sequence of measurements for one particular set of polarization potential and time conditions, results obtained under the four possible conditions were compared. The difference between results obtained with the staircase and the rectangular programme was negligible while for ascending and descending changes of potential, results were significantly different (because for ascending potentials, changes of state of

the oxide film can still be occurring). Between these two, the ascending potential programme was applied which provided almost perfect reproducibility of experimental results and the best surface characterization. The Tafel plots for the oxide formed at 2.1 V, RHE and higher reveal two linear regions in which the Tafel slopes, $b = dE/d \log t$, have different values, designated as b_1 and b_2 (b_1 refers to the first region between 1.70 V and the inflection point {usually between 1.9 and 1.95 V, RHE}, while b_2 refers to the second region between the inflection point and the upper potential limit). The values of b_1 and b_2 are listed in Tables 3.5 and 3.6.

Section I

Figs. 3.21-3.24 show the Tafel plots for polarization at 2.0, 2.1, 2.2 and 2.3 V, RHE, for various polarization times; the values of the Tafel slopes, b_1 and b_2, are summarized in Table 3.5.

An interesting feature is the curvature of the Tafel plots between 1.7 and 1.8 V, RHE, for 0 and short polarization times. This behaviour is attributed to further development of the OC1 state. However, once the BS and OC3 states have been formed, the relation becomes linear. Further increase of the polarization potential does not change the slopes (Table 3.5) but moves the whole profile towards higher current densities due to increase of the real surface area (see Section 3.1).

Section II

In this Section, only two sets of Tafel plots will be shown for the polarization time, t_h, of 30 min and 1 h. These examples are sufficient for showing the general behaviour of changes in the Tafel slopes. Fig. 3.25 and 3.26 show Tafel plots for the polarization potential, E_h, of 2.0, 2.1, 2.2 and 2.3 V, RHE; the values of the Tafel slopes, b_1 and b_2, are summarized in Table 3.6.

There are two interesting features in these two sets of Tafel plots: first, the value of

Table 3.5

Polarization potential E_h / V, RHE	Polarization time t_h / h	Tafel slope		Comments
		in region 1 b_1 / mV	in region 2 b_2 / mV	
2.0	0 0.1 1 4 12 94	130 125 116 116 115 115	- - - - - -	Tafel plots too short to determine b_2 without making a big error
2.1	0 0.5 3 8.5 19	115 111 112 111 110	69 70 71 69 69	For long t_h, the Tafel plots shift toward larger current densities due to increase of the real surface area
2.2	0 0.15 1.6 3.5 6.5	112 109 106 106 106	64 63 67 66 67	As in the case of E_h = 2.1 V but the shift is even greater
2.3	0 0.15 0.5 1 2	109 109 106 105 105	65 65 68 71 74	As in the case of E_h = 2.1 and 2.2 V but the shift is the greatest and the time required for it is the shortest

Table 3.6

Polarization time t_h / h	Polarization potential E_h / V, RHE	Tafel slope		Comments
		in region 1 b_1 / mV	in region 2 b_2 / mV	
0.5	2.0 2.1 2.2 2.3	119 111 107 106	- 69 67 68	The plots shift towards larger current densities due to increase of the electrode real surface area
1.0	2.0 2.1 2.2 2.3	116 111 107 106	- 71 67 71	As above but the shift is greater since thicker films have been established

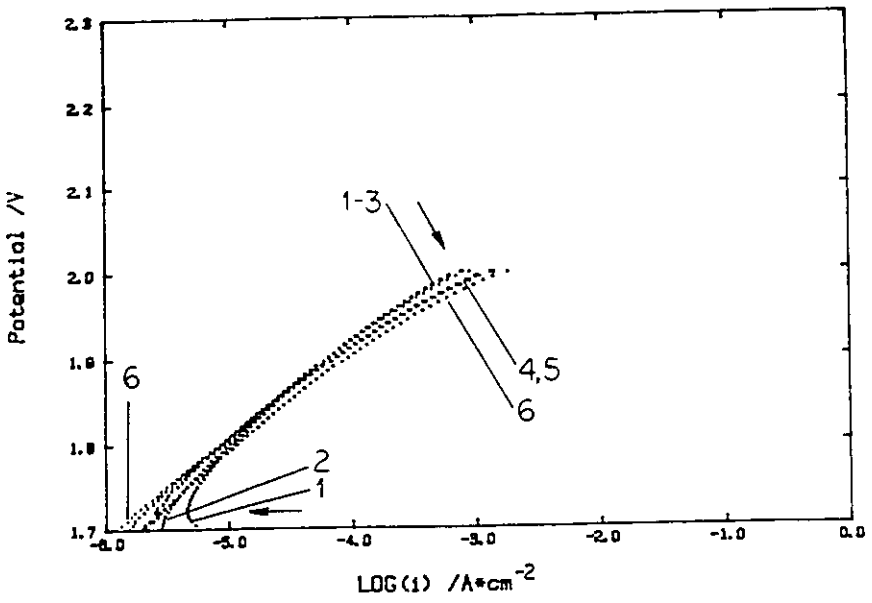

Fig. 3.21 Tafel relations for anodic O_2 evolution in 0.5 M aq. H_2SO_4 (298 K) on pre-oxidized Pt at E_h = 2.0 V, RHE, for various times; curve (1) 0 min; (2) 5 min; (3) 1 h; (4) 4 h; (5) 12 h; and (6) 94 h (arrows indicate changes in the Tafel plots).

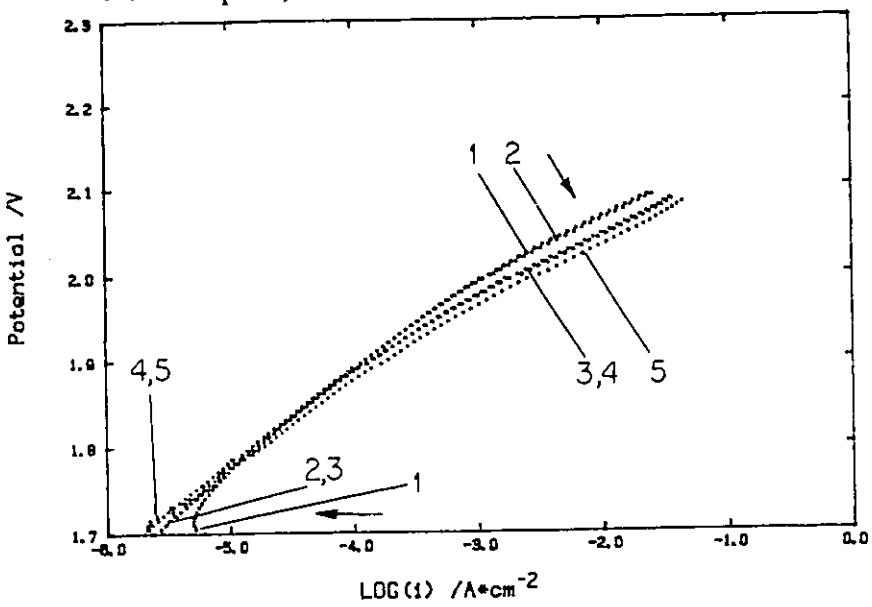

Fig. 3.22 Tafel relations for anodic O_2 evolution in 0.5 M aq. H_2SO_4 (298 K) on pre-oxidized Pt at E_h = 2.1 V, RHE, for various times; curve (1) 0 min; (2) 30 min; (3) 3 h; (4) 8.5 h; and (5) 19 h (arrows indicate changes in the Tafel plots).

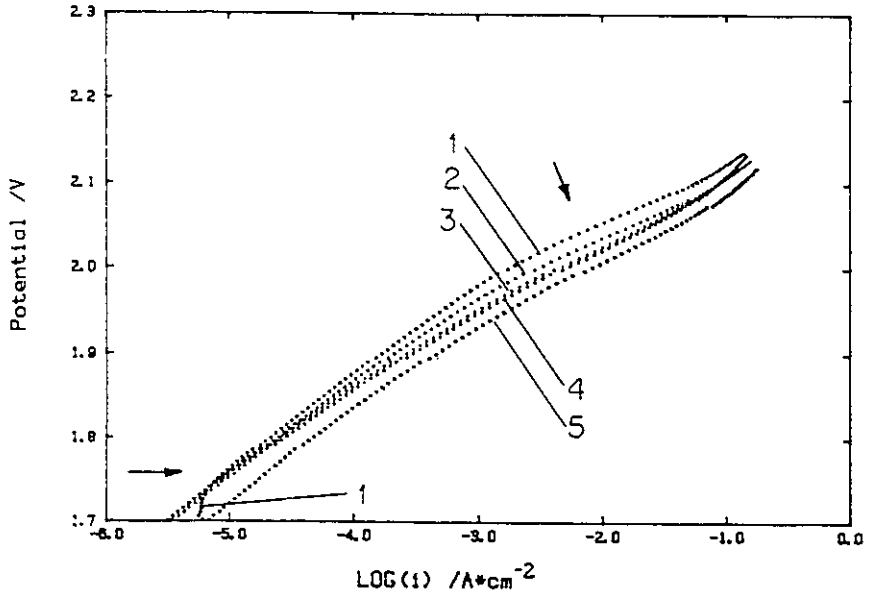

Fig. 3.23 Tafel relations for anodic O_2 evolution in 0.5 M aq. H_2SO_4 (298 K) on pre-oxidized Pt at E_h = 2.2 V, RHE, for various times; curve (1) 0 min; (2) 10 min; (3) 100 min; (4) 3.5 h; and (5) 6.5 h (arrows indicate changes in the Tafel plots).

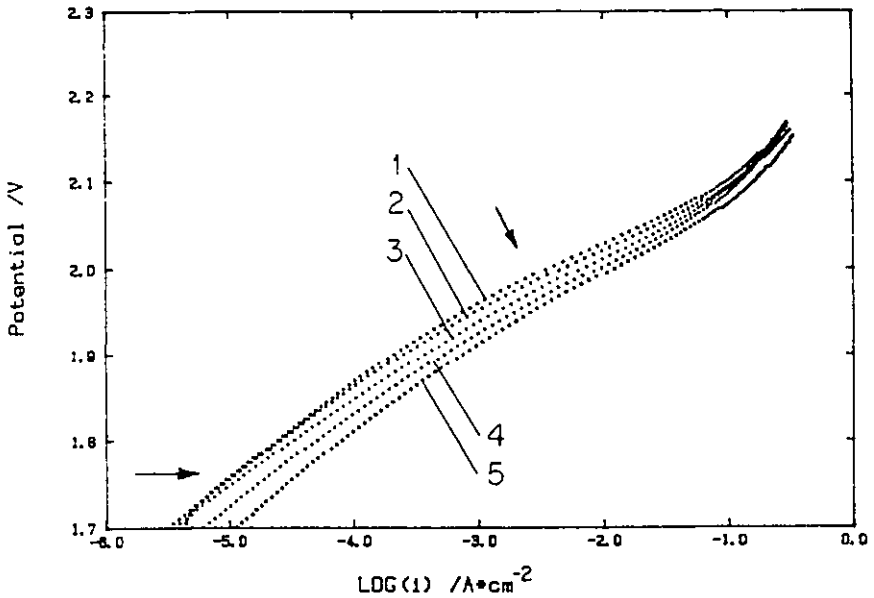

Fig. 3.24 Tafel relations for anodic O_2 evolution in 0.5 M aq. H_2SO_4 (298 K) on pre-oxidized Pt at E_h = 2.3 V, RHE, for various times; curve (1) 0 min; (2) 10 min; (3) 30 min; (4) 65 min; and (5) 2 h (arrows indicate changes in the Tafel plots).

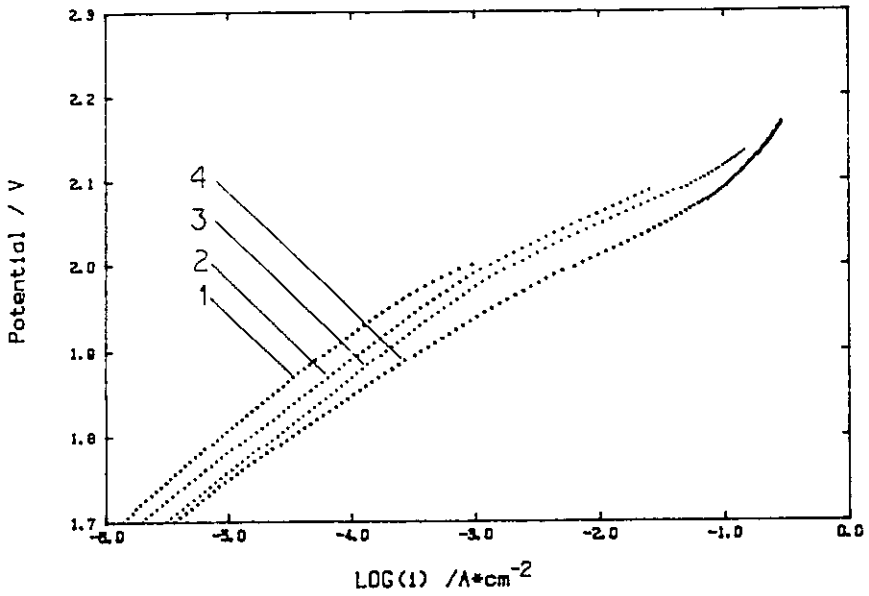

Fig. 3.25 Tafel relations for anodic O_2 evolution in 0.5 M aq. H_2SO_4 (298 K) on pre-oxidized Pt for t = 30 min at various polarization potentials; curve (1) 2.0 V; (2) 2.1 V; (3) 2.2 V; and (4) 2.3 V, RHE.

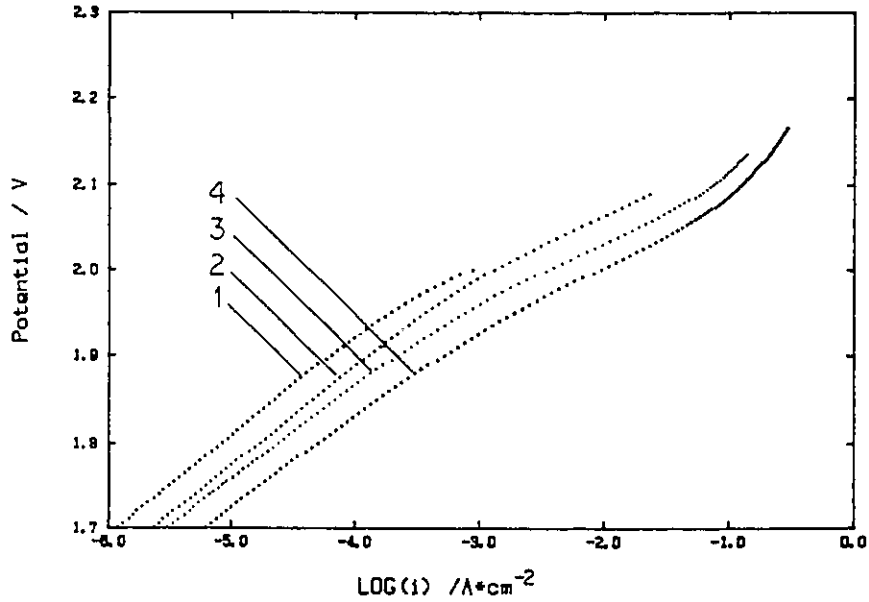

Fig. 3.26 Tafel relations for anodic O_2 evolution in 0.5 M aq. H_2SO_4 (298 K) on pre-oxidized Pt for t_h = 1 h at various polarization potentials; curve (1) 2.0 V; (2) 2.1 V; (3) 2.2 V; and (4) 2.3 V, RHE.

the Tafel slope b_2 remains essentially constant while b_1 decreases; and second, the Tafel plots shift towards higher current densities due to the increase of the real surface area of the electrode as a result of thick-oxide film formation.

The Tafel relations for anodic O_2 evolution in 0.5 M aq. H_2SO_4 solution, reproducibly exhibit two linear regions having different Tafel slopes (see Tables 3.5 and 3.6). The values of b_1 are close to the earlier results obtained in this laboratory [184,190,224,225], while the values of b_2 are between 10 and 15 mV greater. The value of the transition potential, E_{tr}, is between 1.90 and 1.95 V, RHE, and is higher than the previously reported value of ca. 1.83 V, RHE [184,190,224,225]. Apart from the discrepancies mentioned above, the behaviour reported here is in agreement with the other early results [184,190,218] and corresponds formally to participation of two processes in the overall reaction pathway which are in a parallel relation to one another, so that the one with lower Tafel slope is the preferred current-carrying pathway at higher overpotentials.

Relation between the Thick-oxide Films and the OER

As has already been mentioned in this Section, the Tafel slopes above E_{tr}, i.e. the inflection point, are different from those below it. In acidic solutions, the change of the slope was attributed by Schultze and Haga [218] to onset of electron transfer via "resonance tunnelling" and by Conway and Liu [190] to intervention of a redox mediation step involving higher oxidation states of Pt ions in the surface of the Pt oxide film. These attributions might be equivalent since the "resonance tunnelling" can be induced by presence of metal ions of higher oxidation states on the oxide surface. This mechanism, supported by experimental evidence, was discussed by Conway and Liu [184,190] and will not be dealt with in detail here. However, what is directly related to it, is the experimental evidence, presented in this thesis (see Sections 3.2.2-3.2.6), that: (a) Pt in the thick-oxide films exists in the +IV oxidation state, as was also found by other research laboratories [191-194]; and (b) the oxide film in which Pt is in the +IV oxidation state

resides on top of the quasi-2-d oxide film ("PtO") as was demonstrated in Section 3.2.8 and in ref. 189. The conclusion that Pt^{4+} can be in direct contact with the solution is very important for the overall mechanism of the OER taking place at thick oxide films and at potentials above E_{tr}.

Fig. 3.27 shows schematically the role of Pt^{4+} in the process of OH^- discharge on the surface of the oxide film.

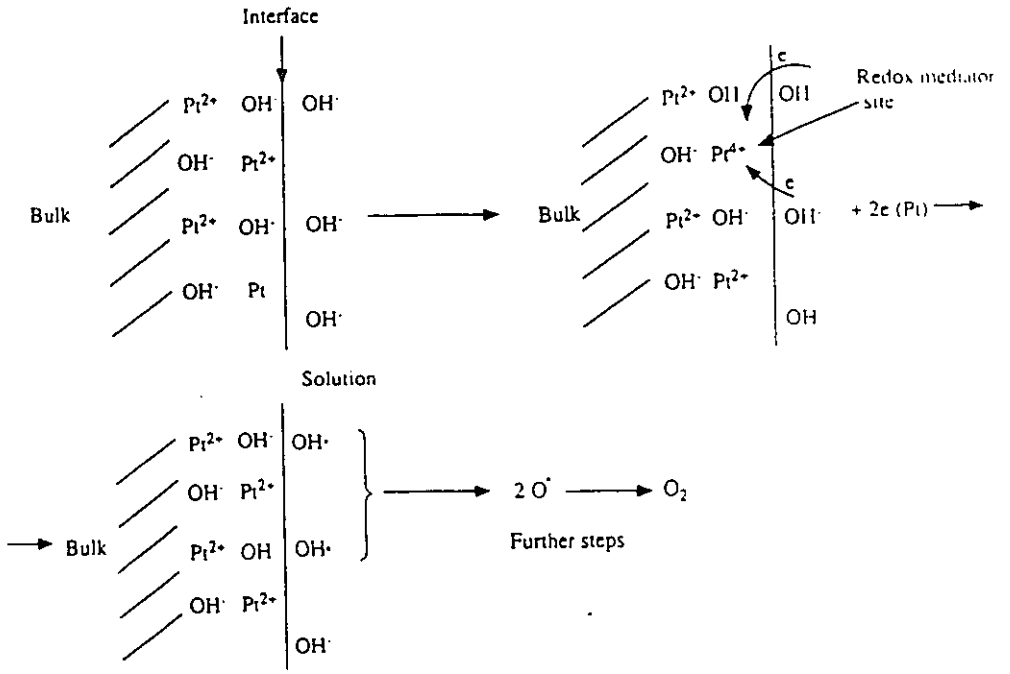

Fig. 3.27 Schematic representation of the role of Pt^{4+} ions as mediator sites in OH^- discharge which eventually leads to O_2 formation [184].

3.3 UPD of H at Pt(111) Electrode Surface after Various Thermal and Electrochemical Pretreatments - A Contribution to the Discussion on the Anomalous H Adsorption Behaviour at Pt(111)

3.3.1 UPD of H at Pt(111)

Within the last decade, the submonolayer states of chemisorbed H at single-crystal Pt electrodes, especially Pt(111), have become a topic of major interest in electrochemical surface science. The commonly applied LEED technique enables single-crystal surface characterization [107-109,230-232] while the cyclic-voltammetry technique [75,76] has demonstrated the existence of more than one state of H adsorption at given single-crystal principal-index surfaces.

The study of UPD of H at polycrystalline Pt by Will and Knorr [76] showed the existence of three H adsorption states. Also re-evaluation of the charging curves by Frumkin and Slygin [118] reveals two distinguishable states (see Section 1.10.1). This behaviour was confirmed by AC impedance [119,120] and optical reflectivity studies [124,125]. The interpretation, at that time, was that the distinguishable peaks arose from H electrosorption at different crystal faces of polycrystalline Pt, as was tested by Will [121] and by Conway et al. [122,123].

The early results of Will [121], who annealed the single-crystal Pt electrodes and pretreated them by prolonged cycling between 0.05 and 1.40 V, RHE, were re-examined by Hubbard et al. [137], who characterized the Pt(111) and Pt(100) surfaces by LEED and cleaned them electrochemically by cycling between 0.05 and 1.40 V, RHE, ten or more times (see Section 1.10.2). The more recent results of Clavilier et al. [140-147] differ substantially from those of Hubbard, but also the experimental procedure applied (heating and quenching) was radically different.

The results of Hubbard and Clavilier were reproduced during the course of the present work and are examined below.

Annealed Pt(111) Surface

Fig. 3.28 shows the C-V profile for the Pt(111) electrode after annealing for 30 min at 900-920°C followed by slow cooling. Since an apparatus for in situ characterization of single-crystal Pt electrodes was not available, the Pt(111) was transferred via air and precleaned in conc. H_2SO_4 prior to immersion in the test solution [9,135,201]. The electrode was cycled 10 times between 0.07 and 1.40 V, RHE, and the C-V profile for UPD of H was recorded (as shown in Fig. 3.28). It was correctly suggested by Więckowski [233] that transfer via air results in some impurity adsorption on the electrode surfaces while storage in conc. H_2SO_4 might form surface oxide. Both of these viewpoints were tested.

The Pt(111) electrode was reannealed and was not cleaned in conc. H_2SO_4. However, prior to its immersion into solution, it was precleaned by heating up to ca. 200°C in an hydrogen-oxygen flame. Such pretreatment neither reconstructs the surface [234] nor introduces any significant amount of stress into the single crystal, but effectively cleans the surface. The C-V profiles obtained at such a pretreated surface were closely similar to those shown in Fig. 3.28. Importantly, there were not signs of the "spike" of Clavilier around the potential of ca. 0.45 V, RHE. The H UPD accommodation, Q_{HUPD}, was found to be 246 (±5) μC cm^{-2}, which is very close to the calculated value of 240 μC cm^{-2} [137] for Pt(111). The peaks of the profile are at 0.125 and 0.260 V, RHE, respectively, while the hump in the "double-layer" region reaches its maximum at 0.55 V, RHE.

Pt (111) Surface Heated at ca. 500°C and Quenched

One of the most important aims of this part of the work was first to reproduce the results of Clavilier et al. [140-147] and then to perform further extended investigations on the "Clavilier" surface. The heating and quenching procedure was not favoured in this laboratory since it seemed to us that such a procedure could not fail to introduce a great

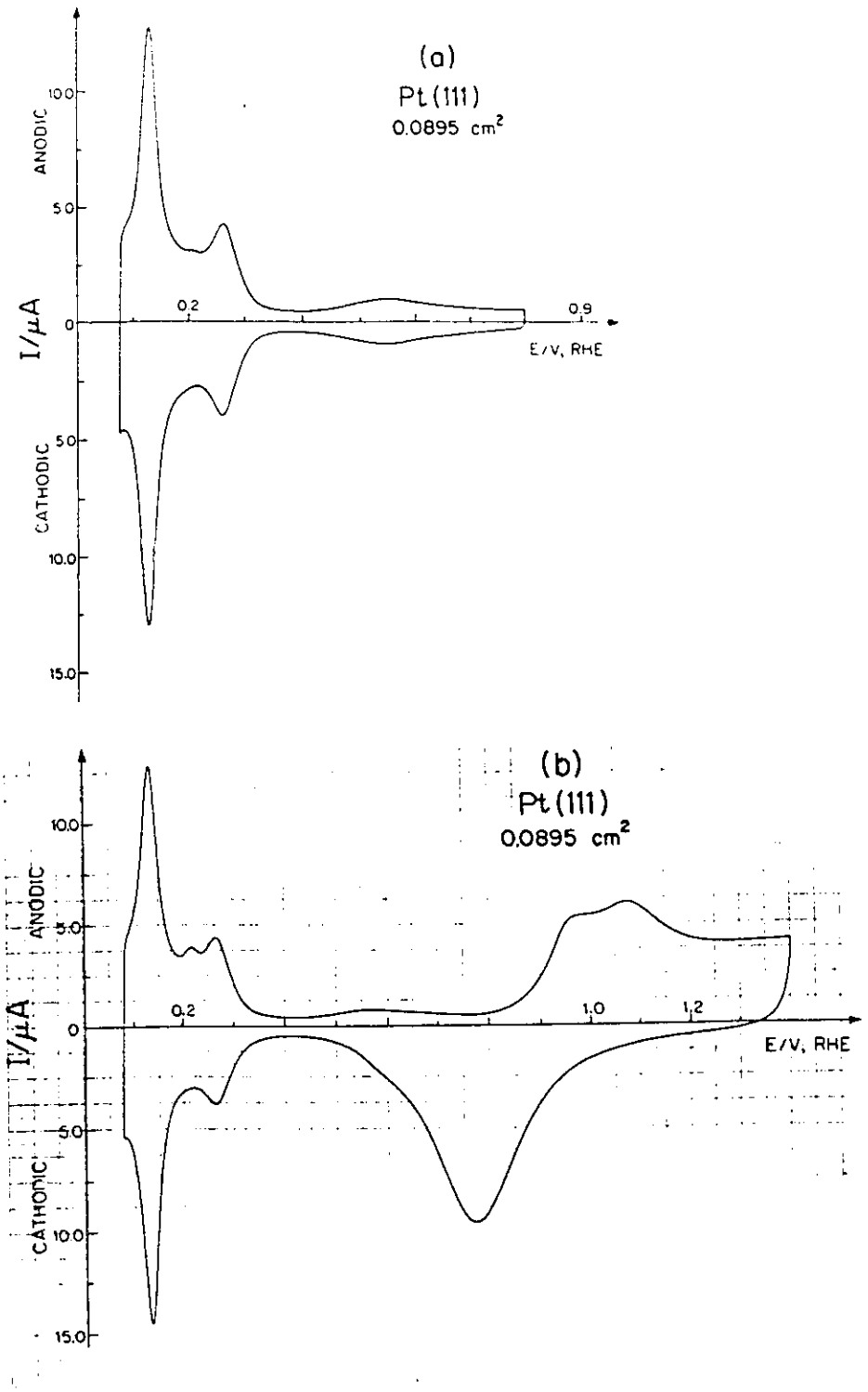

Fig. 3.28 C-V profiles for the Pt(111) electrode after annealing at 900-920°C followed by electrochemical precleaning; (a) H UPD C-V profile up to 0.8 V, RHE; (b) C-V profile up to 1.4 V, RHE (0.5 M aq. H_2SO_4, 298 K).

amount of stress into the crystal and, if repeated a few times, then it could lead to polygonization [195]. To avoid an irreversible destruction of the Pt(111) single crystal, it was heated to ca. 500°C and quenched in pyrolytically-distilled water. Fig. 3.29 shows the C-V profile for such an electrode, taken between 0.07 and 0.70 V, RHE. The H UPD accommodation was found to be 228 (±5) $\mu C\ cm^{-2}$. The peaks in the first "butterfly" are at 0.120 V, RHE, and the second "butterfly" is also well developed. The H UPD C-V profile reveals a small, overlapping peak at 0.46 V, RHE, which later (at higher heating temperatures - see below) becomes the characteristic "spike" [140-142]. Somewhat similar C-V profiles were reported by Clavilier and Armand [143] but after cycling at 50 $V\ s^{-1}$.

Pt(111) Surface Heated at ca. 800°C and Quenched

Fig. 3.30 shows the C-V profile of the Pt(111) electrode after heating at ca 800°C followed again by quenching. In this case, the peaks of the first "butterfly" are less pronounced and arise at 0.125 and 0.260 V, RHE.

The structure of the second "butterfly" became more complex and consisted of the hump with the "spike" at 0.455 V, RHE; a new peak appeared at 0.325 V, RHE. The H UPD charge was found to be 227 (±5) $\mu C\ cm^{-2}$. It is interesting that the H UPD C-V profile became more like the one of Clavilier upon increase of the heating temperature. This suggested that the shape of the H UPD C-V profile might depend on the heating-quenching conditions; evidently a difference of 300°C had led to a substantial change.

Pt(111) Surface Heated at ca. 1000°C and Quenched

Fig. 3.31 shows the C-V profile of the Pt(111) electrode after heating at ca. 1000°C, i.e. above the annealing temperature of Pt which is 900°C, followed by quenching. An interesting feature of this C-V profile is the complex structure between

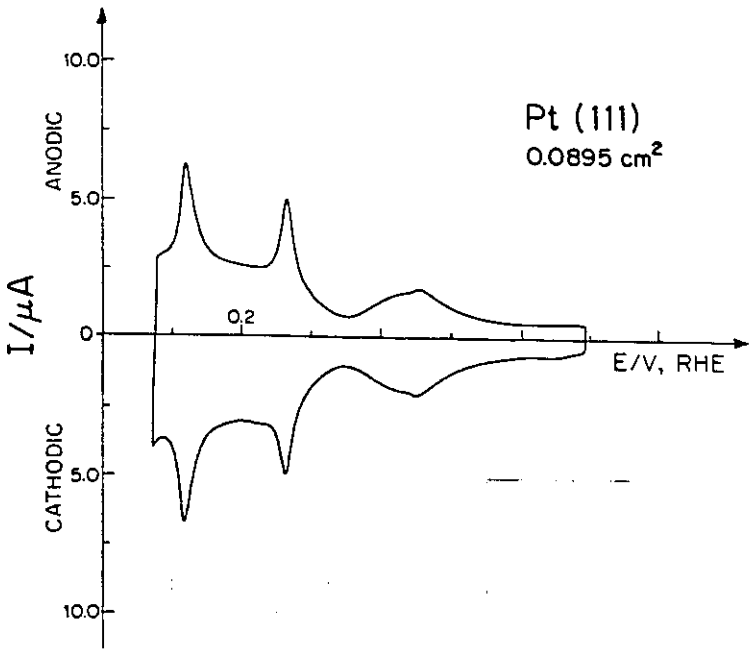

Fig. 3.29 H UPD C-V profile of the Pt(111) electrode after heating at ca. 500°C followed by quenching (0.5 M aq. H_2SO_4, 298 K).

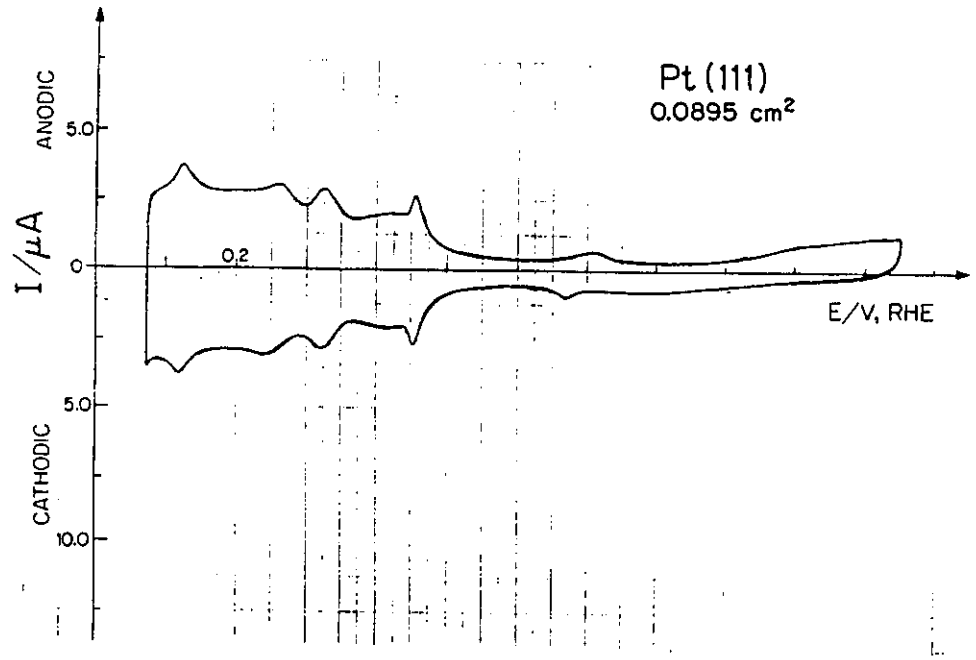

Fig. 3.30 H UPD C-V profile of the Pt(111) electrode after heating at ca. 800°C followed by quenching (0.5 M aq. H_2SO_4, 298 K).

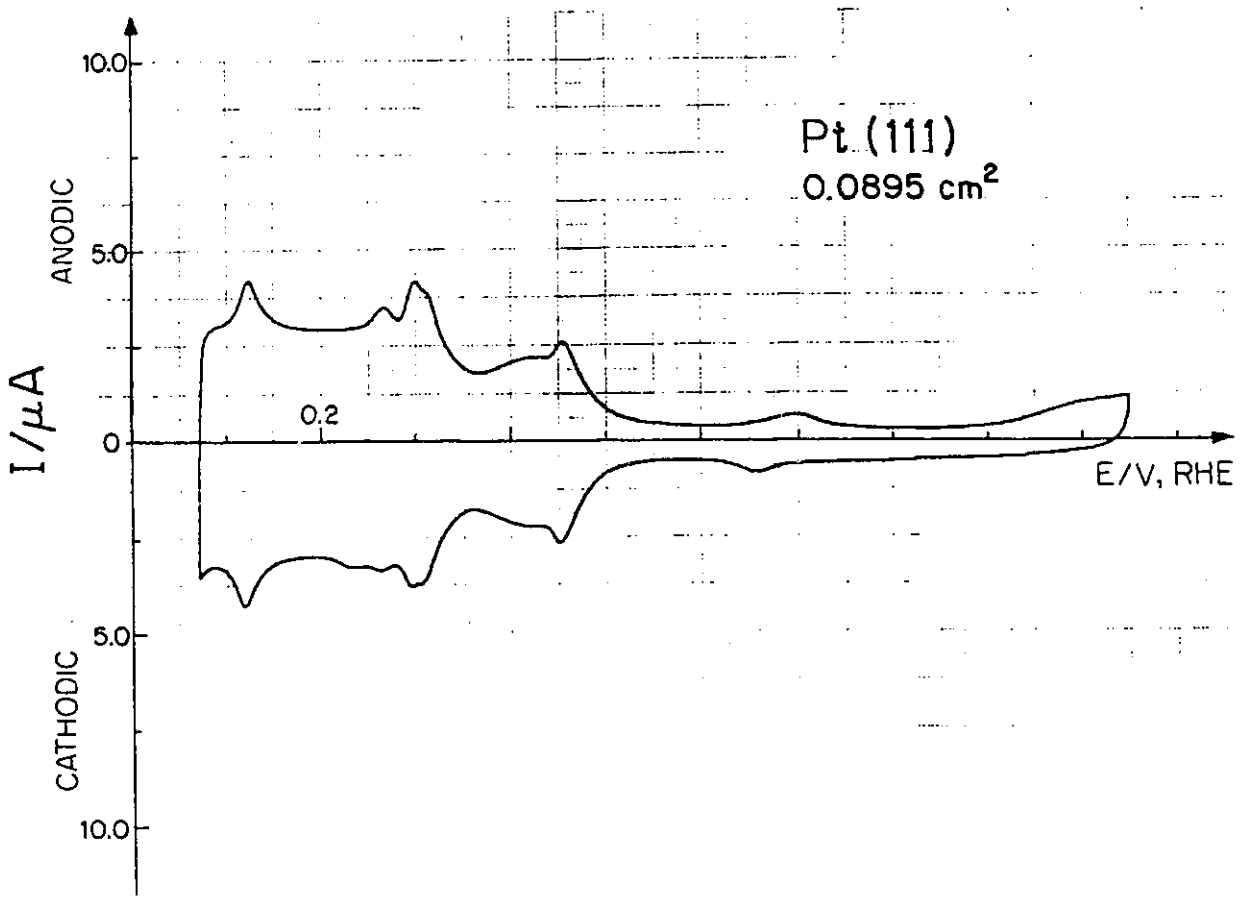

Fig. 3.31 H UPD C-V profile of the Pt(111) electrode after heating at ca. 1000°C followed by quenching (0.5 M aq. H_2SO_4,.298 K).

0.25 and 0.35 V, RHE. However, this could be simply explained by the growth of the peak at 0.325 V (Fig. 3.30). For this case, the complex structure between 0.25 and 0.35 V, RHE, evidently arises from overlapping of the two peaks at 0.265 and 0.325 V, RHE, respectively (see Fig. 3.30).

Figs.3.29-3.31 show clearly that the H UPD C-V profiles of Pt(111) depend substantially on the thermal pretreatment and reveal two characteristic "butterflies". This behaviour has not been observed in other research laboratories and was rather unexpected.

A next question arises whether the fine structure of the "double-butterfly" undergoes any significant changes upon potential cycling to various upper potential limits, e.g. those in which surface oxide is generated and reduced. The results of Aberdam et al. [195] indicate changes in the C-V profiles and LEED patterns of Pt(111) upon cycling up to 1.40 V, RHE, but virtually no data are available in the literature on prolonged cycling to potential limits lower than 1.40 V, RHE.

3.3.2 Behaviour of Heated and Quenched Pt(111) Electrode after Prolonged Cycling up to 1.10 V

Fig. 3.32(a) shows a C-V profile for the Pt(111) electrode after having been heated to ca. 900°C, followed by quenching. The peaks of both "butterflies" become more pronounced upon an increase of the upper potential limit from 0.70 to 1.10 V, RHE, and the H UPD charge increases from 226 to 236 (±5) $\mu C\ cm^{-2}$. An interesting feature is the appearance of an anodic current profile region corresponding to a small amount of surface oxide formed evidently beyond 0.90 V, RHE. This observation differs from that of Clavilier et al. [142] who stated that the C-V profile would stay unchanged as long as the electrode was not cycled into the oxide region which was said to begin at 1.25 V, RHE (i.e. at a much higher potential than that [ca. 0.85 V] at polycrystalline Pt [9]).

Cycling of the Pt(111) overnight (800 cycles) at a sweep-rate of 50 $mV\ s^{-1}$, up to 1.10 V, RHE, resulted in a (not unexpected) drastic change in the C-V profile (Fig.

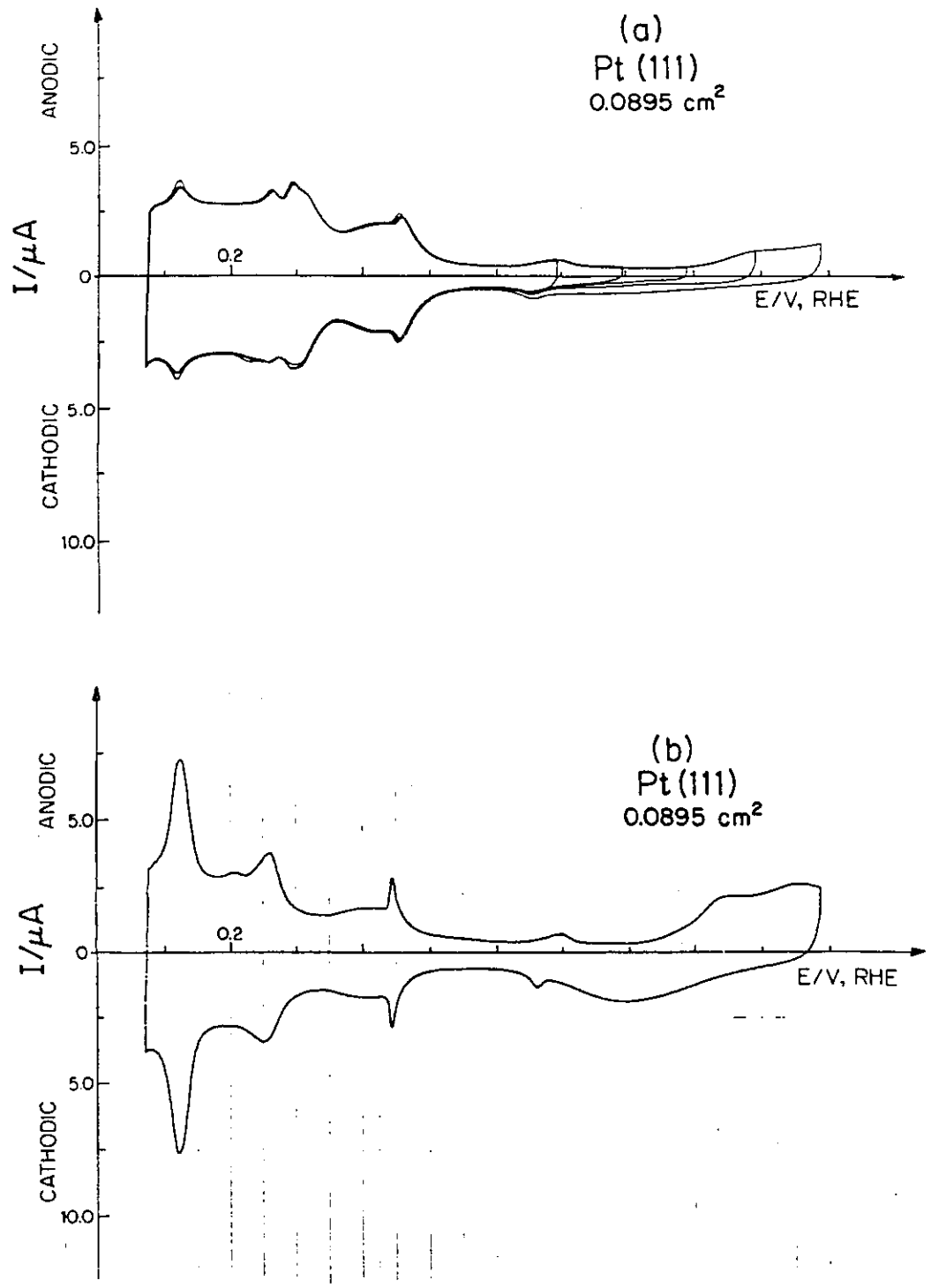

Fig. 3.32 (a) C-V profile of the heated (at ca. 900°C) and quenched Pt(111) electrode; (b) C-V profile of the Pt(111) after 800 cycles up to 1.10 V, RHE at a sweep-rate of 50 mV s^{-1} (0.5 M aq. H_2SO_4, 298 K).

3.32(b)). The overall H UPD C-V profile underwent changes but, importantly, the H UPD accommodation of 236 μC cm^{-2} remained unaffected; however, the quantity of oxide, formed in the anodic sweep and reduced in the cathodic one, significantly increased. An obvious question arises then whether the oxide growth, at the quenched Pt(111), does not take place prior to 1.10 V (or 1.25 V as suggested by Clavilier et al. [142]) but a slow surface restructuring must occur first or, in other words, whether it is only at a restructured surface that oxide growth takes place at potentials as low as 1.10 V, RHE, or less (see Section on oxide formation and ref. 9).

3.3.3 Behaviour of Heated and Quenched Pt(111) Electrode after Cycling up to 1.40 V

As was already shown, the H UPD C-V profile for the Pt(111) electrode strongly depends on the electrode's thermal pretreatment. Interestingly, the C-V profile after cycling up to 1.40 V, RHE, is the same for each of the heating-quenching conditions. This means that the electrode surface tends to the same stable and final state which does not undergo any further changes. Since the initial C-V profiles are different for the various thermal pretreatments, then the intermediate C-V profiles (prior to the attainment of the stable, final C-V profile) do vary but the final one remains virtually invariant (Fig. 3.33). Although major changes arise in the C-V profiles from the "double-butterfly" to the "single-butterfly" shapes, it is remarkable that the total H UPD accommodation remains almost constant, i.e. between 236 and 242 (±5) μC cm^{-2}. Another small but interesting feature, seen in the previous C-V profiles, but not discussed so far, is a small asymmetric hump in the double-layer region with its anodic current maximum at 0.70 V and the cathodic one at 0.66 V, RHE. This feature was also noticed by other researchers and seems to be quite reproducible [140-142,166,195]. However, 5 cycles up to 1.4 V, RHE, are enough to erase it from the C-V profile.

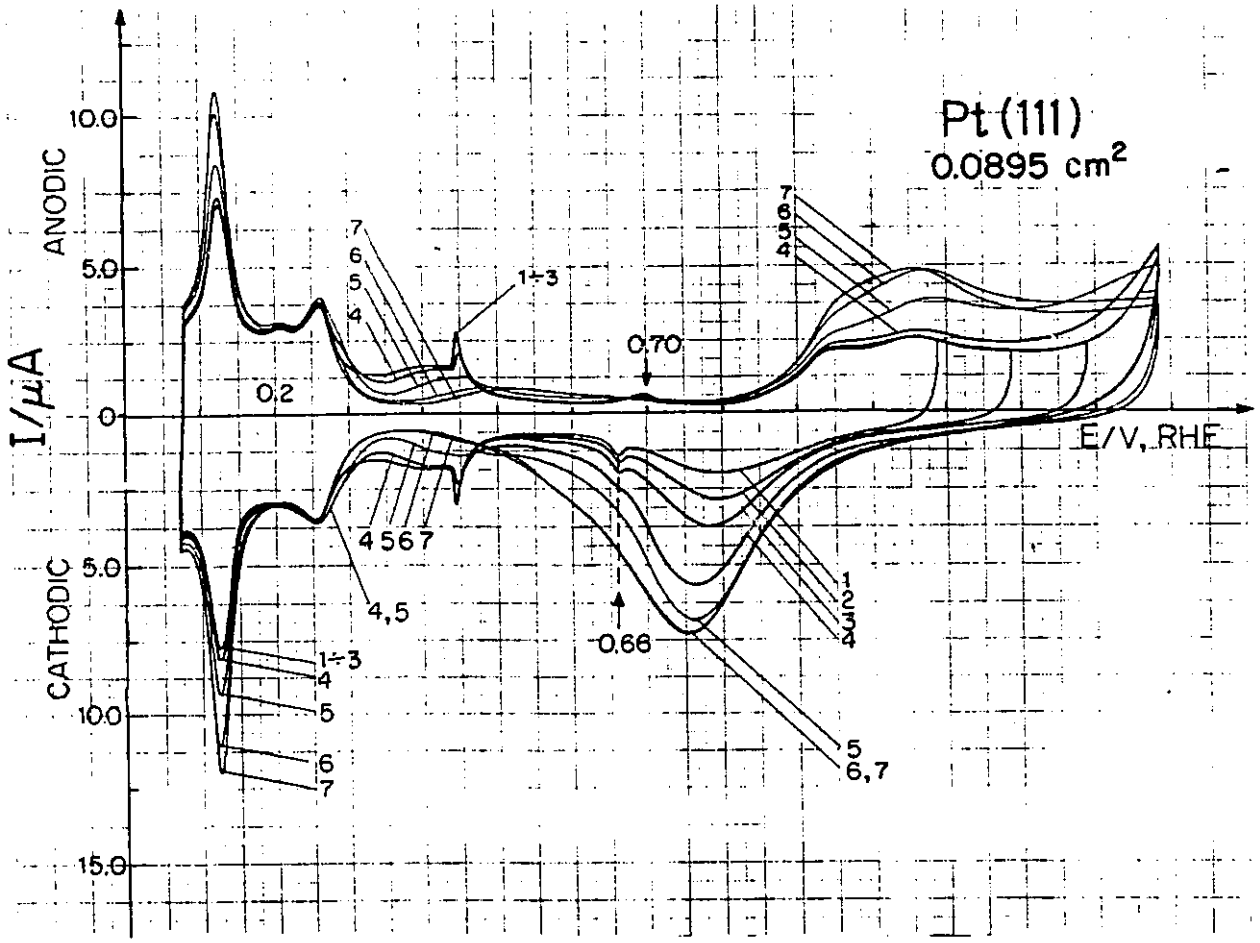

Fig. 3.33 C-V profiles of the heated and quenched Pt(111) electrode (continuation of the experiment the results of which are shown in Fig. 3.32); the upper potential limits of subsequent curves are: (1) 1.1 V; (2) 1.2 V; (3) 1.3 V; (4) 1.4 V (1st cycle); (5) 1.4 V (3rd cycle); (6) 1.4 V (5th cycle); and (7) 1.4 V, RHE (10th cycle).

3.3.4 Introductory Remarks on Oxide Growth at an Heated and Quenched Pt(111) Electrode and on Some Structural Effects upon Prolonged Cycling up to 1.40 V

In the previous Sections of this chapter, it was mentioned that the extent of surface oxide formation at the heated and quenched Pt(111) electrode is much less up to 1.10 V, RHE, than that at polycrystalline Pt [9]; the electrode surface must apparently undergo some restructuring first, by prolonged cycling up to 1.10 V, RHE, in order for surface oxide to be formed at potentials lower than 1.10 V, RHE (Fig. 3.32). This behaviour is not due to any impurity effects since: (a) the H UPD region is well developed with excellently resolved peaks (uncharacteristic of behaviour commonly observed at a poisoned surface); and (b) polycrystalline Pt, in the same solution, gives the normal, well resolved C-V profiles as observed for a clean surface in an ultra-clean solution [9,135,201]. Such a pretreated ("electrochemically annealed" [206]) and possibly restructured [138,139,195] electrode surface, behaves similarly to the polycrystalline Pt electrode at which surface oxide formation region begins already at ca. 0.85 V, RHE [9]. Similar results were reported by Clavilier et al. [140,142] and by Aberdam et al. [195].

Another interesting phenomenon observed at the heated and quenched Pt(111) electrode are the changes in the C-V profile which arise as a result of prolonged cycling between 0.07 and 1.40 V, RHE. Fig. 3.34 shows such changes after 430 cycles. An interesting feature of such C-V profiles is a small peak at 0.215 V, RHE, which appears only on the anodic sweep and becomes more pronounced upon prolonged cycling up to 1.40 V, RHE. This could be attributed to the polygonization of the initially "quenched" Pt(111) surface, as was suggested by Aberdam et al. [195] who noticed surface restructuring as a result of prolonged cycling into the oxide region (cf. Ross and Wagner [138,139]). It is suggested that this process ("restructive polygonization") proceeds through the "electrochemical annealing" mechanism, i.e. repetitive oxide formation and reduction (see Section 3.1.3).

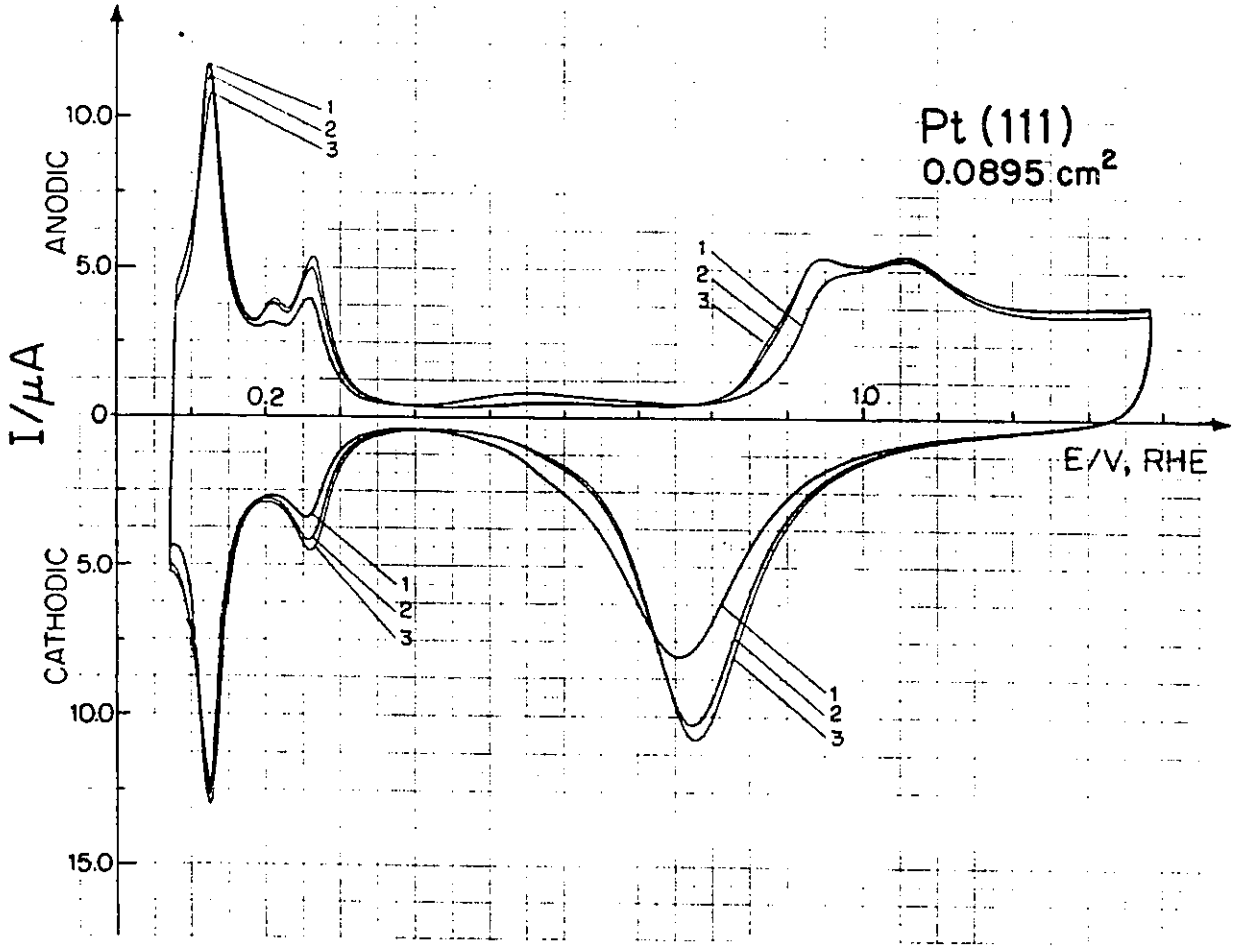

Fig. 3.34 C-V profiles of the heated and quenched Pt(111) electrode after cycling up to 1.40 V, RHE; curve (1) after 20 cycles; (2) 140 cycles; and (3) 430 cycles (continuation of the experiment the results of which are shown in Figs. 3.32 and 3.33).

3.3.5 Continuity of Changes in the C-V Profiles for Heated and Quenched Pt(111) as a Result of Increase of Upper Potential Limit

In the previous Sections of this thesis, it was shown that cycling of the heated and quenched Pt(111) up to or beyond 1.10 V, RHE, leads to a probably restructured surface for which the H UPD C-V profile differs substantially from the initial one and also at which the surface oxidation processes commence beyond 0.90 V, RHE. The behaviour observed seems to indicate that not only the H UPD C-V profile but that over the surface oxide region as well, is a measure of the extent of surface restructuring.

A question arises whether small structural changes are reversible or irreversible. Experiments were conducted in which an heated and quenched Pt(111) surface, having originally a C-V profile such as in Fig. 3.30, was cycled five times up to 1.20 or 1.30 V, RHE, until changes in the H UPD C-V profile were observed. Then, the upper potential limit was reduced to 1.0, 0.9 or 0.8 V, RHE, and the electrode was again cycled up to 70 times. This did not lead to reproduction of the original H UPD C-V profile so that the surface structural changes which lead to the above differences are evidently irreversible.

Another question arises whether the surface structural changes arising after cycling to the various upper potential limits tend to respective characteristic states or whether they are continuous until the final and stable structure, as described in Section 3.3.3, has been attained. In a further set of experiments, the Pt(111) crystal was heated to 1000°C and quenched in pyrolytically-distilled water. The "butterflies" are well pronounced (Fig. 3.35) and the H UPD charge is found to be 240 (±5) $\mu C\ cm^{-2}$. Then the electrode was cycled five times to various upper potential limits of 1.10, 1.15, ..., 1.40 V, RHE. Upon cycling to 1.25 V, RHE, or beyond, the C-V profiles (Fig. 3.36) underwent continuous changes, more significant than those resulting from cycling only to 1.10, 1.15 or 1.20 V, RHE. The successive changes in the C-V profiles of the quenched Pt(111) surface caused by cycling to various positive potential limits are shown in Fig. 3.36. However, the i vs E profiles of this figure cannot be distinguished by differently coloured lines, as on the

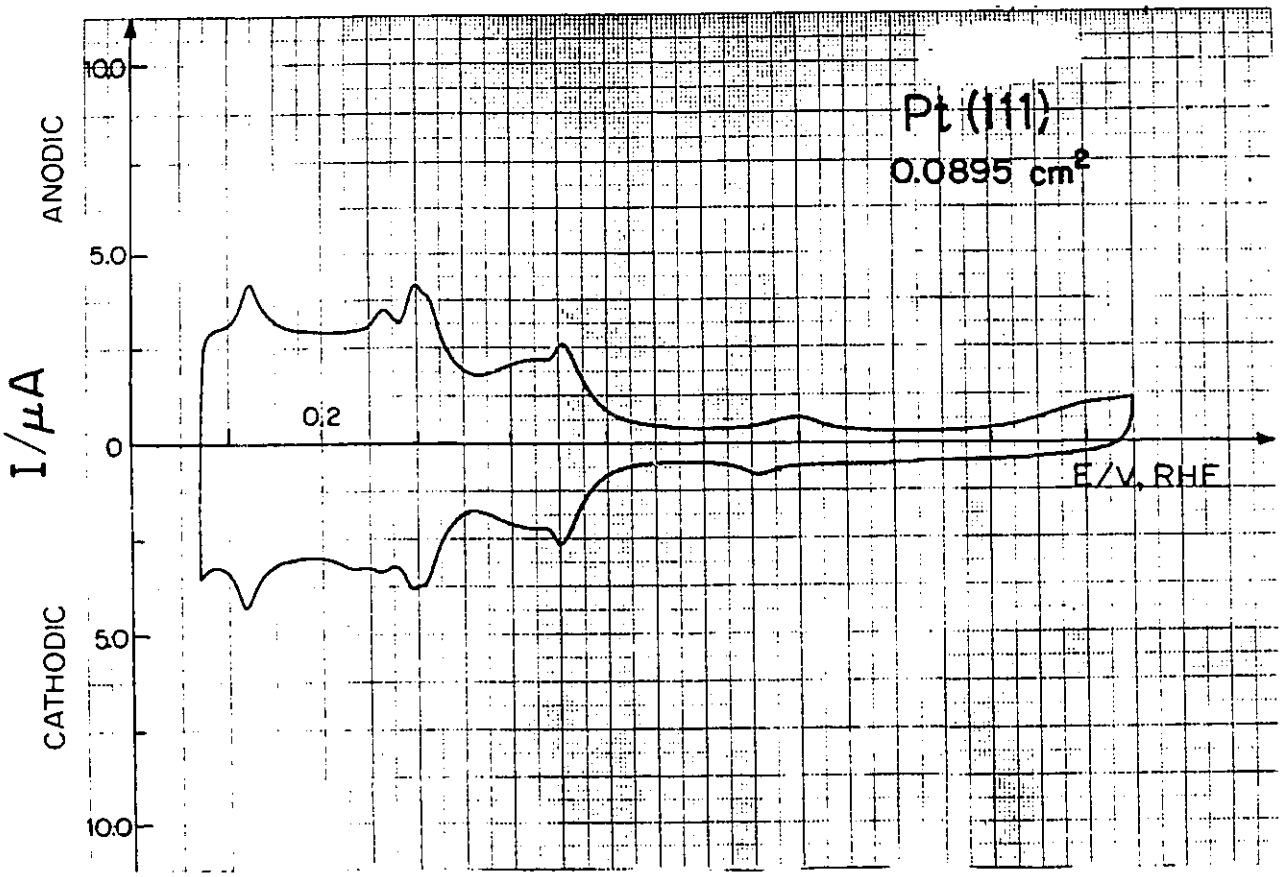

Fig. 3.35 Initial C-V profile of the Pt(111) crystal heated at 1000°C and quenched, with the upper potential limit taken to 1.05 V, RHE, prior to multiple cycling (0.5 M aq. H_2SO_4, 298 K).

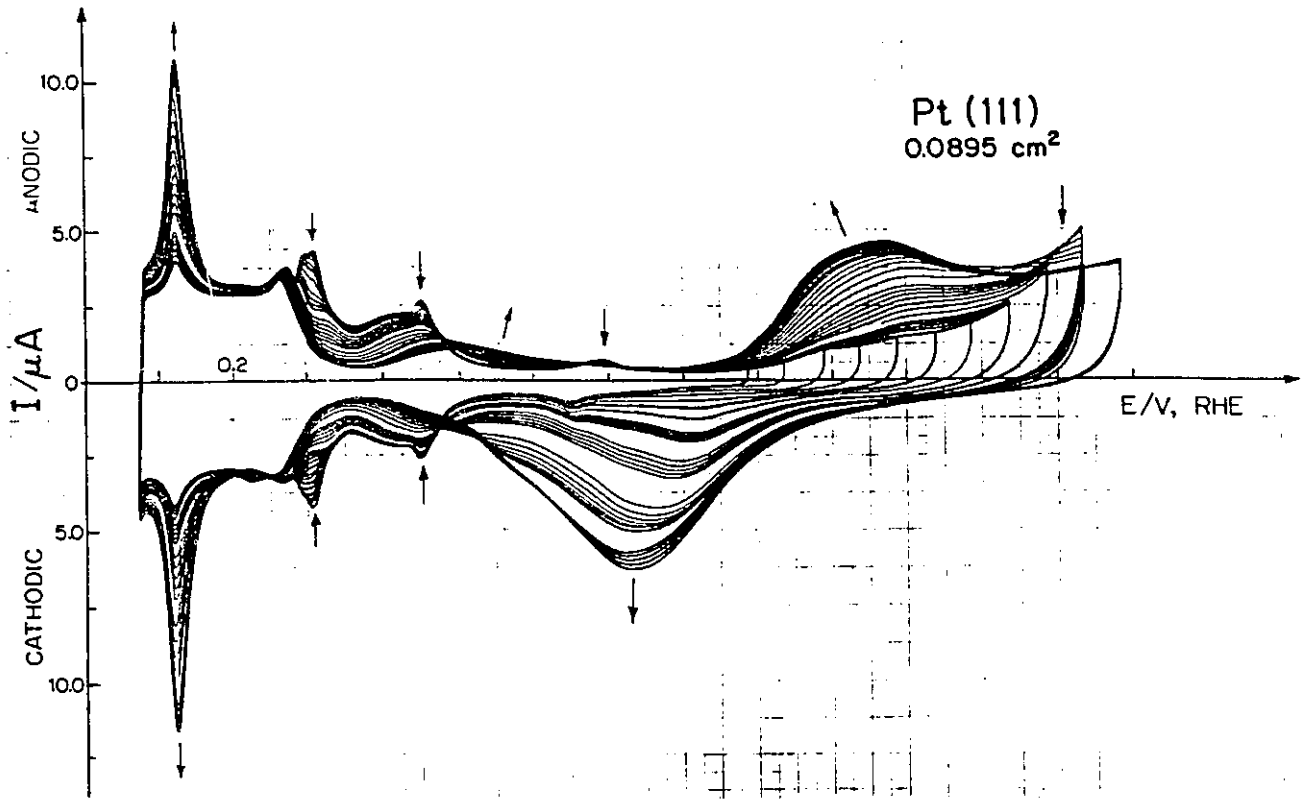

Fig. 3.36 Changes in the C-V profile as a result of cycling five times to various upper potential limits of 1.10, 1.15, ..., 1.40 V, RHE (0.5 M aq. H_2SO_4, 298 K) (arrows indicate the directions of changes in the C-V profiles with successive cycling).

original recordings, so the original profile is shown as Fig. 3.35, the consecutive changes in Fig. 3.36 and the final curves up to 1.40 V, RHE, after 55 cycles, are shown in Fig. 3.37. In general, the higher the upper potential limit, the more pronounced were the structural changes, as revealed by the C-V profiles. Further cycling up to 1.40 V, RHE, led to the same final C-V profile (Fig. 3.37) and presumably corresponding surface structure, though restructured as suggested by Aberdam et al. [195], which again was consistent with the results of Hubbard et al. [137].

3.3.6 Comparison of the H UPD C-V Profile for Heated and Quenched Pt(111) with that for Annealed Pt(111)

In order to attempt to understand the origin of the differences in the H UPD C-V profiles resulting from the various thermal pretreatments, it is necessary to discuss what may happen when a hot Pt(111) crystal is cooled down suddenly. In a lattice, Pt atoms oscillate in three directions and the amplitude of such oscillators is temperature-dependent; in general, the greater the temperature, the greater will be the average amplitudes. It is such oscillations of the Pt atoms in the lattice which can bring them to such excited states that atom migration can occur to extents determined by a Boltzmann distribution. This atom migration leads to atomic displacements to energetically more excited positions on/in the surface lattice (and, to some extent, also in the bulk), in other words to sites for which their potential energies are above their normal minimized ones [240,241].

This idea of thermal displacements of sruface atoms at Pt at elevated temperature finds support in Watts-Tobin's [241] argument, based on similar lines, that the surface of Hg at room temperature (where it is, of course, already liquid) is thermally disordered into a microscopically non-flat configuration due to atomic displacements arising according to Boltzmann statistics.

If a Pt(111) crystal is brought to the annealing temperature, at which amplitudes of

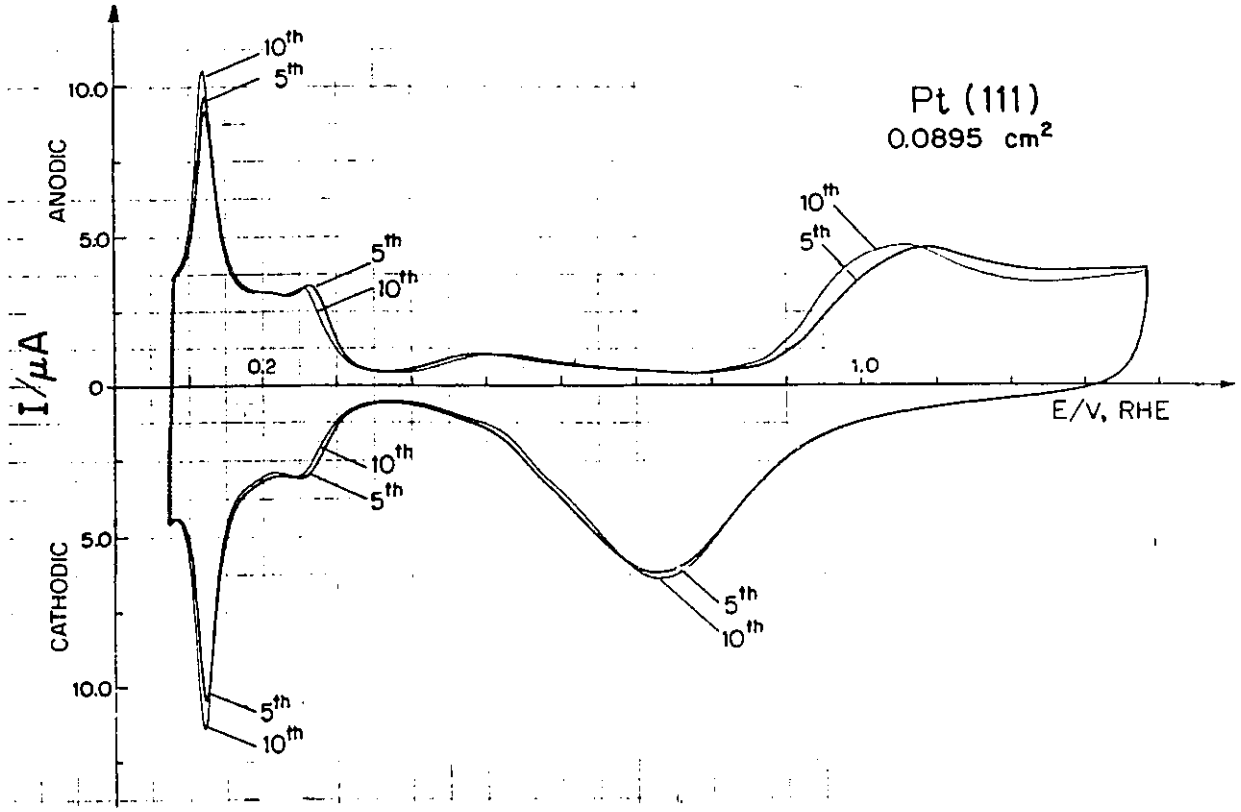

Fig. 3.37 C-V profiles after multiple cycling up to 1.10, 1.15, ..., 1.40 V, RHE (0.5 M aq. H_2SO_4, 298 K).

the oscillations referred to above are sufficient to promote small but significant migration of thermally excited lattice atoms, and is then slowly cooled down, most of the Pt atoms will return to states of minimum potential energy; then, the crystal will be almost free of stresses or cold-work defects, and from surface lattice defects. This is so because slow cooling gradually decreases the amplitudes of the Pt-atom oscillations and allows migrated atoms to return to minimum potential energy sites, simultaneously decreasing the number of thermally displaced atoms and the rate of continuing atom migration. On the contrary, fast cooling (see the cooling and quenching curves in Fig. 3.38), for instance by quenching, would be expected to "freeze" Pt atoms in displaced states, both in the bulk as well as in the surface lattice. In such a pretreated crystal, some Pt atoms could be in relaxed (stable) positions (those energetically most favourable) while others, more significantly, would be "frozen" in displaced positions (those energetically less favourable) associated with the atom migration taking place at high temperatures (Fig. 3.39).

Amongst the present series of experiments on the quenched Pt(111) surface, probably the most critical is that where a quenched crystal that gave the "Clavilier" type "double-butterfly" C-V profile was thermally annealed over 4 hours in vacuo. Following this procedure, the crystal surface was subjected to a single sweep, but not either into or from the oxide region, after heating to ca. 200°C in the top end of an H_2/O_2 flame to remove any impurities that might have become adsorbed on the (111) surface during the annealing and transfer. The resulting C-V profile was immediately that of Hubbard, similar to Fig. 3.28(a). It is difficult to see how and why such an annealing procedure could lead to a more rather than a less disordered surface, i.e. this experiment tends to support the view that it is the "Hubbard" C-V profile that corresponds to a more ideal, ordered surface than vice versa since the conversion from one to the other involved only the thermal annealing procedure and supposedly none of the disordering that is known to arise due to multiple cycling into the oxide region.

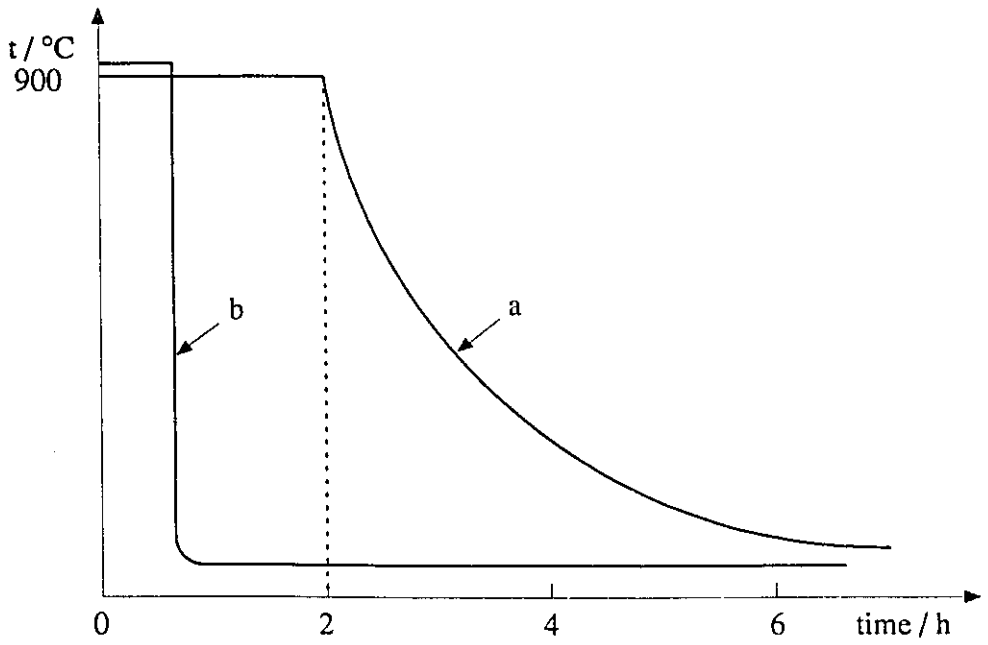

Fig. 3.38 Temperature vs time curves: (a) annealing curve; and (b) quenching curve.

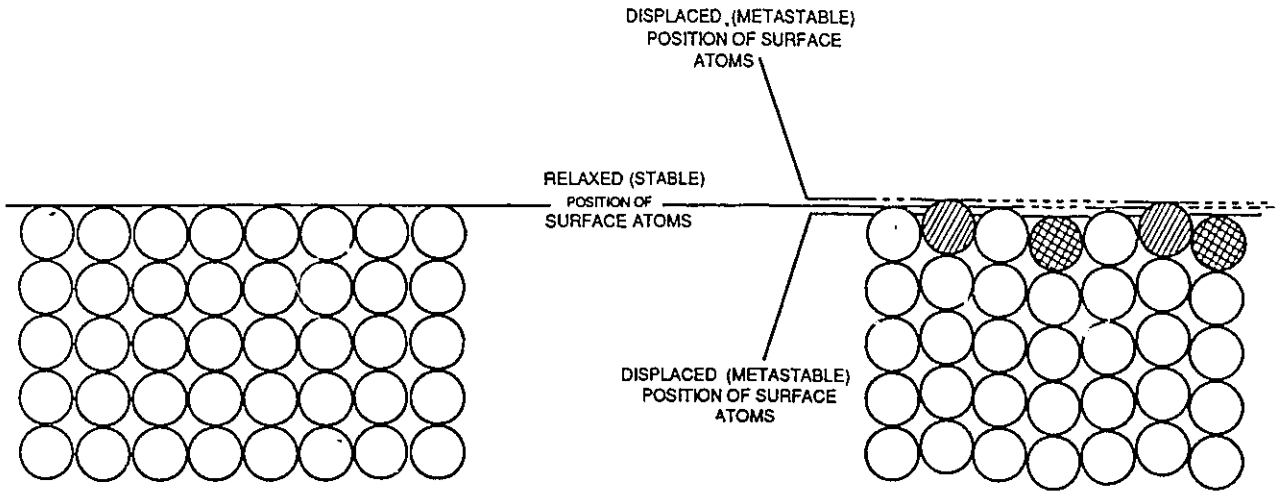

Fig. 3.39 Schematic representation of the relaxed (stable) and displaced (metastable) positions of surface metal atoms; the left-hand-side diagram represents an annealed surface while the right-hand-side represents a heated and quenched surface.

Although the above two surfaces (i.e. the annealed surface and the "quenched" one) exhibit very different C-V profiles, the accommodations for adsorbed H on the two surfaces are identical within 2%; this means that the atom densities per cm^2 are correspondingly almost the same.

A quenched crystal would tend to contain substantial stress (equivalent to cold work), with atomic displacements manifested also in its surface structure. Such displacements (which are overemphasized in Fig. 3.39) might be small (up to 5% of the atomic diameter) and difficult to detect by the LEED technique which gives patterns characteristic only of long-range order. Such stresses or displacements could be released upon further physical or chemical treatment. This would apply not only to the surface atoms but also to bulk atoms near the surface. In other words, the Pt(111) surface atoms of the heated and quenched crystal could be in both relaxed and displaced positions, and the number of atoms in displaced positions would, on average, tend to be greatest in the case for which the highest heating temperature and fastest cooling procedure had been used (cf. the structure of glassy metals resulting from very rapid solidification). Such states of surfaces will be referred to here as metastable surface structures. It would be reasonable to expect them to undergo further changes to a more stable structure, through multiple oxide formation-reduction cycles, allowing reconstruction of the surface lattice [138,139,166,195]. This process is what has been referred to here as "electrochemical annealing" since it releases stress and allows atomic rearrangements not only in the surface layers of the crystal but also probably from layers lying somewhat beneath the surface. However, release of stresses or removal of displacements from deeper layers, through "electrochemical annealing" would be slow or negligible.

It was already mentioned that Fig. 3.39 schematically represents the possible displaced (metastable) positions of surface atoms and that it overemphasizes the extent of displacements which, in reality, are more likely to be less and around 0.1 - 0.2 Å, i.e. close to the limit of LEED sensitivity (resolution) which is about 0.1 Å in the direction

perpendicular to the surface and 0.2 Å in the direction parallel to the surface [107,108]. This could explain why the LEED patterns of "quenched" Pt(111) reveal [171-174,195] all the characteristics of an "ideal" (111) - (1×1) surface.

It must be recorded here that, in the course of this research, no access to either an ex situ or an in situ LEED apparatus was available. However, "calibration relations" to provide surface structures of the single-crystal surface investigated were made by comparisons of C-V profiles obtained in the present work under various conditions with those reported in certain papers (e.g. refs. 137,144,172-174, especially the work of Aberdam et al. [195]) where LEED characterization of surface structures in relation to C-V profiles had been made. In most cases, this enabled useful conclusions to be made on structural changes resulting from various thermal and/or electrochemical treatments of the two single crystals used in the present work. Such conclusions cannot, however, be regarded as entirely firm in the absence of use of LEED in our own actual experiments.

The above discussion is based on the premise that the displacement is perpendicular to the surface. This might not be the real case since the displacement could as well be parallel to the surface. However, it seems to be "directional". In order to test this point of view, a new experiment was designed in which the direction (geometry) of quenching was varied.

Fig. 3.40 shows a schematic diagram of the quenching procedure in which the single-crystal was quenched separately in two different directions. Fig. 3.41 shows the H UPD C-V profile taken between 0.07 and 0.80 V, RHE, for the Pt(111) electrode heated at ca. 800°C and quenched "laterally" in pyrolytically-distilled water. The H UPD accommodation on this surface is 240 $\mu C\ cm^{-2}$ while the C-V profile is different from that for "perpendicular" quenching (see Fig. 3.30). The major difference is that the "spike" is very high while the second "butterfly" (that between 0.32 and 0.45 V, RHE) has a square-like shape. Unfortunately, it is impossible to perform the quenching procedure in such a manner that only the surface of interest (the base of the cylindrical single-crystal) is

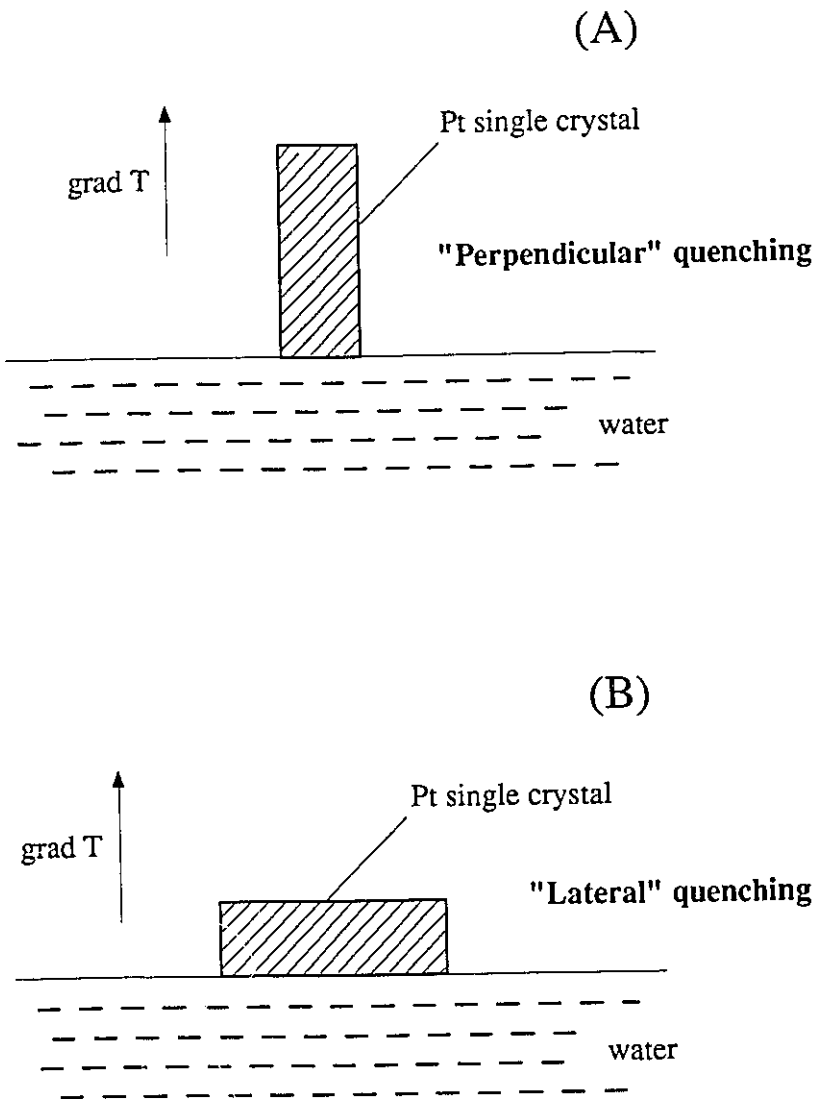

Fig. 3.40 Schematic representation of two different quenching procedures: (A) "perpendicular" quenching in which the grad T (temperature) is perpendicular to the single-crystal surface; and (B) "lateral" (horizontal) quenching in which the grad T is parallel to the single-crystal surface.

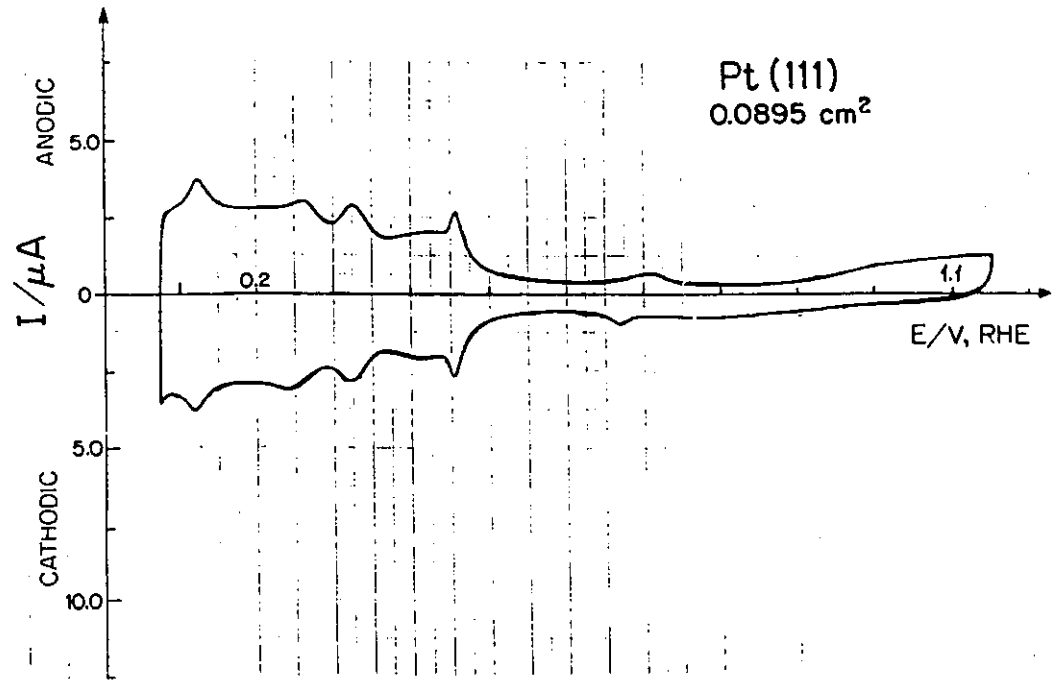

Fig. 3.30 H UPD C-V profile for Pt(111) electrode after heating at ca. 800°C followed by quenching in the "perpendicular" direction (0.5 M aq. H_2SO_4, 298 K).

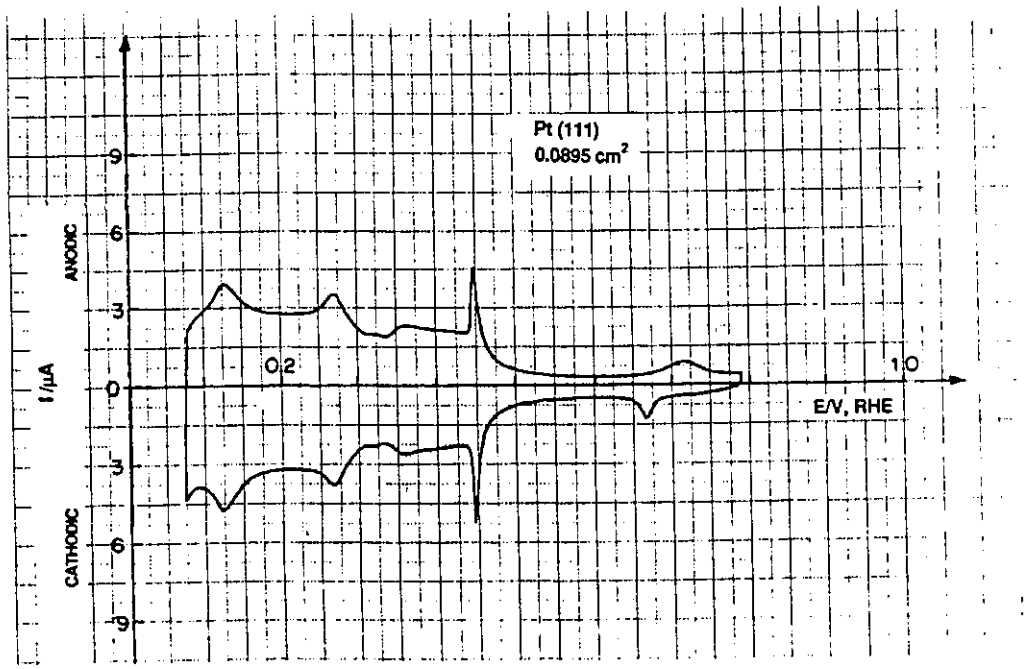

Fig. 3.41 H UPD C-V profile for Pt(111) electrode heated at ca. 800°C and quenched in the "lateral" direction (0.5 M aq. H_2SO_4, 298 K).

in contact with water while the side-wall is not or vice versa. It is postulated that application of bigger single crystals, or of crystals having a disc shape, could lead to more pronounced differences in the H UPD C-V profiles, depending on the direction of quenching.

3.3.7 Interpretation of the H UPD C-V Profiles for Pt(111) Electrodes

One of the most puzzling features of the H UPD C-V profile obtained at the "quenched" Pt(111) surface is its complexity. As was mentioned earlier in this thesis, the present work has shown that the shape of the "double-butterfly" depends on the thermal pretreatment of the Pt(111) electrode (see Section 3.3.1). However, the peaks and the "spike" remain the major components of the H UPD C-V profile but their relative heights vary with the thermal pretreatment applied. In general, the results of the present research indicate that there are four major features in the H UPD C-V profile manifested at the "quenched" Pt(111) surface while, at the annealed one, there are three in the anodic component of the overall profile and two in the cathodic one.

The "ideal" Pt(111) surface is very stable and, out of the three low-index surfaces, is the most stable one [107,108]. This suggests that the H UPD C-V profile obtained at the "ideal" Pt(111) surface should be much simpler, both in aq. H_2SO_4 and $HClO_4$ solutions, even if the "anion effect", i.e. the specific anion adsorption, is taken into consideration [140-146,154,155,175-177,229,235,242]. On the contrary, the H UPD C-V profiles for the "quenched" Pt(111) are always more complex than for the Pt(100) or Pt(110) surfaces, or even polycrystalline Pt, although they are known to be unstable and easily undergo reconstruction [107,108].

Więckowski et al. [175,176] have critically reviewed the various interpretations of the Pt(111) cyclic-voltammograms (see ref. 175 and refs. therein) and proposed their own interpretation which will be discussed later in this Section. However, prior to this, it is essential to present the important results of Aberdam et al. [195] who reproduced the

results of Clavilier [140-144] on the "quenched" Pt(111) and cycled such prepared Pt(111) electrodes up to 1.40 V, RHE, simultaneously taking LEED patterns.

The results of Aberdam et al. [195] can be summarized in the following points:

(a) the Pt(111) electrode was cooled from the annealing temperature (1000-1100 K) to room temperature "as fast as possible", i.e. it was quenched; (b) the Pt(111) electrode after cycling up to 0.95 V, RHE, exhibits the "double-butterfly" of Clavilier [140-146] and gives LEED patterns characteristic of the clean and well-ordered Pt(111) surface; (c) the quality of the LEED patterns was not so much related to the number of cycles into the oxide region as to the level of contamination reached after the electrode transfer in the UHV apparatus; (d) trace amounts of contaminants such as C, O and S (which become spread on the Pt(111) surface) cannot be detected by the AES technique and do not obscure, dramatically, the LEED patterns; (e) these trace amounts of impurities, undetectable by the AES technique, are, however, discernable through their effects on the CV's; (f) 5 cycles into the oxide region (up to 1.40 V, RHE) both in aq. H_2SO_4 and $HClO_4$ solutions change the LEED patterns which then reveal monoatomic steps and (111) terraces which contain at least 11-12 compact rows; (g) after 5 cycles up to 1.40 V, RHE, the second "butterfly" with its "spike" becomes eliminated from the C-V profile for Pt(111); (h) 30 cycles up to 1.40 V in aq. $HClO_4$ solution further change the C-V profile and the LEED patterns then reveal monoatomic steps and (111) terraces which contain at least 10 compact rows; (i) 60 cycles up to 1.40 V in aq. H_2SO_4 solution lead to more changes in the LEED patterns which correspond to (111) terraces containing, on average, 7.5 ± 1 compact rows (note the extremely narrow terrace width distribution) and monoatomic steps; (j) monoatomic steps are not created as a whole by the oxide formation-reduction process which leads, rather, to generation of point defects such as adatoms and vacancies which, upon cycling, tend to cluster into steps; and (k) point defects are created by the place-exchange mechanism between oxygen species and Pt atoms [cf. ref. 234,242].

Some other interesting results on Pt(111), Pt(110) and Pt(100) are those of Kita et al. [242] who showed that the H UPD C-V profiles for Pt(111) depend on the pH of solution and the composition of solution. For instance, the "quenched" Pt(111) does not reveal the second "butterfly" in 0.1 M aq. NaOH solution and its total H UPD accommodation is ca. 170 $\mu C\ cm^{-2}$ only, i.e. it lacks about 30% necessary for a complete monolayer. Furthermore, addition of Na_2SO_4 does not result in formation of the second "butterfly". These observations indicate that: (a) the first "butterfly" is independent of the composition of solution or its pH; and (b) the second "butterfly" depends on the composition and concentration of solution, especially on the anion present, and on its pH. The significance of anions was confirmed by in-situ IR spectroscopy (cf. ref. 175) that HSO_4^- adsorption on Pt(111) increases greatly from the potential of the "spike".

In the light of the rather thorough investigation of Aberdam et al. [195] and the data presented in Section 3.3, the following conclusions or suggestions can be made:

1. If the "double-butterfly" of Clavilier et al. [140-146] in aq. H_2SO_4 solution were characteristic of the clean and well-ordered Pt(111) surface, then one should still observe it after 5 or 10 cycles up to 1.40 V, RHE, since ca. 90% of the surface is still of the (111) orientation according to Aberdam et al. [195], across the terraces;

2. The "double-butterfly" of Clavilier et al. cannot be an artifact, e.g. due to impurity adsorption [138], since the results have been reproduced in several research laboratories world-wide under high-purity conditions;

3. The "double-butterfly" seems to be characteristic of "quenched" Pt(111) surfaces in aq. H_2SO_4 and $HClO_4$ solutions, i.e. it depends on sensitive interactions between the "quenched" Pt(111) surface and HSO_4^- or ClO_4^- anions;

4. Interestingly, the results of Clavilier et al. [142-144] indicate, amongst other things, that contact between a hot Pt single-crystal (800-1300°C) and air or water results evidently in formation of Pt oxide on the Pt single crystal, as was shown by Clavilier et al. [142-144] by recording the first negative-going sweep from ca. 0.90 to 0.05 V, RHE; this

indicated that the "thermal" oxide formation did not reconstruct the surface substantially so that the "double-butterfly" could still be observed;

5. Electrochemical oxide formation seems to be more "destructive" for the "double-butterfly" profile of Clavilier than the thermal formation of the oxide;

6. If the second "butterfly" of Clavilier were due to the subsurface hydrogen, as suggested by Więckowski et al. [175], then one should still see it for the Pt(111) surface after 5-10 cycles up to 1.40 V, RHE, since this surface still contains (111) terraces having 10-12 compact rows; this clearly indicates that the second "butterfly" of Clavilier is not due to a different state of sorbed ("sunken") hydrogen; in the model of Więckowski et al. [175], it is not clear why only ca. 33% of the UPD H is capable of "sinking" beneath the top-most metal layer;

7. The idea of subsurface hydrogen of Więckowski et al. [175] could, however, find support from the early calculations of Ishikawa and Hubbard [136] which clearly support the view that the adsorbed H on Pt(111) lies at surface sites "in between" trigonal arrangements of Pt atoms (characteristic of (111) geometry) rather than "on top" of Pt atoms; however, the potential energy profile for adsorbed H atoms shown in this paper [136], which indicates that H is energetically more stable by residing between the first and the second surface layer of Pt(111), is based upon calculations for a cluster containing not more than five Pt atoms (too few) and does not take into consideration the different electronic states of the Pt atoms in the first and second surface layers, and also different electronic states of H atoms adsorbed on the Pt(111) surface (more different) of H atoms beneath the first surface layer of Pt(111). It should be made clear that the electric charge on the adsorbed H would be different from that of any sorbed H, since the latter donates its electron into the electron conduction band of the Pt metal [236-238]; in other words, the sorbed H atom is more electron-deficient than the adsorbed H atom; the calculations of Desjonquères and Cyrot-Lackmann (see ref. 239 and refs. therein) clearly indicate that asphericity of the H charge density changes when going from surface into the bulk metal.

This is because bulk metal atoms have different orbital occupation numbers (electrical charge, which is less than 0.20 e) from those of surface metal atoms whose orbital occupation number is ca. 0.44 e [239]. The physical origin of this effect is that the surface metal atoms have orbitals protruding from the surface, i.e. some orbitals which do not overlap with orbitals of other atoms due to the asymmetry of atom distribution at a surface;

8. The experimental data [175,243] on HSO_4^- ion adsorption on the "quenched" (called "ordered" in ref. 175) Pt(111), "well-cycled" (called "disordered" in ref. 175) Pt(111) and polycrystalline Pt indicate that: (a) HSO_4^- adsorption on the "quenched" Pt(111) surface is 20% higher than on the "well-cycled" Pt(111) or polycrystalline Pt surface; (b) the potential at which HSO_4^- adsorption begins on the "quenched" Pt(111) surface is ca. 200 mV more positive than on "well-cycled" or polycrystalline Pt surfaces; and (c) the potential dependence of adsorption of HSO_4^- on the "well-cycled" Pt(111) surface is almost identical with that observed on polycrystalline Pt surfaces.

It is suggested that the complexity* of the "double-butterfly" H UPD C-V profile for the "quenched" Pt(111) is due to the specific anion adsorption. It was suggested earlier in this thesis (see Section 3.3.6) that quenching the Pt(111) electrode might, in fact, create a metastable surface in which the surface Pt atoms are only slightly displaced. In such a case, the interatomic distance between adjacent Pt surface atoms and the atoms around them, would not be the normal 2.77 Å but could vary up to ca. 0.2 Å. Such small displacements, it was mentioned, are difficult to detect by LEED (especially if they are not repetitive on a long-range scale) since they are close to the detection limit of LEED analysis. However, such small displacements could be "felt" by the HSO_4^- ions present at

---

* The multiplicity of states of chemisorption of UPD atoms below monolayer coverage, even on single-crystal surfaces, is a general problem in surface science, hitherto not well explained. Qualitatively, it is associated with successive development of different overlay lattices, possibly with 2-d phase transitions between states.

the electrode interface. Since it is supposed that there is a distribution of distances between surface Pt atoms (possibly between 2.57 and 2.97 Å, i.e. 2.77 ± 0.2 Å) in the quenched surfaces, then the HSO_4^- ions could arrange themselves on the Pt(111) electrode surface in such a way (ways) that their overall adsorption would be ca. 20% higher than on the annealed or "well-cycled" Pt(111) surface. This implies not only that HSO_4^- adsorption is greater by some 20% but also that there is a greater range of adsorption energies available to them. Since anion adsorption normally competes with H electrosorption, then different H coverages would tend to arise at different potentials on account of the presence of adsorbed HSO_4^- ions, as observed experimentally. Since HSO_4^- coverage is evidently [175,243] greater on the "quenched" Pt(111) surface due to more strongly-binding sites available to them, an abnormally complicated H UPD C-V profile could arise at the "quenched" Pt(111) surface.

The situation is much simpler in the case of annealed Pt(111), which is presumably freer from small displacements (apart from the step edges of terraces [195]), and in the case of the Pt(111) electrode cycled 30 to 60 times up to 1.40 V, RHE. The first surface is presumably "flat" while the second one evidently contains long (111) terraces and monoatomic steps [195] (but probably without small random displacements). On these two surfaces, the distances between Pt atoms are well defined [107,108,208,209], hence a narrow range of states for HSO_4^- ions to adsorb, and a consequent simpler H UPD C-V profile, could arise.

3.4 UPD of H at the Pt(100) Electrode Surface After Various Thermal and Electrochemical Pretreatments

3.4.1 UPD of H at Pt(100)

The first experimental data on H adsorption at Pt(100) were reported by Will

[121]. However, as was mentioned in Section 1.10.2, his single-crystal Pt electrodes were subjected to prolonged cycling between 0.05 and 1.40 V, RHE, and revealed significant polycrystallinity.

Some of the most interesting results on the Pt(100) electrode are those of Hubbard et al. [137] and Clavilier et al. [142-144,147]. Hubbard et al. characterized the Pt(100) surface by LEED and cleaned it electrochemically by cycling ten or more times between 0.05 and 1.40 V, RHE (see Section 1.10.2 and Fig. 1.10). The results of Clavilier et al. [142-144,147] differ again substantially from those of Hubbard, due, most likely, to the experimental procedure applied, i.e. heating and quenching. The distinguishable results of Hubbard and of Clavilier were reproduced during the course of this work and are presented below. However, prior to the discussion of the experimental results, it should be mentioned that there are much less data on electrochemistry at Pt(100) in the literature than at Pt(111). The Pt(111) electrode surface behaviour was so anomalous that it attracted much attention, world-wide, making it the most investigated system amongst studies on electrochemistry of single crystals. The experimental data on Pt(100) are much less controversial and do not show any special anomalies such as the "spike" in the case of Pt(111). That is presumably why it has not been investigated very extensively.

Annealed Pt(100) Surface

Fig. 3.42(a) shows the C-V profile of the Pt(100) electrode after annealing at ca. 900°C followed by slow cooling over 4 h. Since the electrode was transferred from the furnace to the electrochemical cell via air, the crystal was further heated in an H_2/O_2 flame at ca. 200°C to desorb any impurities that might have become adsorbed (see Section 3.3.1). The electrode was also "electrochemically cleaned" by cycling 5 times up to 1.40 V, RHE; this procedure unblocked some surface sites still occupied by impurities from the air or from the solution but did not cause any significant changes in the C-V profile which reveals the following features: a major peak at 0.27 V, RHE, a small peak at 0.18 V, RHE

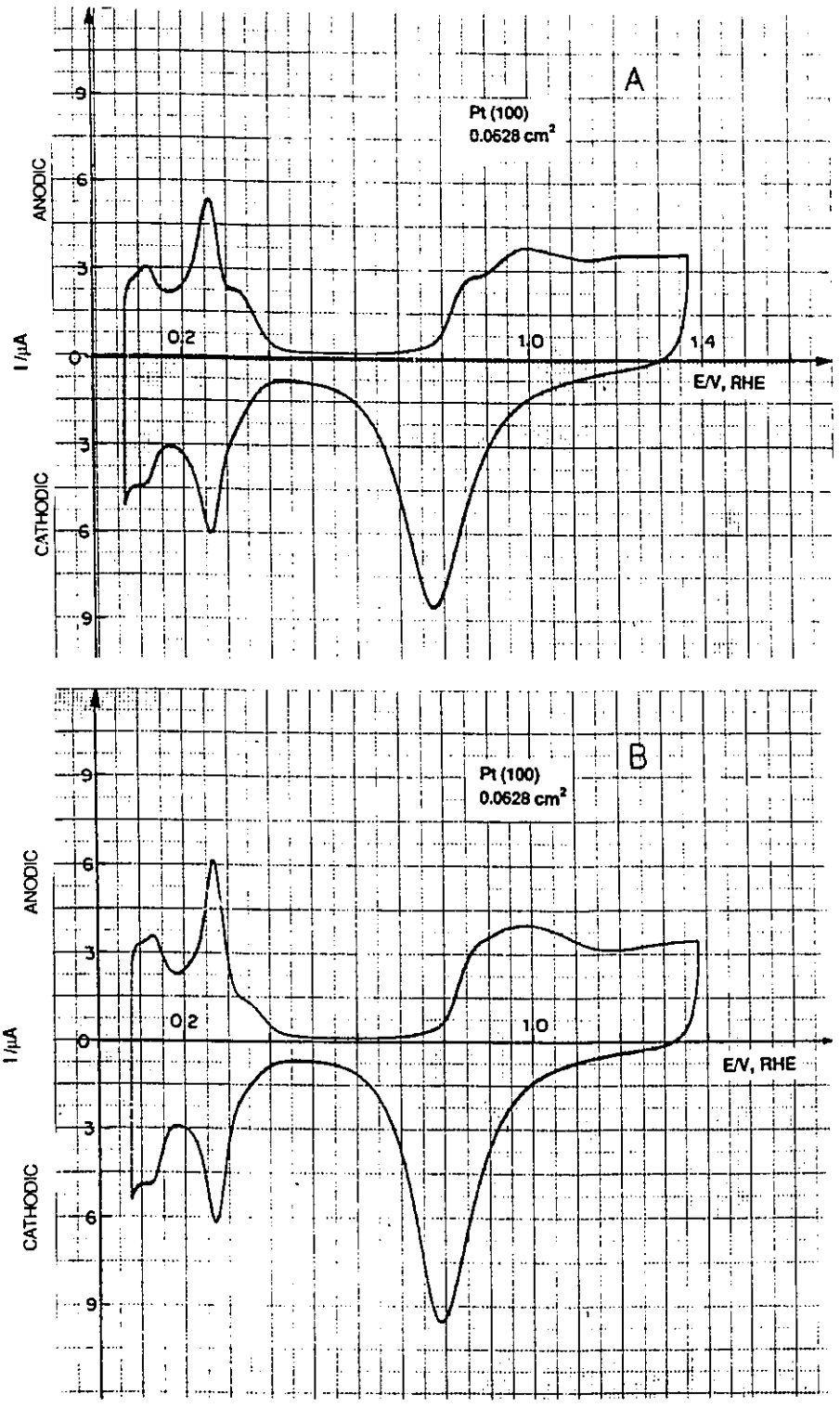

Fig. 3.42 C-V profiles for the Pt(100) electrode after annealing at 900°C followed by electrochemical cleaning: (a) 5th C-V profile up to 1.40 V; (b) C-V profile after prolonged cycling (0.5 M aq. H_2SO_4, 298 K).

and a small hump between ca. 0.32 and 0.42 V, RHE, which overlaps the major peak (Fig. 3.42(a)). After prolonged cycling to 1.40 V, RHE, the H UPD C-V profile underwent some changes, as shown in Fig. 3.42(b), but they were not very significant - the major peak increased, becoming sharper, while the hump became less pronounced. The most interesting feature of both the profiles is the H UPD accommodation which is 282 (±5) μC cm^{-2} for the first one and 286 (±5) μC cm^{-2} for the second (over 70 μC cm^{-2} more than the calculated [137] charge of 208 μC cm^{-2}!; this anomaly will be explained below). Though the C-V profiles in Fig. 3.42 resemble qualitatively those of Hubbard et al. [137] and of Clavilier et al. [142,144], their H UPD accommodation was some 30% too big compared with the charge calculated [137] for 1 H per Pt atom on an unreconstructed [(100)-(1×1)] surface (see below).

Pt(100) Surface Heated at ca. 500°C and Quenched

As for the Pt(111) electrode, the Pt(100) single crystal was heated at ca. 500°C followed by quenching in pyrolytically-distilled water. The H UPD C-V profile for such a pretreated crystal is shown in Fig. 3.43. Here, the peaks at 0.13 and 0.27 V, RHE, are slightly less pronounced while what was a hump between 0.32 and 0.42 V, in the case of the annealed Pt(100) surface, has become a well developed peak at ca. 0.37 V, RHE. The H UPD accommodation was found to be 284 (±5) μC cm^{-2}, still some 76 μC cm^{-2} more than the charge calculated [137] for the "ideal" Pt(100)-(1×1) surface.

Pt(100) Surface Heated at ca. 800°C and Quenched

Fig. 3.44 shows the H UPD C-V profile for the Pt(100) electrode heated at ca. 800°C followed by quenching in pyrolytically-distilled water. This profile is very similar to those of Clavilier et al. [142,144] for quenched Pt(100) surfaces and reveals two peaks at 0.27 and 0.37 V, RHE, respectively, and a small shoulder between them which seems to be a small peak being overlapped by the two major ones. An interesting feature of this

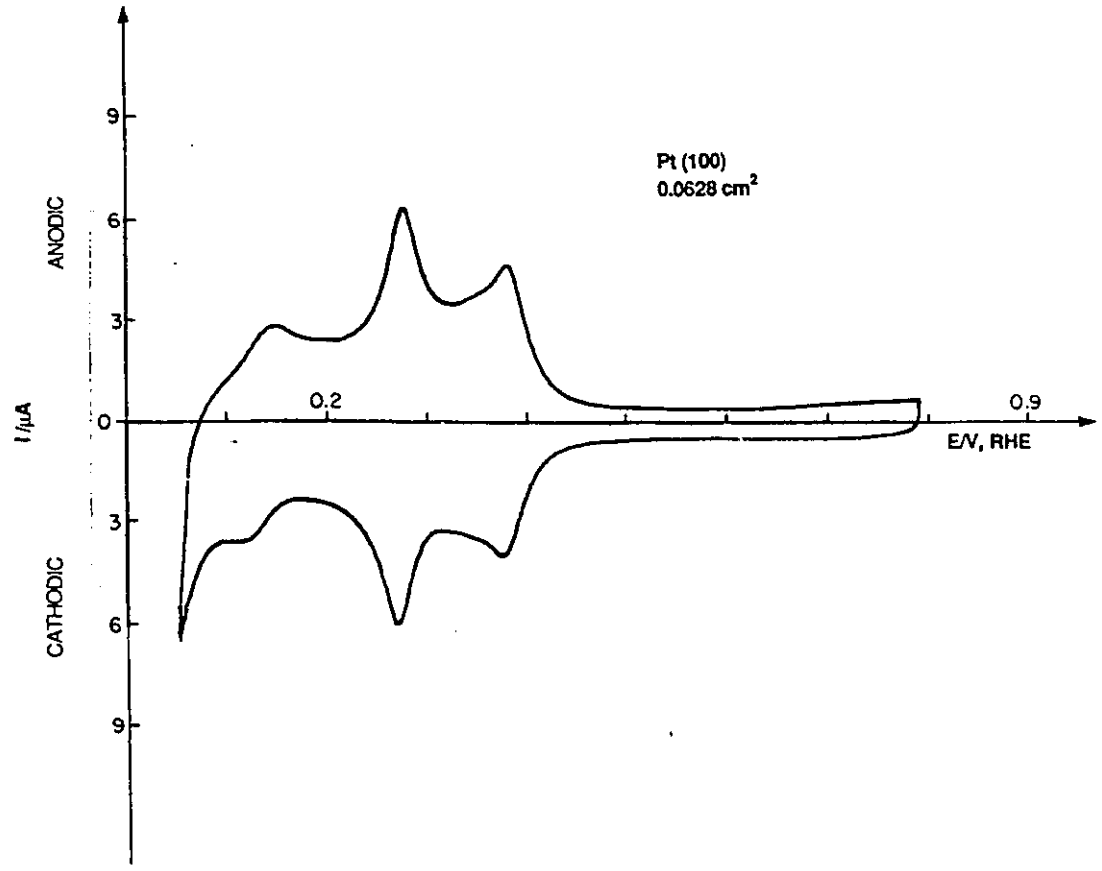

Fig. 3.43 H UPD C-V profile for the Pt(100) electrode heated at ca. 500°C followed by quenching (0.5 M aq. H_2SO_4, 298 K).

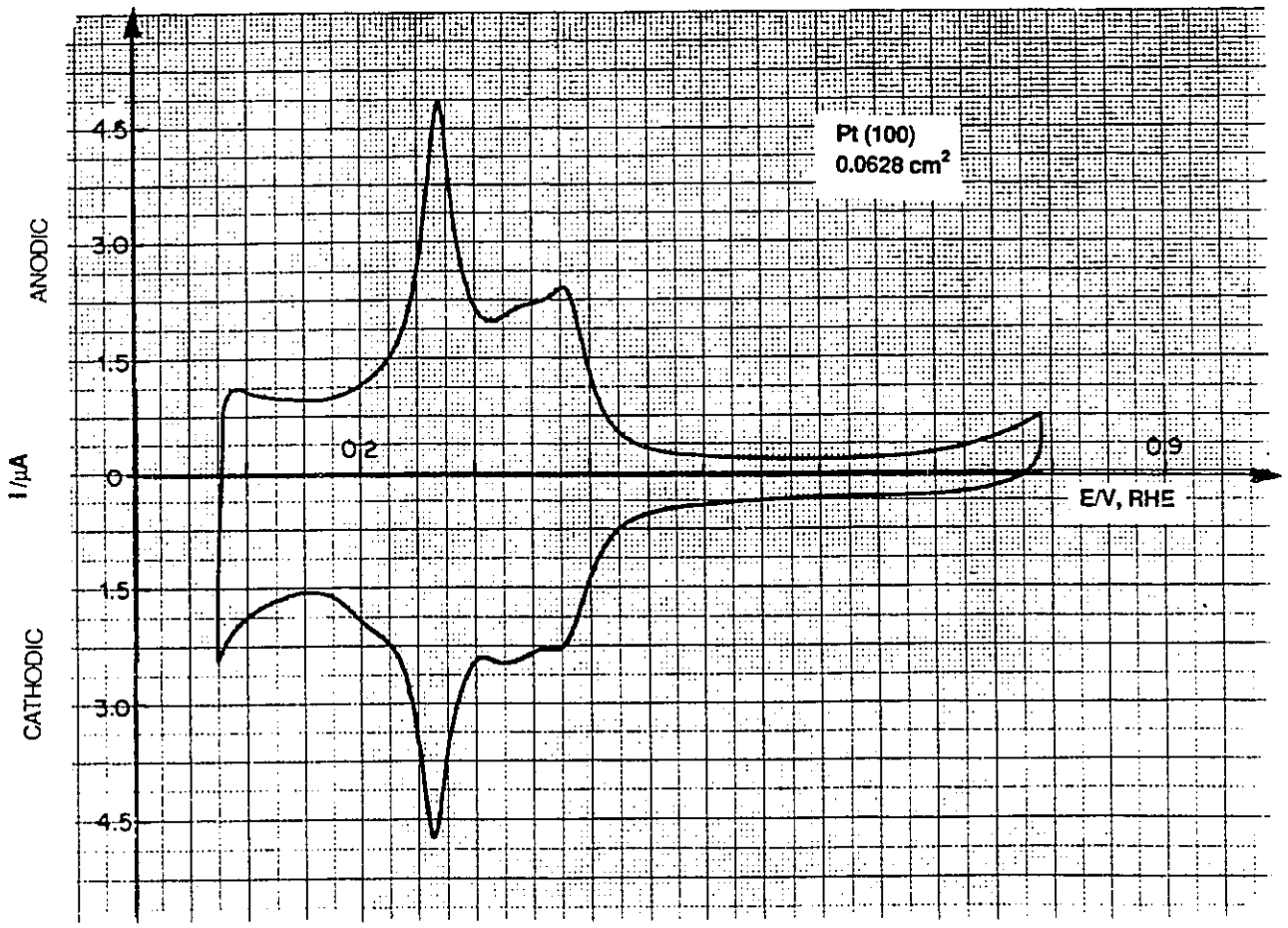

Fig. 3.44 H UPD C-V profile for the Pt(100) electrode heated at ca. 800°C followed by quenching (0.5 M aq. H_2SO_4, 298 K).

profile is the absence of the peak at 0.13 V, RHE, revealed at both the annealed Pt(100) and the Pt(100) heated at ca. 500°C followed by quenching. The H UPD accommodation was found to be 202 (±5) μC cm^{-2}; in this case the apparent cathodic charge is some 20 μC cm^{-2} greater than the anodic one. It is interesting that such a drastic pretreatment of the Pt(100) electrode as heating at ca. 800°C followed by quenching leads to the kind of surface whose H UPD accommodation is close to the calculated value [137] (for explanation see Sections 3.4.3 and 3.4.4). Another interesting detail is the onset of surface oxide formation around 0.80 V, RHE, as will be discussed later (compare with a value of ca. 0.85 V, RHE, for polycrystalline Pt).

3.4.2 Continuity of Changes in the C-V Profiles for Heated and Quenched Pt(100) as a Result of Increase of Upper Potential Limit in Cycling

In the previous Section, it was shown that different thermal pretreatments lead to distinguishable C-V profiles which probably correspond to variously modified Pt(100) surfaces, i.e. surfaces restructured to different extents. A question arises whether these structural changes, as revealed by the C-V, are reversible or irreversible, and what would the C-V profile for "quenched" Pt(100) surfaces be like after cycling to various potential limits between 0.90 and 1.40 V, RHE.

Experiments were conducted in which a heated and quenched Pt(100) surface, having originally a C-V profile as in Fig. 3.45(a) and a Q_{HUPD} of 284 (±5) μC cm^{-2}, was cycled five times to various potential limits of 0.9, 1.0 ..., 1.4 V, RHE. Fig. 3.45(b) shows the changes in both the H UPD and the "oxide region" of the C-V profiles, that arise as a result of increase of the upper potential limit. The C-V profile underwent continuous changes which became more pronounced when the upper potential limit was raised to 1.20 V, RHE, or higher. Fig. 3.45(c) shows the 5th C-V profile up to 1.40 V, RHE. Further cycling causes some further but small changes in the C-V profile which, after prolonged cycling, becomes the C-V profile of Hubbard et al. [137], as shown in Fig. 3.42.

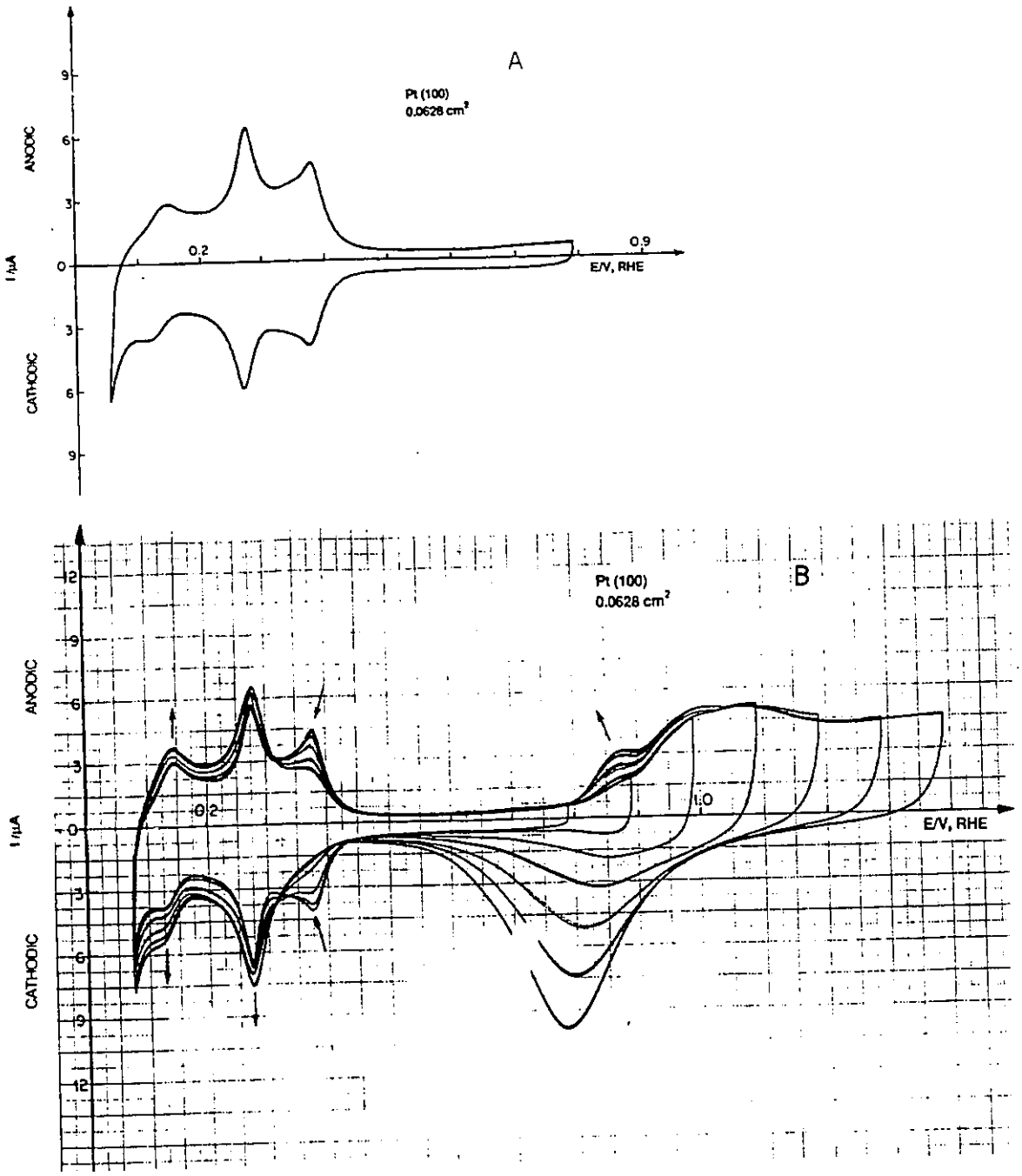

Fig. 3.45 C-V profile for the Pt(100) electrode after heating at ca. 500°C followed by quenching; (a) H UPD C-V profile between 0.07 and 0.80 V, RHE; (b) changes in the C-V profile as a result of cycling five times to various limits of 0.90, 1.00, ..., 1.40 V, RHE (0.5 M aq. H_2SO_4, 298 K) (the second and third cycle are recorded; arrows indicate the directions of changes in the C-V profiles with successive cycling).

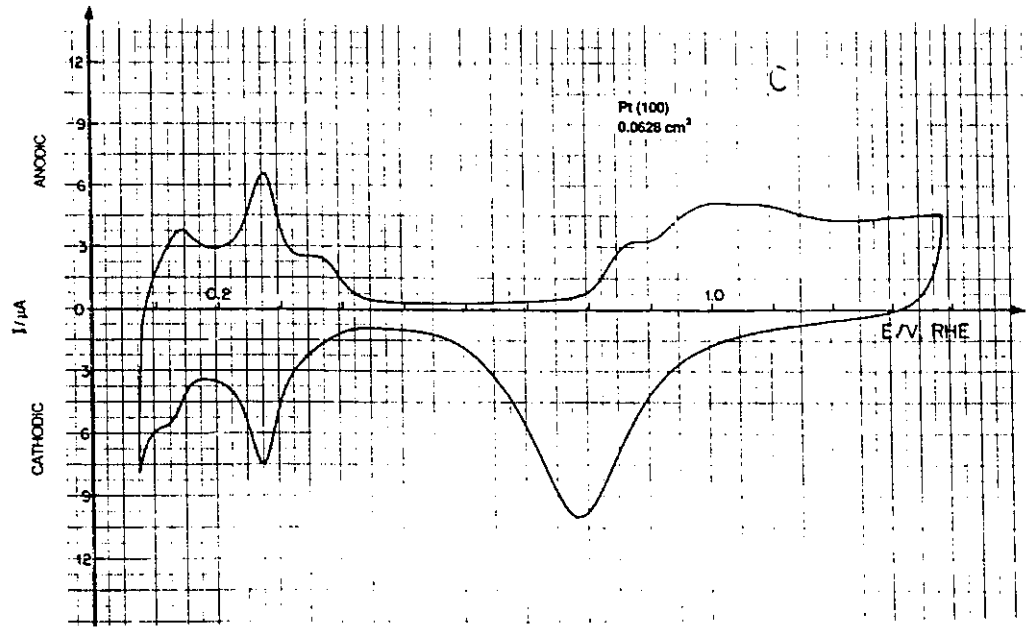

Fig. 3.45 (c) The 5th C-V profile after multiple cycling up to 0.90, 1.00, ..., 1.40 V, RHE.

The changes in the C-V profile, which correspond to surface structural changes of the Pt(100), arising after cycling to the various upper potential limits, are irreversible. This was tested by reducing the upper potential limit to 0.9 or 0.8 V, RHE, after previous cycling up to 1.20 or 1.30 V, RHE. Since this did not lead to reproduction of the original H UPD C-V profile, the surface structural changes were evidently irreversible.

The H UPD accommodation for the C-V profile shown in Fig. 3.45(a) was said to be 284 (±5) μC cm^{-2}. Interestingly, cycling to various upper potential limits did not affect the H UPD charge which basically remains between 278 and 288 μC cm^{-2}.

3.4.3 Explanation of the Anomalous H UPD Accommodation on the Annealed Pt(100)

In Section 3.4.1, it was mentioned that the H UPD accommodation on the annealed Pt(100) surface and on the heated (at ca. 500°C) and quenched Pt(100) surface was some 70 μC cm^{-2} greater than the calculated value [137].

In an early stage of the work, it was thought that this could be due to solution creeping along the side-wall of the Pt(100) single crystal, since the shape of this particular crystal was slightly barrel-like. However, the same abnormally large value of H UPD accommodation was acquired on three different occasions, i.e. when the crystal was annealed and the C-V profiles recorded on different days. At that point it was thought that creepage of the solution was unlikely to be exactly the same on three separate occasions. To solve this problem, the shape of the hanging meniscus was observed by means of a projection apparatus (Olympus, Japan) for measuring contact angles. Fig. 3.46 shows a series of photographs of the Pt(100) single crystal in contact with the 0.5 M aq. H_2SO_4 solution for different heights of the hanging meniscus and for a broken solution-electrode "connection". The data from the photographs reveal that: (a) there is no creep of solution along the side-wall of the Pt(100) crystal; and (b) that the height of the hanging meniscus is not very crucial to the electrochemistry at single-crystal electrodes in 0.5 M aq. H_2SO_4 since the solution does not easily creep along the side-wall of the crystal. The anomalously large value of the H UPD accommodation on the annealed Pt(100) must then be explained in terms of surface restructuring rather than creep of solution, especially since the extra (excess) charge was always ca. 30% of the "normal" H UPD monolayer at Pt(100).

Thermodynamically favoured surfaces are those exposing densely packed planes of atoms. The (111) plane of the fcc lattice is the most densely packed and also the most stable one (similarly, the (110) plane of the bcc lattice). However, the (110) or (100) planes are known to undergo reconstruction [107,108], minimizing the surface free energy.

The physical and chemical origins of such reconstructions are as follows:

(a) the electron cloud attempts to smooth its surface (almost as if there were an electron gas tension) by producing electrostatic forces which draw either the surface atoms closer to each other or the surface atoms towards the substrate;

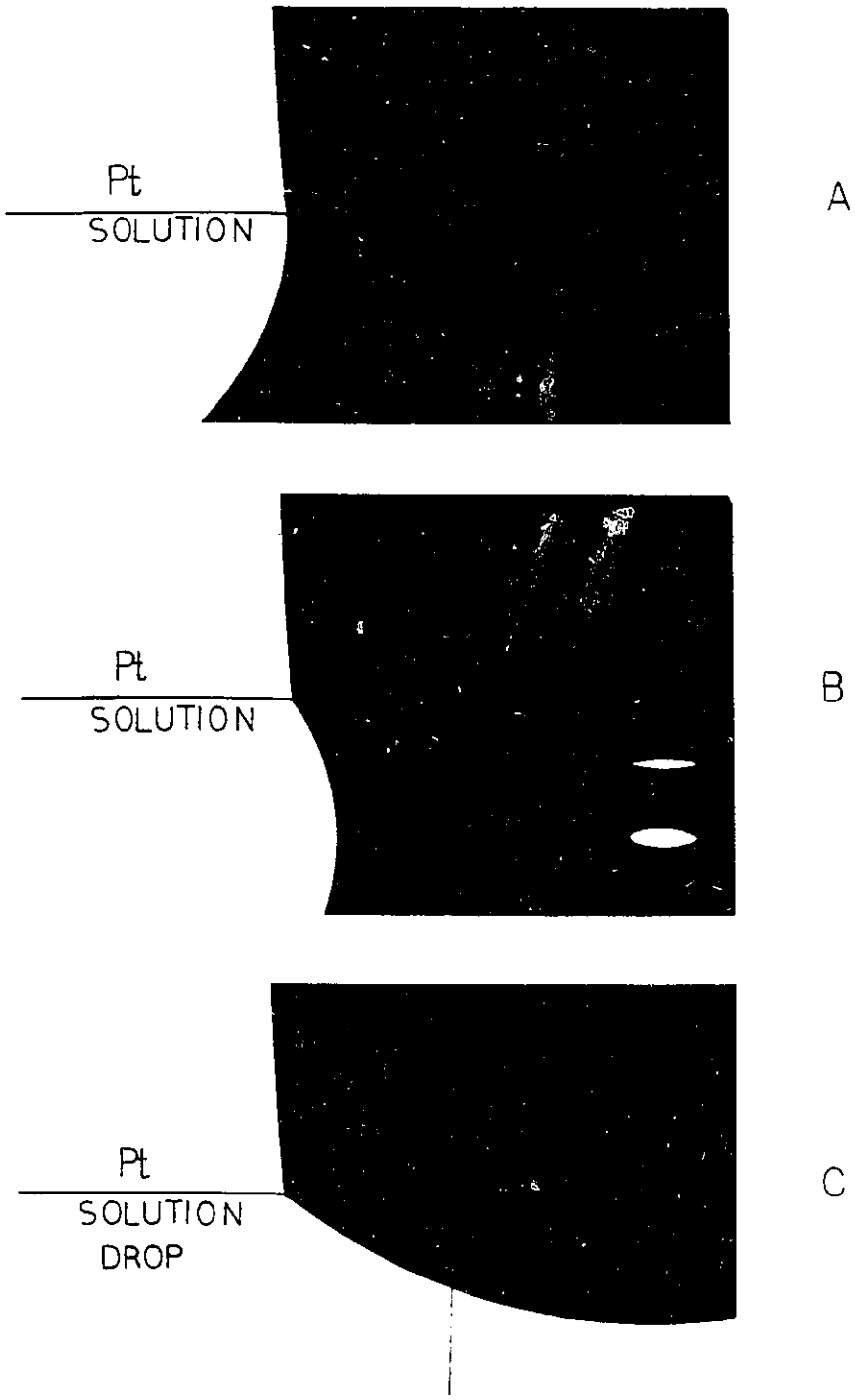

Fig. 3.46 Photographs showing the contact between the Pt(100) single crystal and the 0.5 M aq. H_2SO_4 solution at the hanging-meniscus; (a) and (b) for different heights of the meniscus; (c) a broken contact (meniscus).

(b) with fewer neighbours around, the two-body repulsion energy is smaller and allows greater atomic overlap and therefore more favourable bonding at shorter bond lengths;

(c) in the case of surface atoms, the bonding electrons are partly shifted from the bonding orbitals towards the non-bonding ones (i.e. towards those which are directed outwards from the metal surface) reducing the bond strength between the surface atoms and those lying underneath [107,108].

Clean (100) and (110) surfaces are reconstructed [107,108] and adsorption of CO or some olefinic hydrocarbons may relax them to the "ideal" (1×1) arrangement. However, desorption of adsorbates (or sometimes of impurities, i.e. recleaning) may again reconstruct the surface. It is possible to prepare a clean (100)-(1×1) surface for Pt or Ir, but it is known to be metastable [107,108]. This is done by bombardment with oxygen ions and subsequent careful annealing. However, heating to ca. 300°C reconverts it to the stable, reconstructed state [107,108].

One of the most stable, reconstructed (100) surfaces is the one represented by the "missing row" model, i.e. the (100)-(2×1) surface, as shown in Fig. 3.47. Interestingly, the H UPD accommodation for such a surface is exactly 33% greater than for the (100)-(1×1) surface (see Section 3.4.2 and the experimentally determined Q_{HUPD}).

It may therefore be concluded that the H UPD C-V profile shown in Fig. 3.42 corresponds to the (100)-(2×1) surface whose H UPD accommodation is ca. 278 $\mu C\ cm^{-2}$.

3.4.4 Comparison of the H UPD Profile for Heated and Quenched Pt(100) with that for Annealed Pt(100)

Earlier (see Section 3.4.1), it was said that the H UPD accommodation on the Pt(100) surface quenched from 500°C was 284 (±5) $\mu C\ cm^{-2}$. This value, which is ca. 35% bigger than the calculated value [137], suggests that the surface is probably the one with a "missing row" structure (Fig. 3.47), whose Q_{HUPD} is 278 $\mu C\ cm^{-2}$. However, an

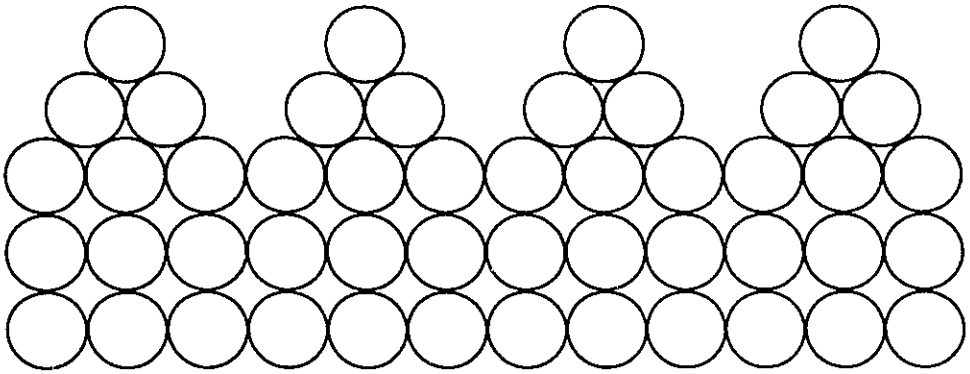

Fig. 3.47 Schematic diagram of the (100) "missing row" surface.

obvious question arises: why, then, is the H UPD C-V profile so different from the one for the annealed Pt(100) surface? It is suggested that this is due to some small atomic displacements of the already reconstructed (100) surface. This reconstructed surface with small (0.1-0.2 Å) displacements would have a wider range of distances between Pt atoms than the surface free of displacements. It might then be expected that the H adsorption, which competes with the HSO_4^- adsorption, would then exhibit a more complex C-V profile than that for the annealed Pt(100) surface (see the analogous discussion for Pt(111) - Section 3.3.7).

In the case of the Pt(100) surface quenched from 800°C, the H UPD charge was 202 (±5) μC cm^{-2}. It is suggested that the hot Pt(100) surface, which is likely to be the (1×1) at high temperatures, is sustained with its "ideal" geometry by rapid cooling (quenching) and possibly by simultaneous thermal formation of the oxide (cf. refs. 107,108). As for the case of the "quenched" Pt(111), the (100)-(1×1) surface structure, we suggest, contains some small but regular displacements which are responsible for the complex character of the H UPD C-V profiles (see Section 3.3.7). Such small displacements are illustrated in Fig. 3.48 and have been observed for Pt(100) and Ir(100) surfaces [107].

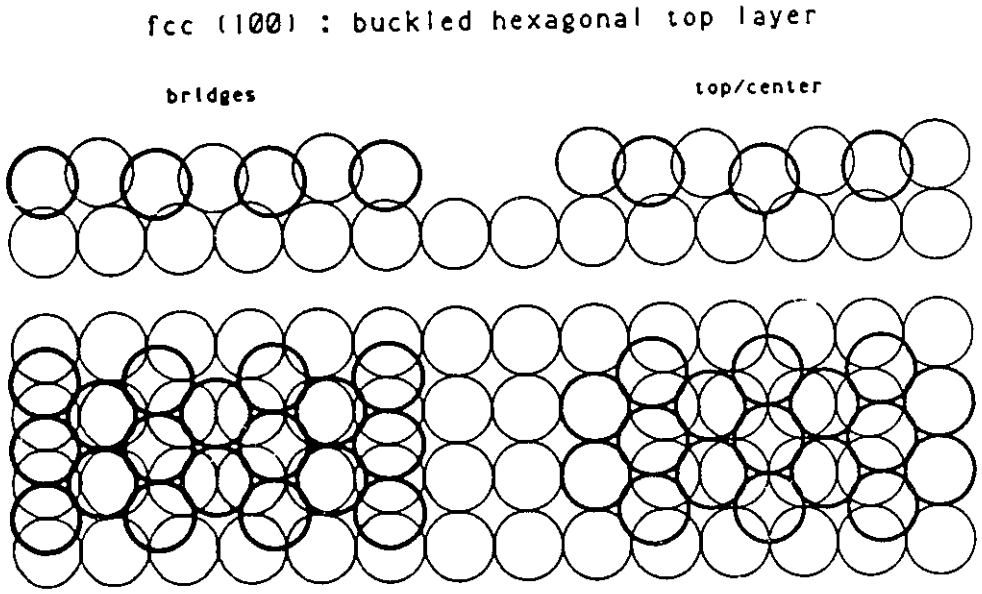

Fig. 3.48 Arrangement of atoms on the reconstructed (100) crystal faces of Pt, Au and Ir; side and top views are shown [107].

At the beginning of Section 3.4, it was mentioned that the Pt(111) surface has been the one most investigated. There are considerably less data on both the Pt(100) and Pt(110) surfaces and thus less controversy. However, it is important to emphasize that these two crystal faces, i.e. (100) and (110), are much less stable, if clean, and then become reconstructed. Some of the most stable but still reconstructed surfaces are those of (n×1) arrangements where n = 2, 3, 4 or 5 in most cases. The H UPD accommodation on these reconstructed surfaces would vary from ca. 208 to 278 $\mu C\ cm^{-2}$. If one takes into account the possibility that each of these reconstructed and stable surfaces can contain some small atomic displacements, then a variety of possible surface structures, and hence possible H UPD C-V profiles, can arise.

3.5 Oxide Growth at Single-Crystal Pt Electrodes

3.5.1 Introductory Remarks

The formation of oxide films at polycrystalline Pt electrodes has been studied extensively. The extension of a submonolayer, through a monolayer, to growth of a multilayer film is quite well understood due to extensive research on this subject, as was indicated in the "Introduction" Chapter. However, very little work on film growth has been done on Pt single crystals.

The data that have arisen from careful analysis of the C-V profiles in aq. H_2SO_4 solutions for single-crystal Pt electrodes recorded by Hubbard et al. [137], Clavilier et al. [140-147] and other researchers [138,139,166,172,173,195] provide only a source of limited information on oxide growth. For example, from results on "quenched" Pt(111), it may be concluded [140-143,147] that the formation of the quasi-2-d oxide does not occur below the potential of 1.10 V, RHE, and beyond that potential and up to 1.40 V, RHE, less than half a monolayer of "O" is formed in a single sweep. This behaviour, however, is not maintained at the "quenched" (111) surface and upon cycling up to 1.40 V, RHE, the electrode surface becomes restructured; the oxide growth at such a restructured surface commences at ca. 0.85 V, RHE. On the other hand, the oxide growth, both at annealed and "quenched" Pt(100), commences at ca. 0.80 V, RHE; qualitative and quantitative changes do occur in the "oxide region" of the C-V profile for Pt(100) upon cycling to 1.40 V, RHE. Even less data are available for the Pt(110) surface and from the existing information [146,147] it may be concluded that the "oxide region" begins between 0.80 and 0.90 V, RHE, depending on the thermal pretreatment of the Pt(110) electrode. Literally no data are available for the "oxide region" of the C-V profile and any possible changes in it resulting from potential cycling to various upper limits.

Pre-electrochemical formation of oxide films on single-crystal and polycrystalline Pt electrodes was observed [142-144] when electrodes were flame-annealed, followed by

quenching. The existence of an oxide film was detected by recording the first negative-going sweep from the rest potential of Pt electrodes, i.e. from ca. 0.90 V, RHE.

An analysis of C-V profiles for single-crystal Pt electrodes up to 1.40 V, RHE, indicates [137,140,141,144,146,147,166,195] that the features of the profiles corresponding to the oxide formation and reduction differ quite substantially from one single-crystal face to another, as also known at Au.

The information above provides some limited qualitative data on quasi-2-d oxide formation and reduction on Pt single-crystal faces. However, virtually no information exists on potentiostatically controlled, direct formation of oxide beyond 1.40 V, RHE, and on any possible surface-restructuring processes which are likely to arise in oxide formation and reduction. In that respect, the results reported in this thesis on this matter are quite original.

3.5.2 Oxide Growth at the Pt(111) Electrode

In Sections 3.3.3 and 3.3.4, it was shown how the "quenched" Pt(111) electrode behaves upon cycling up to 1.40 V, RHE. It was interesting to see that the "quenched" Pt(111) electrode surface after ca. 10 cycles up to 1.40 V, RHE, exhibits the same behaviour as the annealed Pt(111) electrode surface after the same number of cycles. Such surfaces, according to Aberdam et al. [195], consist of (111) terraces in monoatomic steps ca. 10-11 rows long; upon further cycling to 1.40 V, RHE, the terraces are found to become shorter, with 7.5 (±1) atomic rows. The clarification of the question what happens to the (111) surface upon cycling up to 1.40 V, RHE, is very important for further investigations on oxide growth at Pt(111). Having established that the Pt(111) surface contains (111) terraces which are at least 7.5 atomic rows long (i.e. the surface is ca. 88% "pure" (111)), oxide growth at this electrode surface was investigated.

Oxide Growth in a Single Sweep to Potentials between 0.9 and 1.8 V, RHE

Application of single sweeps to 1.80 V, RHE, at 298 K (25°C) results in the formation of the OC1 state, i.e. the quasi-2-d oxide, observed in a following reduction sweep. The oxide-reduction charges are shown in Fig. 3.49. As expected, the larger reduction charge corresponds to a sweep up to 1.80 V, RHE, and is ca. 865 $\mu C\ cm^{-2}$, i.e. 1.79 equivalent "PtO" monolayers while a sweep up to 0.90 V, RHE, results in a reduction charge of ca. 25 $\mu C\ cm^{-2}$, i.e. 0.05 of a "PtO" monolayer or 0.1 of "PtOH". It is interesting that formation of up to 1.79 monolayers of equivalent "PtO" does not cause any significant changes in the surface structure of Pt(111), as was revealed by the first positive-going C-V profile right after the oxide reduction (Fig. 3.50). This implies that, in the case of an annealed Pt(111) surface, the place-exchange process is completely "reversible" from the electrochemical surface structure point of view (i.e. Pt atoms return to their initial sites in the surface lattice after oxide reduction) and does not contribute to any surface restructuring processes which would be detected by the C-V technique. The situation, however, might be different once a thick-oxide film has been grown, as is the case at polycrystalline Pt (see Sections 3.1.1-3.1.3). Formation of thick oxide films might cause some significant restructuring. No thick-oxide films (those having the OC2, OC3 or OC4 states) were grown on single-crystal Pt electrodes during the course of the research reported here so the question of possible restructuring remains unanswered.

Oxide Growth at Pt(111) for Various Polarization Potentials and Times

Oxide film development was followed at different polarization (holding) potentials, E_h, between 0.90 and 1.80 V, RHE, and for various polarization (holding) times, t_h, which were 0, 10, 100 and 1000 s. The logarithmic oxide film-growth rates, $dQ_{ox}/d \log t_h$, were recorded (from the reduction profiles) for each of the E_h values, as shown in Fig. 3.51. The smallest surface oxide coverage was obviously for $E_h = 0.90$ V, RHE, and $t_h = 0$ s, and corresponded to an oxide reduction charge of ca. 27 $\mu C\ cm^{-2}$ (i.e.

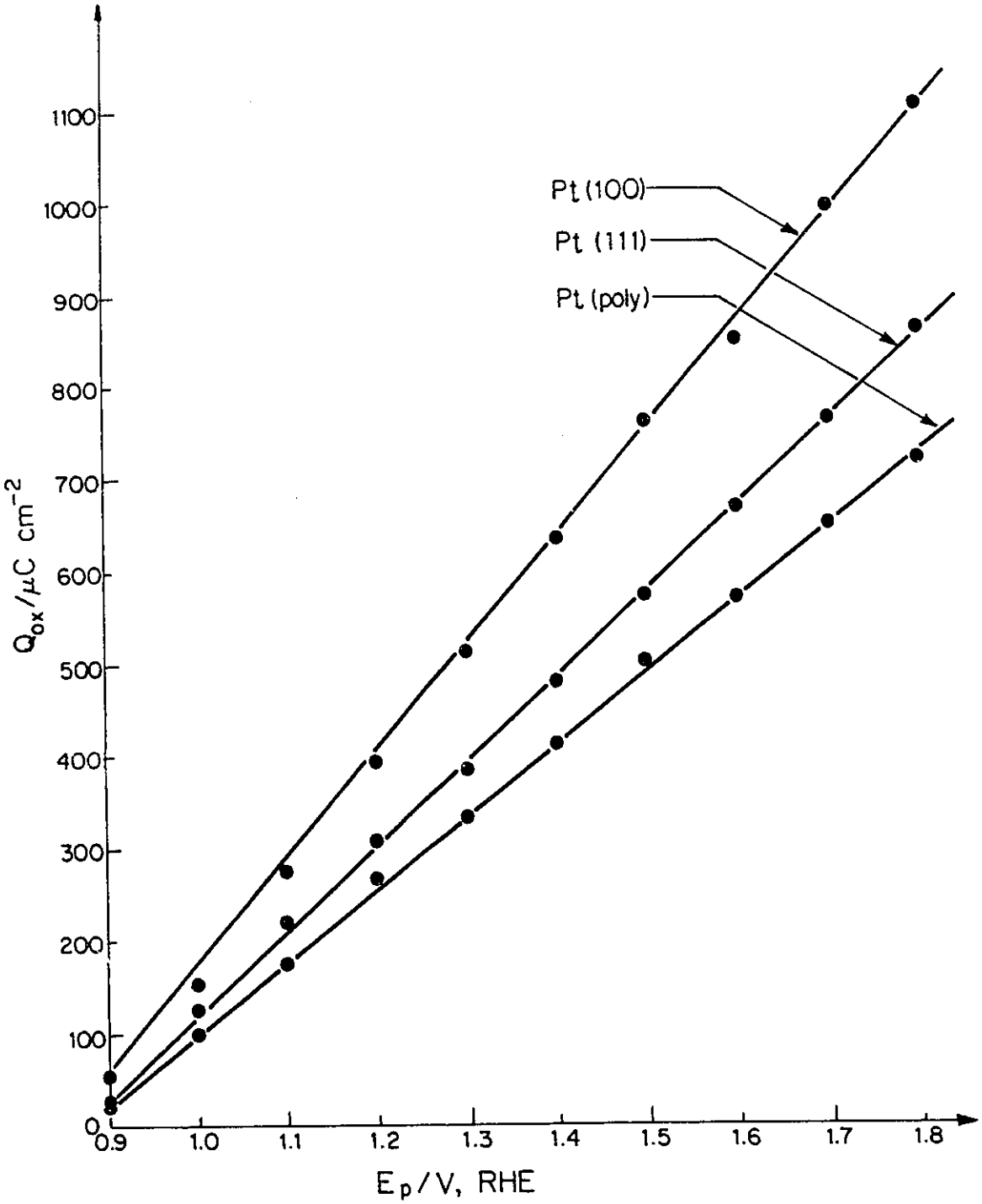

Fig. 3.49 Oxide-reduction charges for Pt(111), Pt(100) and Pt(poly) electrodes upon a single sweep as a function of the upper potential limit (0.5 M aq. H_2SO_4, 298 K).

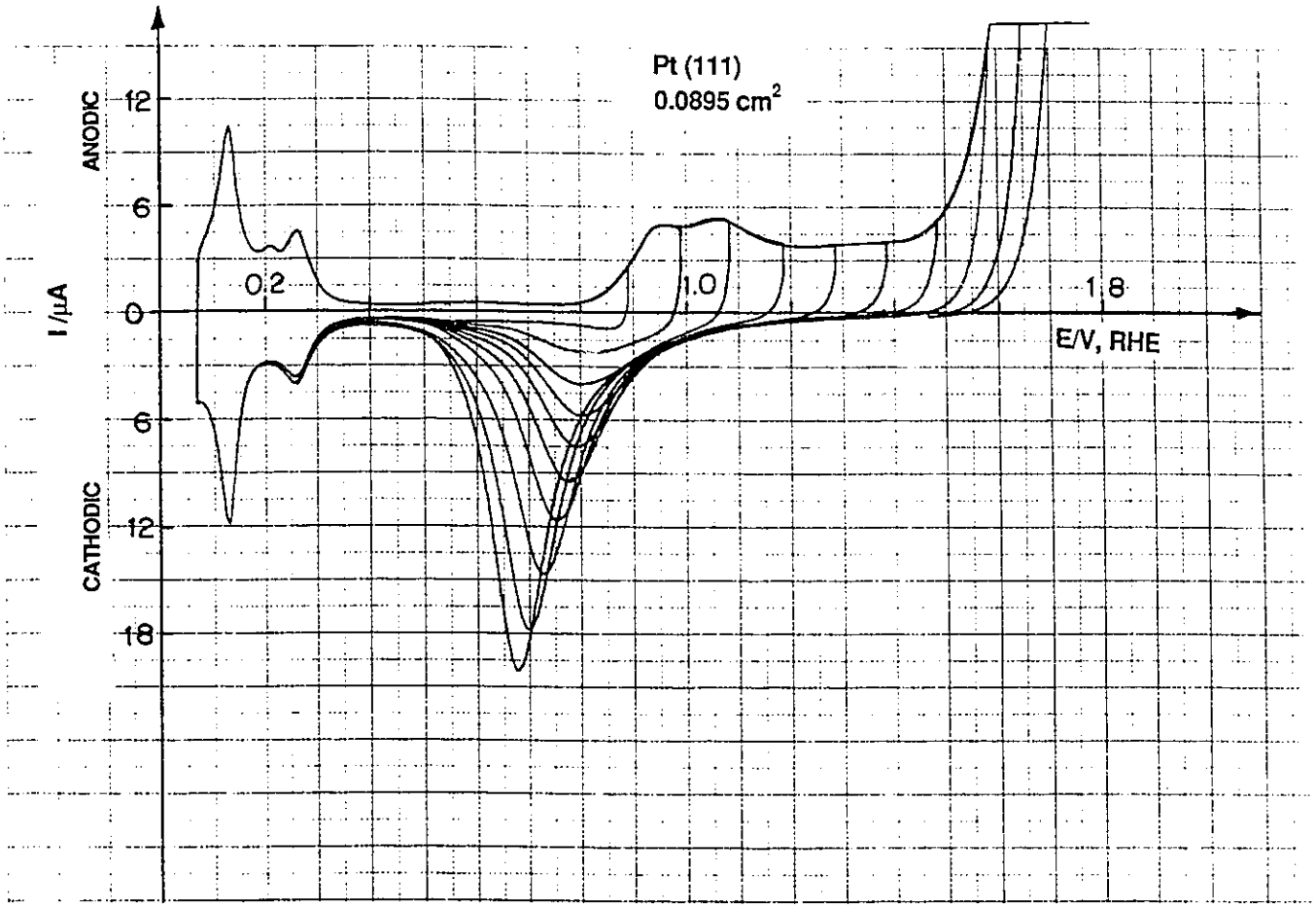

Fig. 3.50 C-V profiles for reduction of surface oxide grown on Pt(111) by application of a single sweep from 0.90 to 1.60 V, RHE (0.5 M aq. H_2SO_4, 298 K); the oxide reduction peak shifts towards less-positive potentials with increase of the upper potential limit (as known previously [9]).

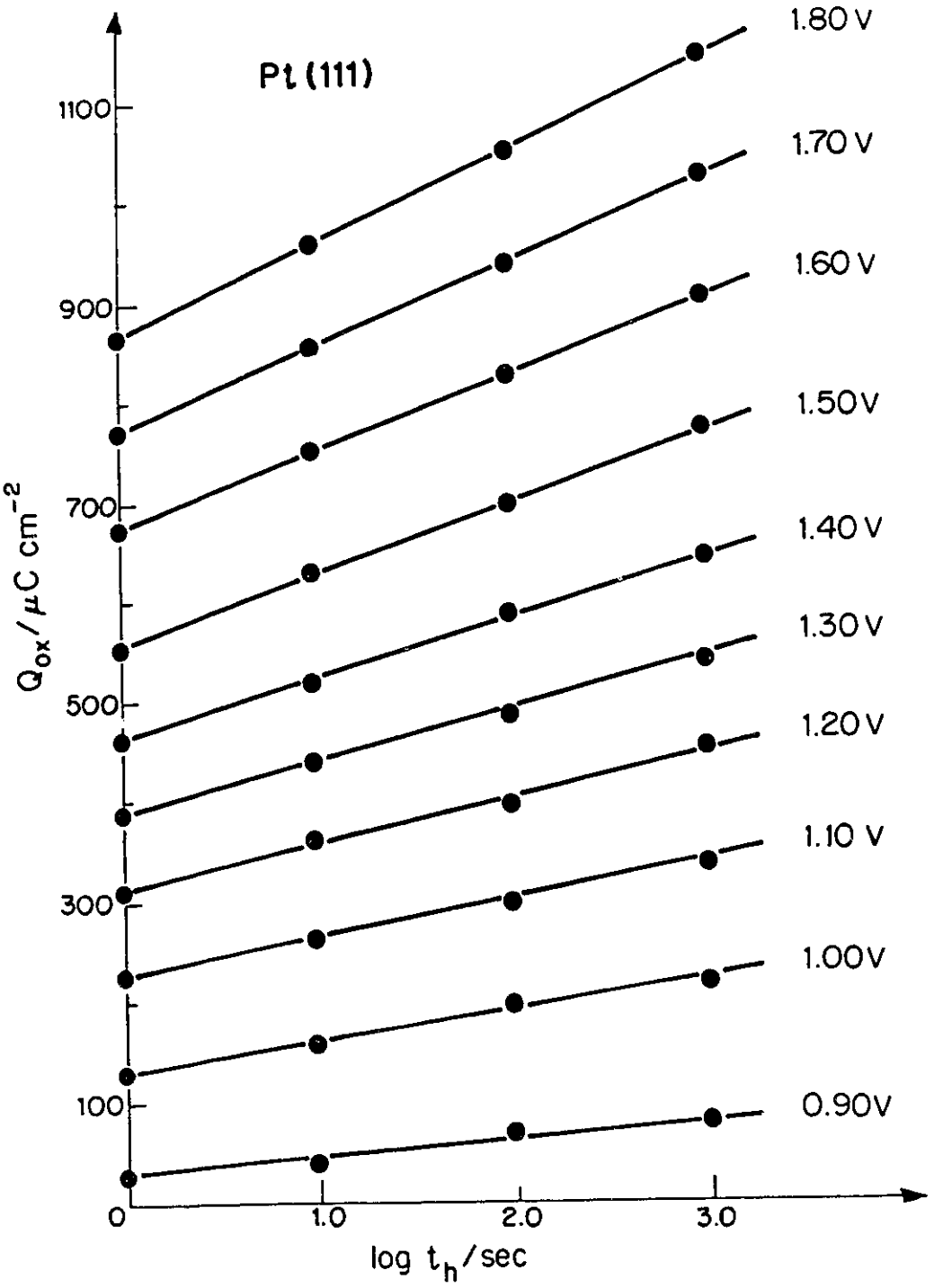

Fig. 3.51 Logarithmic oxide film growth plots, Q_{ox} vs log t_h, at Pt(111) for various polarization potentials (0.5 M aq. H_2SO_4, 298 K).

0.06 of equivalent "PtO" monolayer) while the largest one for E_h = 1.80 V, RHE, and t_h = 1000 s gave an oxide reduction charge of ca. 1300 $\mu C\ cm^{-2}$ (i.e. 2.71 equivalent "PtO" monolayers). Examination of the growth kinetics in terms of $dQ_{ox}/d \log t_h$ plots for various polarization potentials showed that $dQ_{ox}/d \log t_h$ was linear in E_h (Fig. 3.52), a relation having a slope of 89 ($\pm$3) $\mu C\ cm^{-2}$ (decade $t_h)^{-1}\ V^{-1}$.

The kinetics of oxide growth at Pt(111) will be discussed in further detail in Section 3.5.4; however, it should be mentioned that: (a) Q_{ox} vs $\log t_h$ plots are linear, i.e. the oxide growth proceeds according to the direct logarithmic law; (b) the values of the $dQ_{ox}/d \log t_h$ slopes depend on E_h; and (c) the Q_{ox} vs $\log t_h$ plots pass through the monolayer level of oxide charge with no change of slope, i.e. the oxide growth mechanism probably remains unchanged between sub-monolayer and multilayer stages of growth indicating a common mechanism, probably of place-exchange at the Pt/oxide interface.

3.5.3 Oxide Growth at the Pt(100) Electrode

In Section 3.4.2, it was said that the Pt(100) electrode does not reveal an H UPD accommodation which would correspond to the "ideal" (1×1) surface. On the contrary, the H UPD charge was found to be ca. 33% greater than that for the (100)-(1×1) surface. This anomalous behaviour was explained by reconstruction to the (100)-(2×1) "missing row" structure, H UPD accommodation for which would be 278 $\mu C\ cm^{-2}$, a value close to that experimentally determined. However, this surface structure was found to be stable and did not undergo any further changes upon prolonged cycling to 1.40 V, RHE, as was revealed by an analysis of the H UPD C-V profiles. Clarification of this problem, i.e. reconstruction resulting from cycling to 1.40 V, RHE, prior to oxide-film growth studies is essential for proper understanding of the overall mechanism of oxide film growth.

Oxide Growth in a Single Sweep to Potentials between 0.9 and 1.8 V, RHE

A single sweep up to 1.80 V, RHE, at 298 K (25°C) results in the formation of the

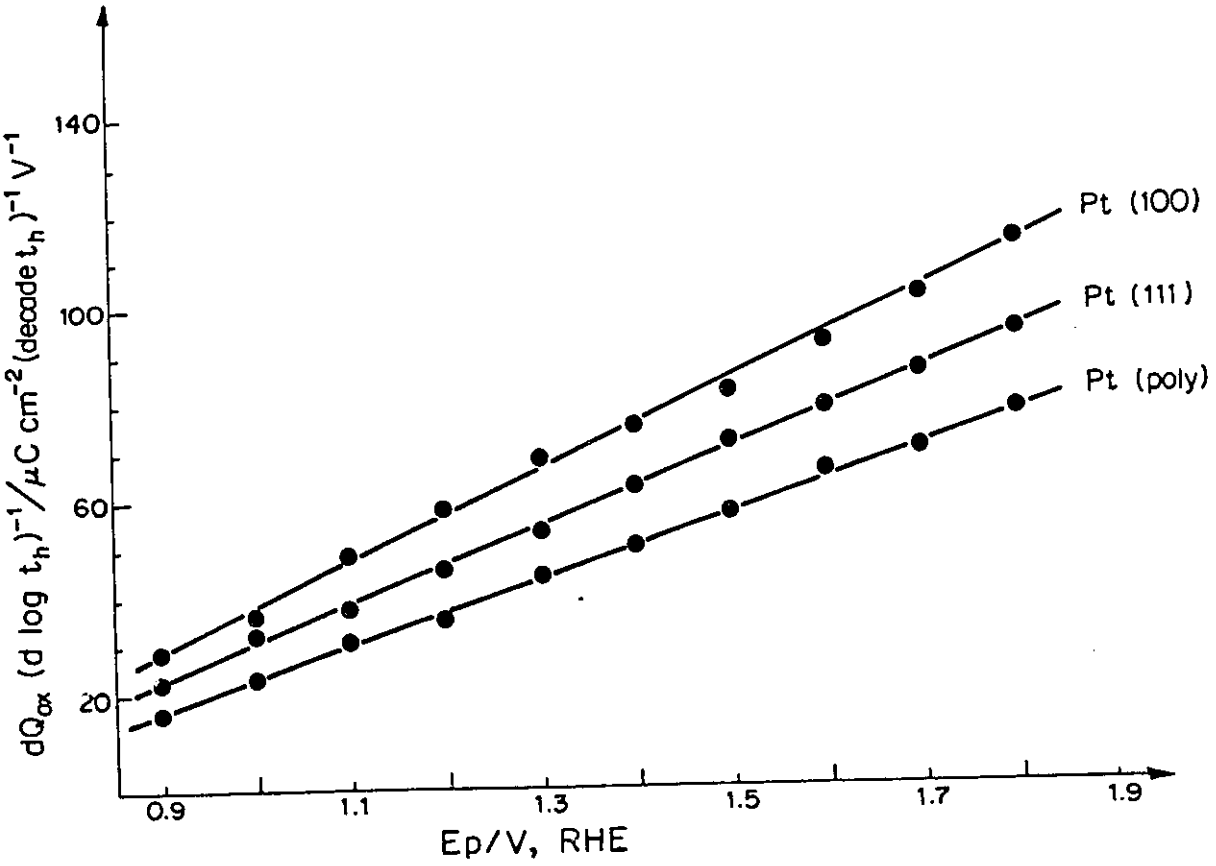

Fig. 3.52 Slopes of the Q_{ox} vs log t_h plots as a function of the polarization (holding) potential, E_h, for the Pt(111), Pt(100) and Pt(poly) electrodes.

OC1 state, as in the case of the (111) electrode. The oxide-reduction charges are shown in Fig. 3.49 and vary from ca. 55 $\mu C\ cm^{-2}$ for E_h = 0.90 V to ca. 1100 $\mu C\ cm^{-2}$ for E_h = 1.80 V, RHE, i.e. from 0.13 to 2.67 equivalent "PtO" monolayers. Similarly to the case of the Pt(111) electrode, the formation of up to 2.67 monolayers of equivalent "PtO" does not cause any significant changes in the structure of Pt(100), as revealed by the form of the first positive-going C-V profile after oxide reduction. This suggests that the "missing row" structure of the (100) face is stable, even after formation and reduction of 2.67 equivalent monolayers of "PtO" (see Fig. 3.53) and that, on the (100)-(2×1) surface, the place-exchange process does not create any new surface arrangement, different from the original one.

Oxide Growth at Pt(100) for Various Polarization Potentials and Times

Oxide film formation was studied as for the case of the Pt(111) electrode, i.e. for polarization potentials between 0.90 and 1.80 V, RHE, and for polarization times up to 1000 s (see Section 3.5.2). The logarithmic oxide growth rates, $dQ/d \log t_h$, are shown in Fig. 3.54. The thickest oxide film (grown at E_h = 1.80 V for t_h = 1000 s) corresponded to 3.50 equivalent monolayers of "PtO". Interestingly, even such a thick film did not cause any significant surface restructuring, based on the subsequent C-V profiles! The growth kinetics were again logarithmic in t_h and the plot of $dQ/d \log t_h$ against E_h (Fig. 3.52) was linear with a slope of 94 (±3) $\mu C\ cm^{-2}$ (decade $t_h)^{-1} V^{-1}$.

As for the case of Pt(111), the following conclusions can be drawn: (a) Q_{ox} vs $\log t_h$ plots are linear, i.e. the growth proceeds according to the direct logarithmic law; (b) the $dQ_{ox}/d \log t_h$ values depend on E_h; and (c) there is no change in the oxide growth mechanism as the oxide film passes through the monolayer level, as also found at polycrystalline Pt.

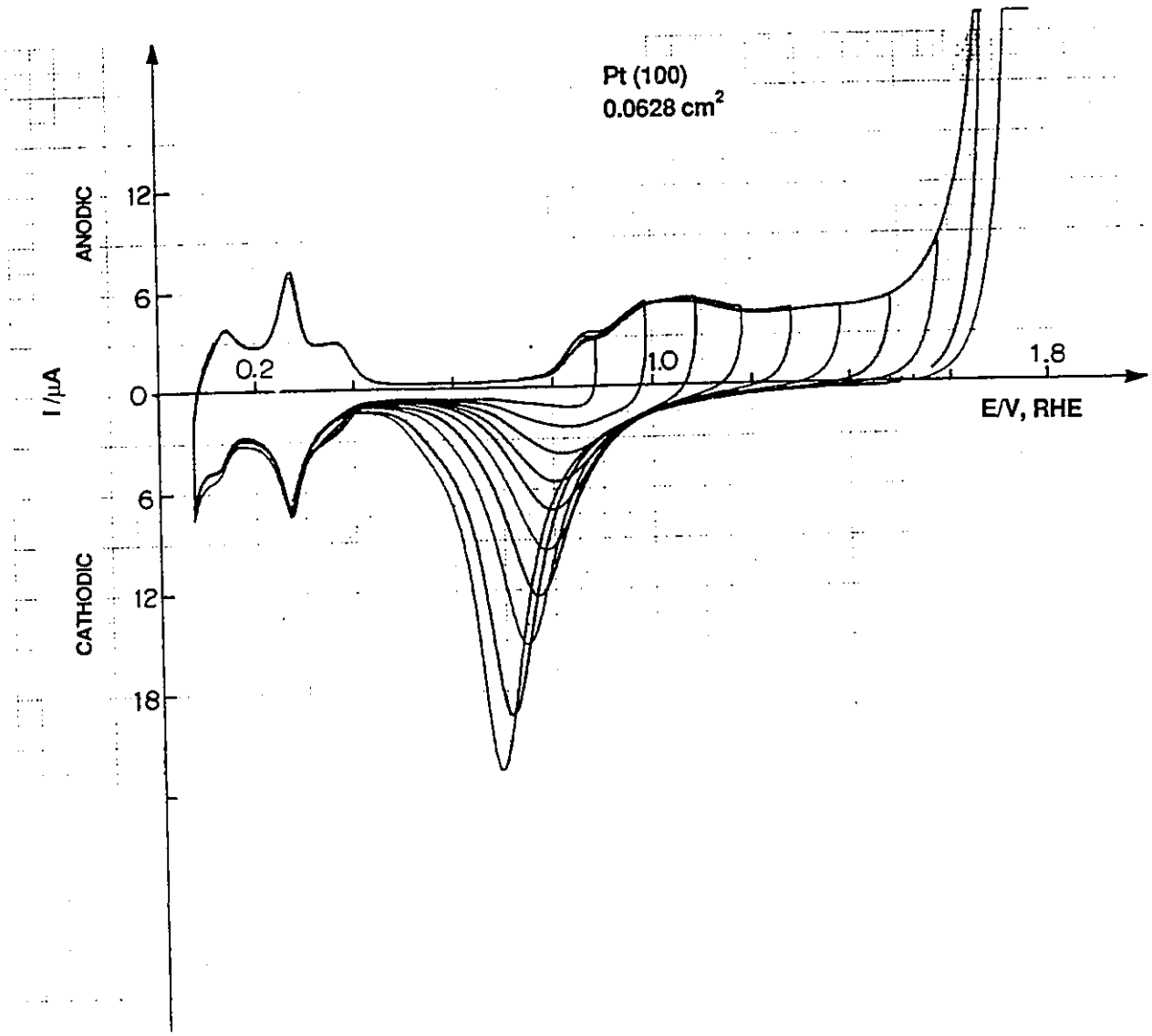

Fig. 3.53 C-V profiles for formation and reduction of surface oxide grown on Pt(100) by an application of single sweeps from 0.90 to 1.80 V, RHE (0.5 M aq. H_2SO_4, 298 K). (The oxide reduction peaks shift towards less-positive potentials with increase of the upper potential limit, as for other Pt surfaces [9]).

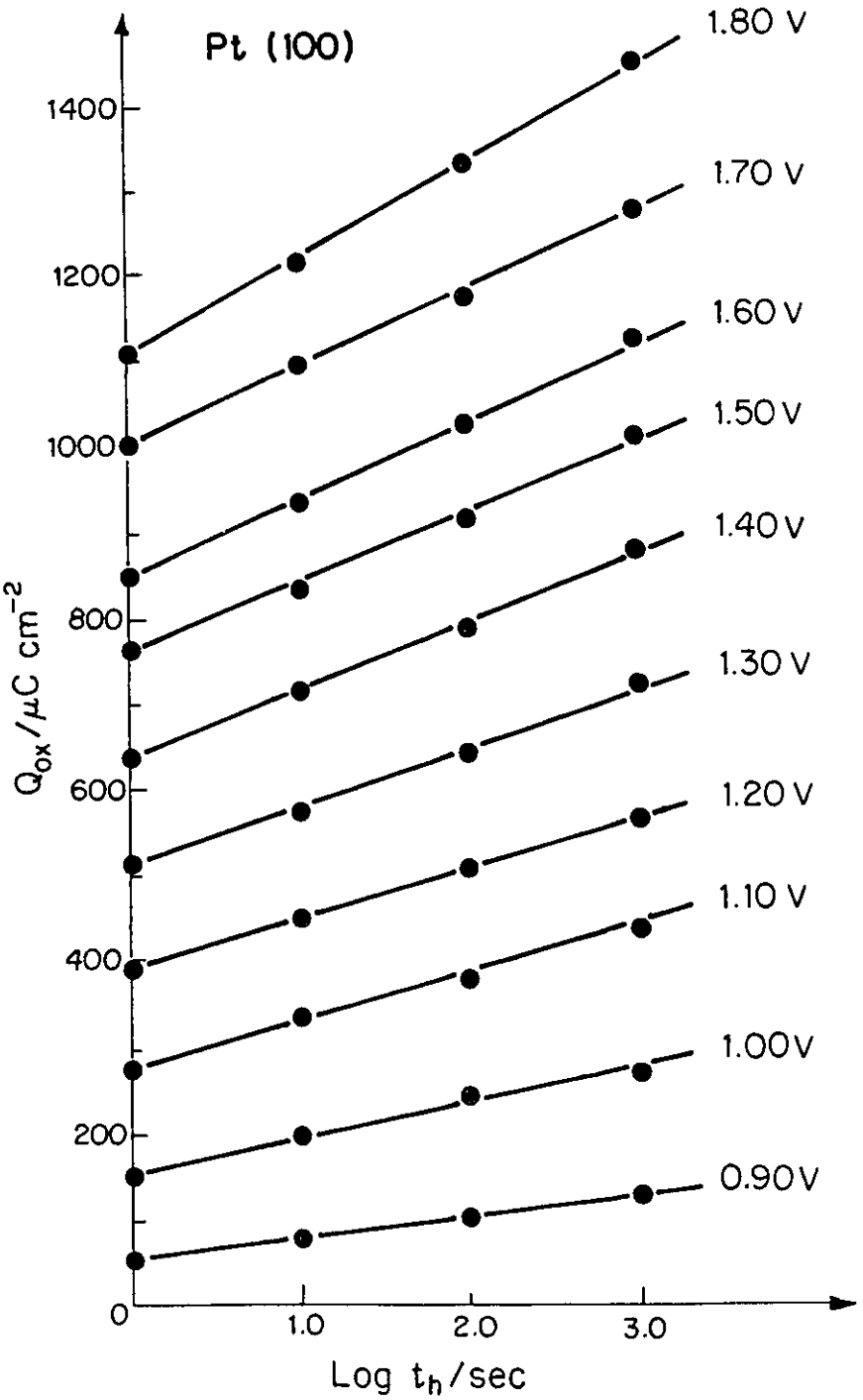

Fig. 3.54 Logarithmic oxide film growth plots, Q_{ox} vs log t_h, at Pt(100) for various polarization potentials (0.5 M aq. H_2SO_4, 298 K).

3.5.4 Discussion on the Oxide Growth at Pt(111), Pt(100) and Pt(poly) Electrode Surfaces

Comparison of the kinetics of oxide growth at various low-index single-crystal faces of Pt cannot be made in a direct quantitative way since different faces contain different numbers of Pt atoms per cm^2. For a qualitative and quantitative discussion, it is therefore essential to introduce a normalization factor for H accommodation for each of the principal low-index faces so that, after the normalization, the results for each face would refer to the same number of Pt atoms per actual cm^2, though in different coordination geometries. This requires definition of a "standard surface". [Acceptance of the polycrystalline Pt electrode surface as the standard surface is convenient at this point in the research so that quantitative comparison between different single-crystal and polycrystalline Pt surfaces is possible. However, upon further characterization of other single-crystal faces, the Pt(111) surface will be proposed as the standard and reference surface because it is the most stable one.] The polycrystalline Pt electrode, with its H UPD accommodation of 210 $\mu C\ cm^{-2}$, is accepted as the standard surface. The H UPD charge divided by the electron charge, e, gives the standard number of Pt atoms per cm^2 of polycrystalline electrode surface. Once having defined the standard surface, the normalization factor would be evaluated according to the following formula:

$$n_f = \frac{\text{number of atoms per 1 cm}^2\text{ of polycrystalline Pt surface}}{\text{number of atoms per 1 cm}^2\text{ of single-crystal Pt surface}} \qquad (3.12)$$

The values of the normalization factors for the principal low-index single-crystal faces are then as follows:

$$n_f(111) = 0.9154$$

$$n_f(110) = 1.4950$$

$$n_f(100) = 1.0571$$

$n_f(poly) = 1.0000$

The normalized values of such experimentally determined quantities as oxide reduction charges or H UPD accommodations are then derived by multiplying them by the appropriate normalization factor.

Oxide Growth in a Single Sweep to Potentials between 0.9 and 1.8 V, RHE

Fig. 3.55 shows the normalized oxide-reduction charges for oxide films grown by application of a single sweep up to 1.80 V, RHE, in 0.5 M aq. H_2SO_4 solution at 298 K. The data shown in this figure clearly indicate that the oxide growth rate at Pt(100) is appreciably faster than at Pt(111). This behaviour could be expected, knowing that the oxide growth proceeds through the place exchange mechanism. In the case of the (111) surface, each Pt atom is surrounded by 9 atoms (6 lying in the same plane and 3 in the plane underneath) while, for (100), only by 8 atoms (4 lying in the same plane and 4 underneath). The situation is more complex for reconstructed surfaces where there might be two or more kinds of surface atoms, each having its own characteristic surface coordination number. The assumption that all low-index surfaces have the ideal (1×1) structure, though a simplification, is satisfactory enough at this stage of the discussion. In the case of the (111) surface, the rate of place-exchange of Pt atoms with the O-containing species would tend to be slower than that for the (100) surface (see Fig. 3.56 for the schematic representation of the place-exchange process). The oxide-reduction charge for Pt(poly) falls close to that for Pt(111) indicating that the polycrystalline Pt surface contains a substantial fraction of crystallites having exposures of (111) or restructured (111) faces.

Oxide Growth at Various Polarization Potentials and Polarization Times

As for the oxide films formed by application of a single-sweep, the logarithmic

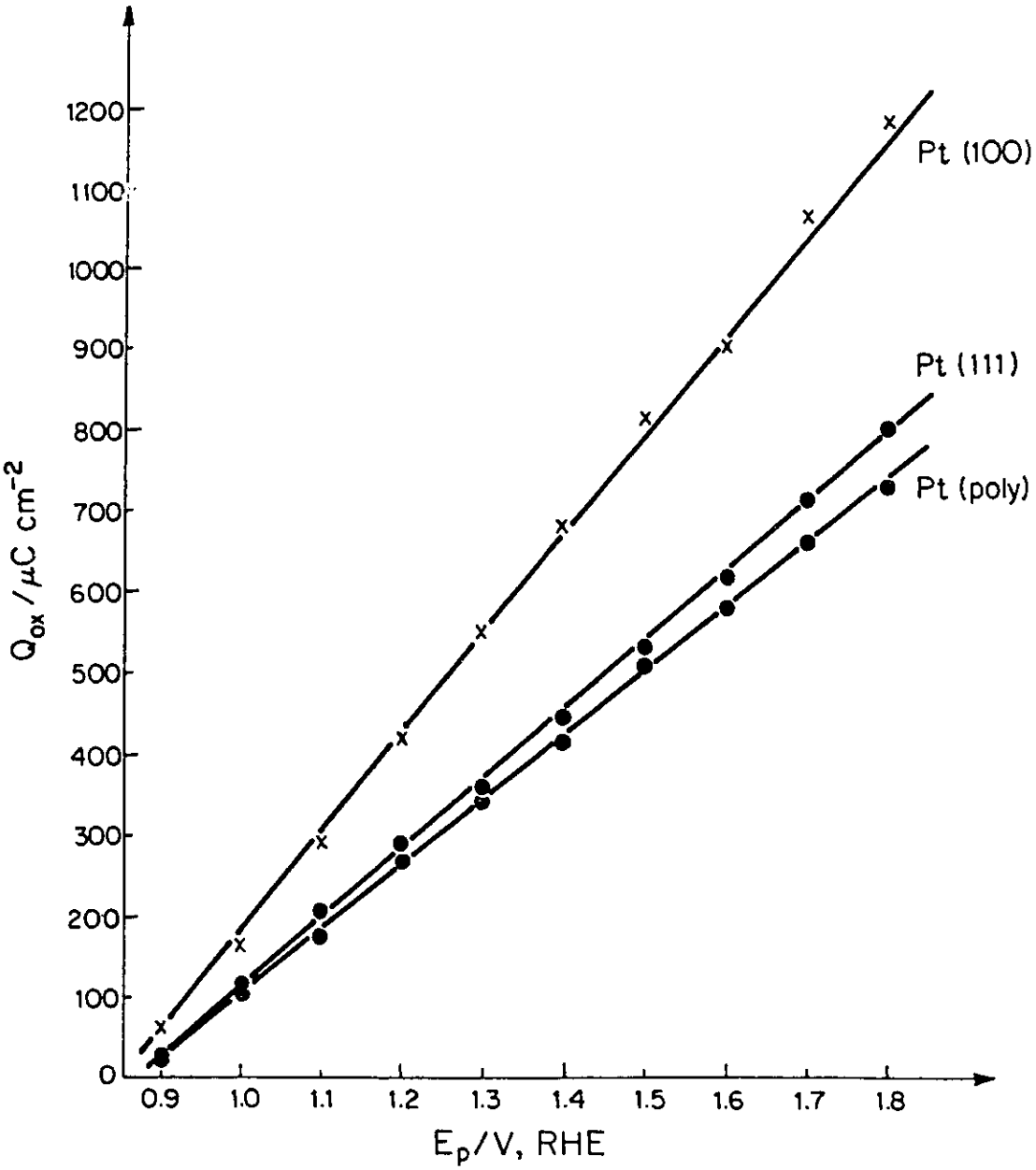

Fig. 3.55 Normalized oxide-reduction charges for Pt(111), Pt(100) and Pt(poly) electrodes upon a single sweep as a function of the upper potential limit (0.5 M aq. H_2SO_4, 298 K).

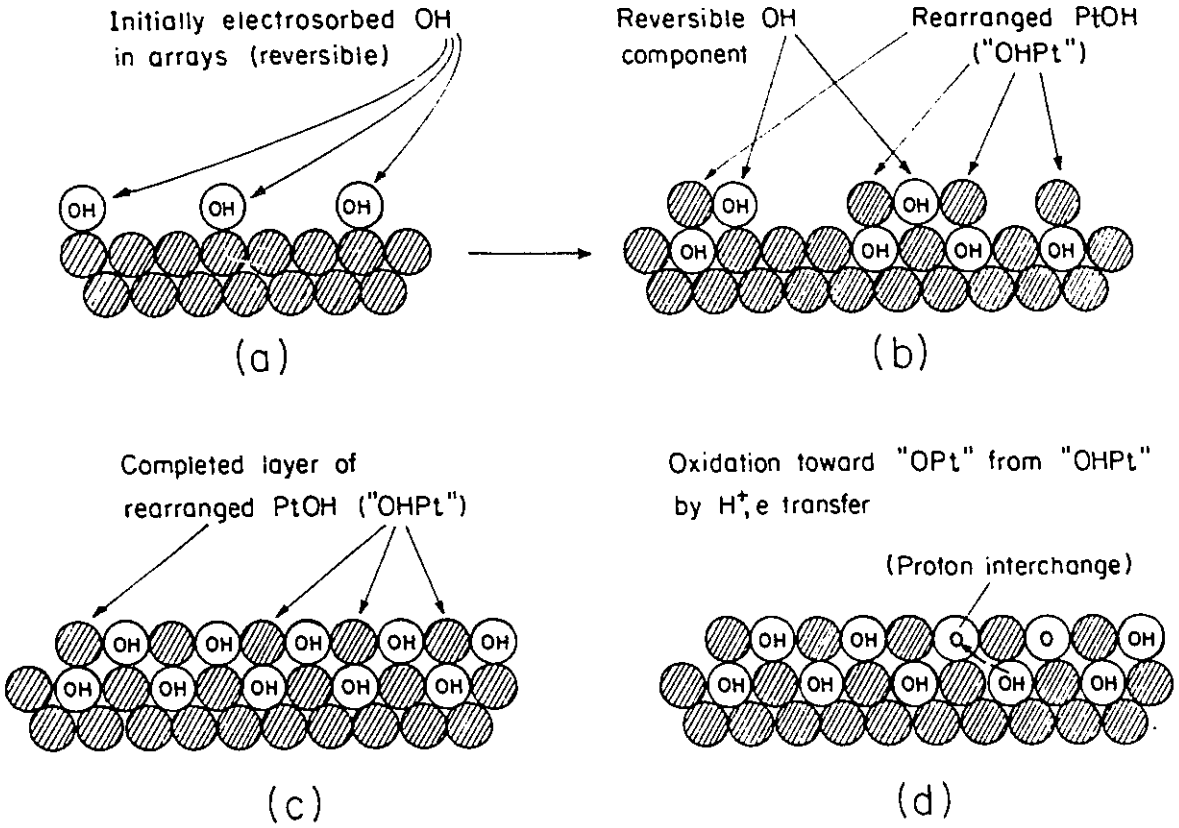

Fig. 3.56 Model for transition between oxide film formation initially in a sub-monolayer and in subsequent place-exchanged domains, prior to complete occupancy of the free-metal surface by electrodeposited OH and later O species [15].

growth rates for Pt(111) and Pt(100) were normalized, as shown in Figs. 3.57 and 3.58. Fig. 3.59 shows the logarithmic oxide growth rates for polycrystalline Pt. The slopes of the normalized Q_{ox} vs log t_h plots as a function of the polarization (holding) potential, E_h, are shown in Fig. 3.60 and are different from those prior to the normalization operation, as expected. The data presented in Figs. 3.57 - 3.59 confirm the observation referred to earlier in this work that the oxide formation proceeds substantially faster at Pt(100) than at Pt(111).

The Q_{ox} vs log t_h plots (see Figs. 3.51, 3.54 and 3.60) for Pt(111), Pt(100) and Pt(poly) were each extrapolated to the zero of charge but did not give a "common intercept" (i.e. when the oxide reduction charges are extrapolated to the zero value, the linear Q_{ox} vs log t_h plots do not tend to the same value of log $t \approx -12$) as had been reported by Gilroy [8] in his work on polycrystalline Pt for various polarization potentials. On the contrary, the intercepts, designated log t_o, were potential-dependent and their values are shown in Fig. 3.61. For the potential range from 0.9 to 1.8 V, RHE, the values of log t_o vary from ca. -1 to -10 but on a fairly common line (Fig. 3.61) for each of the three surfaces. It is informative to attempt to give to "log t_o" some physico-chemical meaning. Roscoe and Conway [185] suggested that t_o represents the small but finite time required for the potential to become adjusted across the electrode/solution interphase. The observation that the Q_{ox} vs log t_h plots do not have the same common intercept is of importance for proper understanding of the oxide growth mechanism. The "nucleation-and-growth" mechanism of Gilroy [8] was based on the observation that the intercept of the Q_{ox} vs log t_h plots was common so that the

$$Q_{ox} = B \log (t/t_o) \tag{3.13}$$

formula was the basis of the first step in his derivation of a kinetic equation for the oxide formation rate. The validity of the approach of Gilroy was questioned by Conway et al.

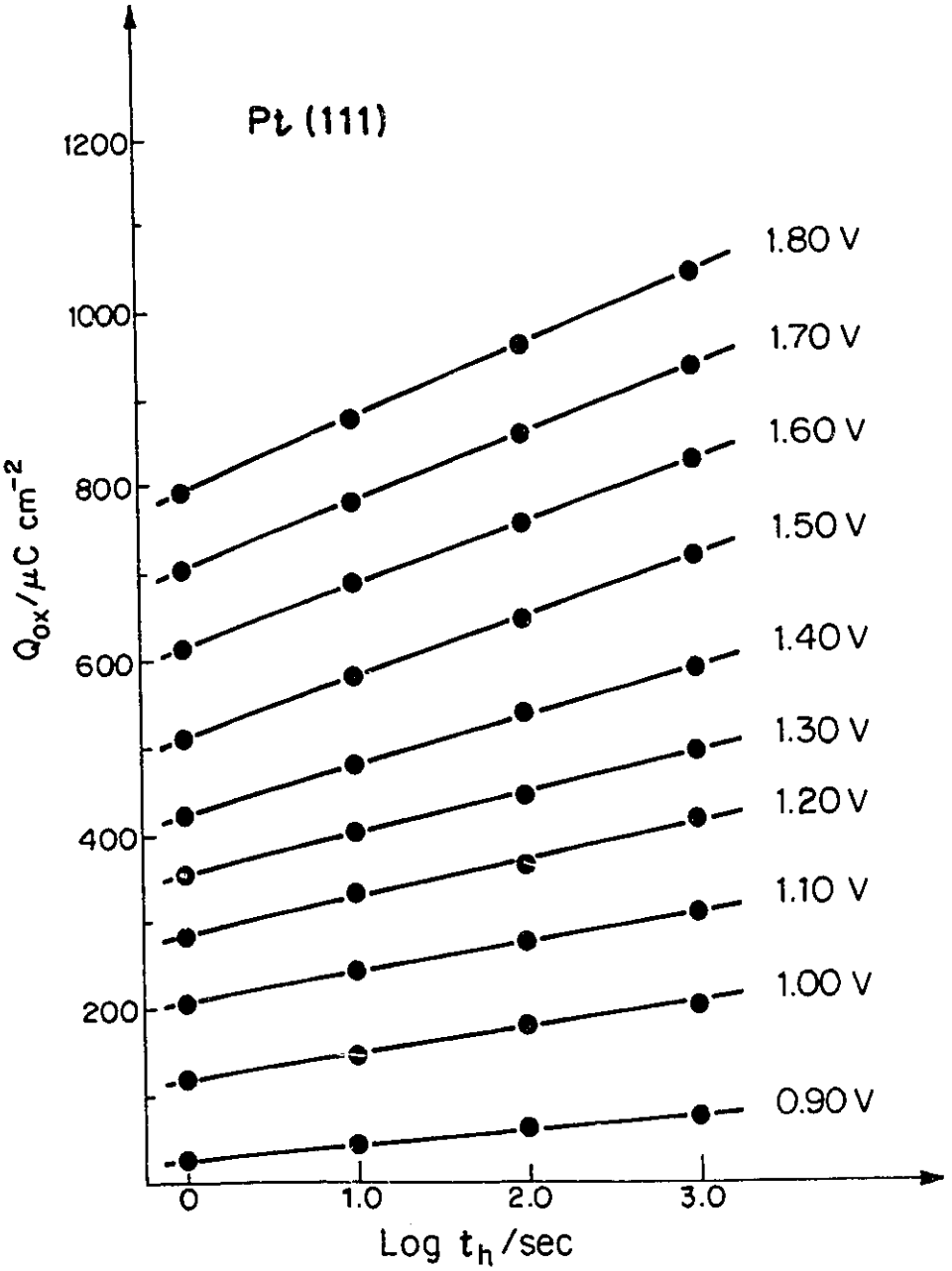

Fig. 3.57 Normalized logarithmic oxide film growth plots, Q_{ox} vs log t_h, at Pt(111) for various polarization potentials (0.5 M aq. H_2SO_4, 298 K).

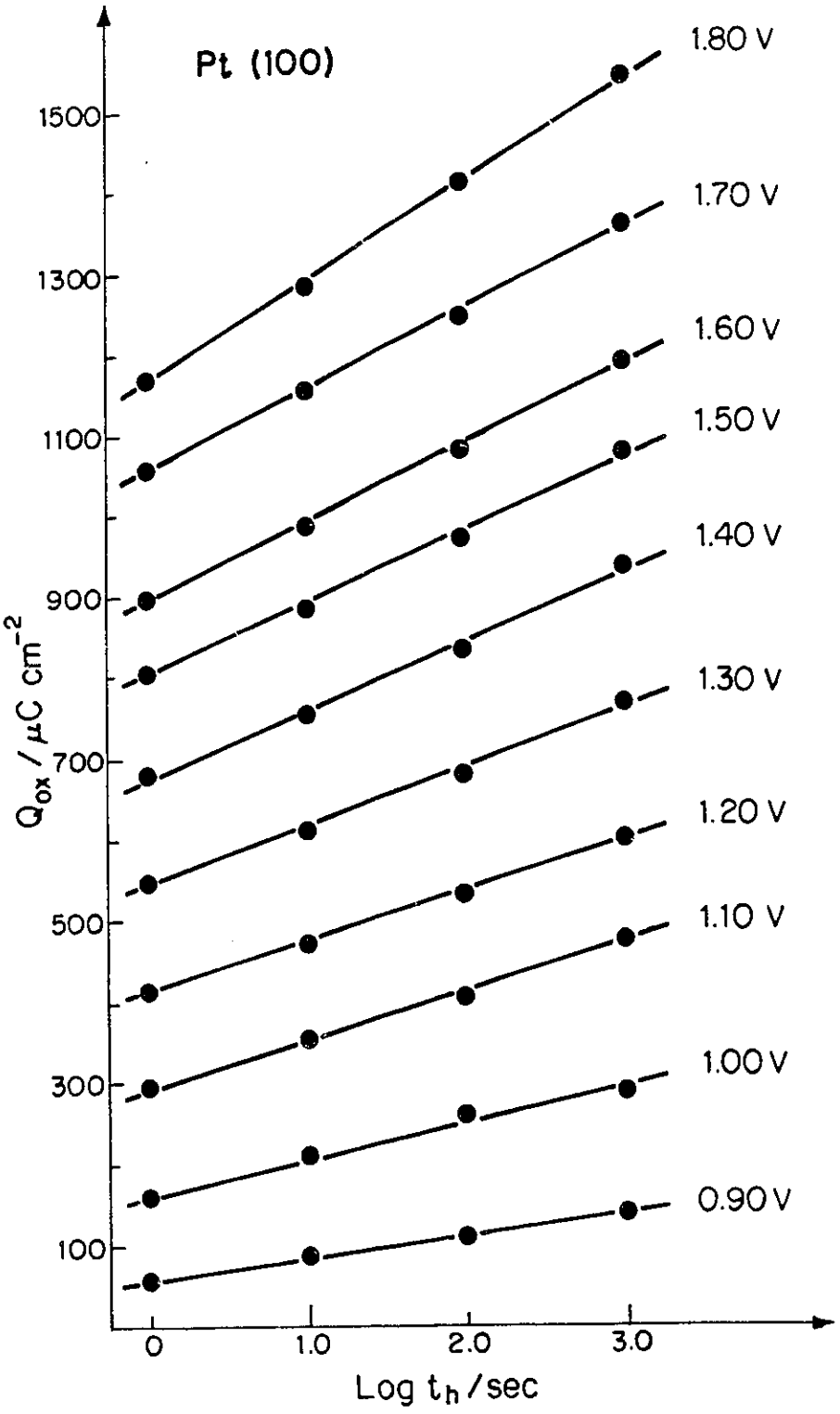

Fig. 3.58 Normalized logarithmic oxide film growth plots, Q_{ox} vs log t_h, at Pt(100) for various polarization potentials (0.5 M aq. H_2SO_4, 298 K).

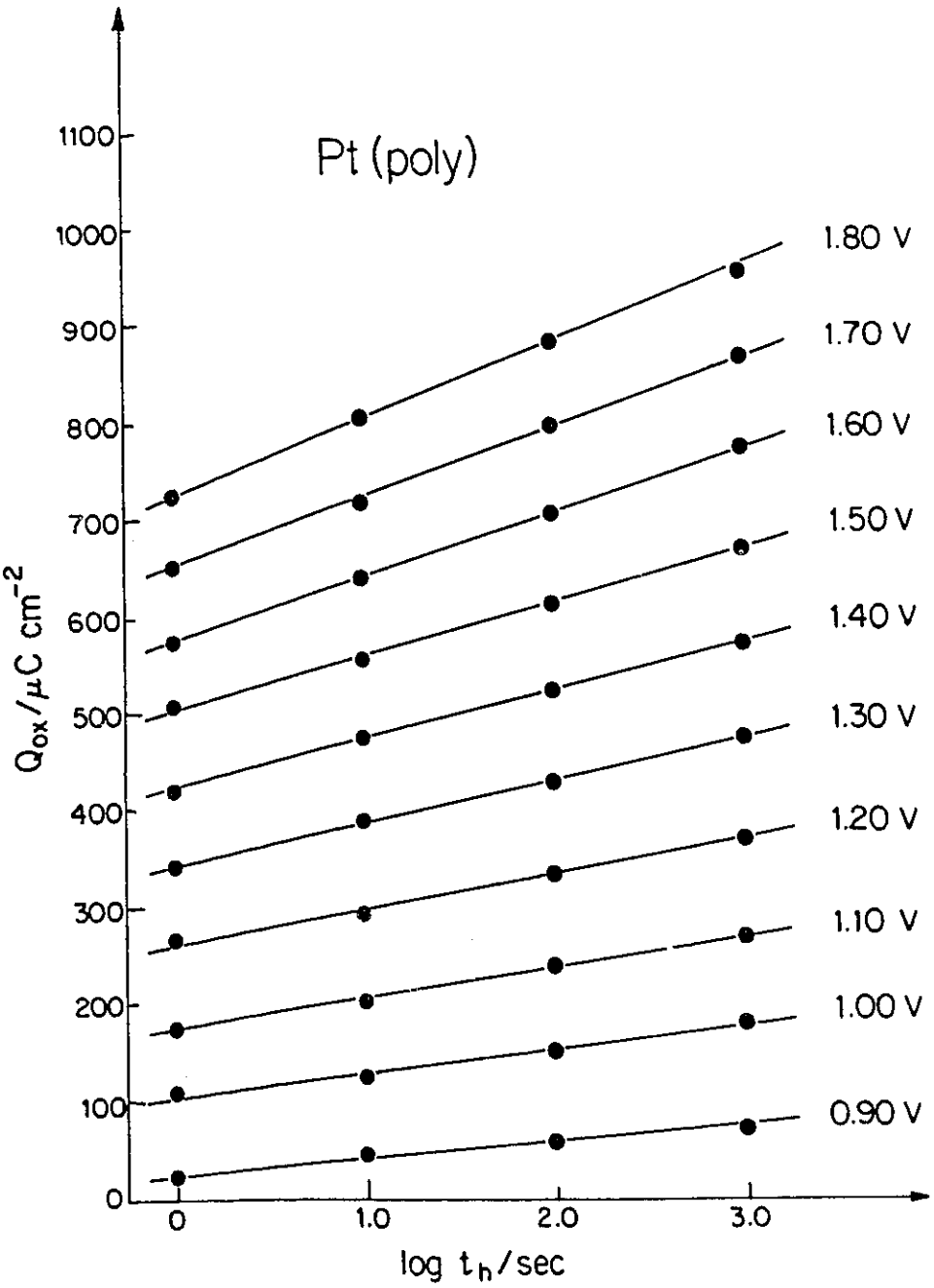

Fig. 3.59 Logarithmic oxide film growth plots, Q_{ox} vs log t_h, at Pt(poly) for various polarization potentials (0.5 M aq. H_2SO_4, 298 K). (Pt(poly) is taken as the "reference" case for the normalization operation in Figs. 3.57 and 3.58; see two previous pages).

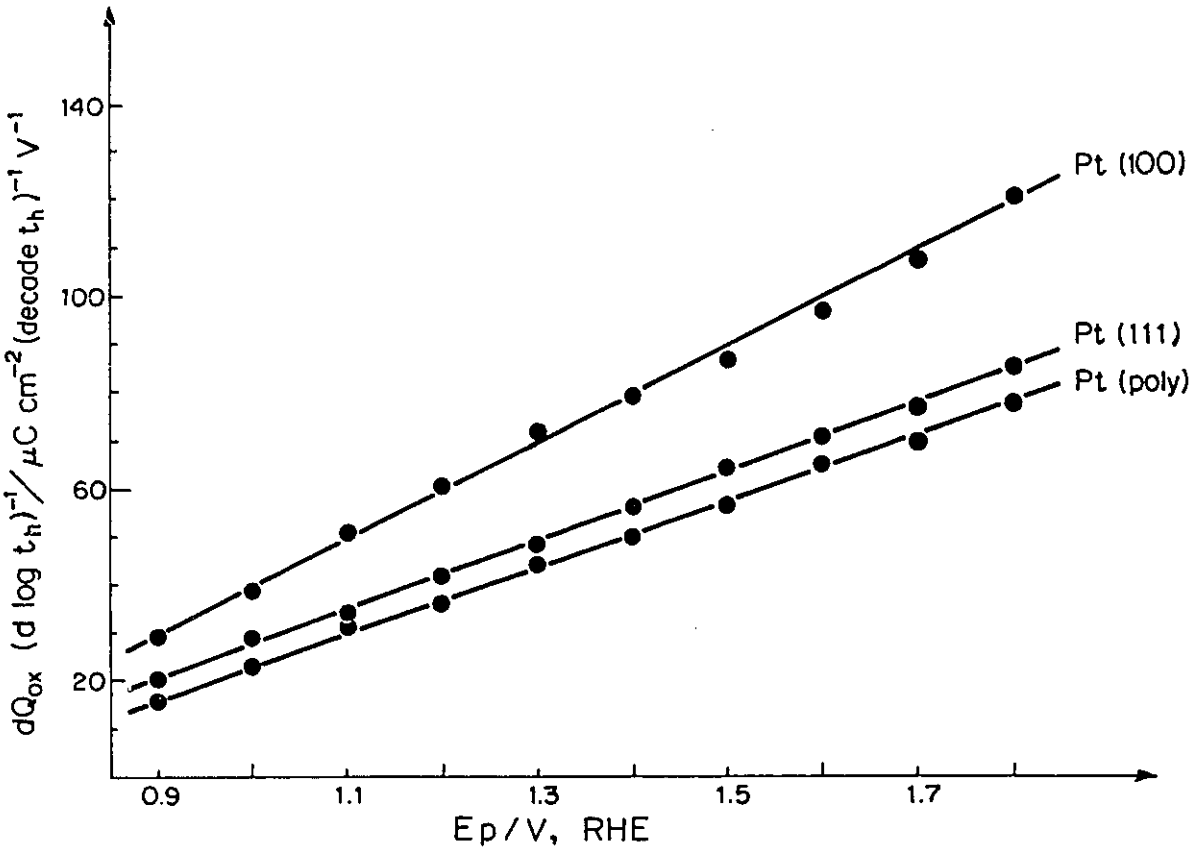

Fig. 3.60 Normalized slopes of the plots of Q_{ox} vs log t_h as a function of the polarization (holding) potential, E_h, for the Pt(111) and Pt(100) surfaces. (The slopes for Pt(poly) are not changes upon normalization, as this is the "reference" surface).

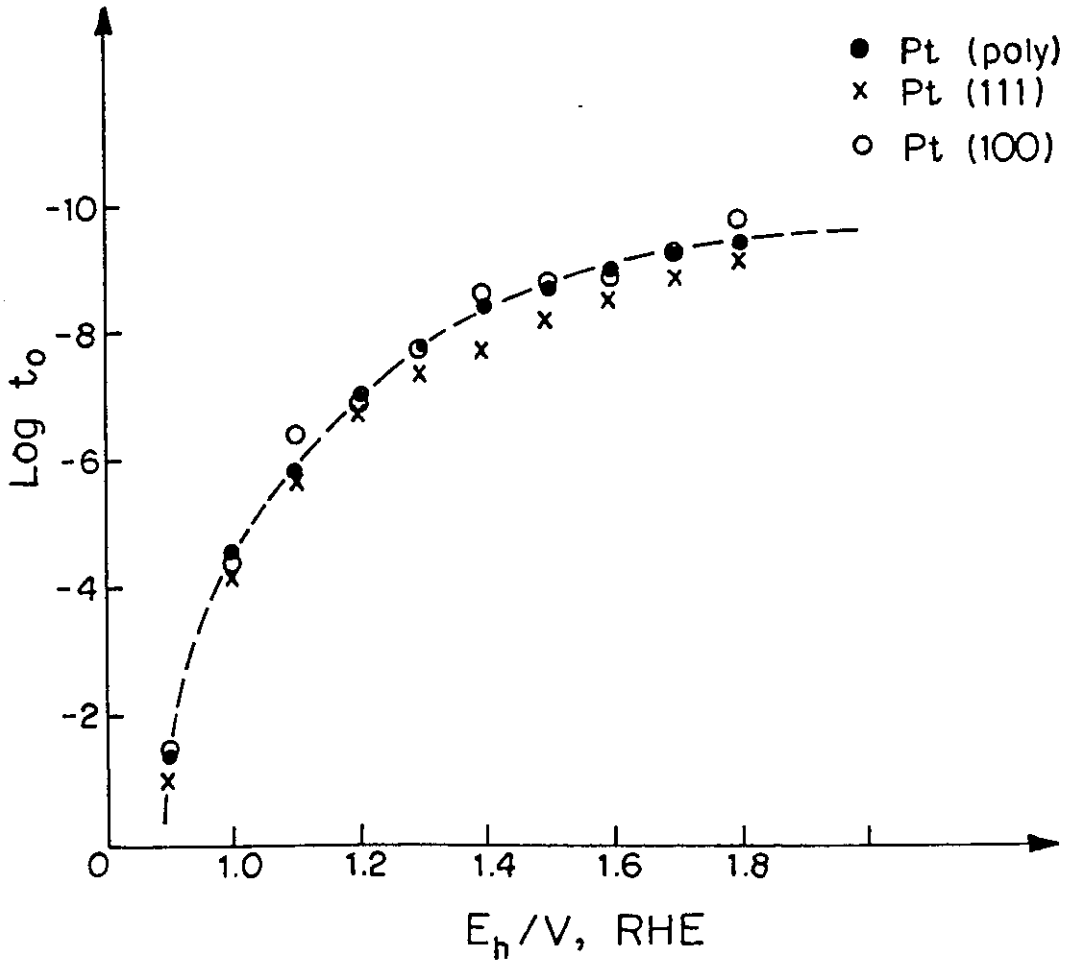

Fig. 3.61 The log t_o vs E_h relations for Pt(111), Pt(100) and Pt(poly) electrodes in 0.5 M aq. H_2SO_4 at 298 K.

[15] who suggested that the experimentally observed features of initial formation of the quasi-2-d oxide film reveal rather an "underpotential-deposition" kind of behaviour than a "nucleation-and-growth" one.

The results for oxide growth at Pt(111), Pt(100) and Pt(poly) electrodes can be summarized as follows:

1. For a given polarization potential and polarization time, the oxide growth rate at Pt(100) is greater than at Pt(111) or Pt(poly);

2. The oxide growth rate at Pt(poly) is only slightly lower than at Pt(111) which indicates that the polycrystalline Pt surface must predominantly consist of crystallites having the (111) orientation;

3. Q_{ox} vs log t_h plots for Pt(111), Pt(100) and Pt(poly) are linear which means that the oxide growth proceeds according to the direct logarithmic law;

4. Q_{ox} vs log t_h plots are significantly potential-dependent; this observation is in agreement with the observation of Gilroy [8] but contrary to some earlier results acquired in this laboratory [15,185] (this could be due to different oxidizability of Pt electrodes which at that time were not "electrochemically annealed");

5. The Q_{ox} vs log t_h plots pass through the nominal monolayer coverage limits for OH or O without any inflection indicating that the growth process is not directly coverage-dependent;

6. Q_{ox} vs log t_h plots do not have a common intercept [8]; this observation impairs the "nucleation-and-growth" mechanism of Gilroy for the oxide growth in its initial stages.

The fact that oxide film growth rates clearly depend (Figs. 3.55, 3.60) on the orientation of the Pt surface at which they grow calls for further comment. It is unlikely that the growing 3-d oxide film can maintain any epitaxial relation to the structure of the underlying metal surface from which it develops since the structure and molar volume of "PtO" or "PtO_2" states must be very different from that of crystalline Pt. Therefore, the specificity of oxide growth kinetics to the surface from which the film develops must

originate, it is suggested, from the different rates at which contunuing place-exchange occurs at the inner interface of the oxide film with the metal. This would be expected to be dependent on the geometry and coordination of that particular oriented surface. Alternatively, the rate of Pt ion injection into the growing film (under "Mott-Cabrera" mechanism conditions) would also probably be dependent on the orientation and coordination of the metal surface from which such Pt ions originate.

Finally, these results on the specificity of oxide film growth of single crystal surfaces imply that the same orientation of the given underlying surface is maintained during progressive extension of the oxide film to appreciable thicknesses.

CHAPTER 4

Summary and Conclusions

In this final Section,it is convenient to present a variety of detailed conclusions, in summary form, under several headings as follows:

4.1 Characterization of Polycrystalline Pt Electrodes

1. The experiments described led to a precise and reproducible characterization of polycrystalline Pt electrodes, revealing the same surface-oxidizability behaviour over a long period of time (in some cases up to 6 months of work on extensive oxide formation followed by reduction and cycling between 0.05 and 1.40 V, RHE).

2. Experiments in the present work have shown that heating and quenching of polycrystalline electrodes leads to surfaces, the real surface areas of which are ca. 20% smaller than those of "electrochemically annealed" or annealed polycrystalline Pt electrodes of the same apparent area.

3. The H UPD C-V profiles of "quenched" polycrystalline Pt electrodes taken between 0.05 and 0.80 V, RHE, differ significantly from corresponding profiles of "well-cycled" polycrystalline Pt electrodes, i.e. the HA3 peak was absent while the HA2 and HC2 were sharp and of the same heights as HA1 and HC1.
   The H UPD C-V profiles of "quenched" Pt electrodes undergo irreversible changes

upon cycling into the oxide region; the sharpness of the HA2 and HC2 disappears after a single sweep to 1.40 V, RHE, while the HA3 appears and increases with cycling.

4. The distribution of the H UPD accommodation after quenching the Pt electrodes not only changes quantitatively but also qualitatively. However, upon prolonged cycling between 0.05 and 1.40 V,RHE, it reaches a constant characteristic form for almost all the Pt electrodes studied.

5. The roughness of well-cycled ("electrochemically annealed") Pt electrodes, which serve as a standard surface, is almost always 1.59 (±0.03). Polycrystalline Pt electrodes, when subjected to different thermal and/or electrochemical pretreatments, tend to the same, final state having the same roughness factor and almost the same values of the i_{HA1}/i_{HC1} and i_{HA2}/i_{HC2} ratios.

6. The real surface area of the Pt electrodes may increase some 300% or more as a result of strong anodic polarization, leading to 50 equivalent monolayers of "O" or more. Such a surface has a different distribution of UPD H between the principal states, and the first positive-going sweep, following the thick oxide reduction, shows that the HA1 peak is often smaller than the HA2. The experimental behaviour shows that the surface having increased area can be qualitatively and quantitatively returned to its initial state (prior to oxide formation) by prolonged cycling between 0.05 and 1.40 V, RHE.

7. Restructuring of the electrode surfaces having increased area, to the final and stable state, proceeds through an "electrochemical annealing" mechanism. This is a phenomenon in which restructuring of an high-energy surface (the enhanced-area

one) to a low-energy surface takes place via formation and reduction of the quasi-2-d oxide, or an high-stress surface (a cold-worked one) to a low-stress one through the same mechanism.

8. It is proposed that the roughness of a Pt electrode should be described by two factors: R_l, the macro-roughness factor, and R_m, the micro-roughness factor. The macro-roughness factor accounts for such surface imperfections as scratches, cracks, pores, etc. while the micro-roughness factor describes the atomic-level imperfections such as steps, terraces, kinks, etc. existing at the micro-level, i.e. in the surface of grains.

9. The overall roughness factor, R_t, of a given Pt electrode is the product of R_l and R_m. For a freshly heated and quenched electrode, $R_m < 1$ but upon cycling $R_m \rightarrow 1$. For an electrode at which a thick-oxide film has been grown and reduced, $R_m > 1$ but upon further cycling $R_m \rightarrow 1$.

4.2 Growth of Thick-oxide Films at Polycrystalline Pt Electrodes

10. Potentiostatic polarization of polycrystalline Pt electrodes at E_h = 1.8, 1.9, ..., 2.3 V, RHE, for up to 48 h leads to formation of up to five states of the oxide film which are distinguishable, in reduction, in linear-sweep voltammetry (cyclic-voltammetry) experiments.

11. The extent of formation of the oxide film at Pt does not attain any limit, contrary to some indications in earlier literature that such a limit is attained when ca. 2.6 O atoms per Pt atom are deposited. Up to 50 equivalent monolayers of "O" can, in

fact, be formed on a smooth polycrystalline Pt electrode given sufficient time and a high enough potential for the anodization. Mechanical disturbance of the electrode surface, by subjecting it to rubbing by emery paper, is not essential for the thick-oxide film to be formed. On the contrary, such a drastic pretreatment contributes to irreproducibility of experimental results.

12. The OC1 state reaches a limit of ca. 880 $\mu C\ cm^{-2}$ which corresponds to two monolayers of "PtO". This limit is maintained even when the Pt electrode is polarized up to 4.0 V, RHE, by a single sweep at room and elevated temperatures.

13. The sequence of formation of distinguishable states of the oxide depends on the time and potential of anodization, and the extents of growth at various potentials are logarithmic in time; the logarithmic growth rates, $dQ/d \log t_h$, linearly increase with anodization potential.

14. The distinguishable states, OC1, OC2, OC3 and OC4, do not represent simply oxide species in which Pt is in different oxidation states, since the species produced under the strongest oxidation conditions are reduced at the least positive potentials. The observed behaviour is interpreted in terms of stability of the oxide phases and their different energetic states but some kinetic effects do arise.

15. At Pt surfaces at which the thick quasi-3-d oxide film states have been formed, the 2-d oxide film can be independently reduced and re-formed on the already oxidized surface with all the characteristics of 2-d film formation on an initially bare Pt metal surface. This implies that the processes of 2-d film formation and reduction at Pt can take place independently of the presence of a thick oxide film on the Pt surface, and that the 2-d film exists and can be re-formed on the Pt metal surface, beneath the

thick oxide film that is therefore porous and permeable to water and protons.

16. After films having an equivalent reduction charge of ca. 1800 $\mu C\ cm^{-2}$ have been formed, the oxide growth rate increases some 400-fold, probably due to onset of a new process (Mott-Cabrera mechanism) of film growth involving Pt ion injection into the oxide film initially formed by a place-exchange mechanism. The major change of growth rate is probably associated with increase of specific resistivity of the oxide film.

17. It is suggested that the formation of the first equivalent monolayer of the "PtO_2" state (880 $\mu C\ cm^{-2}$) on top of 2 monolayers of "PtO" (a further 880 $\mu C\ cm^{-2}$) is a slow process but once the "PtO_2" layer has been formed, the oxide growth rate drastically increases.

18. The bulk-type oxide can be formed in a single sweep but only beyond ca. 3.0 V, RHE, at temperatures of, but not less than, 333 and 348 K. However, such conditions lead to the formation of the OC1, BS and OC3 states only.

19. Although formation of increasing quantities of surface oxide is a logarithmically slow process, extending over many minutes or hours, the oxide film thus developed can be reduced in a single sweep over a time of ca. 33 s or less.

20. ESCA examination indicates a +IV oxidation state of Pt in the OC2, OC3 + OC4 oxide states and +II in th OC1 state.

21. EDX mapping analyses indicate differential extents of oxide film growth on distinguishable crystal grains at the surface of smooth polycrystalline Pt.

22. Rates of anodic O_2 evolution (at a given potential) depend on the state of the oxide on which the O_2 evolution occurs, i.e. electrocatalysis in that process depends on the state of the anodically generated film, determined by the time of anodic film growth and the potential at which it was conducted.

23. Thick oxide films formed at Pt are stable (in the absence of H_2 and other reducing agents) and their states remain unchanged for lengthy periods under open-circuit conditions. This is of practical importance for experiments on electrode-kinetics of other reactions, e.g. Cl_2 evolution and the Kolbe reaction, cond cted on pre-formed Pt oxide films. Thick-oxide films at Pt are also stable under ultra-high vacuum conditions but probably undergo dehydration.

24. The kinetics of the OER at pre-oxidized Pt electrodes were investigated by steady-state Tafel polarization measurements, these being conducted at different stages of development of the oxide film,i.e. either prior to or after formation of the OC2, OC3 and/or OC4 states.

25. The Tafel plots for the OER, thus determined, reveal two linear regions with a transition (at a potential, E_{tr}) between 1.90 and 1.95 V, RHE. The value of the Tafel slope b_1 (between 1,70 and E_{tr}) varies between 105 and 116 mV, and of the b_2 (between E_{tr} and the upper potential limit) from 64 to 74 mV, depending on the pre-oxidation conditions.

26. The Tafel slopes for the OER at pre-oxidized Pt electrodes confirm that there are two parallel processes in the reaction, i.e. the OER proceeds through the pathway having a lower Tafel slope at higher overpotentials.

27. The Tafel plots for zero and short polarization times exhibit curvature between 1.70 and 1.80 V, RHE. This corresponds to further development of the OC1 state until the other ones (OC2, OC3 and/or OC4) are formed. This anomalous behaviour is referred to as a passivation effect.

28. In the case of long polarization times, the whole Tafel plots are shifted towards higher current densities as a result of formation of a thick-oxide film, the real surface area of which is greater than that of the initially oxide-free Pt electrode. This behaviour is more pronounced the greater is the polarization time and the higher is the polarization potential. These effects of changing real area were not recognized in previous works.

29. In earlier work from this laboratory, it was suggested that the change of the Tafel slope could be due to intervention of a redox mediation step involving higher oxidation states of Pt ions in the surface layer of the oxide film. Evidence presented in this thesis proves that Pt can exist in the +IV oxidation state in the oxide film and that the "PtO_2" is in direct contact with the solution by residing on top of "PtO"; this supports the role of intervention of a redox mediation step in the overall mechanism of anodic O_2 evolution which takes place on the exterior surface of the outer film.

4.3 Characterization and UPD of H at the Pt(111) Electrode Surface

30. Heating Pt(111) electrodes to various temperatures (500, 800 and 1000°C), followed by quenching, leads to H UPD C-V profiles which are clearly distinguishable from one another.

31. Annealed, and annealed and "electrochemically cleaned" Pt(111) electrodes give C-V profiles similar to that of Hubbard et al. [137].

32. Oxide film extension at a heated and quenched Pt(111) electrode arises only at a positive potential substantially higher than that required for surface oxide formation at polycrystalline Pt. Thus, only a small quantity is formed at potentials higher than 0.85 V, RHE, relative to that observable at polycrystalline Pt over the same range of potential. The extent of oxide formation on "quenched" Pt(111) is less than half an equivalent "O" monolayer upon the first sweep to 1.40 V, RHE.

33. Prolonged cycling of a heated and quenched Pt(111) surface up to 1.10 V, RHE, drastically changes the H UPD profile, presumably as a result of changes of surface structure brought about by sub-monolayer oxide film formation, with restructuring; the total H UPD charge remains, however, unaffected and near the calculated value of 240 $\mu C\ cm^{-2}$ for a (111) surface.

34. Cycling of a heated and quenched Pt(111) electrode up to 1.40 V, RHE, changes the H UPD profile which, after a few or several cycles, becomes close to that for thermally annealed and electrochemically precleaned Pt(111); further cycling does not cause any additional significant changes in the H UPD C-V profile; the H UPD charge remains, in fact, unaffected and close to 240 $\mu C\ cm^{-2}$.

35. The surface structural changes of the heated and quenched Pt(111), resulting from cycling up to 1.20 V, RHE or beyond, are irreversible.

36. Heating and especially quenching of a Pt(111) electrode, it is proposed, introduces small displacements of surface atoms corresponding to development of a metastable

surface structure; prolonged cycling into the surface oxide formation potential region releases stress and enables displaced atoms to become relaxed to stable states through an "electrochemical annealing" mechanism which leads to a restructured surface structure.

37. The displacements mentioned above might be of the order of 0.1-0.2 Å, i.e. close to the limit of LEED sensitivity (resolution). In such a case, the possible metastable surfaces with their displacements could be detected only by a more sensitive technique such as RHEED with use of grazing angles of incident and emergent beams.

38. Experiments conducted for two different quenching geometries, i.e. "lateral" and "perpendicular" to the (111) surface, demonstrate that the supposed displacements of Pt atoms are directional. Interestingly, the H UPD accommodation is still close to 240 $\mu C\ cm^{-2}$ while the H UPD C-V profiles show some qualitative differences. This experiment could provide more unambiguous information if the crystal were bigger or of a different shape such as a disc.

39. The H UPD C-V profile for "quenched" Pt(111) is surprisingly complex though the "ideal" (111)-(1×1) surface is the most stable one out of the three low-index surfaces. The complexity of the "double-butterfly" profile cannot be easily explained even if an "anion adsorption effect" is taken into account.

40. It has been suggested that the "double-butterfly" profile is due to specific HSO_4^- ion adsorption on the "quenched" Pt(111) surface which contains small displacements. The HSO_4^- ions may arrange themselves on this surface in such a way that their overall adsorption is 20% greater than on polycrystalline Pt. In other words, the

"double-butterfly" profile is characteristic of a "quenched" or "fast-cooled" Pt(111) surface in contact with aq. H_2SO_4 solution only, and is sensitive to interactions between the surface-structures or the (111) and HSO_4^- or SO_4^{2-} ions. These interactions are found to depend strongly on pH of the solution.

41. The "quenched" Pt(111) surface does not seem to be the "ideal" (111)-(1×1) one since, after five cycles up to 1.40 V, RHE (which leads to a restructured surface consisting of (111) terraces 11-12 atomic rows long and one atom in height), the "double-butterfly" disappears from the C-V profile.

42. The second "butterfly" is unlikely to be due to subsurface H atoms since, after the 5-10 cycles up to 1.40 V, RHE, some 90% of the surface still has (111) orientation (on the 12-atom row terraces) while the profile is completely different and does not reveal the second "butterfly".

43. The idea that some of the UPD H is sorbed in subsurface states, though supported by some early calculations of Ishikawa and Hubbard, does not take into consideration that: (a) the adsorbed and sorbed H bear different electric charges (electronic states); (b) surface metal atoms have hybrid d-orbitals protruding from the surface; and (c) surface and bulk metal atoms have different orbital occupation numbers. In the light of such information, the potential energy profiles of Ishikawa and Hubbard for adsorbed and subsurface H carry less significance. Apart from this, there is no explanation why only ca. 33% of the H monolayer should exist as subsurface H.

4.4 Characterization and UPD of H at the Pt(100) Electrode Surface

44. Annealing, or heating and quenching Pt(100) electrodes leads to H UPD C-V profiles which are clearly distinguishable from one another.

45. The H UPD C-V profiles for annealed Pt(100) are qualitatively consistent with that of Hubbard et al. but their H UPD accommodation is some 33% greater than that calculated for the (100)-(1×1) geometry. This could arise on account of reconstruction of the "ideal" (100)-(1×1) structure, which is unstable when clean, to the (100)-(2×1) "missing row" structure the Q_{HUPD} of which is 278 $\mu C\ cm^{-2}$, i.e. close to the experimentally determined value.

46. The H UPD accommodation for Pt(100), heated at 800°C and quenched, is close to the value calculated for the (100)-(1×1) structure. This is likely because quenching, which results in a thermally formed oxide film, presents a surface structure which is close to the "ideal" one, though possibly with small displacements.

47. At both the annealed Pt(100) and that heated at 500°C and quenched, the H UPD charges are the same but the C-V profiles are different. This observation suggests that these two surfaces must differ on account of some small surface displacements but not major restructuring; however, the anion adsorption on these surfaces is different, leading to complexity of the H UPD C-V profiles.

48. Cycling of heated and quenched Pt(100) into the oxide region changes the H UPD profile, presumably as a result of surface structural changes brought about by oxide film formation and reduction. After a few or several cycles up to 1.40 V, RHE, the H UPD C-V profile becomes close to that for thermally annealed Pt(100). These

surface structural changes are irreversible, as expected.

49. Surface structural changes of the "quenched" Pt(100), resulting from cycling into the oxide region, become more pronounced when an upper limit of 1.20 V, RHE, has been exceeded.

50. Both the (100) and (110) surfaces are unstable when clean and become easily reconstructed to stable (n×1) structures (n=2,3,4,5). This suggests that different thermal pretreatments may lead to various surface structures having different accommodations for chemisorbed H.

4.5 Oxide Growth at Single-Crystal Pt Electrodes

51. Formation of quasi-2-d oxide does not occur on "quenched" Pt(111) below 1.10 V, RHE, and between that limit and 1.40 V, RHE, less than half a monolayer is formed. On the contrary, oxide formation on annealed Pt(111) commences at ca. 0.85 V, RHE, like that at polycrystalline Pt.

52. Formation of the quasi-2-d oxide, both on "quenched" and annealed Pt(100), commences around 0.80 V, RHE, and does not depend on the thermal pretreatment.

53. The Pt(111) and Pt(100) electrodes, after cycling up to 1.40 V, RHE or beyond, reveal and sustain the H UPD profiles characteristic of annealed surfaces.

54. Oxidation of Pt(111) by application of a single sweep up to 1.80 V, RHE, results in formation of the OC1 state only to the extent of ca. 1.79 equivalent "O" monolayers.

The oxide formation by the place-exchange mechanism is completely "reversible" from the electrochemical surface science point of view (i.e. Pt atoms return to their initial sites in the surface lattice after oxide reduction) and does not contribute to any significant surface structural changes.

55. Similarly, oxidation of Pt(100) by application of a single sweep up to 1.80 V, RHE, also results in formation of the OC1 state only, to the extent of ca. 2.67 equivalent "O" monolayers. The formation of this oxide film does not lead to any significant surface restructuring; this suggests that the so-called "missing row" structure of Pt(100) is stable under such anodization conditions.

56. The oxide growth measurements at Pt(111) at various polarization potentials between 0.90 and 1.80 V, RHE, and for polarization times up to 1000 s, show that: (a) Q_{ox} vs log t_h plots are linear, i.e. a direct logarithmic law of oxide growth applies; (b) the slopes of the dQ_{ox}/d log t_h plots depend linearly on potential, with a slope of 89 $\mu C\ cm^{-2}$ (decade $t_h)^{-1}\ V^{-1}$; (c) Q_{ox} vs log t_h plots pass through the monolayer level without inflection, indicating uniformity of the oxide growth mechanism below, through and above monolayer formation; and (d) no changes in the H UPD C-V profiles are observed upon oxide formation and reduction under the above-mentioned conditions.

57. In the case of oxidation of Pt(100), for various polarization potentials and times, the observations are exactly the same as (a), (b), (c) and (d) in Conclusion 56 with the only difference being that the dQ_{ox}/d log t_h vs E_h plot has a slope of 94 $\mu C\ cm^{-2}$ (decade $t_h)^{-1}V^{-1}$.

58. Quantitative comparison of oxide growth rates at various low-index single-crystal

faces of Pt and polycrystalline Pt is possible only by introduction of a normalization factor so that, after normalization, the results for each low-index single-crystal or polycrystalline Pt surface would refer to the same number of Pt atoms per real cm^2 but having different coordination geometries, of course.

59. Normalization of the data for oxide growth rates at Pt(111), Pt(100) and Pt(poly) indicates that the oxide formation at Pt(100) is appreciably faster than at Pt(111) or Pt(poly). This behaviour can be rationalized in tems of the oxide film growth which proceeds through the place-exchange mechanism. In the case of Pt(111), the "turn-over" process is much slower than in the case of Pt(100), since its surface Pt atoms are coordinated by another 9 Pt atoms, while in the case of Pt(100) by 8 atoms only (i.e. Pt atoms in the (100) surface are held less strongly than in the (111) one and hence can "turn-over" much faster).

60. The oxide formation rates for polycrystalline Pt fall close to those of Pt(111) indicating that the polycrystalline Pt surface consists mainly of crystallites or domains having the (111) orientation.

61. Since it is very unlikely that an anodically grown, thick-oxide film (beyond the level of two monolayers) on single-crystal Pt surfaces would maintain epitaxial with the underlying geometry of the parent Pt metal surface, it follows that the differences of oxide-film growth rates, that are specific to the surface on which the films grow, are determined by the inner metal/metal oxide-film interface. This implies that the growth depends on the rate of place-exchange, or Pt ion injection, at the inner metal/metal oxide-film interface. The rate of "place-exchange", or Pt ion injection, is specific to the surface geometry of the metal at this inner interface. This specific metal surface geometry, it appears, is maintained throughout growth of the oxide

films and gives rise to linear Q_{ox} vs log t_h plots having slopes specific to the geometry of the surface from which the oxide growth originates.

62. Contrary to earlier observations of Gilroy, the Q_{ox} vs log t_h plots for Pt(111), Pt(100) and Pt(poly) do not have a "common intercept" (i.e. when the oxide reduction charges are extrapolated to the zero value of Q_{ox}, the linear Q_{ox} vs log t_h plots do not tend to the same value of log $t \approx -12$). This observation impairs the applicability of Gilroy's "nucleation-and-growth" mechanism for the initial stages of oxide growth at Pt.

Contributions to Original Research

1. Qualitative and quantitative evaluation of polycrystalline Pt electrodes after various thermal and/or electrochemical pretreatments, and evaluation of surface structural changes resulting from cycling into the oxide formation-reduction region.

2. Discovery and evaluation of the "electrochemical annealing" phenomenon.

3. Description of a standard procedure for preparation of polycrystalline Pt electrodes which reveal the same physical and electrochemical properties.

4. Introduction of a new procedure for characterization of polycrystalline Pt electrodes which involves the macro-roughness factor and the micro-roughness factor.

5. Differentiation and characterization of five distinguishable oxide states at Pt as a function of the polarization potential and the polarization time required for their formation.

6. Experimental evidence that a direct logarithmic oxide growth law extends to polarization potentials higher than 1.8 V, RHE.

7. Proof that oxide film growth at Pt does not tend to any limit, contrary to the claim in earlier literature.

8. Proof that the OC1 state (quase-2-d oxide film) reaches a limit of 2 monolayers of "PtO" under various experimental conditions.

9. Direct evidence and proof that the OC1 state (quasi-2-d oxide film) can be reduced and re-formed independently of the presence of a thick phase-oxide film at high potentials and long anodization times.

10. Experimental proof that the quasi-2-d oxide film (the OC1 state) resides between Pt metal and the thick phase-oxide film.

11. Explanation that formation of the first monolayer of "PtO_2" on top of two monolayers of "PtO" is a slow process and its completion is essential for the oxide growth rate to increase 400-fold.

12. Evidence that oxide growth rates are different at various grains of polycrystalline Pt electrodes.

13. Evaluation of anodic O_2 evolution kinetics on various states of a developing thick oxide film on Pt.

14. Investigations in order to clarify the significance of the Clavilier "double-butterfly" H UPD C-V profile in relation to that for annealed Pt(111) and earlier C-V profiles of Hubbard.

15. Demonstration of further evidence that H UPD C-V profiles for Pt(111) and Pt(100) strongly depend on the thermal and/or electrochemical pretreatment procedures.

16. Evaluation of changes in the H UPD C-V profiles for "quenched" Pt(111) and Pt(100) resulting from cycling into the oxide region.

17. Suggested explanation of the complexity of the H UPD C-V profiles for "quenched" Pt(111) and Pt(100), and basis of effects of quenching on the surface structure of Pt(111) and Pt(100).

18. Evaluation of different previous explanations of the "double-butterfly" H UPD C-V profile for Pt(111).

19. For the first time, evaluation of oxide growth rates on Pt single-crystal faces by direct potentiostatic anodization.

20. Evidence and explanation that the oxide growth rate at Pt(100) is greater than that at Pt(111), while that at Pt(poly) is similar to that at Pt(111).

21. Demonstration that a direct logarithmic oxide growth rate describes oxide growth at Pt single-crystal electrodes.

22. Indication that oxide growth at Pt(poly), Pt(111) or Pt(100) does not proceed through the "nucleation-and-growth" mechanism.

REFERENCES

1. C. Wagner and W. Trand, *Z. Elektrochem.* **44** (1938) 391.
2. A.N. Frumkin and A. Aladjova, *Acta Physicochim. USSR* **19** (1944) 1.
3. H. Uhlig (Ed.), *"Corrosion Handbook"*, John Wiley and Sons, New York (1943).
4. U.R. Evans, *"An Introduction to Metallic Corrosion"*, Edward Arnold Publishers, London (1963).
5. I. Young, *"Anodic Oxide Films"*, Academic Press, New York (1961).
6. T.P. Hoar, Chapter XXX in *Modern Aspects of Electrochemistry*, Vol. 2, Ed. J.O'M. Bockris, Academic Press, New York (1959).
7. D. Gilroy and B.E. Conway, *Can. J. Chem.* **46** (1968) 875.
8. D. Gilroy, *J. Electroanal. Chem.* **71** (1976) 257; see also *J. Electroanal. Chem.* **83** (1977) 329.
9. H. Angerstein-Kozlowska, B.E. Conway and W.B.A. Sharp, *J. Electroanal. Chem.* **43** (1973) 9.
10. W.B.A. Sharp, Ph.D. Thesis, University of Ottawa (1976).
11. H. Angerstein-Kozlowska, B.E. Conway, A. Hamelin and L. Stoicoviciu, *J. Electroanal. Chem.* **228** (1987) 429.
12. H. Angerstein-Kozlowska, B.E. Conway, A. Hamelin and L. Stoicoviciu, *Electrochim. Acta* **31** (1986) 1051.
13. H. Angerstein-Kozlowska, B.E. Conway, K. Tellefsen and B. Barnett, *Electrochim. Acta* **34** (1989) 1045.
14. B. Barnett, Ph.D. Thesis, University of Ottawa (1981).
15. B.E. Conway, B. Barnett, H. Angerstein-Kozlowska and B.V. Tilak, *J. Chem. Phys.* **93** (1990) 8361.
16. B. Beden, D. Floner, J.M. Leger and C. Lamy, *Surf. Sci.* **162** (1985) 822.

17. R. Simpraga and B.E. Conway, *J. Electroanal. Chem.* **280** (1990) 341.

18. H.A. Laitinen and C.G. Enke, *J. Electrochem. Soc.* **107** (1960) 773.

19. K.J. Vetter and J.W. Schultze, *J. Electroancl. Chem.* **34** (1972) 131; 141.

20. J.L. Ord and F.C. Ho, *J. Electrochem. Soc.* **118** (1971) 46.

21. A.K.N. Reddy, M. Genshaw and J.O'M. Bockris, *J. Chem. Phys.* **48** (1968) 671.

22. A. Damjanović and A.T. Ward, *J. Electrochem. Soc.* **121** (1974) 113 C; **126** (1973) 593d; **126** (1979) 555.

23. A. Damjanović and V. Birss, *J. Electrochem. Soc.* **130** (1983) 1688.

24. S. Gottesfeld and B.E. Conway, *J. Chem. Soc., Faraday Trans. I* **69** (1973) 1090.

25. T. Biegler and R. Woods, *J. Electroanal. Chem.* **20** (1969) 73; **29** (1971) 269.

26. D.A.J. Rand and R. Woods, *J. Electroanal. Chem.* **35** (1972) 209.

27. S. Shibata, *J. Electroanal. Chem.* **89** (1978) 37.

28. S. Shibata and M. Sumino, *Electrochim. Acta* **20** (1975) 739.

29. S. Shibata, *Electrochim. Acta* **22** (1977) 175.

30. Y.B. Vassilyev, V.S. Bagotzky and O.A. Khazova, *J. Electroanal. Chem.* **181** (1984) 219.

31. Y.B. Vassilyev, V.S. Bagotzky and V.A. Gromyko, *J. Electroanal. Chem.* **178** (1984) 247.

32. S.D. James, *J. Electrochem. Soc.* **116** (1969) 1681.

33. J. Balej and O. Spalek, *Coll. Czech. Chem. Comm.* **37** (1972) 499.

34. L.D. Burke and M.B.C. Roche, *J. Electroanal. Chem.* **137** (1982) 175.

35. L.D. Burke, Chapter 4 in *Modern Aspects of Electrochemistry*, Vol. 18, Eds. R.E. White, J.O'M. Bockris and B.E. Conway, Plenum Press, New York (1986).

36. M. Farebrother, M. Goledzinowski, G. Thomas and V.I. Birss, *J. Electroanal. Chem.* **297** (1991) 469.

37. P. Stonehart, H.A. Kozlowska and B.E. Conway, *Proc. R. Soc. London* **A310** (1969) 541.

38. B.E. Conway, *Rev. Pure Appl. Chem.* **18** (1968) 105.

39. B.E. Conway, Chapter 10 in *Progress in Kinetics*, Vol. 4, Ed. G. Porter, Pergamon Press, Oxford (1967).

40. B. MacDougall, H. Angerstein-Kozlowska and B.E. Conway, *J. Electroanal. Chem.* **32** (1971) App. 15.

41. B.E. Conway, B. MacDougall and H.A. Kozlowska, *Trans. Faraday Soc.* **68** (1972) 1566.

42. H. Angerstein-Kozlowska, B. MacDougall and B.E. Conway, *J. Electroanal. Chem.* **39** (1972) 287.

43. B. MacDougall, Ph.D. Thesis, University of Ottawa (1972).

44. K. Tellefsen, Ph.D. Thesis, University of Ottawa (1988).

45. B.E. Conway, *"Ionic Hydration in Chemistry and Biophysics"*, Elsevier, Amsterdam (1981).

46. J.O'M. Bockris and A.K.N. Reddy, *"Modern Electrochemistry"*, Plenum Press, New York (1973).

47. C.A. Vincent, F. Bonino, M. Lazzari and B. Scrosati, *"Modern Batteries"*, Edward Arnold, Baltimore (1984).

48. M.J. Dignam, Chapter 5 in *Comprehensive Treatise of Electrochemistry*, Vol. 4, Eds. J.O'M Bockris, B.E. Conway, E. Yeager and R.E. White, Plenum Press, New York (1981).

49. D.B. Gibbs, B. Rao, R.A. Griffins and M.J. Dignam, *J. Electochem. Soc.* **122** (1975) 1167.

50. G. Belanger and A.K. Vijh, in *Oxides and Oxide Films*, Vol. 5, Ed. A.K. Vijh, Marcel Dekker, New York (1977).

51. N.F. Mott and N. Cabrera, *Rept. Prog. Phys.* **12** (1949) 163; *Trans. Faraday Soc.* **36** (1940) 472.

52. F.P. Fehlner and N.F. Mott, *Oxidation of Metals* **2** (1970) 59.

53. A.K. Vijh, *"Electrochemistry of Metals and Semiconductors"*, Marcel Dekker, New York (1973).

54. U.R. Evans, *"The Corrosion and Oxidation of Metals"*, St. Martins, New York (1960).

55. K. Hauffe, *"Oxidation of Metals"*, Plenum Press, New York (1965).

56. D.A. Vermilyea, Chapter 4 in *Advances in Electrochemistry and Electrochemical Engineering*, Vol. 3, Eds. P. Delahey and C.W. Tobias, Interscience, New York (1963).

57. U.R. Evans, *Electrochim. Acta* **16** (1971) 1825.

58. M.J. Weaver, *J. Electroanal. Chem.* **51** (1974) 231.

59. A. Damjanović and A.T. Ward, in *Int. Rev. of Science, Physical Chem., Series Two*, Vol. 6, Ed. J.O'M. Bockris, Butterworths, Toronto (1976).

60. S. Trasatti (Ed.), *"Electrodes of Conductive Metallic Oxides"*, Part A and B, Elsevier, New York (1980, 1981).

61. S.W. Feldberg, C.G. Enke and C.E. Bricker, *J. Electrochem. Soc.* **110** (1963) 863.

62. D. Dickertmann, J.W. Schultze and K.J. Vetter, *J. Electroanal. Chem.* **55** (1974) 429.

63. M.M. Lohrengel and J.W. Schultze, *Electrochim. Acta* **21** (1976) 957.

64. J.W. Schultze and M.M. Lohrengel, *Ber. Busengesl* **80** (1976) 552.

65. W.E. Reid and J. Kruger, *Nature* **203** (1964) 402.

66. A.C. Makrides, *J. Electrochem. Soc.* **113** (1966) 1158.

67. B.E. Conway, B. Barnett and H. Angerstein-Koziowska, *J. Chem. Phys.* **93** (1990) 8361.

68. M.A.H. Lanyon and B.M.W. Trapnell, *Proc. Roy. Soc.* **A227** (1955) 387.

69. N. Sato nad M. Cohen, *J. Electrochem. Soc.* **111** (1964) 512; 519; 624.

70. G. Tammann and W. Koster, *Z. Anorg. Chem.* **123** (1922) 196.

71. N.F. Mott, *Trans. Faraday Soc.* **35** (1939) 1175.

72. N.F. Mott, *Trans. Faraday Soc.* **43** (1947) 429.

73. R. Ghez, *J. Chem. Phys.* **58** (1973) 1838.

74. A. Hickling, *Trans. Faraday Soc.* **38** (1942) 27.

75. A. Sevcik, *Coll. Czech. Chem. Comm.* **13** (1948) 349.

76. F.G. Will and C.A. Knorr, *Z. Electrochem.* **64** (1960) 258.

77. P. Delahay, *"New Instrumental Methods in Electrochemistry"*, Robert E. Krieger, Huntington, New York (1980).

78. Southampton Electrochemistry Group, *"Instrumental Methods in Electrochemistry"*, John Wiley and Sons, New York (1985).

79. B.E. Conway, *"Theory and Principles of Electrode Processes"*, The Ronald Press, New York (1965).

80. J.S. Chacha, Ph.D. Thesis, University of Ottawa (1989).

81. E. Heitz and G. Kreysa, *"Principles of Electrochemical Engineering"*, VCH Publishers, W. Germany, New York (1986).

82. J.E.B. Randles, *Trans. Faraday Soc.* **44** (1948) 327.

83. P. Delahay and G. Perkins, *J. Phys. Coll. Chem.* **55** (1951) 586; 1146.

84. R.S. Nicholson and I. Shain, *Anal. Chem.* **36** (1964) 706.

85. R.S. Nicholson and I. Shain, *Anal. Chem.* **37** (1965) 178; 190.

86. R.S. Nicholson, *Anal. Chem.* **37** (1965) 1351.

87. S. Srinivasan and E. Gileadi, *Electrochim. Acata* **11** (1966) 321.

88. B.E. Conway, *Sci. Prog., Oxf.* **71** (1987) 479.

89. J.A.V. Butler, *Proc. Roy. Soc. London* **19** (1924) 734.

90. J.A.V. Butler, *Proc. Roy. Soc. London* **A 157** (1936) 423.

91. M. Volmer and T. von Erdey-Gruz, *Z. Physik. Chem.* **A 150** (1930) 203.

92. J.A.V. Butler, *Proc. Roy. Soc. London* **A 112** (1926) 129.

93. J. Tafel, *Z. Phys. Chem.* **50** (1905) 641.

94. R. Parsons, *Trans. Faraday Soc.* **47** (1951) 1332.

95. B.E. Conway, *Trans. Roy. Soc. Can., Sec. III* **54** (1960) 19.

96. B.D. Cullity, *"Elements of X-ray Diffraction"*, Addison-Wesley, USA (1958).

97. B.E. Warren, *"X-ray Diffraction"*, Addison-Wesley, USA (1969).

98. C.S. Barnet and T.B. Masalski, *"Structure of Metals; Crystallographic Methods, Principles and Data"*, McGraw-Hill, London (1966).

99. A. Hamelin, Chapter 1 in *Modern Aspects of Electrochemistry*, Vol. 16, Eds. B.E. Conway, R.E. White and J.O'M. Bockris, Plenum Press, New York (1985).

100. A.B. Greninger, *Zeit. für Krist.* A **91** (1935) 424.

101. I.M. Watt, *"The Principles and Practive of Electron Microscopy"*, Cambridge University Press, Cambridge (1985).

102. O.C. Wells, *"Scanning Electron Microscopy"*, McGraw-Hill, New York (1974).

103. K. Siegbahn et al., *"ESCA - Atomic, Molecular and Solid State Structure Studied by Means of Electron Spectroscopy"*, Uppsala, Sweden (1967).

104. R.S. Swingle and W.M. Riggs, *Anal. Chem.* **47** (1975) 21.

105. J.M. Blakely, *"Introduction to the Properties of Crystal Surfaces"*, Pergamon Press, New York (1973).

106. A. Oles, *"Metody Eksperymentalne Fizyki Ciala Stalego"*, WN-T, Warsaw (1983).

107. G.A. Somarjai, *"Chemistry in Two Dimension: Surfaces"*, Cornell University Press, Ithaca, New York (1981).

108. G.A. Somorjai, *"Principles of Surface Chemistry"*, Prentice-Hall, New Jersey (1972).

109. J.B. Pendry, *"Low Energy Electron Diffraction"*, Academic Press, New York (1974).

110. I. Langmuir, *J. Am. Chem. Soc.* **38** (1916) 1145.

111. I. Langmuir, *Trans. Faraday Soc.* **17** (1921) 621.

112. I. Langmuir, *J. Am. Chem. Soc.* **38** (1916) 2221; **40** (1918) 1361.

113. K.J. Laidler, *"Chemical Kinetics"*, Harper and Row, New York (1987).

114. B.E. Conway, H. Angerstein-Kozlowska and H.P. Dhar, *Electrochim. Acta* **19** (1974) 455.

115. T. Hill, *"Introduction to Statistical Thermodynamics"*, Addison-Wesley, Reading, Massachusetts (1960).

116. M. Temkin and V. Pyzhev, *Acta Physicochim., USSR* **2** (1935) 473.

117. J.G. Klinger, Ph.D. Thesis, University of Ottawa (1977).

118. A.N. Frumkin and A. Slygin, *Acta Physicochim., USSR* **3** (1935) 791; **4** (1936) 991; **5** (1936) 819.

119. P. Dolin and B.V. Ershler, *Acta Physicochim., USSR* **13** (1940) 747.

120. M.W. Breiter, *Trans. Symposium on Electrode Processes* **1759** (The Electrochemical Society), 307, John Wiley and Sons, New York (1961).

121. F.G. Will, *J. Electrochem. Soc.* **112** (1965) 481.

122. H. Angerstein-Kozlowska, W.B.A. Sharp and B.E. Conway, *Proceedings of the Symposium on Electrocatalysis*, The Electrochemical Society (1974) 94.

123. B.E. Conway, *Chemistry in Canada* **28 (8)** (1976).

124. J.D. McIntryre and Peck, *Faraday Discussion*, (Chem. Soc., London) Oxford (1973).

125. B.E. Conway, H. Angerstein-Kozlowska and L. Laliberte, *J. Electrochem. Soc.* **121** (1974) 1596.

126. P. Stonehart, *Electrochim. Acta* **15** (1970) 1853.

127. R. Woods, *J. Electroanal. Chem.* **49** (1974).

128. B.E. Conway, H. Angerstein-Kozlowska and F.C. Ho, *J. Vac. Sci. Technol.* **14** (1977) 351.

129. P.J. Estrup and J.A. Anderson, *J. Chem. Phys.* **45** (1966) 2254.

130. L.H. Gerner and A.U. McRae, *Proc. Natl. Acad. Sci.* **48** (1962) 991.

131. E.G. Bauer, *Phys. Rev.* **123** (1961) 1206.

132. L.D. Schmidt, *Cat. Rev., Sci. Eng.***9** (1974) 115.

133. J.A. Paritz, *J. Vac. Sci. and Technol.* **11** (1974) 206.

134. S. Tsuchiya, Y. Amenomiya and R.J. Cvetanovic, *J. Catalysis* **19** (1970) 245.

135. B.E. Conway, W.B.A. Sharp, H. Angerstein-Kozlowska and E.E. Criddle, *Anal. Chem.* **45** (1973) 1321.

136. R.M. Ishikawa and A.T. Hubbard, *J. Electroanal. Chem.* **69** (1976) 317.

137. A.T. Hubbard, R.M. Ishikawa and J. Katekaru, *J. Electroanal. Chem.* **86** (1978) 271.

138. F.T. Wagner and P.N. Ross, Jr., *J. Electroanal. Chem.* **150** (1983) 141.

139. P.N. Ross and F.T. Wagner, Chapter 2 in *Advances in Electrochemistry and Electrochemical Engineering*, Vol. 13, Ed. H. Gerischer, John Wiley and Sons, New York (1984).

140. J. Clavilier, R. Faure, G. Guinet and R. Durand, *J. Electroanal. Chem.* **107** (1980) 205.

141. J. Clavilier, *J. Electroanal. Chem.* **107** (1980) 211.

142. J. Clavilier, D. Armand and B.L. Wu, *J. Electroanal. Chem.* **135** (1982) 159.

143. J. Clavilier and D. Armand, *J. Electroanal. Chem.* **199** (1986) 187.

144. J. Clavilier, R. Durand, G. Guinet and R. Faure, *J. Electroanal. Chem.* **127** (1981) 281.

145. J. Clavilier, D. Armand, S.G. Sun and M. Petit, *J. Electroanal. Chem.* **205** (1986) 267.

146. D. Armand and J. Clavilier, *J. Electroanal. Chem.* **263** (1989) 109.

147. J. Clavilier, K. El Achi, M. Petit, A. Rodes and M.A. Zamakhchari, *J. Electroanal. Chem.* **295** (1990) 333.

148. J. Clavilier, R. Parsons, R. Durand, C. Lamy and J.M. Leger, *J. Electroanal. Chem.* **124** (1981) 321.

149. J. Clavilier, C. Lamy and J.M. Leger, *J. Electroanal. Chem.* **125** (1981) 249.

150. C. Lamy, J.M. Leger, J. Clavilier and R. Parsons, *J. Electroanal. Chem.* **150** (1983) 71.

151. F. El Omar and R. Durand, *J. Electroanal. Chem.* **178** (1984) 343.

152. J. Clavilier and S.G. Sun, *J. Electroanal. Chem.* **199** (1986) 471.

153. J. Clavilier, J.M. Feliu and A. Aldaz, *J. Electroanal. Chem.* **243** (1988) 419.

154. D. Armand and J. Clavilier, *J. Electroanal. Chem.* **225** (1987) 205.

155. D. Armand and J. Clavilier, *J. Electroanal. Chem.* **233** (1987) 251.

156. S.G. Sun, J. Clavilier and A. Bewick, *J. Electroanal. Chem.* **240** (1988) 147.

157. S.G. Sun and J. Clavilier, *J. Electroanal. Chem.* **236** (1987) 95.

158. R. Albalat, J. Claret, J.M. Feliu and J. Clavilier, *J. Electroanal. Chem.* **288** (1990) 277.

159. J.M. Feliu, A. Fernandez-Vega, A. Aldaz and J. Clavilier, *J. Electroanal. Chem.* **256** (1988) 149.

160. J. Clavilier, J.M. Feliu, A. Fernandez-Vega and A. Aldaz, *J. Electroanal. Chem.* **269** (1989) 175.

161. J.M. Feliu, J.M. Orts, A. Fernandez-Vega, A. Aldaz and J. Clavilier, *J. Electroanal. Chem.* **296** (1990) 191.

162. B. Love, K. Seto and J. Lipkowski, *J. Electroanal. Chem.* **199** (1986) 219.

163. R.R. Adzić, A.V. Tripković and V. Vesović, *J. Electroanal. Chem.* **205** (11986) 335.

165. R. Adzić, Chapter 5 in *Modern Aspects of Electrochemistry*, Vol. 21, Eds. R.E. White, J.O'M. Bockris and B.E. Conway, Plenum Press, New York (1990).

166. G. Jerkiewicz and B.E. Conway, *Journal de Chimie Physique*, in press.

167. E. Morallon, J.L. Vasquez and A. Aldaz, *J. Electroanal. Chem.* **288** (1990) 217.

168. M.-C. Morin, C. Lamy, J.-M. Leger, J.-L. Vasquez and A. Aldaz, *J. Electroanal. Chem.* **283** (1990) 287.

169. T.E. Felter and A.T. Hubbard, *J. Electroanal. Chem.* **100** (1979) 473.

170. G.A. Garwood, Jr. and A.T. Hubbard, *Surf. Sci* **92** (1980) 617.

171. A.T. Hubbard, J.L. Stickney, S.D. Rosasco, M.P. Soriaga and D. Song, *J. Electroanal. Chem.* **150** (1983) 165.

172. A. Więckowski, B.C. Schardt, S.D. Rosasco, J.L. Stickney and A.T. Hubbard, *Surf. Sci.* **146** (1984) 115.

173. A. Więckowski, S.D. Rosasco, B.C. Schardt, J.L. Stickney and A.T. Hubbard, *Inorg. Chem.* **23** (1984) 565.

174. D. Zurawski, L. Rice, M. Hourani and A. Więckowski, *J. Electroanal. Chem.* **230** (1987) 221.

175. A. Więckowski, P. Zelenay and K. Varga, *Journal de Chimie Physique*, in press.

176. E.K. Krauskopf and A. Więckowski, Chapter in *"Frontiers in Electrochemistry"*, Eds. P.N. Ross and J. Lipkowski, VCH Verlag, in press.

177. K. Al Jaaf-Golze, D.M. Kolb and A.D. Scherson, *J. Electroanal. Chem.* **200** (1986) 353.

178. A. Bewick, K. Kunimatsu, J. Robinson and J.W. Russell, *J. Electroanal. Chem.* **239** (1988) 413.

179. T. Toya, *J. Res. Inst. Catalysis, Hokkaido University* **10** (1962) 236.

180. J. Horiuti and T. Toya, in *"Solid State Surface Science"*, ed. M. Green, Marcel Dekker, New York (1969).

181. J.D.E. McIntyre, W.F. Peck, J. Lipkowski and B. Love, paper presented at the 194th Meeting of the American Chemical Society in New Orleans (1987).

182. K.J. Vetter and D. Berndt, *Z. Electrochem.* **62** (1958) 378.

183. W. Böld and M. Breiter, *Electrochim. Acta* **5** (1961) 145.

184. B.E. Conway and T.C. Liu, *Langmuir* **6** (1990) 268.

185. S.G. Roscoe and B.E. Conway, *J. Electroanal. Chem.* **224** (1987) 163.

186. A.K. Vijh and B.E. Conway, *Chem. Rev.* **67** (1967) 623.

187. F.C. Anson, *J. Amer. Chem. Soc.* **81** (1959) 1554; *Anal. Chem.* **33** (1961) 934.

188. A.J. Appleby, *J. Electrochem. Soc.* **120** (1973) 1205.

189. B.E. Conway, G. Tremiliosi-Filho and G. Jerkiewicz, *J. Electroanal. Chem.* **297** (1991) 435.

190. B.E. Conway and T.C. Liu, *Proc. Roy. Soc., London* **A429** (1990) 375.

191. J.S. Hammond and N. Winograd, *J. Electroanal. Chem.* **78** (1977) 55.

192. K.S. Kim, N. Winograd and R.E. Davis, *J. Am. Chem. Soc.* **93** (1971) 6296.

193. M. Peuckert, *Electrochim. Acta* **29** (1984) 1315.

194. G.C. Allen, P.M. Tucker, A. Capon and R. Parsons, *J. Electroanal. Chem.* **50** (1973) 335.

195. D. Aberdam, R. Durand, R. Faure and F. El-Omar, *Surface Sci.* **171** (1986) 303.

196. G.A. Somarjai and M.A. Van Hove, *Progress in Surface Science,* **80** (1988) 201.

197. J. Mozota, Ph.D. Thesis, University of Ottawa (1981).

198. D.F. Tessier, Ph.D. Thesis, University of Ottawa (1985).

199. E. Heitz and G. Kreysa, *"Principles of Electrochemical Engineering"*, VCH Verlag, W. Germany (1986).

200. B.E. Conway, *Proc. Roy. Soc., London* **A256** (1960) 128.

201. H. Angerstein-Kozlowska, Chapter 9 in *"Comprehensive Treatise of Electrochemistry"*, Vol. 9, Eds. E. Yeager, J.O'M. Bockris, B.E. Conway and S. Sarangapani, Plenum Press, New York (1984).

202. J. Lipkowski, private communication.

203. J. Clavilier and J.P. Chauvineau, *J. Electroanal. Chem.* **100** (1978) 461.

204. H. Melville and B.G. Gowenlock, *"Experimental Methods in Gas Reactions"*, London (1964).

205. D.J. Ives and G.J. Janz, *"Reference Electrodes, Theory and Practice"*, Academic Press, New York (1961).

206. G. Tremiliosi-Filho, G. Jerkiewicz and B.E. Conway, *Langmuir*, in press.

207. H. Angerstein-Kozlowska, B.E. Conway, B. Barnett and J. Mozota, *J. Electroanal.*

Chem. **100** (1979) 417.

208. M.F. Ashby and D.R.H. Jones, *"Engineering Materials 1"*, Pergamon Press, New York (1980).

209. M.F. Ashby and D.R.H. Jones, *"Engineering Materials 2"*, Pergamon Press, New York (1986).

210. Z. Wendorff, *"Metaloznawstwo"*, WNT, Warszawa (1972).

211. P.N. Ross, *J. Electrochem. Soc.* **126** (1979) 67.

212. J. Mozota and B.E. Conway, *J. Electochem. Soc.* **128** (1981) 214; see also *Electrochim. Acta* **28** (1983) 119.

213. B.V. Tilak, H. Angerstein-Kozlowska and B.E. Conway, *J. Electroanal. Chem.* **48** (1973) 1.

214. R.K. Burshtein, *Elektrokhim.***3** (1967) 349.

215. J.A.V. Butler and J. Drever, *Trans. Faraday Soc.* **32** (1936) 427.

216. B.V. Ershler and Y. Proskurnin, *Acta Phys-Chim. USSR* **6** (1937) 195.

217. J.O'M. Bockris and A.K.M.S. Huq, *Proc. R. Soc. London* **A237** (1956) 227.

218. J.W. Schultze and M. Haga, *Z. Phys. Chem.* **104** (1977) 73.

219. W. Schmickler and J.W. Schultze, *Z. Phys. Chem.* **110** (1978) 277.

220. J.O'M. Bockris, *J. Phys. Chem.* **24** (1956) 817.

221. S. Trasatti, *J. Electroanal. Chem.* **115** (1980) 125.

222. A.C.C. Tseung and S.M. Jasem, *Electrochim. Acta* **22** (1976) 501.

223. A. Damjanović, L.S.R. Yeh and J.F. Wolf, *J. Electrochem. Soc.* **127** (1980) 784; 1951.

224. T.C. Liu and B.E. Conway, *J. Appl. Electrochem.* **17** (1987) 983.

225. B.E. Conway and T.C. Liu, *Materials Chem. and Phys.* **22** (1989) 163.

226. T. Dickinson, A. Povey and P.M.A. Sherwood, *J. Chem. Soc. Faraday Trans. I* **71** (1975) 298.

227. J. Willsau, D. Wolter and J. Heitbaum, *J. Electroanal. Chem.* **195** (1985) 299.

228. B.E. Conway and P.L. Bourgault, *Can. J. Chem.* **37** (1959) 292.

229. D. Armand and M.-L. Rosinberg, *J. Electroanal. Chem.* **302** (1991) 191.

230. G.A. Somorjai, Ed., *"The Structure and Chemistry of Solid Surfaces"*, John Wiley and Sons, New York (1969).

231. G.A. Somorjai and H.H. Farrell, *Adran. Chem. Phys.* **20** (1970) 215.

232. G. Ertl and J. Küppers, *"Low Energy Electrons and Surfaces Chemistry"*, Verlag Chemie, Weinheim (1979).

233. A. Więckowski, private communication.

234. S. Motoo and N. Furuya, *J. Electroanal. Chem.* **172** (1984) 339; see also N. Furuya and S. Koide, *Surface Sci.* **20** (1989) 18.

235. P. Zelenay, G. Horányi, C.K. Rhee and A. Więckowski, *J. Electroanal. Chem.* **300** (1991) 499.

236. F.A. Lewis, *"The Palladium Hydrogen System"*, Academic Press, New York (1967).

237. K.M. MacKay, *Hydrogen Compounds of the Metallic Elements"*, E. & F.M. Spon, London (1966).

238. G. Bambakidis, *"Metal Hydrides"*, Plenum Press, New York (1981).

239. M.C. Desjonquères and F. Cyrot-Lackmann, *J. Chem. Phys.* **64** (1976) 3707.

240. N.F. Mott and R.J. Watts-Tobin, *Electrochim. Acta* **4** (1961) 79.

241. R.J. Watts-Tobin, *Phil. Mag.* **6** (1961) 133.

242. H. Kita, S. Ye, A. Aramata and N. Furuya, *J. Electroanal. Chem.* **295** (1990) 317.

243. A. Bewick, *Ext. Abstr., 40th ISE Meeting*, Kyoto, Japan (1989) p. 828.

List of Symbols and Abbreviations

A	Surface area
A_{gcom}	Geometric surface area
α	Transfer coefficient
b	Tafel slope
BS	Broad shoulder
β	Symmetry factor
c	Concentration
C	Capacitance
CE	Counter Electrode
d(h,k,l)	Lattice constant
D	Diffusion constant
e	Electron charge
E	Potential
E°	Standard potential
E_b	Binding energy
E_f	Final potential
E_h	Holding (polarization) potential
E_i	Initial potential
$E_{i=0}$	Potential of zero current
E_{IR}	"IR" drop
E_k	Kinetic energy
E_{obs}	Observed potential
E_p	Peak potential
EDX (or EDS)	Energy-Dispersive X-Ray Spectrometry

ESCA	Electron Spectroscopy for Chemical Analysis
F	Faraday constant
g	Parameter in Temkin isotherm
$\Delta^{\ddagger}G$	Gibbs energy of activation
h	Planck constant
ΔH_{ads}	Enthalpy of adsoption
HA1, HA2, HA3	UPD H desorption peaks
HC1, HC2	UPD H adsorption peaks
HER	Hydrogen Evolution Reaction
η	Overpotential
θ	Coverage
i	Current density
i_o	Exchange current density
i_p	Peak current
i_{HA1}, i_{HA2}, i_{HA3}	Principle H UPD anodic peak current density
i_{HC1}, i_{HC2}	Principle H UPD cathodic peak current density
k	Boltzmann constant
k	Rate constant
k_b	Rate constant of the backward reaction
k_f	Rate constant of the forward reaction
K_1	Equilibrium constant
LEED	Low Energy Electron Diffraction
λ	Wavelength
n	Number of electrons exchanged
n_f	Normalization factor
ν	Frequency
OER	Oxygen Evolution Reaction

OC1-OC4	Cathodic oxide reduction peaks
q	Charge density
q_1	Monolayer charge density
Q_{ox}	Oxide reduction charge
$Q_{H\ UPD}$	H UPD charge
R	Gas constant
R_F	Faradaic charge-transfer resistance
R_S	Solution resistance
$R \equiv R_1$	Roughness (macro) factor
R_m	Micro-roughness factor
R_t	Total (overall) roughness factor
RHE	Reference Hydrogen Electrode
RHEED	Reflectance High Energy Electron Diffraction
s	Sweep mode
SEM	Scanning Electron Microscopy
STM	Scanning Tunnelling Microscopy
t	Time
t_h	Holding (polarization) time
T	Temperature in Kelvins
T_m	Melting point
Tafel plot	Overpotential (η) vs log current density (log i) plot
τ	Transmission coefficient
UPD	Under Potential Deposition
UPD H	Under Potential Deposition of Hydrogen
XPS	X-ray Photoelectron Spectroscopy
WE	Working Electrode
z	Number of electrons exchanged